

2011

Formation and Stabilization of Combustion-Generated Environmentally Persistent Free Radicals on Transition Metal Oxides Supported on Silica

Eric Warren Pimentel Vejerano

Louisiana State University and Agricultural and Mechanical College

Follow this and additional works at: https://digitalcommons.lsu.edu/gradschool_dissertations

 Part of the [Chemistry Commons](#)

Recommended Citation

Vejerano, Eric Warren Pimentel, "Formation and Stabilization of Combustion-Generated Environmentally Persistent Free Radicals on Transition Metal Oxides Supported on Silica" (2011). *LSU Doctoral Dissertations*. 1109.
https://digitalcommons.lsu.edu/gradschool_dissertations/1109

This Dissertation is brought to you for free and open access by the Graduate School at LSU Digital Commons. It has been accepted for inclusion in LSU Doctoral Dissertations by an authorized graduate school editor of LSU Digital Commons. For more information, please contact gradetd@lsu.edu.

**FORMATION AND STABILIZATION OF COMBUSTION-GENERATED
ENVIRONMENTALLY PERSISTENT FREE RADICALS ON
TRANSITION METAL OXIDES SUPPORTED ON SILICA**

A Dissertation

Submitted to the Graduate Faculty of the
Louisiana State University and
Agricultural and Mechanical College
in partial fulfillment of the
requirements for the degree of
Doctor of Philosophy

in

The Department of Chemistry

by

Eric Warren P. Vejerano
B.S., University of the Philippines Los Baños, 1999
May 2011

DEDICATION

for Joaquin, Andre, Che, and Nanay

ACKNOWLEDGMENTS

The journey of a thousand miles begins with a single step- Chinese Proverb.

A milestone as essential as this, had lots of people behind it. It is my greatest honor and humility to have received their support, and helped me achieve this penultimate goal of graduate school life. It is therefore proper to give thanks and acknowledgments to them.

I extend my deepest gratitude to my adviser, Dr. Barry Dellinger, for giving me a *research home* and allowing me to work in his group, and for his trust on my ability. I am deeply indebted to Dr. Slawomir Lomnicki for his invaluable assistance and understanding. I would also like to thank Dr. Lavrent Khachatryan and Dr. Zofia Maskos for their assistance and inputs. I would like to thank my committee members, Dr. Erwin Poliakoff, Dr. Bin Chen, Dr. Robert Cook, and Dr. Michael Benton for their invaluable comments. I am also thankful to the LSU Chemistry Department, especially to Ms. Kim Mollere, Ms. Sherry Wilkes, and to good ‘Ole Mr. Roy. To the members of the Dellinger group; Dr. Hongyi Wu for his numerous help, Dr. Shadrack Nganai, Albert de la Cruz, Lucy Kiruri, William Gehling, Joshua Kibet, and most especially to Ms. Tina Black for her concerns, support, and understanding—Thank You.

I and my family are thankful to the Filipinos at LSU for their support and understanding, and for providing a community. We are grateful to Drs. Zorabel and Jason Lejeune for their numerous help — a heartfelt appreciation for all the things you have done.

I, Andre, Joaquin, and my lovely wife Che, are grateful for the sacrifices, care, *love*, *understanding*, and benedictions from our families. *Salamat!*

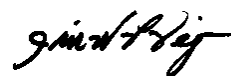


TABLE OF CONTENTS

DEDICATION	ii
ACKNOWLEDGMENTS	iii
LIST OF TABLES	viii
LIST OF FIGURES	ix
LIST OF SCHEMES.....	xii
LIST OF ABBREVIATIONS.....	xiv
ABSTRACT.....	xv
CHAPTER I. INTRODUCTION.....	1
1.1 Nature and Origin of Combustion Generated Particulate Matter and Free Radicals.....	2
1.2 Transition Metals in Combustion System.....	5
1.3 Sources, Origin, and Nature of Radical Precursors	7
1.4 Environmental and Health Implications	10
1.5 Nature, Structure, and Origin of Phenoxy and Semiquinone Radicals.....	14
1.5.1 Formation of Phenoxy Radical and Semiquinone Radical in the Gas Phase	14
1.5.2 Surface-mediated Formation of Semiquinone and Phenoxy Radical	15
1.6 Formation of PCDD and PCDF in Combustion System.....	18
1.7 Research Objectives.....	18
1.8 Summary of Key Findings on Particulate Matter in the Literature	20
1.9 References.....	24
CHAPTER II. EXPERIMENTAL	43
2.1 Vacuum and Thermoelectric Furnace System	43
2.1.1 The Vacuum System	43
2.1.2 Vacuum Exposure Chamber	44
2.1.3 The Extraction Cell.....	45
2.1.4 The High Temperature Ceramic Heater.....	46
2.2 Particulate Matter Sample.....	46
2.2.1 Particulate Matter Sample Matrix Preparation	46
2.2.2 Determination of Metal Content in Sample Particulate Matter	48
2.3 Detailed Adsorption Procedure.....	49
2.4 EPR Analysis	51
2.4.1 Analysis and Calculation	51
2.4.2 Calibration Curve.....	52
2.5 Determination of Surface-Bound Radical Stability and Persistency	53

2.5.1	Calculation of 1/e Half-life	54
2.6	GC-MS Analyses of EPFR Extracts	55
2.7	Interaction of EPFRs with Biological Compounds.....	56
2.8	Determination of the Interaction of Particulate Matter with Biological Fluids	56
2.9	Spin Trapping of Reactive Oxygen Species	57
2.9.1	Materials	57
2.9.2	EPFR Surrogate Synthesis	57
2.9.3	Calculation of OH Radical Concentration	57
2.9.4	Comparison with EPR Spectra in the Literature.....	58
2.9.5	<i>In Vitro</i> Studies	58
2.9.6	EPR Measurements.....	60
2.10	Basics of Electron Paramagnetic Resonance Spectroscopy (EPR)	60
2.11	EPR Instrumentation.....	62
2.12	References.....	63
CHAPTER III. RESULTS		65
3.1	Formation of Paramagnetic Species on the Surface of Transition Metal Oxide on Silica Particles.....	65
3.1.1	Formation of g1 on Fe(III) ₂ O ₃ and Ni(II)O on Silica Surface	67
3.1.2	Formation of g2 and g3 Radicals on Fe(III) ₂ O ₃ /Silica Surface	68
3.1.2.1	Phenol.....	70
3.1.2.2	Hydroquinone and Catechol.....	70
3.1.2.3	1,2-Dichlorobenzene and 2-Monochlorophenol	70
3.1.2.4	Monochlorobenzene.....	71
3.1.3	Formation of g2 and g3 Radical on Ni(II)O on Silica Surface	73
3.1.3.1	Phenol.....	73
3.1.3.2	Monochlorobenzene.....	81
3.1.3.3	1,2-Dichlorobenzene and 2-Monochlorophenol	82
3.1.3.4	Catechol and Hydroquinone.....	83
3.2	Comparative Yields of the EPFRs on Ni(II)O, Cu(II)O, and Fe(III) ₂ O ₃ /Silica Surface	85
3.3	Persistence and Lifetime of EPFRs on Transition Metal Oxide/Silica Surface....	86
3.3.1	Persistence and Lifetime of EPFRs on Fe(III) ₂ O ₃ /Silica Surface	86
3.3.2	Persistence and Lifetime of EPFRs on Ni(II)O/Silica Surface	87
3.3.3	Persistence and Lifetime of EPFRs on Zn(II)O/Silica Surface	88
3.4	Comparative Lifetimes of EPFRS on Different Transition Metal Oxide on Silica Surface	90
3.5	Molecular Products from Extraction of EPFRs	93
3.5.1	Molecular Products from Extraction of EPFRs on Cu(II)O/Silica	93
3.5.2	Molecular Products from the Extraction of EPFRs on Fe(III) ₂ O ₃ /Silica Surface	94
3.5.3	Molecular Products from Extraction of EPFRs on Ni(II)O/Silica.....	97
3.6	Biological Studies with EPFRs.....	100
3.6.1	Decay of EPFR Signal on Biological Fluids.....	102
3.6.2	Interaction of Some Biological Compounds with EPFRs	104

3.7 Spin Trapping Studies.....	104
3.7.1 Spin Trapping of Hydroxyl Radical.....	104
3.7.2 Trapping of $O_2^{\cdot -}$ by DMPO in Different Solvents.....	106
3.8 References.....	109
CHAPTER IV. DISCUSSION.....	110
4.1 General Mechanism of EPFR Formation on Transition Metal Oxide Surface ...	110
4.2 Metal <i>F</i> -center Formation (g1) in Fe(III) ₂ O ₃ and Ni(II)O.....	111
4.3 Adsorbate EPFR Formation (g2 and g3 radicals) on Fe(III) ₂ O ₃ and Ni(II)O.....	112
4.3.1 Phenol.....	112
4.3.2 Hydroquinone and Catechol.....	113
4.3.3 1,2-Dichlorobenzene and 2-Monochlorophenol.....	116
4.3.4 Monochlorobenzene.....	119
4.4 Comparative Yields of EPFRs on Different Transition Metal Oxide/Silica Surface	121
4.5 Persistence and Lifetimes of EPFRs on Fe(III) ₂ O ₃ , Ni(II)O, and Zn(II)O Surface	121
4.6 Formation of Molecular Products from Radical Recombination.....	127
4.7 Interaction of EPFRs with Biological Compounds.....	131
4.8 Spin Trapping Studies.....	134
4.8.1 Hydroxyl Radical Generation.....	137
4.8.2 The Effect of Superoxide Dismutase (SOD) and Catalase (CAT)	139
4.8.3 Trapping of Superoxide Radical by DMPO in Aprotic Solvents	141
4.9 References.....	145
CHAPTER V. SUMMARY.....	152
5.1 EPFR Formation on Transition Metal Oxide/Silica Surface	152
5.2 Formation and Stabilization of EPFRs on Fe(III) ₂ O ₃ and Ni(II)O on Silica Surface	153
5.3 Temperature Dependence of EPFR Yields.....	154
5.4 Persistence of EPFRs on Transition Metal Oxide/Silica Surface.....	156
5.5 Formation of Molecular Products from Radical-Radical Recombination	156
5.6 <i>In Vitro</i> Studies and Interaction of EPFRs with Biological Compounds	157
5.7 Concluding Remarks.....	159
5.8 References.....	160
APPENDIX 1. VARIATION OF G-VALUE AND $\Delta H_{P,P}$ WITH TIME ON Fe(III) ₂ O ₃ , Ni(II)O, AND Zn(II)O ON SILICA SURFACE WITH AIR.....	164
APPENDIX 2. PROPOSED REACTION MECHANISMS FOR THE FORMATION OF MOLECULAR PRODUCT FROM RADICALS.....	172
APPENDIX 3. PEAK FITTING ANALYSIS EXAMPLE OF EPR SPECTRA FOR CT, HQ, PH, 1,2-DCBz, MCBz, AND 2-MCP	175

APPENDIX 4. EPFRs ON Cu(II)O AND Fe ₂ (III)O ₃ /SILICA EXPOSED TO SUNLIGHT AT AMBIENT CONDITION	177
APPENDIX 5. AMERICAN CHEMICAL SOCIETY'S POLICY ON THESES AND DISSERTATIONS.....	178
VITA.....	179

LIST OF TABLES

Table 1.1. Summary of the key findings on particulate matter, its nature, origin, composition, and environmental and health implications	21
Table 2.1. Properties of silica gel and Cab-O-Sil.....	47
Table 3.1. Summary of the peak fitting results for the different adsorbates dosed on Fe(III) ₂ O ₃ /silica at different temperatures	74
Table 3.2. Radical concentration (g ₂ +g ₃) of surface-bound EPFRS (spin/g of Fe(III) ₂ O ₃ /silica) at different temperatures dosed on Fe(III) ₂ O ₃ /silica	76
Table 3.3. Summary of the peak fitting results for the different adsorbates dosed on Ni(II)O/silica at different temperatures	77
Table 3.4. Radical concentration (g ₂ +g ₃) (spins/g of Ni(II)O/Silica) at different temperatures dosed on Ni(II)O/Silica.....	79
Table 3.5. Molecular extraction products from radical recombination of EPFRs on Cu(II)O/silica for different temperatures and adsorbates extracted by methanol	91
Table 3.6. Molecular extraction products from radical recombination of EPFRs on Cu(II)O/silica for different temperatures and adsorbates extracted by dichloromethane	92
Table 3.7. Molecular extraction products from radical recombination of EPFRs on Fe(III) ₂ O ₃ /silica for different temperatures and adsorbates extracted by methanol	95
Table 3.8. Molecular extraction products from radical recombination of EPFRs on Fe(III) ₂ O ₃ /silica for different temperatures and adsorbates extracted by dichloromethane	96
Table 3.9. Molecular extraction products from radical recombination of EPFRs on Ni(II)O/silica for different temperatures and adsorbates extracted by methanol	98
Table 3.10. Molecular extraction products from radical recombination of EPFRs on Ni(II)O/silica at different temperatures and adsorbates extracted by dichloromethane	99
Table 4.1. EPR measured parameters of DMPO-OH adduct in water solution as a function of AcN concentration.....	144

LIST OF FIGURES

Figure 1.1. Zone theory of combustion in the formation of surface-mediated free radical	3
Figure 1.2. Generation of ROS catalyzed by surface-bound semiquinone radical	13
Figure 1.3. Structures of hydroquinone and catechol and their corresponding radicals	14
Figure 1.4. Molecular precursors of chloro(phenoxy) radicals and their structures	15
Figure 2.1. The vacuum and high temperature thermoelectric furnace system	43
Figure 2.2. EPR extraction cell with a detachable EPR tube	45
Figure 2.3. EPR tube for DPPH standard	53
Figure 2.4. The Zeeman effect	61
Figure 2.5. First-derivative EPR spectrum	62
Figure 2.6. Instrument set-up of the Bruker EMX2.0/2.7 EPR spectrometer	62
Figure 3.1. Temperature dependence of the EPR spectra of different adsorbates dosed at different temperatures on Fe(III) ₂ O ₃ on silica surface	66
Figure 3.2. Peak fitting procedure done on catechol at 250 °C dosed on Fe(III) ₂ O ₃ /silica surface	67
Figure 3.3. Yield of organic EPFRs (g ₂ + g ₃) adsorbed on 5% Fe(III) ₂ O ₃ /silica for different adsorbates and dosing temperatures	68
Figure 3.4. Intensity of g ₂ and g ₃ radicals on 5% Fe(III) ₂ O ₃ /silica from deconvolution of EPR spectra for different adsorbates and dosing temperatures	69
Figure 3.5. Ratio of g ₂ and g ₃ components of the different adsorbates as a function of dosing temperature on Fe(III) ₂ O ₃ /silica surface	71
Figure 3.6. Temperature dependence of the EPR spectra of different adsorbates dosed on 5% Ni(II)O/silica	72
Figure 3.7. Yield of the g ₂ and g ₃ radicals on 5% Ni(II)O/silica for different adsorbates and dosing temperatures	80
Figure 3.8. Yield of organic radical (g ₂ +g ₃) for different precursors and dosing temperatures dosed on 5% Ni(II)O/silica	81
Figure 3.9. Ratio of the yield of the g ₂ and g ₃ organic radical for different adsorbates and dosing	

temperatures on Ni(II)O/silica	82
Figure 3.10. Comparative yield of the EPFR intensity (g2 +g3) for Cu(II)O, Fe(III) ₂ O ₃ , and Ni(II)O for different adsorbates and temperatures.....	84
Figure 3.11. First-order decay profile of CT, HQ, PH and 2-MCP in 5% Fe(III) ₂ O ₃ /silica dosed at 230 °C and exposed to air at ambient condition.....	87
Figure 3.12. First-order decay profile of CT, HQ, PH and 2-MCP in 5% Ni(II)O/silica dosed at 230 °C and exposed to air at ambient condition.....	88
Figure 3.13. First-order decay profile of CT, HQ, PH and 2-MCP in 5% Zn(II)O/silica dosed at 230 °C and exposed to air at ambient condition.....	89
Figure 3.14. EPR spectrum of EPFRs from 2-MCP adsorbed on 5% Cu(II)O/ silica UFP with mice serum and BALF.....	100
Figure 3.15. Decay of EPFR concentration with the interaction of 2-MCP adsorbed on 5% Cu(II)O/silica UFP with serum and BALF from mice	101
Figure 3.16. Time dependence of the EPR spectra of 2-MCP adsorbed on 5% Cu(II)O/silica UFP with mice serum and BALF.....	102
Figure 3.17. EPR spectra of 2-MCP dosed on 5% Cu(II)O/silica UFP at 230 °C on the interaction of the EPFRs with hydrocortisone, epinephrine, retinoic acid and BEAS-2B cells.....	103
Figure 3.18. Time evolution of the DMPO-OH adduct signal in the presence of non-EPFR- and EPFR-containing particles	104
Figure 3.19. EPR spectra of DMPO-OH.....	105
Figure 3.20. EPR spectra of DMPO-O ₂ ⁻ in AcN.....	106
Figure 3.21. EPR Spectra of DMPO-OH in different solvent systems.....	107
Figure 3.22. The inhibition effect of SOD and CAT on EPFRs	108
Figure 4.1. Comparison of the half-lives of EPFRs over 5% Fe(III) ₂ O ₃ , Cu(II)O, Ni(II)O, and Zn(II)O on silica surface dosed at 230 °C and exposed in air at room temperature.	124
Figure 4.2. Relative persistency and stability of EPFRs on metal oxide surface	125
Figure 4.3. Dependence of the EPFR half-lives with the standard reduction potential.....	126
Figure 4.4: Structure of epinephrine, hydrocortisone, and retinoic acid	132
Figure 4.5. A hypothesis of a redox cycle of EPFRs originating from hydroquinone molecule	

adsorbed on Cu(II)O domain in biological system 134

Figure 4.6: A hypothesis of a red-ox cycle of EPFRs originating from 2-MCP molecule
adsorbed on Cu(II)O domain in biological system 135

LIST OF SCHEMES

Scheme 1.1. Gas phase formation of (chloro)phenoxy radical	16
Scheme 1.2. Gas phase formation of semiquinone radicals	16
Scheme 4.1. General mechanism of the formation of EPFRs on a metal oxide/silica surface from adsorption of chlorinated and hydroxylated benzenes	110
Scheme 4.2. Formation of phenoxy radical on Fe(III) ₂ O ₃ surface from H ₂ O elimination.....	113
Scheme 4.3. Formation of cyclopentadienyl radical from decomposition of surface-bound phenoxy radical through CO elimination on Fe(III) ₂ O ₃ surface.....	113
Scheme 4.4. Formation of <i>o</i> -semiquinone radical from adsorption of catechol on an Fe(III) ₂ O ₃ surface via double-H ₂ O elimination.....	114
Scheme 4.5. Formation of <i>p</i> -semiquinone radical from hydroquinone on an Ni(II)O/silica surface.....	115
Scheme 4.6. Formation of 2-chlorophenoxy radical and <i>o</i> -semiquinone radical from 2-monochlorophenol on an Fe(III) ₂ O ₃ /silica surface.....	116
Scheme 4.7. Formation of 2-chlorophenoxy radical and <i>o</i> -semiquinone radical from 1,2-dichlorobenzene on an Fe(III) ₂ O ₃ /silica surface.....	117
Scheme 4.8. Chlorination mechanism of benzene catalyzed by surface formation of hypochlorite species and subsequent formation of <i>o</i> -semiquinone radicals	120
Scheme 4.9. Formation of dibenzofuran from recombination of two keto forms of phenoxy radical.....	127
Scheme 4.10. Formation of dibenzo- <i>p</i> -dioxin from reaction of 2-monochlorophenol and chlorophenoxy radical.....	128
Scheme 4.11. Formation of 2,3'-dichloro-2'-hydroxydiphenyl ether	129
Scheme 4.12. Formation of (chloro)ferrocene from cyclopentadienyl radical	130
Scheme 4.13. Formation of 2,6-dichlorophenol by surface hypochlorite chlorination.....	131
Scheme 4.14. Formation of naphthalene and chloronaphthalene from recombination of cyclopentadienyl radical	131
Scheme 4.15. Formation of DMPO-OH adduct.....	136
Scheme 4.16. Conversion of molecular oxygen to hydroxyl radical catalyzed by EPFRs	138

Scheme 5.1. Formation of cyclopentadienyl radical from decomposition of surface-bound phenoxyl radical through CO elimination..... 153

Scheme 5.2. Surface decomposition of *o*-semiquinone radical to phenoxyl radical and subsequent conversion to cyclopentadienyl radical through CO elimination..... 155

LIST OF ABBREVIATIONS

1,2-DCBz	—	1,2-dichlorobenzene
2-MCP	—	2-monochlorophenol
BALF	—	bronchoalveolar lavage fluid
CAT	—	catalase
CT	—	catechol
DMPO	—	5,5-dimethyl-1-pyrroline-N-oxide
DPPH	—	2,2-di(4-tert-octylphenyl)-1-picrylhydrazyl
EPFRs	—	environmentally persistent free radicals
EPR	—	electron paramagnetic resonance
GC-MS	—	gas chromatography-mass spectrometry
HQ	—	hydroquinone
MCBz	—	monochlorobenzene
NO _x	—	nitrogen oxides
PH	—	phenol
PM	—	particulate matter
ROS	—	reactive oxygen species
SOD	—	superoxide dismutase
TEMPOL	—	4-hydroxyl-2,2,6,6-tetramethylpiperidine-1-oxyl
UFP	—	ultrafine particle
DMSO	—	dimethylsulfoxide
PCDD/F	—	polychlorinated dibenzodioxin and dibenzofuran
AcN	—	acetonitrile
DETAPAC	—	diethylenetriaminepentacetic acid
PBS	—	phosphate buffer saline
NADPH	—	nicotinamide adenine dinucleotide phosphate
DFM	—	deferoxamine mesylate
UV-Vis-NIR	—	ultraviolet-visible-near infrared
XANES	—	X-ray absorption near edge structures

ABSTRACT

The formation of environmentally persistent free radicals in combustion system was investigated from chemisorptions of chlorine- and hydroxy-substituted benzenes on transition metal oxide surface under post-combustion conditions. This manuscript reports the formation of EPFRs on silica particles containing 5% Fe(III)₂O₃, Ni(II)O, and Zn(II)O. The EPFRs are formed by the chemisorption of substituted aromatic molecular adsorbates on the metal cation center followed by electron transfer from the adsorbate to the metal ion at temperatures from 150 to 400 °C. Depending on the nature of the adsorbate and the temperature, two organic EPFRs were formed: a phenoxy-type radical, which has a lower *g*-value of 2.0023-2.0043, and a second semiquinone-type radical, with a *g*-value of 2.0044-2.0085. In general, the yield of EPFRs on Ni(II)O are similar to Cu(II)O and differs by ~10× compared to Fe(III)₂O₃. The persistency of the EPFRs is highly dependent on the metals they are associated with. The half-lives of EPFRs on iron and nickel ranged from 24 to 111 and 36 to 128 h, respectively, compared to the half-lives on copper of 27 to 74 min. However, the half-lives measured for the EPFRs on zinc are remarkably higher which range from 72 to 1752 h. The higher oxidation potential of the metals is believed to result in increased stabilization of the EPFR once formed, resulting in the longer half-lives.

The half-life of EPFRs on BALF was ~2× higher than in serum. On average, twice as much DMPO-OH spin adducts was formed in the presence of EPFR-containing particle compared to non-EPFR-containing particles at higher incubation time. A 10:1 ratio of OH radical concentration formed to the number of EPFR radicals indicates a cyclic process. The inability to identify superoxide radicals in aqueous media, while a DMPO-O₂⁻ spin adduct is detected in the

aprotic solvents, suggests a very quick transformation of the $O_2^{\cdot-}$ in aqueous environment, thus, the superoxide anions self-dismutates in protic environment and forms OH radicals.

CHAPTER I. INTRODUCTION

The research described herein is the detailed study on the formation of environmentally persistent free radicals (EPFRs) in combustion system. The objectives of the study are threefold.

First, is to investigate how EPFRs are formed on the surface of combustion-generated particulate matter containing different metal oxides supported on silica from aromatic adsorbates. In our study, we used surrogate metal oxides (copper, iron, nickel, and zinc) since they are the dominant transition metals in combustion-generated particulate matter. We investigated the interaction of the formation of EPFRs with various chlorinated and hydroxylated aromatic adsorbates (catechol, hydroquinone, phenol, 1,2-dichlorobenzene, monochlorobenzene, and 2-monochlorophenol) using electron paramagnetic resonance (EPR) spectroscopy. GC-MS analyses were performed from methanol and dichloromethane extracts of EPFR-particle systems to elucidate the structure and facilitate identification of EPFRs. The persistency of EPFR-particle system was performed by exposing them in air at ambient condition and determining their half-lives.

In the second objective, the EPFR-particle systems generated from 2-monochlorophenol adsorbate were studied to understand the interaction with biological systems. Exposure of these EPFR-particle system with bronchoalveolar lavage fluid (BALF) and serum extracted from mice were performed. Additionally, kinetic studies were performed to determine the half-lives of EPFR-particle system in these biological media. Moreover, studies were performed to determine whether EPFR-particle system can produce new organic radicals from biological components, such as epinephrine, retinoic acid, and hydrocortisone.

Thirdly, we investigated the propensity of EPFR-particle systems in generating reactive oxygen species (ROS), specifically, hydroxyl and superoxide radicals in phosphate buffered saline solution. We used spin trapping technique to elucidate and understand the mechanism of

EPFR-induced ROS formation.

1.1 Nature and Origin of Combustion Generated Particulate Matter and Free Radicals

One of the major sources of air pollution is basically derived from combustion and thermal processes (1). Over 70% and 90% of airborne fine and ultrafine particles comes from combustion-generated processes (2) like internal combustion engine, industrial heating, power generation, flaring of hydrocarbon in refineries, and biomass burning (3-12). Combustion-generated particles can be classified as primary and secondary. Primary combustion-generated particles come from direct emission from its source like vehicular emission, industrial processes, and biomass burning. On the other hand, secondary combustion-generated particles are formed when supersaturated vapors nucleate to form particles from gas phase compounds (1). These

The formation of particulate matter from combustion is explained by the zone theory of combustion which divides the combustion process (13, 14) into four zones: zone 1, the free flame (fuel zone), zone 2, the high temperature flame zone, zone 3, the postflame thermal zone, and zone 4, the gas quench cool zone and the surface catalysis zone. This combustion-generated particulate matter contains free radicals. Free radicals are not expected to be formed or stabilized on the surface in the first three zones since the temperature is very high. But in the post combustion zone which is the cool zone region whose temperature ranges from about 150 to 400 °C surface-mediated reactions can occur to form environmentally persistent free radicals (15-19).

In these combustion process, highly resonance-stabilized semiquinone and phenoxy radicals are formed and stabilized by their association with transition metals (16). Also, it has been shown that PCDD/Fs are formed at this zone (20, 21), since the temperature is low enough and the pollutants are not destroyed, which can desorb from the surface and released to the atmosphere and the formation of these products is known to be catalyzed by transition metals (22-24).

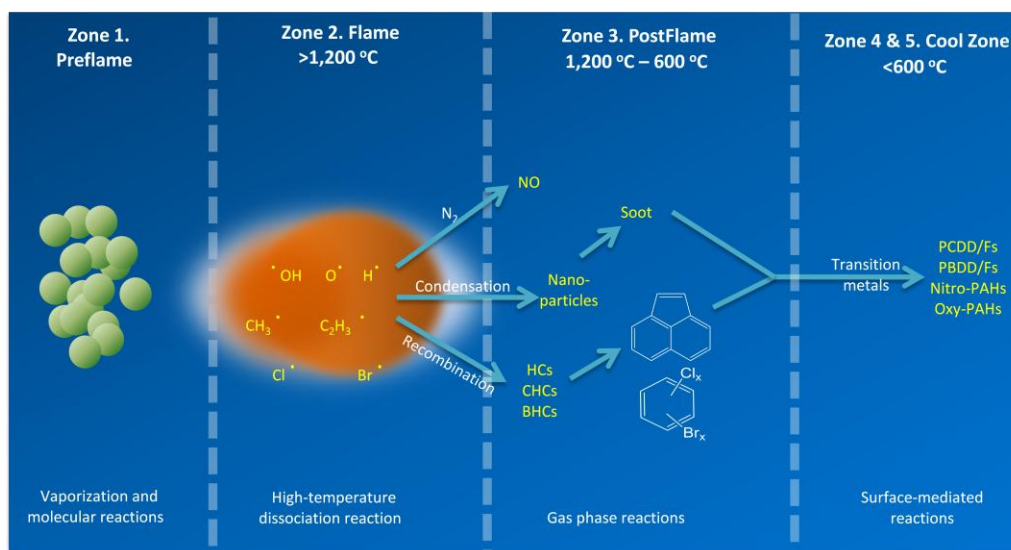


Figure 1.1. Zone theory of combustion in the formation of surface-mediated free radical

Free radicals are chemical species which contain unpaired electrons. Although, most free radicals are very reactive and can indefinitely exist in vacuum at low concentration, radicals in large quantities, can, under special conditions be stabilized. The use of vacuum, low temperature condition, spin-trapping techniques, and various spectroscopic methods render them to be observed and quantified. Some radicals are sufficiently stable at ambient condition and can become environmentally persistent free radicals (EPFRs) (15, 25, 26). For a radical to be persistent, it must first be stable, meaning, it will not decompose after it was formed at elevated temperature and it has a low reactivity with air at ambient condition, since most radicals decay upon contact with small molecules such as molecular oxygen (27). Free energy calculations suggest that reactions of phenoxyl and semiquinone radicals, which are abundant in combustion systems and thermal processes with molecular oxygen are highly endothermic process (16). Thus, the very large energy required for the reaction to proceed explains their unusual stability. Moreover, these radicals can be formed on the surface of particles containing transition metals where they are further stabilized (28). Because of this persistency, they can be transported over

long distances from their source where they can exert their adverse health effects (15, 25, 26).

Defining and characterizing particulate matter is no trivial task, but it is loosely defined as the material which contains extremely small particles and liquid droplets. Size analysis of particulate matter shows that it can be divided in three categories: coarse (accumulation mode), fine, and ultrafine particles, the latter two defined as the nucleation mode. The coarse particles are those with mean aerodynamic diameter larger than 2.5 μm . The fine particles called PM_{2.5}, are particles that have mean aerodynamic diameter of less than 2.5 μm , while the ultrafine particles are those which are smaller than 0.1 μm . The aerodynamic diameter of a particle is defined as the diameter of a sphere of unit density with the same terminal velocity as the particle in question (29).

Primary combustion-generated particles are still not well characterized because of their physical and chemical complexity, however, analysis of particulate matter showed that it primarily contains elemental carbon, carbonaceous material, organic carbon (*e.g.* soot), organic compounds, inorganic species like silica, alumina, nitrates, and sulfates; and trace and transition metals (2, 30, 31). Nitrates and sulfates can be found in particles larger than 0.2-0.3 μm in diameter (32). The composition of PM varies from site and location (6-11), for instance particulate matter in Europe are higher in sulfate and organic compounds due to the prevalent use of coal which contributes to submicron size particles (10, 33), thus, PM from industrial sites and urban sites would have a different chemical composition than those found in non-urban settings (34).

The coarse particle fraction is hazardous but it is not the primary concern because it can be filtered by the nose and engulfed by mucous (35). The principal concern for particulate matter is the fine and ultrafine fractions. Although, the mass of the ultrafine particles has a small contribution to the total mass of particulate matter, it dominates the number concentration (36-

38). In PM_{2.5}, it constitutes to only 20% by mass concentration but accounts 80% by number concentration (26, 39). Because of their size and number concentration, these give them higher surface area, where large amount of toxic pollutants such as organic compounds and transition metals to condense and adsorb on the surface (36). Moreover, the risks associated with the ultrafine PM and those in the nanoparticle range are, they cannot be captured efficiently by air pollution control devices due to their small size and are transported over long distances (40, 41).

Studies revealed that high concentration of atmospheric ultrafine particles have been ubiquitous and are observed in places ranging from the frigid arctic areas, the remote region, coastal marine location, and urban environment (42). In urban air, airborne fine and ultrafine particles make up most of particle pollutions. In one measurement alone in Pasadena, California, the ultrafine particle pollution was determined to be $1.3 \times 10^4 \pm 8.9 \times 10^3$ particles/cm³ which would deposit 10^{11} particles in a person's respiratory tract (32). Human exposure to particulate matter comes from vehicular emission, poor air quality especially in areas where coal combustion and biomass burning are the primary source of energy which pose a significant and chronic health risks (43). Indoor exposure from particulate mainly come from cigarette smoking, use of gas-oven cooking, wood-fired oven in developing countries (43). Although, the ultrafine particulate fraction is more hazardous it is not regulated by the current air quality standard as it regulates mass concentration in PM and not by number concentration.

1.2 Transition Metals in Combustion System

The formation and stability of environmentally persistent free radical and PCDD/Fs are enhanced in the presence of transition metals (16, 28, 44, 45). A number of studies have shown that the typical size of metals from combustion-derived processes is within the ultrafine size range (46). Generally, high temperature is required for ultrafine metallic aerosols to form (46) and such high temperature processes are caused by burning of wood and other biomass,

industrial activities, combustion-fired power generation, and other anthropogenic activities, although non-anthropogenic sources like natural fires and volcanic eruptions also contribute to the formation of ultrafine transition metals (47). Transition metals like copper and iron are abundant and other metals like nickel and zinc are present in combustion system and thermal processes (9, 48-51). It has been shown that these metals, specifically, copper and iron enhance the formation of PCDD/Fs (23, 45, 52-55). Analysis and characterization of the materials from combustion systems show that iron is the most abundant catalytic transition metals there is (56) and in municipal incineration system alone, iron (III) oxide and copper(II) oxide account up to 2.35% and 0.05% by mass, respectively (57). Characterization of ambient particulate matter reveals that it contains iron and other transition metal that originates from anthropogenic sources as well as from non-anthropogenic sources and are present in combustion-generated particle (58). Many transition metals in particulate matter are complexed with sulfate which resulted from atmospheric reactions of sulfur from burning coal (59). Urban particulate matter contains available transition metal (2, 31, 40, 48, 60) and iron dominates the metal concentration in ambient particle air pollution, which accounts about 4.6% by mass (60-64). It has been reported that the bulk iron content in urban atmosphere is about 5-15%, with iron oxides and hydroxides contributing to 10-70% of it (65). The concentrations of iron in fine particles and ultrafine particles are between 115-790 ng/m³ and 148.3 ng/m³, respectively, while zinc is 7.01-12.00 ng/m³ and 6.56 ng/m³, respectively (66). In PM₁₀ alone, iron reaches gram per m³ concentration compared to copper, nickel, and zinc which are present only in nanogram levels per m³ (66) and in fog water and urban aerosol its concentration is almost 1mM (67, 68).

Copper has a significant contribution in biomass and has been found to exist in cigarette smoke along with cooking using gas stove and contribute significantly to ultrafine transition metals in particulate matter in indoor environment (69). Copper, iron, nickel, and zinc are

present in high concentration in PM₁₀ and PM_{2.5} (9, 48, 49). They are also emitted from vehicular sources from fuel and lubrication oil which contains iron, zinc copper, and nickel in higher amounts than other metals (70). Analysis of ambient fine and ultrafine particulate matter correlates with the high presence of zinc and copper in high traffic areas.

Nickel in the environment are mainly derived from rock weathering, volcanic eruptions, and may also originate from combustion of oil additives and metallurgical processes (71, 72). However, unlike other metal it is present only in small concentration (*ppm* level) compared to other metals like copper, iron, and zinc. In fly ash, nickel is typically present at approximately 240 ppm and in ambient urban air it ranges from 5 to 50 ng/m³ (73). Analysis of PM determines that nickel exists as metallic, sulfidic, and oxidic form, with the latter as the most abundant, which accounts to approximately 50% (73).

These transition metals are highly oxidizing and are involved in various electron transfer reactions where they can mediate the formation of radicals from organic compounds (58). Moreover, it has been shown that iron and copper contribute to the formation of chlorinated aromatic compounds formation in fly ash (16, 28, 44, 45).

1.3 Sources, Origin, and Nature of Radical Precursors

The formation of EPFRs is dependent on two things: catalytically active transition metals and organic compounds (16, 28), which the latter are present and abundant in the environment and combustion systems. Chlorinated aromatic precursors such as 1,2-dichlorobenzene, monochlorobenzene, and 2-monochlorophenol are found in municipal and hazardous wastes (74, 75). On the other hand, hydroxylated aromatic precursors such as phenol and its hydroxylated derivatives, catechol, and hydroquinone are not only abundant in nature especially in biomass (76-82), but can also come from anthropogenic inputs from industrial processes (83). Studies have demonstrated that phenol, hydroquinone, and catechol are the most abundant organic

components in cigarettes (84-89), and they are naturally present in onions, apples, and other natural products. Catechol, hydroquinone, and phenol are also found in the environment as metabolites in urine from compounds containing phenol as the parent structure (90). Moreover, they may also come from environmental degradation of phenol through microbial hydroxylation (91). Industrial sources of hydroquinone mainly comes from its use as monomer inhibitor in polymer syntheses and in the manufacture of rubber (80). The use of catechol in photography and in the synthesis of pharmaceutical products also contributes to its environment presence (83).

Phenol can come from animal waste and as product of organic material decomposition (92, 93). Anthropogenic sources of phenol mainly originated from oil refineries as it is a major component of its waste and it is also a constituent of the waste from coal conversion process (94) and from pharmaceutical industries through leaching of industrial waste and from municipal waste treatment plant (94). Agricultural and domestic activities, specifically herbicide applications contribute to phenol sources in the environment as it is a metabolite of phenoxyherbicides (93, 95). Phenol is also present in vehicular exhaust and atmospheric reactions responsible for cloud formation (96). They are the basic structure of many compounds like the amino acid, tyrosine (97), the hormone, epinephrine, and the neurotransmitter, serotonin in humans, and plants are plentiful source of phenol as transformation products of phenolic substances (96).

The presence and abundance of phenol and its derivatives in nature, point to their importance as one of the basic structures for synthesizing various compounds essential for myriads of cellular and metabolic processes (98). However, while there are plentiful uses for them, their combustion products may lead to the formation of radicals (99) and other harmful organic pollutants, which are detrimental to our health and the environment. Catechol and

hydroquinone are known precursors of semiquinone radical and phenol of phenoxy radical in combustion systems (100).

The major anthropogenic sources of chlorinated aromatics in the environment come from thermal and combustion processes (101, 102), which include PCDD/Fs, biphenyls, and chlorobenzenes. It has been shown that municipal waste incineration system generates high amounts of chlorinated aromatics (74, 75). One anthropogenic source of chlorinated aromatics comes from electronic waste or e-waste (103, 104). Especially, now that there a higher demand for consumer electronics, and after the end of their usable life most of them end up being incinerated or simply open-burned, especially in developing countries where no stringent regulations and/or regulations at all exist and are sources of precursor for the formation of EPFRs and other hazardous substances.

Chlorinated phenols are synthetic molecules and there is no significant occurrence of it in nature (96). Environmental input of this contaminant like 2-monochlorophenol comes from leaching of wood treated with 2-monochlorophenol used in their preservation and can also come from the breakdown of agricultural pesticides (105). Research shows that chlorination of polyaromatic compounds either by combustion reaction or as metabolites of microbial degradation also contributes to 2-monochlorophenol sources in the environment (105). 2-Monochlorophenol is also formed from the chlorine-bleaching process in paper and pulp and has been found in water from the chlorination process of natural organic matter in source water (106).

The other precursors that were studied, monochlorobenzene and 1,2-dichlorobenzene can be found in the environment from anthropogenic sources as there are no known occurrence of them in nature. The industrial production of 1,2-dichlorobenzene relies on its use as solvents and chemical intermediates in many synthetic reactions and as starting materials and intermediates

in pharmaceuticals and agricultural products, especially herbicides (107). On its own, it is used as insecticide and fumigant for beetles, grubs and termites (108). Research shows that majority of 1,2-dichlorobenzene in the environment is released through the air from its industrial production. It is estimated that 5-10% of the 1,2-dichlorobenzene production in the US are lost and leak to the atmosphere (109, 110) and may sink in aquatic or terrestrial environments.

The sources of chlorinated compounds in the environment are mainly of anthropogenic origin but it has also been discovered that non-anthropogenic sources also contribute to chlorinated aromatics such as those from higher fungi which contribute significantly to biomass in terrestrial environment (93, 111-113). The risk involved in many of these chlorinated compounds is they can ascend the food chain like PCDD/Fs (114) and are precursors of EPFRs in combustion system. They are volatile and easily bioaccumulate in both terrestrial and aquatic system (114, 115). Moreover, some of them are suspected carcinogen and may interfere with reproductive functions (114-117).

1.4 Environmental and Health Implications

In various studies done by researchers investigating particulate matter, it has been shown that there is a high correlation between episodes of air pollution and diseases and even mortality and morbidity (118-125). While correlational studies abound implicating PM with a plethora of diseases, the components which are responsible for its toxicity and the observed adverse effects are still not well established (126, 127). But some recent findings are beginning to shed answers to this fundamental and important question. Many researchers who investigate the toxicology of PM acknowledge that both the chemical composition (128) and particle size (129) are important in understanding its toxicity. The serious health risk associated with particulate matter especially the ultrafine is that it has higher surface area and number concentration where large amount of toxic pollutants can condense on its surface (36). Their size enables them to penetrate deep into

the interstitial spaces of the lungs where it can be deposited to the alveoli, bronchi, and other parts of the lower respiratory system (130-132). It is thought, that their number concentration alone can lessen the effectivity of macrophages which are responsible for engulfing foreign bodies (133). At the cellular level, ultrafine particles can be deposited in mitochondria causing oxidative stress and ultimately some major structural damage (134). Other researchers even believe that the high risk associated with ultrafine particles is they can circulate systemically and circumvent the very tight blood-brain barrier (132, 135-137) and can ultimately be translocated to the brain (138) where it can exert deleterious effects, although, the studies have yet to find more conclusive findings (138). The ability of PM to induce damage, and, hence, its biological potency depends on the redox cycling ability of organic compounds adsorbed on its surface (134).

A number of toxicological studies have emerged demonstrating that PM can produce immunological (139-141) and inflammatory responses in cells. Particulate matter are highly deleterious to adults and children with pre-existing condition and those who are susceptible like the elderly, infants and the young ones, especially those with existing cardiovascular and respiratory problems (139-141). Ultrafine and fine particles have been shown to correlate with increase asthma incidence both in adults and children (142-145) due decline in lung functions, which are thought to arise from the inflammation of the respiratory tract (143, 144). Studies have shown that airborne and combustion-generated particles contains significant amount of EPFRs (15, 16, 25, 28, 146-148). Previous studies with PM_{2.5} collected from six cities across the United States revealed that sufficient amount of radical species that have chemical properties similar to semiquinone radicals are present in the PM_{2.5} fraction (15, 16, 25, 28, 146-152). Furthermore, they have shown that these particles can damage DNA (15, 19, 153, 154). Thus, EPFRs are posited to induce oxidative stress and diseases to exposed and susceptible individuals.

The adverse health effects due to exposure to high level of particulate matter both the coarse and fine fractions are believed to include cardiovascular (*130-132*), pulmonary and respiratory problems (*139*), myocardial infarction, and stroke (*127, 155-157*). Particulate matter is also implicated with the incidence of cancer (*158, 159*) especially lung cancer, although there are still no strong evidences supporting it in human and animal studies. Moreover, an increase in mortality and decrease in life expectancy with high emission of PM_{2.5} were observed (*118, 120-125, 160, 161*). Association between mortality of specific causes associated with PM_{2.5} is higher than PM₁₀ (*127, 162-164*), which shows that much of the risk in particulate matter is due to the fine and ultrafine fractions.

One consistent finding on the toxicological effect associated with particulate matter, is that its main toxic effect is primarily through the generation of reactive oxygen species (ROS) (*165-168*), which include hydrogen peroxide, superoxide, and hydroxyl radical, the latter which by far the most damaging of all the ROS (*169-172*). ROS are essential in the maintenance of cellular processes, such as energy source, chemical signal transduction, and immune function, but the overproduction of ROS can make the defense system to fail and cause structural damage to cellular components (*128*). Many of the acute and chronic diseases exerted by particulate matter is attributed to the generation of ROS (*173, 174*), which cause oxidative stress whereby the body over reacts to a stimulus and triggers a stress response (*35, 127, 150, 175-180*). Some of the metals in particulate matter can also catalyze ROS (*166*), specifically, iron, and is recognized they can produce proinflammatory effects (*126, 153, 181*).

One of the generally accepted models in the toxicity of particulate matter proposes semiquinone-type radical produces superoxide from molecular oxygen (*83, 149, 154, 178-180, 182-185*). The semiquinone radical undergoes dismutation (*186*) with biological reducing agents like NADPH to produce hydrogen peroxide, which can then react to form hydroxyl radical with

transition metals like iron via Fenton reaction which then damage DNA (83, 179, 182, 186). Since, the hydroxyl radical has a very short lifetime of 10^{-9} s it is thought they are generated in very close proximity to the DNA molecule to induce damage (186). The problem though is, exogenous iron in PM is inactive toward Fenton reaction since they exist as Fe^{3+} rather than Fe^{2+} and are immobilized in the particle (187). Moreover, it has been shown that endogenous Fe is bound in biological system and not readily available to participate in Fenton reaction. However, a recent study have discovered that superoxide does not only dismutate to hydrogen peroxide, but can also attack Fe-S cluster protein in biological system to liberate the bound iron making it available for the Fenton reaction (188). **Figure 1.2** depicts the schematic mechanism of the

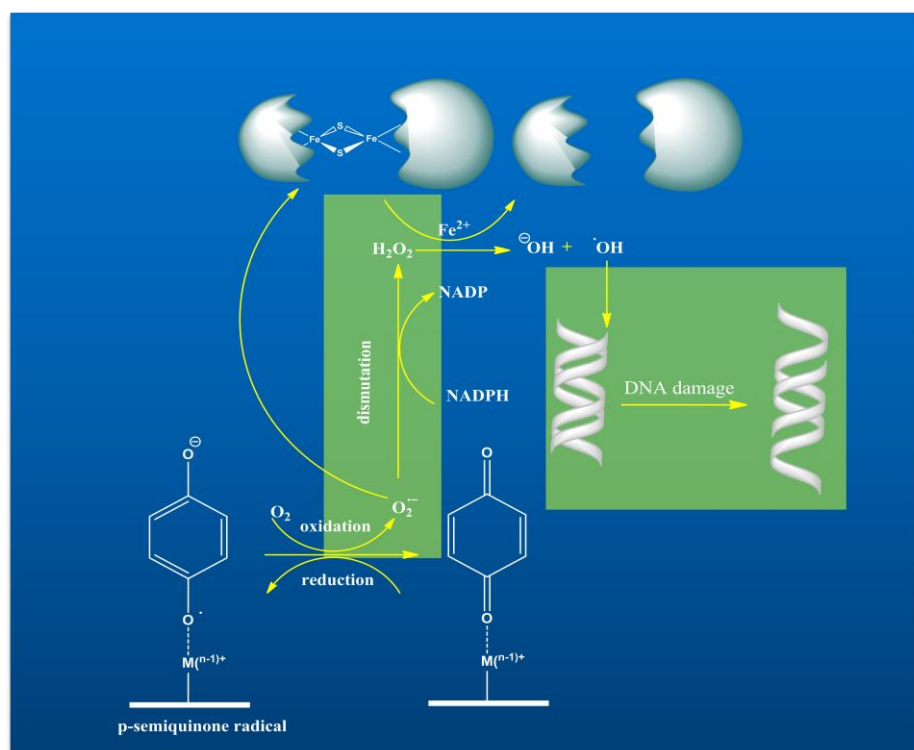


Figure 1.2. Generation of ROS catalyzed by surface-bound semiquinone radical

production of ROS from surface-stabilized semiquinone-type radical and consequent damage of the generated hydroxyl radical to the DNA molecule by a single strand nicking (186).

1.5 Nature, Structure, and Origin of Phenoxy and Semiquinone Radicals

It has been shown that semiquinone radical is commonly found in combustion sources (15, 193). Catechol and hydroquinone are known molecular precursors of semiquinone radical (100). They are isomeric to each other and the only difference in their structure lies in the position of the hydroxyl substituent which is in the *ortho* position for catechol and *para* position for hydroquinone to generate the corresponding *ortho*- and *para*-semiquinone radicals, respectively as shown in **Figure 1.3**. Phenol, monochlorobenzene, 1,2-dichlorobenzene, and 2-monochlorophenol are precursors of phenoxy and 2-chlorophenoxy radical whose structures are given in **Figure 1.4** and their corresponding radicals. The doubly substituted benzenes generate a

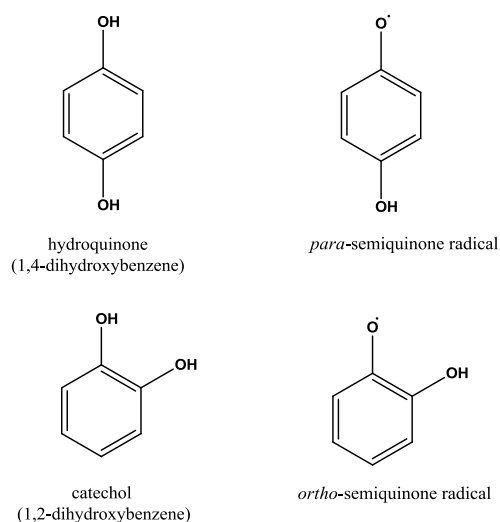


Figure 1.3. Structures of hydroquinone and catechol and their corresponding radicals

chlorophenoxy radical and also semiquinone radicals, while the monosubstituted ones generate a phenoxy radical.

1.5.1 Formation of Phenoxy Radical and Semiquinone Radical in the Gas Phase

Aside from semiquinone radical, phenoxy radical is also abundant in combustion system. In combustion system, the generation of phenoxy radical is similar to semiquinone radical where

a hydrogen atom on the hydroxyl substituent of phenol is abstracted by another hydrogen atom or by an alkyl radical to form the corresponding phenoxy radical. **Scheme 1.1** shows the general mechanism for the formation of phenoxy radical and the contributing resonance structure in the gas phase which is believed to be the major source of phenoxy radical in combustion system (194, 195). In combustion system semiquinone radical are generated both in the gas phase (196, 197) and in the surface of fly ash (28). Phenoxy and semiquinone radical are primary products of oxidation (198). The scheme given in **Scheme 1.2** depicts the general mechanism of the formation of *ortho*- and *para*-semiquinone radicals which are thought to arise from abstraction of a hydrogen atom or an alkyl radical which are abundant in combustion system. The formed semiquinone radical is resonance-stabilized due to the delocalization of the electron on the benzene ring and also on the oxygen atom.

1.5.2 Surface-mediated Formation of Semiquinone and Phenoxy Radical

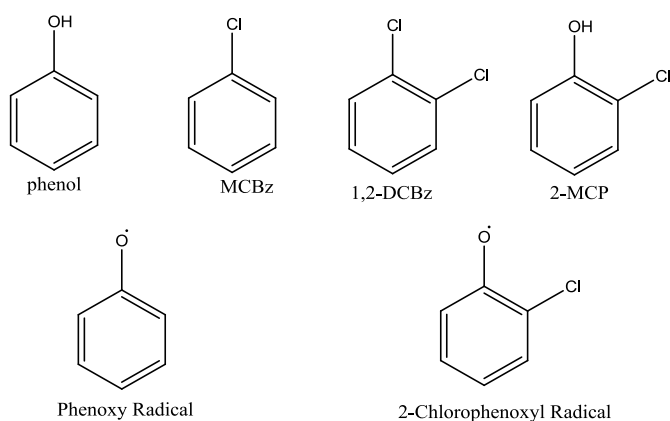
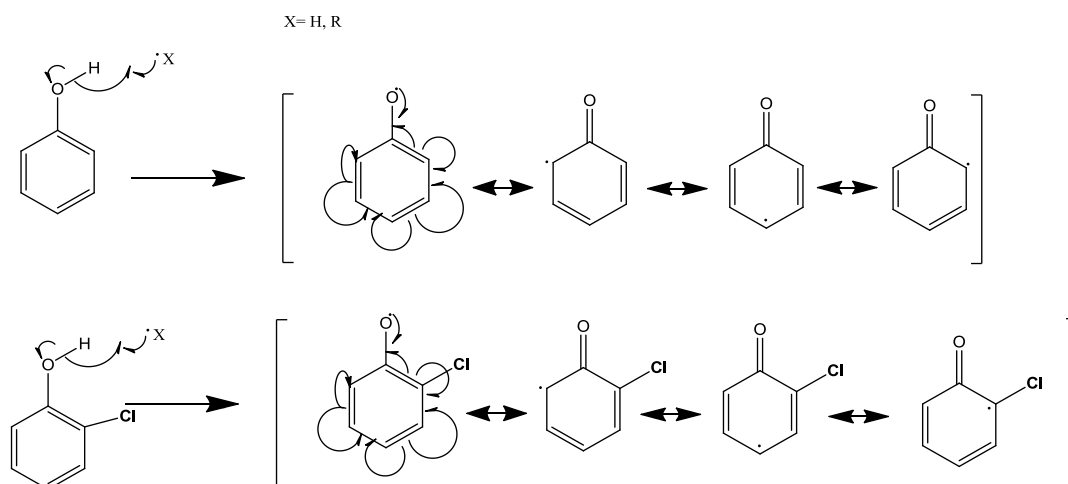


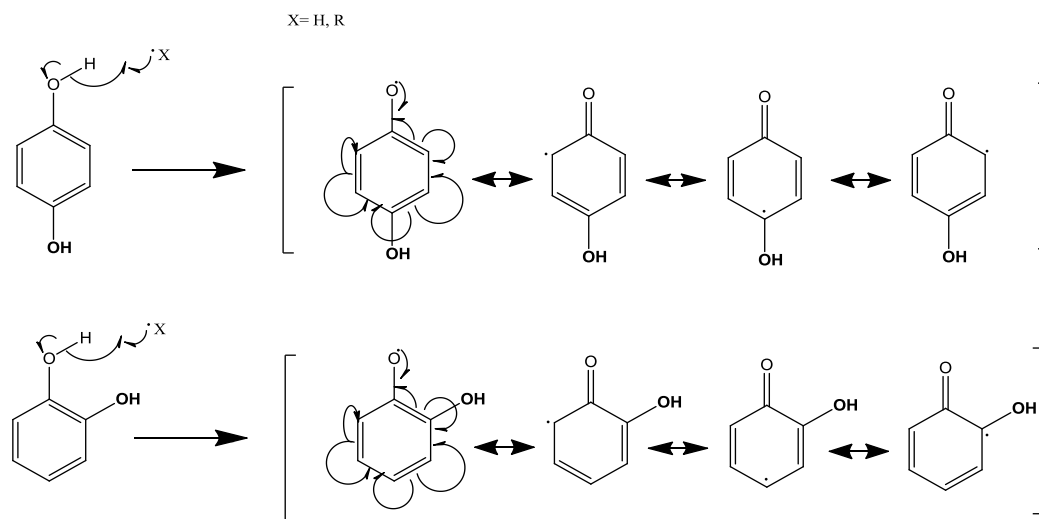
Figure 1.4. Molecular precursors of chloro(phenoxy) radicals and their structures

Semiquinone and phenoxy radicals are stable in the gas phase (15), but they can be further stabilized by association with transition metals in the surface of fly ash. Fly ashes in combustion system contain significant amount of transition metals which may be catalytically

active. The formation of phenoxyl radical on the surface is thought to proceed through the following steps.



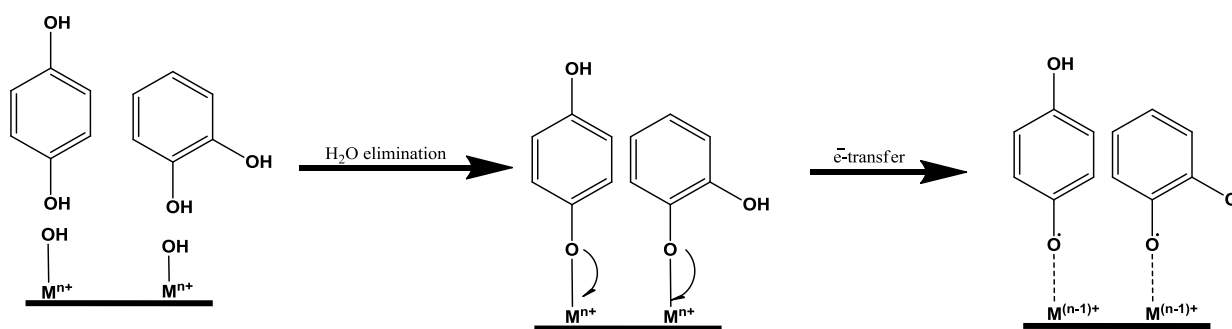
Scheme 1.1. Gas phase formation of (chloro)phenoxyl radical



Scheme 1.2. Gas phase formation of semiquinone radicals

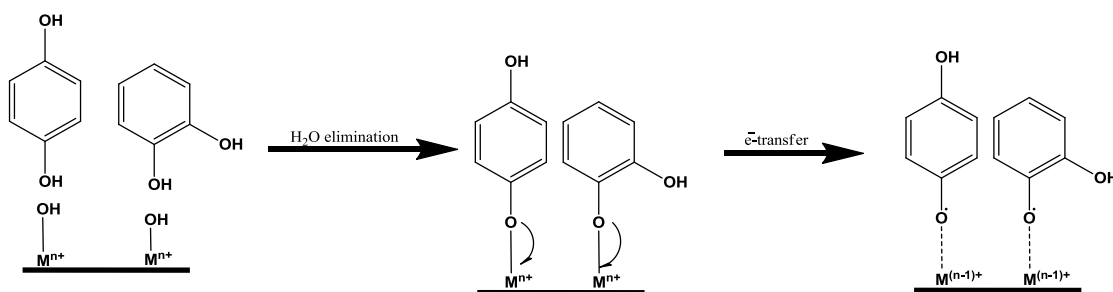
Initially, the chlorinated molecular precursor in the gas phase physisorbs on the surface through hydrogen bonding. Then it chemisorbs on the surface by elimination of hydrogen

chloride to form surface-associated species which reduces the metal by accepting an electron from the oxygen atom as depicted in **Scheme 1.3**.



Scheme 1.3. Formation of surface-associated (chloro)phenoxy radical via HCl elimination on metal oxide surface

On the other hand, the formation of surface-associated semiquinone radical also occurs by the same mechanism. The only difference is that the surface-associated species chemisorbs on the surface by water elimination to form the corresponding semiquinone radical and subsequent electron transfer from the oxygen to the metal which reduces the metal. The mechanism of this surface reaction in the formation of semiquinone from catechol and hydroquinone on the surface of transition metal is given in **Scheme 1.4**. Once the radical are formed on the surface, they can exist for a very long time depending on the metal it is bound to. They may also recombine via



Scheme 1.4. Formation of surface-bound semiquinone radical from hydroquinone and catechol on metal oxide surface

radical-radical or radical-molecule interactions where PCDD/Fs can be produced along with numerous toxic and hazardous substances.

1.6 Formation of PCDD and PCDF in Combustion System

Semiquinone and phenoxy radical can recombine to form myriads of toxic pollutants in combustion and thermal processes, but much of the attention is focused on the formation of polychlorinated dibenzo-*p*-dioxins and polychlorinated dibenzofurans (PCDD/Fs) in combustion systems. These compounds are the most toxic and potent species known to man. Moreover, they are known to be carcinogenic, mutagenic, teratogenic, and are endocrine disruptors (114, 116, 117).

One of the two hypotheses in PCDD/Fs formation is that chloroaromatic compounds are precursors for their formation. It is already an accepted theory, that metal can catalyze the formation of dioxins and furans by providing a surface where they can react (22). The formation of PCDD/Fs can also be through the interaction of a surface-bound organic radical and gas phase molecules. It is generally thought, that the main mechanism by which PCDDs are formed is through the Eley-Rideal mechanism, where a gas phase molecule and a surface-associated radical react to form PCDDs (199). On the other hand, the PCDFs are formed mainly through the Langmuir-Hinshelwood mechanism where two surface-bound phenoxy radicals react to form the corresponding PCDF (199).

1.7 Research Objectives

The objectives of the study are threefold. First, is to investigate how EPFRs are formed on the surface of surrogate combustion-generated particulate matter on metal oxide surface and to determine which metals are capable of forming and stabilizing EPFRs. Second, is to determine how EPFRs interact with compounds in biological media. Thirdly, to investigate how ROS are generated from EPFR-particle system *in vitro* and to elucidate the mechanism of their formation.

This study focuses on the role of transition metal specifically copper, iron, nickel, and zinc as they are the more dominant transition metals found in combustion generated- particulate matter (58) and how do they interact with organic precursor to form surface-associated EPFRs. Thus, we report our detailed laboratory study of the formation, structure, and persistence of EPFR formed from various molecular precursors on particle substrate of 5% Cu(II)O, Fe(III)₂O₃, Ni(II)O, and Zn(II)O on silica particles.

To carry-out the first objective synthetic particulate matter was synthesized from silica gel, which serves as a surrogate fly ash system by doping with different transition metals such as Cu, Fe, Ni, and Zn to form the corresponding metal oxide by impregnation method. We used 5% concentration of the metal oxide relative to silica for comparison with existing studies on PCDD/F formation. Based from previous study, copper is catalytically active in the formation and stabilization of free radicals (28) and iron was chosen, as it is the most dominant transition metal in combustion sources (56, 60-62, 65), and much research has focused on its role in ROS production, oxidative stress, and the toxicity of fine and ultrafine particles. Nickel and zinc were chosen as they are present in significant concentration in combustion system and particulate matter (9, 48). Moreover, many industrial applications rely heavily on the use of zinc, and, therefore, are of high environmental and health concerns. These transition metals are known to be very oxidizing and can catalyze the formation of radicals from organic compounds (58).

In the adsorption study, the particulate matter was dosed with different chlorinated and hydroxylated benzenes in a specially-designed vacuum exposure chamber from 150-400 °C, which is the temperature range for the post-combustion zone where surface-mediated reactions occur. The chlorinated aromatic adsorbates used as EPFRs precursor were 1,2-dichlorobenzene, monochlorobenzene, and 2-monochlorophenol, which are present in combustion sources containing chlorine, such as hazardous waste and municipal waste incinerators (200-202). The

hydroxylated aromatic adsorbates such as catechol, hydroquinone, and phenol were chosen as they are dominant component of combustion system especially in biomass (76-81). The formation of EPFR was analyzed by using EPR spectroscopy. In addition, the dosed particulate matter was extracted with dichloromethane and methanol, and the extracts were analyzed by GC-MS to determine the molecular products, which result from EPFR recombination. Kinetic studies were done to determine the persistency and stability of the EPFRs by exposing the EPFRs formed over Fe(III)₂O₃, Ni(II)O, and Zn(II)O at 230 °C to air at ambient condition and their EPFR intensities were measured as a function of time.

In the second objective, the EPFR-containing particles were studied by determining its interaction with some biological system like bronchoalveolar lavage fluid (BALF) and serum extracted from mice. Other compounds in biological system were studied such as adrenaline, retinoic acid, and hydrocortisone. Kinetics studies were done to determine half-lives of EPFR dosed with 2-monochlorophenol on both BALF and serum from mice.

In the last objective, *in vitro* studies were performed with both non-EPFR- and EPFR-containing particles to determine their ability to catalyze smaller and more damaging radical such as superoxide and hydroxyl radicals, and determine the mechanisms governing their formation to help us better understand their toxicology. Spin trapping studies were performed using 5,5-dimethyl-pyrroline-N-oxide (DMPO) as the suitable spin trap and were conducted on different solvent systems (protic and aprotic solvents). *In vivo* studies were also conducted to determine the effect of EPFRs on biological system and samples were sent to our collaborators in LSU-HSC, both in Shreveport and New Orleans.

1.8 Summary of Key Findings on Particulate Matter in the Literature

Table 1.1 summarizes the major findings on the nature, origin, composition, and environmental and health impacts of particulate matter.

Table 1.1. Summary of the key findings on particulate matter, its nature, origin, composition, and environmental and health implications

Author (Year)	Title	Key Findings	Ref.
Balakrishna, S., Lomnicki, S., McAvey, K. M., Cole, R. B., Dellinger, B. and Cormier, S. (2009)	Environmentally persistent free radicals amplify ultrafine particle mediated cellular oxidative stress and cytotoxicity	Significant increase in ROS production upon exposure of BEAS-2B cell with combustion generated particle containing MCP230. Cell death increases due to low cellular antioxidant activity. MCP230 is cytotoxic due to its ability to enhance cellular oxidative stress and reduction in antioxidant ability of epithelial cells.	(189)
Nganai, S., Lomnicki, S., and Dellinger, B. (2009)	Ferric Oxide Mediated Formation of PCDD/Fs from 2-Monochlorophenol	Maximum yield of PCDD/F occurs at higher temperature for Fe ₂ O ₃ compared to CuO. Fe metal contributes between 5-125x PCDD/F in full scale combustor compared to CuO	(55)
Lomnicki, S., Truong, H., Vejerano, E. and Dellinger, B. (2008)	Copper oxide-based model of persistent free radical formation on combustion-derived particulate matter	Particles containing environmentally persistent free radical are formed and stabilized on the surface of CuO surfaces. These radical are identified as semiquinone- and phenoxyl-type radicals based on their g-values	(28)
Valavanidis, A., Fiotakis, K., Bakeas, E., and Vlahogianni, T. (2005)	Electron paramagnetic resonance study of the generation of reactive oxygen species catalysed by transition metals and quinoid redox cycling by inhalable ambient particulate matter	PM contains active transition metals, quinoids and PAHs and induces the production of ROS. The water-soluble fraction of PM induces DNA damage from hydroxyl radical generated by transition metal by a Fenton-type reaction involving quinoids.	(190)
Cormier, S. A., Lomnicki, S., Backes, W., and Dellinger, B. (2006)	Origin and health impacts of emissions of toxic by-products and fine particles from combustion and thermal treatment of hazardous wastes and materials	Summary on the effects of ultrafine particles and its health impact on the induction of cardiovascular disease and cancer. Discusses the sources of pollutants and its association with combustion-generated particles.	(191)

Table Cont'd

Author (Year)	Title	Key Findings	Ref.
Maskos, Z, Khachatryan, L., and Dellinger, B. (2005)	Precursors of radicals in tobacco smoke and the role of particulate matter in forming and stabilizing radicals	Suggested that some constituents in tobacco forms free radicals or constituents in TPM from tobacco stabilizes radical or forms radical	(192)
Ning, L., Sioutas, C., Cho, A., Schmitz, D., Misra, C., Sempf, J., Meiying, W., Oberley, T., Froines, J., and Nel, A. (2003)	Ultrafine Particulate Pollutants Induce Oxidative Stress and Mitochondrial Damage	The biological potency of UFP is determined by the presence of redox cycling adsorbed organic compounds on the particle	(134)
Shi, T., Knaapen, A. M., Begerow, J. B. W., Borm, P. J. A., and Schins, R. P. F. (2003)	Temporal variation of hydroxyl radical generation and 8-hydroxy-2'-deoxyguanosine formation by coarse and fine particulate matter	Hydroxyl radical is generated by both coarse and fine PM which consequently induce formation of 8-OgdG. Demonstrated the variability of OH production based on the fractions of PM and the sampling time.	(18)
Soares, S. R. C. Bueno-Guimaraes, H. M., Ferreira, C. M., Rivero, D. H. R. F., De Castro, I., Garcia, M. L. B., and Saldiva, P. H. N. (2003)	Urban air pollution induces micronuclei in peripheral erythrocytes of mice in vivo	Exposure of rodents with urban air pollution increase micronuclei frequency which indicates that somatic mutation in mice occurs.	
Pope III, C.A., Burnett, R.T., Thun, M.J., Calle, E.E., Krewski, D., Ito, K., and Thurston, G.D. (2002)	Lung Cancer, Cardiopulmonary Mortality, and Long-term Exposure to Fine Particulate Air Pollution	Association between fine particles and sulfur-oxide containing pollutants with incidence of lung cancer and cardiopulmonary mortality suggesting that combustion-related fine particulate air pollution as a risk factor for the development of these diseases	(158)

Table Cont'd

Author(Year)	Title	Key Findings	Ref.
Saldiva, P.H.N., Clarke, R.W., Coull, B.A., Stearns, R.C., Lawrence, J., Murthy, G.G.K. Diaz, E.; Koutrakis, P., Suh, H., Tsuda, A., Godleski, J.J. (2002)	Lung inflammation induced by concentrated ambient air particles is related to particle composition	Significant inflammatory reaction in rodents is induced by concentrated particulate matter from Boston	(181)
Dellinger, B. Pryor, W. A. Cueto, R., Squadrito, G. L., Hegde, V., and Deutsch, W. A. (2001)	Role of Free Radicals in the Toxicity of Airborne Fine Particulate Matter	Large quantities of radicals similar to that of semiquinone were present in PM2.5 as determined by EPR. Formation of ROS causes DNA damage from aqueous extract of PM2.5	(19)
Peters, A., Dockery, D. W., Muller, J. E., and Mittleman, M. A. (2001)	Increased particulate air pollution and the triggering of myocardial infarction	Increased in FP concentration correlated with increase incidence of myocardial infarction after a 2-hour period. Symptoms appear after 24 hours indicating delayed response.	(127)
Ghio, A. J., Stonehuerner, J., Dailey, L. A., and Carter, J. D. (1999)	Metals associated with both the water-soluble and insoluble fractions of an ambient air pollution particle catalyze an oxidative stress	PM suspensions and particle-free filtrates induce DNA strand breaks in human alveolar epithelial cells by the generation of hydroxyl radical from metal-dependent reaction in the presence of H ₂ O ₂ .	(58)

1.9 References

1. Sarofim, A.F.; Lightly, J.S.; Edding, E.G. Fine particles: Health effects, characterization, mechanisms of formation and modelling. *Fuel Chemistry Division Preprints* **2002**, *47*, 2, 618-621.
2. Cass, G.R.; Hughes, L.A.; Bhave, P.; Kleeman, M.J.; Allen, J.O.; Salmon, L.G. The chemical composition of atmospheric ultrafine particles. *Philos. Trans. R. Soc. London, Ser. A* **2000**, *358*, 1775, 2581-2592.
3. Chen, Y.Z.; Shah, N.; Huggins, F.E.; Huffman, G.P. Comparison of micron-sized and ultrafine particulate matter from pulverized coal combustion. *Abstr. Pap. Am. Chem. Soc.* **2005**, *229*, U866-U866.
4. Chen, Y.; Shah, N.; Huggins, F.E.; Huffman, G.P.; Dozier, A. Characterization of ultrafine coal fly ash particles by energy-filtered TEM. *J. Microsc-Oxford* **2005**, *217*, 3, 225-234.
5. Huffman, G.P.; Huggins, F.E.; Shah, N.; Huggins, R.; Linak, W.P.; Miller, C.A.; Pugmire, R.J.; Meuzelaar, H.L.C.; Sehra, M.S.; Manivannan, A. Characterization of fine particulate matter produced by combustion of residual fuel oil. *J. Air Waste Manage. Assoc.* **2000**, *50*, 7, 1106-1114.
6. Chen, Y.; Shah, N.; Huggins, F.E.; Huffmann, G.P., *Investigation of the microcharacteristics of PM2.5 in residual oil fly ash by analytical transmission electron microscopy*. Vol. 38. **2004**, Washington, DC, ETATS-UNIS: American Chemical Society8.
7. Kleeman, M.J.; Schauer, J.J.; Cass, G.R. Size and composition distribution of fine particulate matter emitted from motor vehicles. *Environ. Sci. Technol.* **2000**, *34*, 7, 1132-1142.
8. Linak, W.P.; Miller, C.A.; Wendt, J.O.L. Comparison of particle size distributions and elemental partitioning from the combustion of pulverized coal and residual fuel oil. *J. Air Waste Manage. Assoc.* **2000**, *50*, 8, 1532-1544.
9. Okeson, C.D.; Riley, M.R.; Fernandez, A.; Wendt, J.O.L. Impact of the composition of combustion generated fine particles on epithelial cell toxicity: Influences of metals on metabolism. *Chemosphere* **2003**, *51*, 10, 1121-1128.
10. Kleeman, M.J.; Schauer, J.J.; Cass, G.R. Size and composition distribution of fine particulate matter emitted from wood burning, meat charbroiling, and cigarettes. *Environ. Sci. Technol.* **1999**, *33*, 20, 3516-3523.

11. Kleeman, M.J.; Cass, G.R. Effect of emissions control strategies on the size and composition distribution of urban particulate air pollution. *Environ. Sci. Technol.* **1999**, *33*, 1, 177-189.
12. Chen, Y.Z.; Shah, N.; Huggins, F.E.; Huffman, G.P. Transmission electron microscopy investigation of ultrafine coal fly ash particles. *Environ. Sci. Technol.* **2005**, *39*, 4, 1144-1151.
13. Taylor D, D.; Flagan R, C., *Aerosols from a laboratory pulverized coal combustor*, in *Atmospheric aerosol*. 1981, AMERICAN CHEMICAL SOCIETY: WASHINGTON, D. C. p. 157-172.
14. Dellinger, B.; Taylor, P.H. Chemical aspects of combustion of hazardous wastes. *Cent. Eur. J. Public Health* **1998**, *6*, 79-87.
15. Dellinger, B.; Pryor, W.A.; Cueto, R.; Squadrito, G.L.; Deutsch, W.A. Combustion-generated radicals and their role in the toxicity of fine particulate. *Organohalogen Compd.* **2000**, *46*, 302-305.
16. Dellinger, B.; Lomnicki, S.; Khachatryan, L.; Maskos, Z.; Hall, R.W.; Adoukpe, J.; McFerrin, C.; Truong, H. Formation and stabilization of persistent free radicals. *Proc. Combust. Inst.* **2007**, *31*, 1, 521-528.
17. Li, N.; Sioutas, C.; Cho, A.; Schmitz, D.; Misra, C.; Sempf, J.; Wang, M.; Oberley, T.; Froines, J.; Nel, A. Ultrafine particulate pollutants induce oxidative stress and mitochondrial damage. *Environ. Health Perspect.* **2003**, *111*, 4, 455-60.
18. Shi, T.; Knaapen, A.M.; Begerow, J.; Birmili, W.; Borm, P.J.A.; Schins, R.P.F. Temporal variation of hydroxyl radical generation and 8-hydroxy-2'-deoxyguanosine formation by coarse and fine particulate matter. *Occup. Environ. Med.* **2003**, *60*, 5, 315-321.
19. Dellinger, B.; Pryor, W.A.; Cueto, R.; Squadrito, G.L.; Hegde, V.; Deutsch, W.A. Role of free radicals in the toxicity of airborne fine particulate matter. *Chem. Res. Toxicol.* **2001**, *14*, 10, 1371-1377.
20. Altwicker, E.R. Some laboratory experimental designs for obtaining dynamic property data on dioxins. *Sci. Total Environ.* **1991**, *104*, 1-2, 47-72.
21. Gullett, B.K.; Lemieux, P.M.; Dunn, J.E. Role of combustion and sorbent parameters in prevention of polychlorinated dibenzo-p-dioxin and polychlorinated dibenzofuran formation during waste combustion. *Environ. Sci. Technol.* **1994**, *28*, 1, 107-18.

22. Olie, K.; Addink, R.; Schoonenboom, M. Metals as catalysts during the formation and decomposition of chlorinated dioxins and furans in incineration processes. *J. Air Waste Manage. Assoc.* **1998**, *48*, 2, 101-105.
23. Addink, R.; Olie, K. Mechanisms of formation and destruction of polychlorinated dibenzo-p-dioxins and dibenzofurans in heterogeneous systems. *Environ. Sci. Technol.* **1995**, *29*, 6, 1425-1435.
24. Gullett, B.K.; Touati, A.; Lee, C.W. Formation of chlorinated dioxins and furans in a hazardous-waste-firing industrial boiler. *Environ. Sci. Technol.* **2000**, *34*, 11, 2069-2074.
25. Lomnicki, S.; Dellinger, B. A detailed mechanism of the surface-mediated formation of PCDD/F from the oxidation of 2-chlorophenol on a CuO/silica surface. *J. Phys. Chem. A* **2003**, *107*, 22, 4387-4395.
26. Rodriguez, S.; Van, D.R.; Putaud, J.P.; Dell'Acqua, A.; Pey, J.; Querol, X.; Alastuey, A.; Chenery, S.; Ho, K.F.; Harrison, R.; Tardivo, R.; Scarnato, B.; Gemelli, V. A study on the relationship between mass concentrations, chemistry and number size distribution of urban fine aerosols in Milan, Barcelona and London. *Atmos. Chem. Phys.* **2007**, *7*, 9, 2217-2232.
27. Barckholtz, C.; Fadden, M.J.; Hadad, C.M. Computational study of the mechanisms for the reaction of $\text{O}_2(3\text{f}\text{g})$ with aromatic radicals. *J. Phys. Chem. A* **1999**, *103*, 40, 8108-8117.
28. Lomnicki, S.; Truong, H.; Vejerano, E.; Dellinger, B. Copper oxide-based model of persistent free radical formation on combustion-derived particulate matter. *Environ. Sci. Technol.* **2008**, *42*, 13, 4982-4988.
29. Hinds, W.C., *Aerosol technology: Properties, behavior, and measurement of airborne particles*. **1999**, New York: John Wiley and Sons.
30. Allouis, C.; Beretta, F.; D'Alessio, A. Sizing soot and micron carbonaceous particle in spray flames based on time resolved LII. *Exp. Therm Fluid Sci.* **2003**, *27*, 4, 455-463.
31. Lighty, J.S.; Veranth, J.M.; Sarofim, A.F. Combustion aerosols: Factors governing their size and composition and implications to human health. *J. Air Waste Manage. Assoc.* **2000**, *50*, 9, 1565-1618.
32. Hughes, L.S.; Cass, G.R.; Gone, J.; Ames, M.; Olmez, I. Physical and chemical characterization of atmospheric ultrafine particles in the Los Angeles area. *Environ. Sci. Technol.* **1998**, *32*, 9, 1153-1161.

33. Kleeman, M.J.; Hughes, L.S.; Allen, J.O.; Cass, G.R. Source contributions to the size and composition distribution of atmospheric particles: Southern California in September 1996. *Environ. Sci. Technol.* **1999**, *33*, 23, 4331-4341.
34. Noll, K.E.; Pontius, A.; Frey, R.; Gould, M. Comparison of atmospheric coarse particles at an urban and non-urban site. *Atmos. Environ.* **1985**, *19*, 11, 1931-1943.
35. Oberdorster, G.; Celein, R.M.; Ferin, J.; Weiss, B. Association of particulate air pollution and acute mortality: Involvement of ultrafine particles? *Inhal. Toxicol.* **1995**, *7*, 1, 111-124.
36. Oberdorster, G. Pulmonary effects of inhaled ultrafine particles. *Int. Arch. Occup. Environ. Health* **2001**, *74*, 1, 1-8.
37. Peters, A.; Wichmann, H.; Tuch, T.; Heinrich, J.; Heyder, J. Respiratory effects are associated with the number of ultrafine particles. *Am. J. Respir. Crit. Care Med.* **1997**, *155*, 4, 1376-1383.
38. Seaton, A.; Godden, D.; MacNee, W.; Donaldson, K. Particulate air pollution and acute health effects. *The Lancet* **1995**, *345*, 8943, 176-178.
39. Woo, K.S.; Chen, D.R.; Pui, D.Y.H.; McMurry, P.H. Measurement of Atlanta aerosol size distributions: Observations of ultrafine particle events. *Aerosol Sci. Technol.* **2001**, *34*, 1, 75-87.
40. D'Alesio, A.; D'Anna, A.; Gambi, G.; Minutolo, P.; Sgro, L.A.; Violi, A. Combustion generated nanoparticles. *Chim. Ind.* **1999**, *81*, 1001-1006.
41. Pekkanen, J.; Peters, A.; Hoek, G.; Tiittanen, P.; Brunekreef, B.; de Hartog, J.; Heinrich, J.; Ibald-Mulli, A.; Kreyling, W.G.; Lanki, T.; Timonen, K.L.; Vanninen, E. Particulate air pollution and risk of ST-segment depression during repeated submaximal exercise tests among subjects with coronary heart disease: The exposure and risk assessment for fine and ultrafine particles in ambient air (ultra) study. *Circulation* **2002**, *106*, 8, 933-938.
42. Kulmala, M.; Vehkamäki, H.; Petaja, T.; Dal, M.M.; Lauri, A.; Kerminen, V.M.; Birmili, W.; McMurry, P.H. Formation and growth rates of ultrafine atmospheric particles: A review of observations. *J. Aerosol Sci.* **2004**, *35*, 2, 143-176.
43. See, S.W.; Balasubramanian, R. Chemical characteristics of fine particles emitted from different gas cooking methods. *Atmos. Environ.* **2008**, *42*, 39, 8852-8862.

44. Kobylecki, R.P.; Ohira, K.; Ito, I.; Fujiwara, N.; Horio, M. Dioxin and fly ash free incineration by ash pelletization and reburning. *Environ. Sci. Technol.* **2001**, *35*, 21, 4313-4319.
45. Stieglitz, L.; Zwick, G.; Beck, J.; Roth, W.; Vogg, H. On the de-novo synthesis of PCDD/PCDF on fly-ash of municipal waste incinerators. *Chemosphere* **1989**, *18*, 1-6, 1219-1226.
46. Flagan, R.C. *Droplet effects in combustion*. 1976: Hemisphere Publ. Corp.
47. Andre, E.; Stoeger, T.; Takenaka, S.; Bahnweg, M.; Ritter, B.; Karg, E.; Lentner, B.; Reinhard, C.; Schulz, H.; Wjst, M. Inhalation of ultrafine carbon particles triggers biphasic pro-inflammatory response in the mouse lung. *Eur. Respir. J.* **2006**, *28*, 2, 275-285.
48. Allouis, C.; Beretta, F.; D'Alessio, A. Structure of inorganic and carbonaceous particles emitted from heavy oil combustion. *Chemosphere* **2003**, *51*, 10, 1091-1096.
49. Nielsen, M.T.; Livbjerg, H.; Fogh, C.L.; Jensen, J.N.; Simonsen, P.; Lund, C.; Poulsen, K.; Sander, B. Formation and emission of fine particles from two coal-fires power plants. *Combust. Sci. Technol.* **2002**, *174*, 2, 79 - 113.
50. Catallo, W.J.; Shupe, T.F.; Gambrell, R.P. Hydrothermal treatment of CCA- and penta-treated wood. *Wood Fiber Sci.* **2004**, *36*, 2, 152-160.
51. Wasson, S.J.; Linak, W.P.; Gullett, B.K.; King, C.J.; Touati, A.; Huggins, F.E.; Chen, Y.; Shah, N.; Huffman, G.P. Emissions of chromium, copper, arsenic, and PCDDs/Fs from open burning of CCA-treated wood. *Environ. Sci. Technol.* **2005**, *39*, 22, 8865-8876.
52. Tuppurainen, K.A.; Ruokojaervi, P.H.; Asikainen, A.H.; Aatamila, M.; Ruuskanen, J. Chlorophenols as precursors of PCDD/Fs in incineration processes: Correlations, PLS modeling, and reaction mechanisms. *Environ. Sci. Technol.* **2000**, *34*, 23, 4958-4962.
53. Gullett, B.K.; Bruce, K.R.; Beach, L.O. The effect of metal-catalysts on the formation of polychlorinated dibenzo-para-dioxin and polychlorinated dibenzofuran precursors. *Chemosphere* **1990**, *20*, 10-12, 1945-1952.
54. Addink, R.; Altwicker, E.R. Formation of polychlorinated dibenzo-p-dioxins and dibenzofurans on secondary combustor/boiler ash from a rotary kiln burning hazardous waste. *J. Hazard. Mater.* **2004**, *114*, 1-3, 53-58.

55. Nganai, S.; Lomnicki, S.; Dellinger, B. Ferric oxide mediated formation of PCDD/Fs from 2-monochlorophenol. *Environ. Sci. Technol.* **2009**, *43*, 2, 368-373.
56. Dreher, K.L.; Jaskot, R.H.; Lehmann, J.R.; Richards, J.H.; McGee, J.K.; Ghio, A.J.; Costa, D.L. Soluble transition metals mediate residual oil fly ash induced acute lung injury. *J. Toxicol. Environ. Health* **1997**, *50*, 3, 285-305.
57. Karamanov, A.; Pelino, M.; Salvo, M.; Metekovits, I. Sintered glass-ceramics from incinerator fly ashes. Part II. The influence of the particle size and heat-treatment on the properties. *J. Eur. Ceram. Soc.* **2003**, *23*, 10, 1609-1615.
58. Ghio, A.J.; Stonehuerner, J.; Dailey, L.A.; Carter, J.D. Metals associated with both the water-soluble and insoluble fractions of an ambient air pollution particle catalyze an oxidative stress. *Inhal. Toxicol.* **1999**, *11*, 1, 37-49.
59. Miceli, J.; Stuehr, J. Ligand penetration rates into metal ion coordination spheres. Aluminum(III), gallium(III), and indium(III) sulfates. *J. Amer. Chem. Soc.* **1968**, *90*, 25, 6967-72.
60. Smith, K.R.; Aust, A.E. Mobilization of iron from urban particulates leads to generation of reactive oxygen species in vitro and induction of ferritin synthesis in human lung epithelial cells. *Chem. Res. Toxicol.* **1997**, *10*, 7, 828-834.
61. Demuyneck, M.; Rahn, K.A.; Janssens, M.; Dams, R. Chemical analysis of airborne particulate matter during a period of unusually high pollution. *Atmos. Environ.* **1976**, *10*, 1, 21-6.
62. Dodd, J.A.; Ondov, J.M.; Tuncel, G.; Dzubay, T.G.; Stevens, R.K. Multimodal size spectra of submicrometer particles bearing various elements in rural air. *Environ. Sci. Technol.* **1991**, *25*, 5, 890-903.
63. Mamane, Y. Estimate of municipal refuse incinerator contribution to Philadelphia aerosol - I. Source analysis. *Atmos. Environ.* **1988**, *22*, 11, 2411-18.
64. Vossler, T.L.; Lewis, C.W.; Stevens, R.K.; Dzubay, T.G.; Gordon, G.E.; Tuncel, S.G.; Russwurm, G.M.; Keeler, G.J. Composition and origin of summertime air pollutants at Deep Creek Lake, Maryland. *Atmos. Environ.* **1989**, *23*, 7, 1535-47.
65. Dedik, A.N.; Hoffmann, P.; Ensling, J. Chemical characterization of iron in atmospheric aerosols. *Atmos. Environ. Part A* **1992**, *26*, 14, 2545-2548.

66. Hughes, L.S.; Allen, J.O.; Kleeman, M.J.; Johnson, R.J.; Cass, G.R.; Gross, D.S.; Gard, E.E.; Galli, M.E.; Morrical, B.D.; Fergenson, D.P.; Dienes, T.; Noble, C.A.; Silva, P.J.; Prather, K.A. Size and composition distribution of atmospheric particles in southern California. *Environ. Sci. Technol.* **1999**, *33*, 20, 3506-3515.
67. Jacob, D.J.; Waldman, J.M.; Munger, J.W.; Hoffmann, M.R. Chemical composition of fogwater collected along the California coast. *Environ. Sci. Technol.* **1985**, *19*, 8, 730-6.
68. Waldman, J.M.; Munger, J.W.; Jacob, D.J.; Flagan, R.C.; Morgan, J.J.; Hoffmann, M.R. Chemical composition of acid fog. *Science (Washington, D. C., 1883-)* **1982**, *218*, 4573, 677-80.
69. Cyrus, J.; Stolzel, M.; Heinrich, J.; Kreyling, W.G.; Menzel, N.; Wittmaack, K.; Tuch, T.; Wichmann, H.E. Elemental composition and sources of fine and ultrafine ambient particles in Erfurt, Germany. *Sci. Total Environ.* **2003**, *305*, 1-3, 143-156.
70. Miller, A.L.; Stipe, C.B.; Habjan, M.C.; Ahlstrand, G.G. Role of lubrication oil in particulate emissions from a hydrogen-powered internal combustion engine. *Environ. Sci. Technol.* **2007**, *41*, 19, 6828-6835.
71. *Locating and estimating air emissions from sources of nickel*. U.S. Environmental Protection Agency. Office of Air and Quality Planning and Standards, Research Triangle Park, NC, March 1984, EPA-450/4-84-007f
72. *Documentation for the 1996 base year national toxics inventory for onroad sources*. U.S. Environmental Protection Agency. Emission Factor and Inventory Group (MD-14); Emissions, Monitoring, and Analysis Division, Research Triangle Park, NC, June 2000
73. Fuechtjohann, L.; Jakubowski, N.; Gładtke, D.; Klockow, D.; Broekaert, J.A.C. Speciation of nickel in airborne particulate matter by means of sequential extraction in a micro flow system and determination by graphite furnace atomic absorption spectrometry and inductively coupled plasma mass spectrometry. *J. Environ. Monit.* **2001**, *3*, 6, 681-687.
74. Ballschmiter, K.; Braunmiller, I.; Niemczyk, R.; Swerev, M. Reaction pathways for the formation of polychloro-dibenzodioxins (PCDD) and --dibenzofurans (PCDF) in combustion processes: II. Chlorobenzenes and chlorophenols as precursors in the formation of polychloro-dibenzodioxins and --dibenzofurans in flame chemistry. *Chemosphere* **1988**, *17*, 5, 995-1005.
75. Olie, K.; Vermeulen, P.L.; Hutzinger, O. Chlorodibenzo-p-dioxins and chlorodibenzofurans are trace components of fly ash and flue gas of some municipal incinerators in the Netherlands. *Chemosphere* **1977**, *6*, 8, 455-459.

76. Fine, P.M.; Cass, G.R.; Simoneit, B.R.T. Chemical characterization of fine particle emissions from the wood stove combustion of prevalent United States tree species. *Environ. Eng. Sci.* **2004**, *21*, 6, 705-721.
77. Hays, M.D.; Fine, P.M.; Geron, C.D.; Kleeman, M.J.; Gullett, B.K. Open burning of agricultural biomass: Physical and chemical properties of particle-phase emissions. *Atmos. Environ.* **2005**, *39*, 36, 6747-6764.
78. Hogl, O. Some non-volatile extracts of coffee. *Mitteilungen aus dem Gebiete der Lebensmitteluntersuchung und Hygiene* **1958**, *49*, pp. 433-441.
79. Sheesley, R.J.; Schauer, J.J.; Chowdhury, Z.; Cass, G.R.; Simoneit, B.R.T. Characterization of organic aerosols emitted from the combustion of biomass indigenous to south Asia. *J Geophys Res-Atmos* **2003**, *108*, D9, -.
80. Varagnal, J., *Hydroquinone, resorcinol, and catechol* 3rd ed. Kirk-othmer. Encyclopedia of chemical technology., ed. D.E. M. Grayson, G.J. Bushey, C.I. Eastman, A. Klingsberg, L. Spiro and M. Wainwright. Vol. 13. **1981**, New York John Wiley & Sons pp. 39-69.
81. Visser, R.; Harbers, A.A.M.; Hovestad, A.; Stevens, T.W. *Identification of organic compounds in waste water of wood gasifiers with capillary gas chromatography*. 1985: Huethig.
82. Lee, S.H.; Jew, S.S.; Chang, P.S.; Hong, I.J.; Hwang, E.S.; Kim, K.S.; Kim, K.T. Free radical scavenging effect and antioxidant activities of barley leaves. *Food Sci. Biotechnol.* **2003**, *12*, 3, 268-273.
83. Schweigert, N.; Acero, J.L.; von, G.U.; Canonica, S.; Zehnder, A.J.; Eggen, R.I. DNA degradation by the mixture of copper and catechol is caused by DNA-copper-hydroperoxo complexes, probably DNA-Cu(I)OOH. *Environ. Mol. Mutagen.* **2000**, *36*, 1, 5-12.
84. Daisey, J.M.; Mahanama, K.R.R.; Hodgson, A.T. Toxic volatile organic compounds in simulated environmental tobacco smoke: Emission factors for exposure assessment. *J. Expo. Anal. Environ. Epidemiol.* **1998**, *8*, 313-334. .
85. Riveles, K.; Roza, R.; Talbot, P. Phenols, quinolines, indoles, benzene, and 2-cyclopenten-1-ones are oviductal toxicants in cigarette smoke. *Toxicol. Sci.* **2005**, *86*, 1, 141-151.

86. Schlotzhauer, W.S.; Walters, D.B.; Snook, M.E.; Higman, H.C. Characterization of catechols, resorcinols, and hydroquinones in an acidic fraction of cigarette-smoke condensate. *J. Agric. Food Chem.* **1978**, *26*, 6, 1277-1288.
87. Carmella, S.G.; Hecht, S.S.; Tso, T.C.; Hoffmann, D. Chemical studies on tobacco-smoke .77. Roles of tobacco cellulose, sugars, and chlorogenic acid as precursors to catechol in cigarette-smoke. *J. Agric. Food Chem.* **1984**, *32*, 2, 267-273.
88. Font, R.; Esperanza, M.; Garcia, A.N. Toxic by-products from the combustion of kraft lignin. *Chemosphere* **2003**, *52*, 6, 1047-1058.
89. Simoneit, B.R.T. Biomass burning - a review of organic tracers for smoke from incomplete combustion. *Appl. Geochem.* **2002**, *17*, 3, 129-162.
90. Waidyanatha, S.; Rothman, N.; Li, G.L.; Smith, M.T.; Yin, S.N.; Rappaport, S.M. Rapid determination of six urinary benzene metabolites in occupationally exposed and unexposed subjects. *Anal. Biochem.* **2004**, *327*, 2, 184-199.
91. Moiseeva, O.V.; Solyanikova, I.P.; Kaschabek, S.R.; Groning, J.; Thiel, M.; Golovleva, L.A.; Schlomann, M. A new modified ortho cleavage pathway of 3-chlorocatechol degradation by *Rhodococcus opacus* 1cp: Genetic and biochemical evidence. *J. Bacteriol.* **2002**, *184*, 19, 5282-5292.
92. Luten, J.B.; Ritskes, J.M.; Weseman, J.M. Determination of phenol, guaiacol and 4-methylguaiacol in wood smoke and smoked fish-products by gas-liquid-chromatography. *Z Lebens Unters For* **1979**, *168*, 4, 289-292.
93. Swarts, H.J.; Verhagen, F.J.M.; Field, J.A.; Wijnberg, J.B.P.A. Trichlorinated phenols from *hypoholoma elongatum*. *Phytochemistry* **1998**, *49*, 1, 203-206.
94. Bruce, R.M.; Santodonato, J.; Neal, M.W. Summary review of the health effects associated with phenol. *Toxicol. Ind. Health* **1987**, *3*, 4, 535-568.
95. Martínez, D.; Pocurull, E.; Marcé, R.M.; Borrull, F.; Calull, M. Separation of eleven priority phenols by capillary zone electrophoresis with ultraviolet detection. *J. Chromatogr. A* **1996**, *734*, 2, 367-373.
96. Michałowicz, J.; Duda, R.O.W. Analysis of chlorophenols, chlorocatechols, chlorinated methoxyphenols and monoterpenes in communal sewage of ŁÓDŹ and in the Ner river in 1999–2000. *Water. Air. Soil Pollut.* **2005**, *164*, 1, 205-222.

97. Tsuruta, Y.; Watanabe, S.; Inoue, H. Fluorometric determination of phenol and p-cresol in urine by precolumn high-performance liquid chromatography using 4-(N-phthalimidinyl)benzenesulfonyl chloride. *Anal. Biochem.* **1996**, *243*, 1, 86-91.
98. Barbehenn, R.; Cheek, S.; Gasperut, A.; Lister, E.; Maben, R. Phenolic compounds in red oak and sugar maple leaves have prooxidant activities in the midgut fluids of *Malacosoma disstria* and *orgyia leucostigma* caterpillars. *J. Chem. Ecol.* **2005**, *31*, 5, 969-988.
99. Hansch, C.; McKarns, S.C.; Smith, C.J.; Doolittle, D.J. Comparative QSAR evidence for a free-radical mechanism of phenol-induced toxicity. *Chem. Biol. Interact.* **2000**, *127*, 1, 61-72.
100. Thompson, R.H., "*Structure and reactivity of phenolic compounds*" in *Biochemistry of phenolic compounds*, J.B. Harborne, Editor. 1964, Academic Press: New York.
101. Bumb, R.; Crummett, W.; Cutie, S.; Gledhill, JR; Hummel, R.; Kagel, R.; Lamparski, L.; Luoma, E.; Miller, D.; Nestrick, T.; Shadoff, L.; Stehl, R.; Woods, J. Trace chemistries of fire: A source of chlorinated dioxins. *Science* **1980**, *210*, 4468, 385-390.
102. Czuczwa, J.M.; Hites, R.A. Environmental fate of combustion-generated polychlorinated dioxins and furans. *Environ. Sci. Technol.* **1984**, *18*, 6, 444-450.
103. Wong, A.S. Export of toxic chemicals-a review of the case of uncontrolled electronic-waste recycling. *Environ. Pollut.* **2007**, *149*, 2, 131-140.
104. Brigden, K.; Labunska, I.; Santillo, D.; Allsop, M., Recycling of electronic wastes in China and India: Workplace and environmental contamination: Greenpeace Research Laboratories Technical Note 09/2005, Publ. Greenpeace International, August 2005: 56 pp.
105. Róžański, L., *Przemiany pestycydów w organizmach żywych i środowisku* Agra-enviro lab. **1998**, Poznań234.
106. Rodriguez, M.J.; Serodes, J.B.; Levallois, P. Behavior of trihalomethanes and haloacetic acids in a drinking water distribution system. *Water Res.* **2004**, *38*, 20, 4367-4382.
107. Budavari, S., *The Merck Index*. 13th ed. **2001**, Whitehouse station, NJ: Merck Co1299-1367.

108. Hayes, W.C.; Hanley, T.R.; Gushow, T.S.; Johnson, K.A.; John, J.A. Teratogenic potential of inhaled dichlorobenzene in rats and rabbits. *Fundam. Appl. Toxicol.* **1985**, *5*, 1, 190-202.
109. <http://www.epa.gov/ttnchie1/le/chlorbnz.pdf>.
110. http://oehha.ca.gov/water/phg/pdf/12dcb_c.pdf.
111. De, J.E.; Field, J.A.; Dings, J.A.F.M.; Wijnberg, J.B.P.A.; De, B.J.A.M. De-novo biosynthesis of chlorinated aromatics by the white-rot fungus *Bjerkandera* sp. Bos55. Formation of 3-chloro-anisaldehyde from glucose. *FEBS Lett.* **1992**, *305*, 3, 220-4.
112. De, J.E.; Field, J.A.; Spinnler, H.E.; Wijnberg, J.B.P.A.; De, B.J.A.M. Significant biogenesis of chlorinated aromatics by fungi in natural environments. *Appl. Environ. Microbiol.* **1994**, *60*, 1, 264-70.
113. Verhagen, F.J.M.; Swarts, H.J.; Wijnberg, J.B.P.A.; Field, J.A. Organohalogen production is a ubiquitous capacity among basidiomycetes. *Chemosphere* **1998**, *37*, 9/12, 2091-2104.
114. Safe, S.; Gasiewicz, T.; J.P. Whitlock, J., *Mechanism of action*. Environmental toxin series 3: Polychlorinated dibenzo-p-dioxins and -furans (PCDDs/PCDFs), ed. S. Safe, O. Huntzinger, and T.A. Hill. **1990**, Berlin: Springer-Verlag, pp. 61-91.
115. Patnaik, P.; . *A comprehensive guide to the hazardous properties of chemical substances*; . **1992**, New York,: Reinhold.
116. Landers, J.P.; Birse, L.M.; Nakai, J.S.; Winhall, M.J.; Bunce, N.J. Chemically induced hepatic cytosol from the sprague-dawley rat: Evidence for specific binding of 2,3,7,8-tetrachlorodibenzo-p-dioxin to components kinetically distinct from the Ah receptor. *Toxicol. Lett.* **1990**, *51*, 3, 295-302.
117. Mitrou, P.I.; Dimitriadis, G.; Raptis, S.A. Toxic effects of 2,3,7,8-tetrachlorodibenzo-p-dioxin and related compounds. *Eur. J. Intern. Med.* **2001**, *12*, 5, 406-411.
118. Evans, J.S.; Tosteson, T.; Kinney, P.L. Cross-sectional mortality studies and air pollution risk assessment. *Environment International* **1984**, *10*, 1, 55-83.

119. Lafitte, S.; Peters, B.; DeMaria, A. Time course of myocardial opacification by real-time echocardiography during coronary occlusion: Value in risk area and infarct size. *Eur. Heart J.* **2001**, *22*, 468-468.
120. Lipfert, F.W. Air pollution and mortality: Specification searches using SMSA-based data. *J. Environ. Econ. Manage.* **1984**, *11*, 3, 208-43.
121. Archer, V.E. Air pollution and fatal lung disease in three Utah counties. *Arch Environ Health* **1990**, *45*, 6, 325-34.
122. Bobak, M.; Leon, D.A. Air pollution and infant mortality in the Czech Republic, 1986-88. *Lancet* **1992**, *340*, 8826, 1010-4.
123. Lave, L.B.; Seskin, E.P. Air pollution and human health. *Science* **1970**, *169*, 947, 723-33.
124. Özkaynak, H.; Thurston, G.D. Associations between 1980 U.S. Mortality rates and alternative measures of airborne particle concentration. *Risk Analysis* **1987**, *7*, 4, 449-461.
125. Mendelsohn, R.; Orcutt, G. An empirical analysis of air pollution dose-response curves. *J. Environ. Econ. Manage.* **1979**, *6*, 2, 85-106.
126. Nel, A.E.; Diaz-Sanchez, D.; Li, N. The role of particulate pollutants in pulmonary inflammation and asthma: Evidence for the involvement of organic chemicals and oxidative stress. *Curr. Opin. Pulm. Med.* **2001**, *7*, 1, 20-6.
127. Peters, A.; Dockery, D.W.; Muller, J.E.; Mittleman, M.A. Increased particulate air pollution and the triggering of myocardial infarction. *Circulation* **2001**, *103*, 23, 2810-2815.
128. Li, N.; Sioutas, C.; Cho, A.; Schmitz, D.; Misra, C.; Sempf, J.; Wang, M.; Oberley, T.; Froines, J.; Nel, A. Ultrafine particulate pollutants induce oxidative stress and mitochondrial damage. *Environ. Health Perspect.* **2003**, *111*, 4, 455-460.
129. Warheit, D.B.; Brock, W.J.; Lee, K.P.; Webb, T.R.; Reed, K.L. Comparative pulmonary toxicity inhalation and instillation studies with different TiO₂ particle formulations: Impact of surface treatments on particle toxicity. *Toxicol. Sci.* **2005**, *88*, 2, 514-524.
130. Calderon-Garciduenas, L.; Mora-Tiscareno, A.; Fordham, L.A.; Chung, C.J.; Garcia, R.; Osnaya, N.; Hernandez, J.; Acuna, H.; Gambling, T.M.; Villarreal-Calderon, A.; Carson, J.;

Koren, H.S.; Devlin, B. Canines as sentinel species for assessing chronic exposures to air pollutants: Part 1. Respiratory pathology. *Toxicol. Sci.* **2001**, *61*, 2, 342-355.

131. Calderon-Garciduenas, L.; Gambling, T.M.; Acuna, H.; Garcia, R.; Osnaya, N.; Monroy, S.; Villarreal-Calderon, A.; Carson, J.; Koren, H.S.; Devlin, R.B. Canines as sentinel species for assessing chronic exposures to air pollutants: Part 2. Cardiac pathology. *Toxicol. Sci.* **2001**, *61*, 2, 356-367.

132. Nemmar, A.; Vanquickenborne, B.; Dinsdale, D.; Thomeer, M.; Hoylaerts, M.F.; Vanbilloen, H.; Mortelmans, L.; Nemery, B. Passage of inhaled particles into the blood circulation in humans. *Circulation* **2002**, *105*, 4, 411-414.

133. Kaan, P.M.; Hegele, R.G. Interaction between respiratory syncytial virus and particulate matter in guinea pig alveolar macrophages. *Am. J. Respir. Cell Mol. Biol.* **2003**, *28*, 6, 697-704.

134. Ning, L.; Sioutas, C.; Cho, A.; Schmitz, D.; Misra, C.; Sempf, J.; Meiyang, W.; Oberley, T.; Froines, J.; Nel, A. Ultrafine particulate pollutants induce oxidative stress and mitochondrial damage. *Environ. Health Perspect.* **2003**, *111*, 4, 455.

135. Frampton, M.W. Systemic and cardiovascular effects of airway injury and inflammation: Ultrafine particle exposure in humans. *Environ. Health Perspect. Suppl.* **2001**, *109*, 4, 529-532.

136. Oberdorster, G. Significance of particle parameters in the evaluation of exposure-dose-response relationships of inhaled particles. *Part. Sci. Technol.* **1996**, *14*, 2, 135-151.

137. Utell, M.J.; Frampton, M.W. Acute health effects of ambient air pollution: The ultrafine particle hypothesis. *J. Aerosol Med.* **2000**, *13*, 4, 355-59.

138. Oberdorster, G.; Sharp, Z.; Atudorei, V.; Elder, A.; Gelein, R.; Kreyling, W.; Cox, C. Translocation of inhaled ultrafine particles to the brain. *Inhal. Toxicol.* **2004**, *16*, 6-7, 437-445.

139. Boezen, M.; Schouten, J.; Rijcken, B.; Vonk, J.; Gerritsen, J.; van, d.Z.S.; Hoek, G.; Brunekreef, B.; Postma, D. Peak expiratory flow variability, bronchial responsiveness, and susceptibility to ambient air pollution in adults. *Am. J. Respir. Crit. Care Med.* **1998**, *158*, 6, 1848-54.

140. Carter, J.D.; Ghio, A.J.; Samet, J.M.; Devlin, R.B. Cytokine production by human airway epithelial cells after exposure to an air pollution particle is metal-dependent. *Toxicol. Appl. Pharmacol.* **1997**, *146*, 2, 180-188.

141. Schwartz, J. What are people dying of on high air pollution days? *Environ. Res.* **1994**, *64*, 1, 26-35.
142. Chestnut, L.G.; Schwartz, J.; Savitz, D.A.; Burchfiel, C.M. Pulmonary function and ambient particulate matter: Epidemiological evidence from NHANES I. *Arch. Environ. Health* **1991**, *46*, 3, 135-44.
143. Tashkin, D.P.; Detels, R.; Simmons, M.; Liu, H.; Coulson, A.H.; Sayre, J.; Rokaw, S. The UCLA population studies of chronic obstructive respiratory disease: XI. Impact of air pollution and smoking on annual change in forced expiratory volume in one second. *Am. J. Respir. Crit. Care Med.* **1994**, *149*, 5, 1209-17.
144. Wang, B.; Peng, Z.; Zhang, X.; Xu, Y.; Wang, H.; Allen, G.; Wang, L.; Xu, X. Particulate matter, sulfur dioxide, and pulmonary function in never-smoking adults in Chongqing, China. *Int. J. Occup. Environ. Health* **1999**, *5*, 1, 14-19.
145. Ackermann-Lieblich, U.; Leuenberger, P.; Schwartz, J.; Schindler, C.; Monn, C.; Bolognini, G.; Bongard, J.; Brandli, O.; Domenighetti, G.; Elsasser, S.; Grize, L.; Karrer, W.; Keller, R.; Keller-Wossidlo, H.; Kunzli, N.; Martin, B.; Medici, T.; Perruchoud, A.; Schoni, M.; Tschopp, J.; Villiger, B.; Wuthrich, B.; Zellweger, J.; Zemp, E. Lung function and long term exposure to air pollutants in Switzerland. Study on air pollution and lung diseases in adults (SAPALDIA) team. *Am. J. Respir. Crit. Care Med.* **1997**, *155*, 1, 122-129.
146. Oettinger, R.; Drumm, K.; Knorst, M.; Krinyak, P.; Smolarski, R.; Kienast, K. Production of reactive oxygen intermediates by human macrophages exposed to soot particles and asbestos fibers and increase in NF-kappa b p50/p105 mRNA. *Lung* **1999**, *177*, 6, 343-54.
147. Sagai, M.; Lim, H.-B.; Ichinose, T. Lung carcinogenesis by diesel exhaust particles and the carcinogenic mechanism via active oxygens. *Inhal. Toxicol.* **2000**, *12*, Suppl. 3, 215-223.
148. Samet, J.M.; Dominici, F.; Curriero, F.C.; Coursac, I.; Zeger, S.L. Fine particulate air pollution and mortality in 20 U.S. Cities, 1987-1994. *N. Engl. J. Med.* **2000**, *343*, 24, 1742-1749.
149. Stone, K.; Bermudez, E.; Zang, L.Y.; Carter, K.M.; Queenan, K.E.; Pryor, W.A. The ESR properties, DNA nicking, and DNA association of aged solutions of catechol versus aqueous extracts of tar from cigarette smoke. *Arch. Biochem. Biophys.* **1995**, *319*, 1, 196-203.
150. Valavanidis, A.; Salika, A.; Theodoropoulou, A. Generation of hydroxyl radicals by urban suspended particulate air matter. The role of iron ions. *Atmos. Environ.* **2000**, *34*, 15, 2379-2386.

151. Tokiwa, H.; Sera, N.; Nakanishi, Y.; Sagai, M. 8-hydroxyguanosine formed in human lung tissues and the association with diesel exhaust particles. *Free Radic. Biol. Med.* **1999**, *27*, 11/12, 1251-1258.
152. Tsurudome, Y.; Hirano, T.; Yamato, H.; Tanaka, I.; Sagai, M.; Hirano, H.; Nagata, N.; Itoh, H.; Kasai, H. Changes in levels of 8-hydroxyguanine in DNA, its repair and OGG1 mRNA in rat lungs after intratracheal administration of diesel exhaust particles. *Carcinogenesis* **1999**, *20*, 8, 1573-6.
153. Kumagai, Y.; Arimoto, T.; Shinyashiki, M.; Shimojo, N.; Nakai, Y.; Yoshikawa, T.; Sagai, M. Generation of reactive oxygen species during interaction of diesel exhaust particle components with NADPH-cytochrome P450 reductase and involvement of the bioactivation in the DNA damage. *Free Radic. Biol. Med.* **1997**, *22*, 3, 479-87.
154. Pryor, W.A.; Hales, B.J.; Premovic, P.I.; Church, D.F. The radicals in cigarette tar: Their nature and suggested physiological implications. *Science* **1983**, *220*, 4595, 425-427.
155. Peters, D.C.; Epstein, F.H.; McVeigh, E.R. Myocardial wall tagging with undersampled projection reconstruction. *Magn. Reson. Med.* **2001**, *45*, 4, 562-567.
156. Anderson, H.R.; Limb, E.S.; Bland, J.M.; Ponce, d.L.A.; Strachan, D.P.; Bower, J.S. Health effects of an air pollution episode in London, December 1991. *Thorax* **1995**, *50*, 11, 1188-93.
157. Firket, J. Fog along the Meuse valley. *Trans. Faraday Soc.* **1936**, *32*, 1192-7.
158. Pope III, C.A.; Burnett, R.T.; Thun, M.J.; Calle, E.E.; Krewski, D.; Ito, K.; Thurston, G.D. Lung cancer, cardiopulmonary mortality, and long-term exposure to fine particulate air pollution. *JAMA* **2002**, *287*, 9, 1132-1141.
159. Dockery, D.W.; Pope, C.A.; Xu, X.; Spengler, J.D.; Ware, J.H.; Fay, M.E.; Ferris, B.G.; Speizer, F.E. An association between air pollution and mortality in six US cities. *N. Engl. J. Med* **1993**, *329*, 1753-1759.
160. Lafitte, S.; Matsugata, H.; Peters, B.; Togni, M.; Strachan, M.; Kwan, O.L.; DeMaria, A.N. Comparative value of dobutamine and adenosine stress in the detection of coronary stenosis with myocardial contrast echocardiography. *Circulation* **2001**, *103*, 22, 2724-2730.

161. Lehnert, B.E.; Ortiz, J.B.; Steinkamp, J.A.; Tietjen, G.L.; Sebring, R.J.; Oberdorster, G. *Mechanisms underlying the redistribution of particles among the lung's alveolar macrophages during alveolar phase clearance*. 1994: Pergamon.
162. Burnett, R.T.; Brook, J.; Dann, T.; Delocla, C.; Philips, O.; Cakmak, S.; Vincent, R.; Goldberg, M.S.; Krewski, D. Association between particulate- and gas-phase components of urban air pollution and daily mortality in eight canadian cities. *Inhal. Toxicol.* **2000**, *12*, Suppl. 4, 15-39.
163. Ostro, B.; Sanchez, J.M.; Aranda, C.; Eskeland, G.S. Air pollution and mortality: Results from a study of Santiago, Chile. *J. Expo. Anal. Environ. Epidemiol.* **1996**, *6*, 1, 97-114.
164. Pope, C.A., 3rd; Verrier, R.L.; Lovett, E.G.; Larson, A.C.; Raizenne, M.E.; Kanner, R.E.; Schwartz, J.; Villegas, G.M.; Gold, D.R.; Dockery, D.W. Heart rate variability associated with particulate air pollution. *Am. Heart J.* **1999**, *138*, 5 Pt 1, 890-9.
165. Han, J.Y.; Takeshita, K.; Utsumi, H. Noninvasive detection of hydroxyl radical generation in lung by diesel exhaust particles. *Free Radic. Biol. Med.* **2001**, *30*, 5, 516-525.
166. Knaapen, A.M.; Shi, T.M.; Borm, P.J.A.; Schins, R.P.F. Soluble metals as well as the insoluble particle fraction are involved in cellular DNA damage induced by particulate matter. *Mol. Cell. Biochem.* **2002**, *234*, 1, 317-326.
167. Prahalad, A.K.; Soukup, J.M.; Inmon, J.; Willis, R.; Ghio, A.J.; Becker, S.; Gallagher, J.E. Ambient air particles: Effects on cellular oxidant radical generation in relation to particulate elemental chemistry. *Toxicol. Appl. Pharmacol.* **1999**, *158*, 2, 81-91.
168. Prahalad, A.K.; Inmon, J.; Dailey, L.A.; Madden, M.C.; Ghio, A.J.; Gallagher, J.E. Air pollution particles mediated oxidative DNA base damage in a cell free system and in human airway epithelial cells in relation to particulate metal content and bioreactivity. *Chem. Res. Toxicol.* **2001**, *14*, 7, 879-887.
169. Breen, A.P.; Murphy, J.A. Reactions of oxyl radicals with DNA. *Free Radic. Biol. Med.* **1995**, *18*, 6, 1033-77.
170. Cohen, G.; Yakushin, S.; Dembiec-Cohen, D. Protein L-dopa as an index of hydroxyl radical attack on protein tyrosine. *Anal. Biochem.* **1998**, *263*, 2, 232-239.
171. Gardner, H.W. Oxygen radical chemistry of polyunsaturated fatty acids. *Free Radic. Biol. Med.* **1989**, *7*, 1, 65-86.

172. Girotti, A.W. Mechanisms of lipid peroxidation. *J. Free Radicals Biol. Med.* **1985**, *1*, 2, 87-95.
173. Hamade, A.K.; Rabold, R.; Tankersley, C.G. Adverse cardiovascular effects with acute particulate matter and ozone exposures: Interstrain variation in mice. *Environ. Health Perspect.* **2008**, *116*, 8, 1033-1039.
174. Li, N.; Xia, T.; Nel, A.E. The role of oxidative stress in ambient particulate matter-induced lung diseases and its implications in the toxicity of engineered nanoparticles. *Free Radic. Biol. Med.* **2008**, *44*, 9, 1689-1699.
175. Gurgueira, S.A.; Lawrence, J.; Coull, B.; Murthy, G.G.K.; Gonzalez-Flecha, B. Rapid increases in the steady-state concentration of reactive oxygen species in the lungs and heart after particulate air pollution inhalation. *Environ. Health Perspect.* **2002**, *110*, 8, 749-755.
176. Oberdorster, G.; Ferin, J.; Finkelstein, J.; Soderholm, S. Thermal degradation events as health hazards: Particle vs gas phase effects, mechanistic studies with particles. *Acta Astronaut* **1992**, *27*, 251-6.
177. Oberdorster, G.; Ferin, J.; Soderholm, S.; Gelein, R.; Cox, C.; Baggs, R.; Morrow, P.E. *Increased pulmonary toxicity of inhaled ultrafine particles: Due to lung overload alone?* 1994: Pergamon.
178. Hirakawa, K.; Oikawa, S.; Hiraku, Y.; Hirosawa, I.; Kawanishi, S. Catechol and hydroquinone have different redox properties responsible for their differential DNA-damaging ability. *Chem. Res. Toxicol.* **2002**, *15*, 1, 76-82.
179. Pryor, W.A.; Stone, K.; Zang, L.Y.; Bermudez, E. Fractionation of aqueous cigarette tar extracts: Fractions that contain the tar radical cause DNA damage. *Chem. Res. Toxicol.* **1998**, *11*, 5, 441-448.
180. Squadrito, G.L.; Cueto, R.; Dellinger, B.; Pryor, W.A. Quinoid redox cycling as a mechanism for sustained free radical generation by inhaled airborne particulate matter. *Free Radic. Biol. Med.* **2001**, *31*, 9, 1132-1138.
181. Saldiva, P.H.N.; Clarke, R.W.; Coull, B.A.; Stearns, R.C.; Lawrence, J.; Murthy, G.G.K.; Diaz, E.; Koutrakis, P.; Suh, H.; Tsuda, A.; Godleski, J.J. Lung inflammation induced by concentrated ambient air particles is related to particle composition. *Am. J. Respir. Crit. Care Med.* **2002**, *165*, 12, 1610-1617.

182. Li, Y.; Trush, M.A. Reactive oxygen-dependent DNA damage resulting from the oxidation of phenolic compounds by a copper-redox cycle mechanism. *Cancer Res.* **1994**, *54*, 7 Suppl, 1895s-1898s.
183. Borish, E.T.; Cosgrove, J.P.; Church, D.F.; Deutsch, W.A.; Pryor, W.A. Cigarette tar causes single-strand breaks in DNA. *Biochem. Biophys. Res. Commun.* **1985**, *133*, 2, 780-6.
184. Church, D.F.; Pryor, W.A. Free radical chemistry of cigarette smoke and its toxicological implications. *Environ. Health Perspect.* **1985**, *64*, 111-126.
185. Pryor, W.A. Cigarette smoke radicals and the role of free radicals in chemical carcinogenicity. *Environ. Health Perspect. Suppl.* **1997**, *105*, 4, 875-882.
186. Pryor, W.A. Oxy-radicals and related species: Their formation, lifetimes, and reactions. *Annu. Rev. Physiol.* **1986**, *48*, 657-67.
187. Kukier, U.; Ishak, C.F.; Sumner, M.E.; Miller, W.P. Composition and element solubility of magnetic and non-magnetic fly ash fractions. *Environ. Pollut.* **2003**, *123*, 2, 255-266.
188. Kohanski, M.A.; Dwyer, D.J.; Hayete, B.; Lawrence, C.A.; Collins, J.J. A common mechanism of cellular death induced by bactericidal antibiotics. *Cell* **2007**, *130*, 5, 797-810.
189. Balakrishna, S.; Lomnicki, S.; McAvey, K.M.; Cole, R.B.; Dellinger, B.; Cormier, S.A. Environmentally persistent free radicals amplify ultrafine particle mediated cellular oxidative stress and cytotoxicity. *Part. Fibre Toxicol.* **2009**, *6*, -.
190. Valavanidis, A.; Fiotakis, K.; Bakeas, E.; Vlahogianni, T. Electron paramagnetic resonance study of the generation of reactive oxygen species catalysed by transition metals and quinoid redox cycling by inhalable ambient particulate matter. *Redox Rep.* **2005**, *10*, 1, 37-51.
191. Cormier, S.A.; Lomnicki, S.; Backes, W.; Dellinger, B. Origin and health impacts of emissions of toxic by-products and fine particles from combustion and thermal treatment of hazardous wastes and materials. *Environ. Health Perspect.* **2006**, *114*, 6,
192. Maskos, Z.; Khachatryan, L.; Dellinger, B. Precursors of radicals in tobacco smoke and the role of particulate matter in forming and stabilizing radicals. *Energy Fuels* **2005**, *19*, 6, 2466-2473.

193. Yi, S.M.; Narasimhulu, K.V.; Samoilova, R.I.; Gennis, R.B.; Dikanov, S.A. Characterization of the semiquinone radical stabilized by the cytochrome aa3-600 menaquinol oxidase of *Bacillus subtilis*. *J. Biol. Chem.* **285**, 24, 18241-18251.
194. Lachocki, T.M.; Church, D.F.; Pryor, W.A. Persistent free radicals in the smoke of common household materials: Biological and clinical implications. *Environ. Res.* **1988**, *45*, 1, 127-139.
195. Igor, V.K.; Kuz'min, V.A. Oxidation-reduction reactions of free radicals. *Russ. Chem. Rev.* **1978**, *47*, 1, 22.
196. Khachatryan, L., Adoukpe, J., Maskos, M., and Dellinger, B. Formation of cyclopentadienyl radicals from the gas-phase pyrolysis of hydroquinone, catechol, and phenol. *Environ. Sci. Technol.* **2006**, *40*, 5071-5076.
197. Ledesma, E.B., Marsh, N.D., Sandrowitz, A.K., and Wornat, M.J. An experimental study on the thermal decomposition of catechol. *Proc. Combust. Inst.* **2002**, *29*, 2299-2306.
198. Blumberg, W.E.; Peisach, J. The optical and magnetic properties of copper in *Chenopodium album* plastocyanin. *Biochim. Biophys. Acta, Biophys. Incl. Photosynth.* **1966**, *126*, 2, 269-273.
199. Lomnicki, S., Dellinger, B. A detailed mechanism of the surface-mediated formation of PCDD/F from the oxidation of 2-chlorophenol on a CuO/silica surface. *J. Phys. Chem. A* **2003**, *107*, 4387-4395.
200. Fine, P.M.; Cass, G.R.; Simoneit, B.R.T. Chemical characterization of fine particle emissions from the fireplace combustion of woods grown in the southern United States. *Environ. Sci. Technol.* **2002**, *36*, 1442-1451.
201. Bonte, J.L.; Fritsky, K.J.; Plinke, M.A.; Wilken, M. Catalytic destruction of PCDD/F in a fabric filter: Experience at a municipal waste incinerator in Belgium. *Waste Manag.* **2002**, *22*, 4, 421-426.
202. Blumenstock, M.; Zimmermann, R.; Schramm, K.-W.; Kaune, A.; Nikolai, U.; Lenoir, D.; Kettrup, A. Estimation of the dioxin emission (PCDD/FI-TEQ) from the concentration of low chlorinated aromatic compounds in the flue and stack gas of a hazardous waste incinerator. *J. Anal. Appl. Pyrolysis* **1999**, *49*, 1-2, 179-190.

CHAPTER II. EXPERIMENTAL

2.1 Vacuum and Thermoelectric Furnace System

The vacuum and thermoelectric furnace system is the working unit used for the entire experiment. This system is used for the adsorption of molecular adsorbates onto the transition metal oxide on silica surface. The vacuum and thermoelectric furnace system consists of five parts: a vacuum system, a high temperature thermoelectric furnace system, a vacuum exposure chamber, an EPR extraction cell, and a dosing vial port.

2.1.1 The Vacuum System

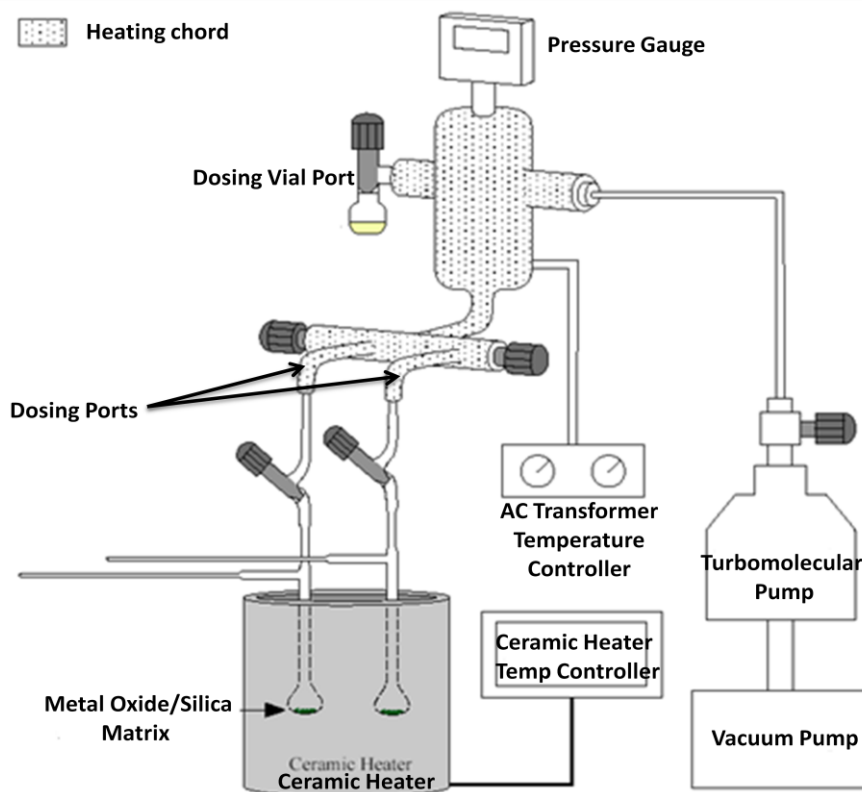


Figure 2.1. The vacuum and high temperature thermoelectric furnace system

The vacuum system is crucial and important in the preparation of the adsorbed EPRs onto the sample particulate matter (cf. **Figure 2.1**). It is used to dry and clean the sample particulate matter with contaminants prior to the adsorption experiment and to dry samples of biological nature. The vacuum system is composed of two vacuums which are connected in series. The first pump is a roughing vacuum pump (Edwards, model E2M0.7) and the second pump is a high vacuum turbomolecular pump (Edwards, model EXT70) with an Edwards active gauge controller. The first vacuum is used all throughout the course of the adsorption experiment while the second pump is used only after the adsorption process is done, the purpose of which is to remove the remaining physisorbed molecular adsorbates from the surface of the glass, the EPR extraction, and most importantly the physisorbed species on the sample. The turbomolecular pump is turned on when the pressure of the system reaches 0.5 Torr using the roughing pump and the turbomolecular pump is used to reach pressure down to 10^{-2} Torr. Since the adsorbates used are harmful, the outlet of the roughing vacuum pump is connected to a carbon capsule (Pall, model 12011) to absorb excess adsorbates and connected to the fume hood to vent.

2.1.2 Vacuum Exposure Chamber

The vacuum exposure chamber is made of glass and contains two dosing ports where the EPR extraction cells can be easily attached and removed for adsorption and cleaning. It is covered with rope heaters (Omegalux, model FGR-080) and wrapped with aluminum foil around the whole chamber to prevent condensation of molecular adsorbates on the glass wall. The rope heaters are connected to a variable AC temperature controller (Electrothermal, model MC240X1) which control the temperature of the whole chamber at around 80 °C. The pressure of the system is monitored by digital pressure gauge (Varian Eyesys ConvecTorr, model L973633200220). The dosing chamber is connected to the vacuum system with a high vacuum adapter with an L-

shaped glass equipped with a double o-ring PTFE valve. A liquid nitrogen-cooled trap is placed in between the vacuum exposure system and the vacuum system to remove excess adsorbates to prevent loss in vacuum performance.

2.1.3 The Extraction Cell

The extraction cell is a 12-inch quartz tube composed of a detachable 9-inch Suprasil™ EPR side arm used for EPR measurement and a reactor bulb where the adsorption on the sample particulate matter at specified temperature occurs. The detachable EPR tube is attached to the body of the EPR extraction cell by a high vacuum adapter fitted with a PTFE o-ring and plastic nut. The reactor bulb of the EPR extraction cell has a rounded bottom which measure 1.5 inch i.d. to increase the exposure of the sample particulate matrix with the adsorbates. When

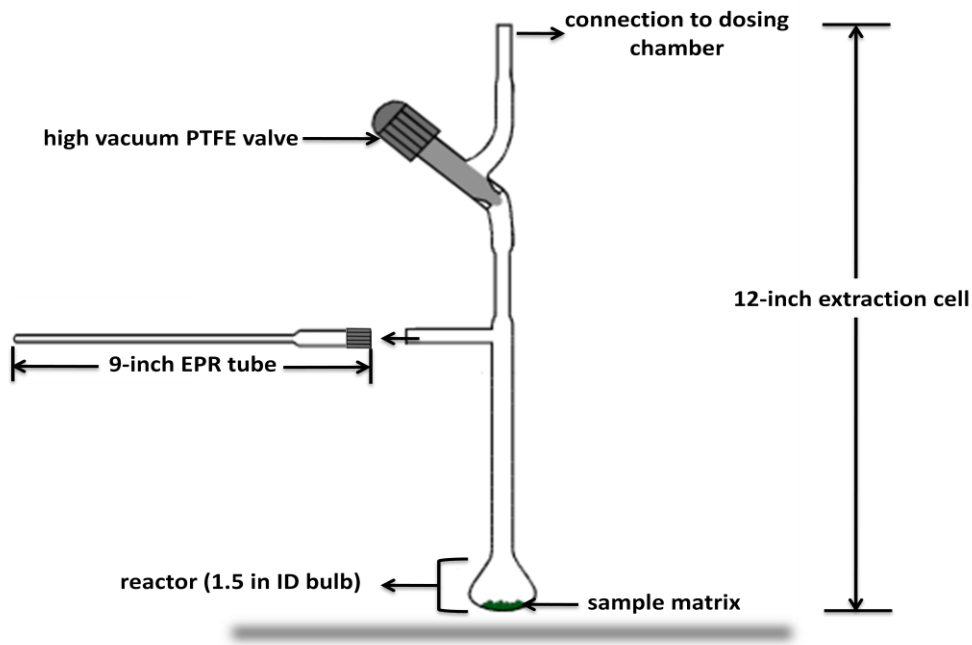


Figure 2.2. EPR extraction cell with a detachable EPR tube

assembled together, they are connected to the vacuum exposure chamber which can accommodate 2 extraction cells using an ultrahigh vacuum adapter (Swagelok, SS-4-UT-6) made of stainless steel. The extraction cell is custom-designed to serve multipurpose role such as adsorption, extraction, and EPR measurement. It was modified from its original design to prevent leak in the whole system and has better seal. In the modified design the sample is introduced in the opening of the extraction cell where the EPR side arm is connected to the body of the EPR extraction cell. This improvement is ideal for adsorption and transfer of the sample matrix from the reaction site to the EPR side arm under vacuum condition. The EPR extraction cell with the EPR tube attachment is illustrated in **Figure 2.2**.

2.1.4 The High Temperature Ceramic Heater

The two reactor bulbs where the sample resides are placed inside a high temperature cylindrical ceramic heater (Omegalux, model CRFC) which can reach temperature as high as 950 °C. The temperature of the heater is controlled by a temperature controller (Omegalux, model SSRL240DC25) which is connected to a relay (Tyco, model SSR-240D25R) and is equipped with a high temperature K thermocouple sensor (Omega, model XCIB-K-2-3-3) which controls the temperature of the ceramic heater.

2.2 Particulate Matter Sample

2.2.1 Particulate Matter Sample Matrix Preparation

Fly ash from combustion system contains various amounts of trace and transition metals (1, 2) which are catalytically and highly redox active, like copper and iron (3). To simulate real environmental sample, the metals used are adsorbed onto silica (silica gel, grade 923, 100-200 mesh) surface which acts as a surrogate for fly ash and also facilitates sample handling. Four different metal oxides were prepared namely, copper, iron, nickel, and zinc. The sample

particulate matter fly ash surrogates were prepared by the method of incipient wetness. Particulate samples of different percentage of the Fe(III)₂O₃, Ni(II)O, Zn(II)O, and Cu(II)O supported on silica on mass loading basis were prepared by impregnation of silica gel with iron(III) nitrate nonahydrate (Sigma Aldrich, 99+%), nickel nitrate hexahydrate (Sigma Aldrich, 99+%), zinc nitrate hexahydrate (Sigma Aldrich, 99+%), and copper nitrate hemipentahydrate (Sigma Aldrich, 99+%), respectively. In this method, the solutions of metal oxide precursors are added to the silica so that the water are trapped in the pore structure and are bound on the adsorption sites so that no bulk water is present in the matrix. In this method, the metal clusters adsorbed on the surface have larger size distribution, which closely resembles the size distribution of metals found in combustion and thermal-derived processes. The detailed procedures in the preparation of 5% Cu(II)O particulate matter are as follow:

- Since bulk water should not be present, the first step is to determine the amount of water needed for incipient wetness to occur for a given amount of silica. Two kinds of silica were used in the experiments: for experiments of biological concerns, Cab-O-Sil was used, and for the regular experiment, silica gel powder (Sigma-Aldrich, grade 923, 100-200 mesh size) was used. The difference in the two forms of silica is that the former is amorphous while the latter is crystalline in structure and has higher porosity. A more detailed inventory of the properties of the two substrates is presented in **Table 2.1**.

Table 2.1. Properties of silica gel and Cab-O-Sil

Substrate	Cab-O-Sil	Silica Gel
Crystallinity	Amorphous	crystalline
Mesh (Mesh size)	230 (63 μm)	100-200 (75-150 μm)
Primary particle size	>20 nm	75-150 μm
Aggregate size	>20-100 nm	---
Pore size	7.5 nm	3.0 nm
Surface area (BET N ₂)	385 m ² /g	500 m ² /g

- When the amount of water is determined, the next step is to determine the

amount of the metal precursor (in hydrated form) that would be added to achieve the necessary mass loading percentage. Different percentages of the metals were prepared like 0.05, 0.1625, 0.275, 0.3875, 0.5, 0.625, 0.75, 0.875, 1, 2, 3, 4, and 5 %.

- To prepare 5% Cu(II)O on mass loading basis, 5g of Cu(II)O and 95 g of SiO₂ (silica) are needed to prepare 100g of Cu(II)O/silica which would need 15 g of Cu(NO₃)₂ 2.5H₂O.
- The Cu(NO₃)₂ 2.5H₂O is dissolve in the predetermined amount of milliOhm distilled water needed for incipient wetness.
- The solution of Cu(NO₃)₂ 2.5H₂O is added to 100 g of silica and stirred to mix well.
- The resulting gel is allowed to stand for 2 h and stirred occasionally at room temperature.
- The resulting gel is oven-dried for 6 h at 120 °C and becomes blue-green after drying.
- The blue-green dried gel is transferred to a crucible, then covered and calcined at 450 °C in the furnace for 12 h to convert Cu(NO₃)₂ 2.5H₂O to Cu(II)O.
- The green powder was thoroughly ground using an agate mortar and pestle.
- The resulting powder was sieved and stored in a vial for use.

2.2.2 Determination of Metal Content in Sample Particulate Matter

To determine the accuracy of the preparation of the sample, the metal content was analyzed by Inductively Coupled Plasma (ICP). As a representative for the metals on silica, 5% Cu(II)O/silica was tested. A sample of 5% Cu(II)O/silica ultrafine particles (Cab-O-Sil® was used as the substrate) weighing 1.889 mg were measured using a microbalance and placed on a conical plastic centrifuge tube. The sample is digested in 2 mL 14% doubly distilled HNO₃

solution for 48 h at room temperature. The sample is then diluted with 10 mL of 3% HNO₃ solution, then, 1 mL aliquot was taken and diluted to 100 mL with 3% HNO₃ solution. Similarly, 2.842 g 5% Cu(II)O/silica, which has been dosed with 2-monochlorophenol using the dosing procedure described in **Section 2.3** (vide infra) was weighed and subjected to the same treatment as the undosed sample. The samples were then analyzed for copper content.

2.3 Detailed Adsorption Procedure

The molecular adsorbates chosen for the study were the substituted benzene: hydroquinone—HQ (Sigma, 99+%), catechol—CT (Aldrich, 99+%), phenol—PH (Aldrich, 99+%), 2-monochlorophenol—2-MCP (Aldrich, 99+%), monochlorobenzene—MCBz (Aldrich, 99.8% anhydrous), and 1,2-dichlorobenzene—1, 2-DCBz (Sigma-Aldrich, 99% HPLC grade) were used as received without further purification. Hydroquinone and catechol were chosen because they are known precursors of semiquinone radicals and previous research in dioxin formation suggested that they are formed on Cu(II)O surfaces so we thought that other transition metals might also catalyze the formation of PCDD/Fs (4). Phenol is the most common partial oxidation product of aromatic species in combustion system (5, 6). 2-Monochlorophenol, monochlorobenzene, and 1,2-dichlorobenzene are all chlorinated aromatics and are suspected precursors of dioxin (7). The detailed procedure for adsorption and the formation of EPFRs is presented below:

- Weigh two 100 mg sample of 5% Cu(II)O/silica and place the weighed sample onto an EPR extraction cell using the side arm opening to introduce the sample onto the cell.
- Close the side arm opening by attaching the EPR tube with a high vacuum plastic threaded screw nut equipped with o-ring. Then, seal the main extraction cell opening with PTFE vacuum valve.

- Attach the two extraction cells into the dosing port of the vacuum exposure chamber. The bottom of the reactors, containing the particles to be dosed, should be placed in the cylindrical high temperature furnace in a vertical orientation. Connect the two EPR extraction cells to the vacuum exposure chamber using a high vacuum Swagelok™ stainless steel adapter and make sure that the reactor part of the extraction cells are on the center of the cylindrical ceramic heater to ensure they do not touch the wall of the heater. Use a high temperature sleeve chord if tying is necessary.
- Switch on the roughing vacuum pump while the turbomolecular pump remains switch off.
- Open the main vacuum valve (the valve connecting the dosing chamber to the vacuum system) of the vacuum exposure system and evacuate.
- Make sure that there are no leaks in the system and all the outlets are initially closed except for the main valve.
- Slowly and carefully open the two valves which connect the extraction cells to the vacuum exposure chamber and evacuate the samples until the particulate matter no longer moves inside the reactors.
- Then, increase the temperature to 120 °C while the vacuum is continuously running to evaporate all the water from the sample for 10 min.
- Increase the temperature to 450 °C and maintain this condition for 1 h to clean, pretreat, and remove any surface contaminants that may have adsorbed on the particulate sample matrix surface.
- Set the temperature of the ceramic heater to the desired adsorption temperature (150 °C to 400 °C).
- Close the valve on the EPR extraction cell.
- When the ceramic heater temperature reaches the set point temperature, attach the vial containing the molecular adsorbates in the dosing vial port with the valve remaining closed. Then, slowly open the valve of the dosing vial port and the dosing vial itself to evacuate air from the adsorbates. The pressure would go up at this point. Wait until the pressure of the system goes down to about 1 Torr before closing the valve on the dosing vial.

- Evacuate further until the pressure decreases to 0.5 Torr.
- Open the water line and turn on the turbomolecular pump and evacuate until the pressure reaches 10^{-2} Torr.
- Turn on the variable AC heater to warm up the vacuum exposure chamber.
- Close the main valve (the valve connecting the whole system to the vacuum pump) and slowly open the valve on the EPR extraction cell.
- Open the valve on the dosing port to introduce the adsorbate to the exposure chamber for 5 min and heat up the metal parts and other uninsulated part of the glass chamber continuously by using a heating gun to prevent condensation of the adsorbates. (CAUTION: Do not heat too much to avoid decomposition of the adsorbate molecules)
- Close the valve on the dosing vial and open the main valve to evacuate the physisorbed adsorbates out of the system at 10^{-2} Torr for 1 h at 120 °C.
- Turn off the variable AC heater and lower the temperature to 25 °C to cool the sample.
- Close the EPR extraction cell valves and then the main valve. Detach the EPR extraction cell from the exposure chamber.
- Transfer the sample from the reactor to the EPR sidearm and do EPR analysis.

2.4 EPR Analysis

The samples were then analyzed by using an electron paramagnetic resonance (EPR) spectroscopy. All EPR measurements were performed using a Bruker EMX-20/2.7 EPR spectrometer with dual cavities, X-band, 100 kHz and microwave frequency, 9.53 GHz. The spectra were obtained at room temperature. The typical operating parameters were: microwave power—1 mW, modulation amplitude—4 G, sweep width—200 G, time constant—40.960 ms, and sweep time—167.7 s, using 1024 points with a receiver gain of 1.0×10^4 .

2.4.1 Analysis and Calculation

The g-factor and the ΔH_{p-p} were calculated and measured using the Bruker WINEPR data

processing software. Peak fitting analysis to determine the number of peaks was done using Origin 7.0 Peak Fitting Module. The spectra were fitted as non-derivative absorption spectra and the overall fit was compared with both the original absorption spectra as well as the first-derivative spectra.

The radical concentrations were calculated using the formula in **equation 1** using the double integration method of the first derivative signal and compared to 2,2-di(4-tert-octylphenyl)-1-picrylhydrazyl (DPPH) as standard using a 3-point calibration curve.

$$C = \frac{Spins \times A \times RG_{DPPH}}{A_{DPPH} \times RG \times m} \quad \text{equation 1}$$

Where: C (spins/g) is concentration of radicals in the sample, A is the area count of sample; RG is receiver gain used to acquire the sample signal; m (grams) is the mass of sample; A_{DPPH} is the area count of DPPH and RG_{DPPH} is receiver gain used to acquire the DPPH signal.

2.4.2 Calibration Curve

To determine the concentration of the radical from the adsorption experiment a calibration curve was prepared. DPPH weighing 2.6 mg was measured using a microbalance with 1 μg accuracy. The DPPH was then dissolved in 25 mL of benzene to make a stock solution with concentration of 104 $\mu\text{g/mL}$. A 1 mL aliquot of the DPPH stock was then diluted to mark with 10 mL of benzene. The concentration of the resulting solution was analyzed using a UV-Vis-NIR spectrophotometer (Shimadzu, model UV-3101PC, double-beam)) using the following parameters: λ_{max} at 520 nm and molar extinction coefficient (ϵ) of 12,800 $\text{M}^{-1} \text{cm}^{-1}$ (8). Then, 0.36 mL, 0.72 mL, and 1.40 mL of the solution were taken and placed on a custom-designed tube made of quartz (cf. **Figure 2.3**). The sample was vacuum-dried and benzene is constantly added to bring down the solid at the tip of the quartz tube. After drying out the benzene from DPPH the

tube was then sealed in vacuum and the EPR spectra were acquired. The area counts were determined using the double-integration method of the first-derivative signal and a calibration curve was generated by plotting the area counts vs. the amount of DPPH.

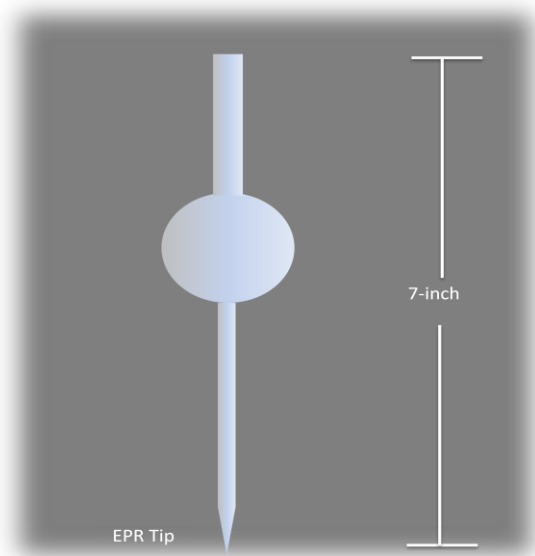


Figure 2.3. EPR tube for DPPH standard

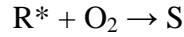
2.5 Determination of Surface-Bound Radical Stability and Persistency

After EPR analysis, the sample is exposed to the atmosphere to determine the persistency of the bound radicals on the metal oxide. Particulate matter dosed with catechol, hydroquinone, phenol, 1,2-dichlorobenzene, monochlorobenzene, and 2-monochlorophenol at the dosing temperature of 230 °C prepared by the procedure discussed in **Section 2.3** were prepared. The sample is exposed to air by opening the PTFE valve on the EPR extraction cells at room temperature. The samples were exposed to air at different time intervals and the EPR spectra were then acquired as a function of time until the sample has decayed and acquisition of the EPR spectra is at the noise level of the instrument. The decay of the relative radical concentration was

plotted vs. time, and the half-lives ($1/e$) were calculated from the fitted data as first-order decay.

2.5.1 Calculation of $1/e$ Half-life

The main mechanism of decay for radical is by its reaction with small molecules such as oxygen. In the exposure studies of the EPFRs with air, we assume that the decay is due to its reaction with molecular oxygen and undergoes this process;



Where R^* is the radical and S is the molecular product. Then the rate equation for the decay of radical R^* can be written as,

$$-\frac{d[R^*]}{dt} = K[O_2][R^*] \quad \text{equation 2}$$

Since the concentration of oxygen is much greater than the concentration of the radical, and the change in oxygen concentration is negligible (*i.e.*, we assume steady-state), that is

$$\frac{d[O_2]}{dt} = 0$$

then, **equation 2** integrates to,

$$d \ln[R^*] = k dt \quad \text{where } k = K[O_2]$$

$$\int_{R_o^*}^{R_f^*} d \ln[R^*] = - \int_0^t k dt$$

$$\ln R_f^* - \ln R_o^* = -kt$$

$$\ln \frac{R_f^*}{R_o^*} = -kt \quad \text{equation 3}$$

$$R_f^* = R_o^* e^{-kt} \quad \text{equation 4}$$

The $1/e$ half-life is the time it takes for the original concentration to decay to $1/e$, that is,

$$R_f^* = 1/e R_o^*$$

Substituting this to **equation 4** yields,

$$1/e R_o^* = R_o^* e^{-kt}$$

Which for a first-order reaction, the $1/e$ half-life is the reciprocal of the rate constant.

$$t_{1/e} = 1/k \quad \text{equation 5}$$

2.6 GC-MS Analyses of EPFR Extracts

To assist in the identification of the EPFRs, the dosed particulate sample was extracted and subjected to GC-MS analyses using dichloromethane and methanol as extracting solvent. The procedures are as follows;

- Dosed the sample particulate matter using the procedure described in **Section 2.3**
- Measure the EPR signals of the bound EPFRs.
- The samples residing in the EPR tube is tilted to transfer it back to the reactor bulb.
- 1 mL of dichloromethane or methanol is added to the sample
- The EPR extraction cell is sealed with a PTFE vacuum valve.
- The sample is then placed in the sonicator (Fisher Scientific, model FS20) and sonicated for 1 h (the sonicator was filled with water up to 1 inch to the brim).
- After 1 h, the sample is transferred to a microcentrifuge tube and centrifuged for 5 min to separate the particles from the liquid fraction. The liquid fraction is carefully decanted to a separate 1.5 mL microvial.
- The decantate is then filtered with 0.45 μm nylon filter to remove smaller particles to prevent clogging of the GC-MS column and transferred to a vial and sealed with a septum cap.
- Then 0.1 μL of the extract is injected to the GC-MS for analyses.

The extracted EPFRs were analyzed by an Agilent 6750 GC-MS instrument with the

following parameters; Column—HP-5MS (30 m, 0.250 μ m I.D), carrier gas—helium,. The parameters for the GC-MS are: injection temperature, 200 °C, and flowrate—1.2 mL/min. The mass-spectral library (NIST 98 version 1.6d) was used to identify the extraction products.

2.7 Interaction of EPFRs with Biological Compounds

The prepared samples were also studied with chemicals found in biological system and lung fluid extracted from mouse. One liter of phosphate buffer solution was prepared by mixing 1.44g of Na_2HPO_4 and 0.24g NaH_2PO_4 in 800 mL deionized water and the pH was adjusted to 7.4 and diluted to mark. Different concentrations of ascorbic acid (Sigma, 99%), epinephrine (Sigma, 98%), 3,3',5-triiodothyronine (Fluka, 98%), hydrocortisone(Sigma, 98%), retinoic acid (Sigma, 98%) and human transferrin (Aldrich, 98%) solutions were prepared by weighing 12.1,11.2, 10.5, 10.2, 3.0, 9.8 mg, respectively, and diluted to 100 mL with phosphate buffer solution. A 0.5 mL of the solution was added to 25 mg of 5% Cu(II)O/silica particles which was previously cleaned by heating in a furnace for 1 h at 450°C. A blank containing the buffer and the particles was also prepared. The samples were then shaken continuously for 1 h at room temperature using a vortex mixer (Fischer Scientific, model G-560). The suspensions of the different solutions were taken with a capillary tube with (i.d., 3 mm). The samples were centrifuged for 5 min and the liquid fraction was taken using a capillary tube. The liquids and the suspensions were then analyzed by EPR. The remaining liquid was discarded and the samples were dried under vacuum at room temperature for 12 h prior to EPR analyses.

2.8 Determination of the Interaction of Particulate Matter with Biological Fluids

Eight samples containing 25 mg of particles dosed with 2-monochlorophenol were prepared. Then 0.5 mL of adult mice BALF solution from LSU-HSC was added to the samples. The suspensions were shaken continuously for 0.5, 1, 3, 4, 5, 6, 8, and 12 h. And at every time

interval, suspensions were taken using a capillary tube (i.d., 3 mm) and the samples were then centrifuged and sample from the liquid fraction was taken with a capillary tube for EPR analysis. The remaining liquid fraction was discarded and the particles were dried in a vacuum for 12 h at room temperature prior to EPR analysis.

2.9 Spin Trapping of Reactive Oxygen Species

2.9.1 Materials

High purity 5,5-dimethyl-1-pyrroline-N-oxide—DMPO (ENZO, > 99.9+%) was used without further purification. L-Ascorbic acid (Fischer, 98+%), β -nicotinamide adenine dinucleotide phosphate—NADPH (Sigma, > 98+%), superoxide dismutase from bovine—SOD (3619 U/mg), catalase from bovine liver—CAT (3809 U/mg), deferoxamine mesylate salt—DFM (assay TLS, 92.5%+) , diethylenetriaminepentacetic acid—DETAPAC (Sigma, 99+%), dimethyl sulfoxide—DMSO (Sigma, 99.9+%), hydrogen peroxide (Fluka, 30%, ACS grade), 2-monochlorophenol—2-MCP (Aldrich, 99+%), Cab-O-Sil® (Cabot, EH-5, 99+%), copper nitrate hemipentahydrate (Aldrich, 99.99+%), Phosphate Buffer Saline—PBS (Fischer, NaCl 0.138M: KCl 0.0027M), acetonitrile—AcN (Fischer, 99.8+%), and 4-hydroxyl-2,2,6,6-tetramethylpiperidine-1-oxyl—TEMPOL (Aldrich, 98+%).

2.9.2 EPFR Surrogate Synthesis

Particles containing EPFRs were synthesized from the method describe in **Section 2.3**. For comparison purposes, undosed Cu(II)O/silica particles, which do not contain stabilized surface EPFRs were also used and referred to as non-EPFRs.

2.9.3 Calculation of OH Radical Concentration

EPR spectra of DMPO-OH adduct were recorded, and it was assumed that one mole of DMPO-OH adduct corresponds to one mole of OH in solution. DMPO-OH adduct

concentration was determined by double integration of the second line (at low magnetic field) of their respective four-line spectra and were compared with 4-hydroxyl-2,2,6,6-tetramethylpiperidine-1-oxyl (TEMPO-OH) or TEMPOL as a standard. The TEMPOL solution in the concentration range of 0.05 – 1 mM was used for calibration (by double integration of second line of TEMPOL with respect to the three-line EPR spectra at low magnetic field) while all conditions were kept the same for both standard and experimental samples. (9). The TEMPOL concentration was verified by using an extinction coefficient of $13.2 \pm 0.1 \text{ M}^{-1}\text{cm}^{-1}$ at 436 nm using UV-Vis measurement. (9).

2.9.4 Comparison with EPR Spectra in the Literature

UN-SCAN-IT Automated Digitizing System, Version 6.0 (Silk Scientific Corporation, <http://www.silkscientific.com/>) was used to digitize scanned EPR spectra published in the literature. The absolute value of the resonance field is different for each original spectrum due to different microwave frequencies. To facilitate comparison of spectra, all experimental and literature X-band spectra were recreated on the same field scale, generally, in a 100-G wide field window.

2.9.5 *In Vitro* Studies

5% Cu(II)O/silica (Cu(II)O deposited on Cab-O-Sil and referred as catalyst) was exposed to vapors of 2-monochlorophenol in a reaction chamber at a temperature of 230 °C to make stable radicals on the catalyst surface (referred as EPFRs) elucidated in **Section 2.3** (4) Two solutions saturated by air have been subjected to EPR examination: 1) A *reference* solution containing; Catalyst (50 µg/mL) + DMPO (150 mM) + additives + buffer, and 2) A *sample* solution containing; EPFRs bound on catalyst (50 µg/mL) + DMPO (150 mM) + additives + buffer. The additives referred to contains, NADPH, ascorbic acid, sodium azide, sodium

formate, SOD, CAT, and chelators. A phosphate buffered saline (PBS, 0.01M) was used to balance and keep the pH at 7.4 with a final sample volume of 200 μL . In both cases, the order of components was added in this sequence; deionized water + reference (sample) solutions + additives + DMPO at a final volume of 200 μL . Before adding DMPO the solutions were sonicated for 5 min with laboratory sonicator (Fisher Scientific, FS-20, 40W power). The solutions were kept in the dark and mixed with a vortex mixer (Fischer, model G-560) for 30 s prior to each measurement. A $\sim 20 \mu\text{L}$ sample was transferred into an EPR capillary tube (i.d. $\sim 1 \text{ mm}$, o.d. $\sim 1.55 \text{ mm}$) and the end was sealed by a Critoseal (Fisherbrand). Then, the capillary was inserted into an ordinary 4 mm EPR tube and was placed into the EPR resonator and the EPR spectra were acquired (10). The intensity of the spectra was reported in arbitrary units, DI/N, which is the double integrated (DI) intensity of the EPR spectrum that has been normalized (N) to account for the conversion time, receiver gain, number of data points, and sweep width [<http://www.bruker-biospin.com/winepr.html?&L=0>]). Each measurement was reproduced at least twice and the intensities of the spectra were averaged over all the experiments performed.

The use of chelators such as deferoxamine mesylate (DFM), DETAPAC, and EDTA were not used to minimize the iron content in solution. The reason was that the chemistry of interaction of chelators upon contact with the catalyst surface is not clear; The addition of these chelators can drastically change the surface reactivity by modifying the redox potential of metals (11) and can probably destroy (or extract) the adsorbed EPFRs which can happen in our case. Additionally, the oxidizing species formed by the Fenton-type reactions are dependent on the nature of the iron chelator (12, 13). These precautions were taken into consideration, and, thus, we have chosen to use a comparative method of analyses (reference and sample solutions) and

excluded the the addition of other components to minimize possible secondary reactions. Additionally, the buffer was prepared in deionized water and treated with Chelex 100 ion-exchange resin (Bio-Rad Laboratories, Hercules, LA) to remove trace heavy metal contaminants (14) with no significant changes on the results of the spin trapping experiment.

2.9.6 EPR Measurements

EPR spectra were recorded on a Bruker EMX-20/2.7 EPR spectrometer (X-band) with dual cavities with the same parameter described in **Section 2.4** with the exception of the power which was set to 10 mW. The exact g-values for key spectra were determined by comparison with DPPH.

2.10 Basics of Electron Paramagnetic Resonance Spectroscopy (EPR)

EPR is a spectroscopic technique which detects species containing one or more unpaired electrons. In the absence of a magnetic field, the two states of electron the α (+1/2, low energy electrons) and β (-1/2, high energy electrons) states are degenerate and the electrons are oriented randomly. When an external magnetic field is applied, the unpaired electrons align either parallel or anti parallel to the external magnetic field. As a consequence, the α and β states have now different energies. This is called the Zeeman effect.

Initially, the Boltzmann population in the α states is greater than the population in the β states. When microwave radiation is applied to the sample this causes the electrons in the α states to jump to the higher energy β state. The magnetic field is then scanned so that the energy of the incident radiation matches the energy of the splitting of the two states.

The field when this condition is achieved is called the field of resonance. The field of resonance is given by the equation:

$$h\nu = g\mu_o B \qquad \text{equation 6}$$

Where: h is a Planck's constant ($h = 6.63 \times 10^{-34}$ J's); ν (Hz) is the frequency of the incident microwave; μ_o is Bohr magneton ($\mu_o = 9.27 \times 10^{-24}$ J T⁻¹); and B (Tesla) is the magnetic field. The first-derivative EPR spectrum is given in **Figure 2.5**.

The g -value is determined as the center of the spectrum which the peak maxima in the absorption spectrum. The ΔH_{p-p} is measured as the distance between the maximum and the minimum features on the spectrum. The signal in EPR is in the first-derivative which arises from the filtering effect as a consequence of field modulation.

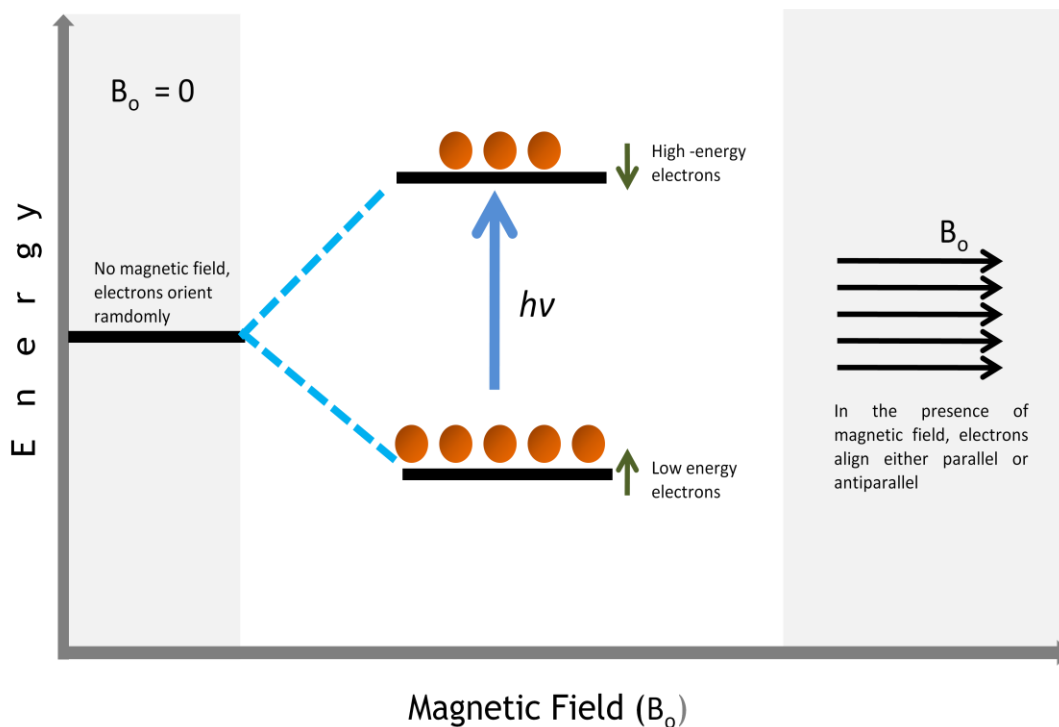


Figure 2.4. The Zeeman effect

2.11 EPR Instrumentation

The Bruker EPR we used consists of four parts: A microwave bridge, a cavity, sample holder, and two large magnets. It also consists of a cooling unit, and a console which controls the

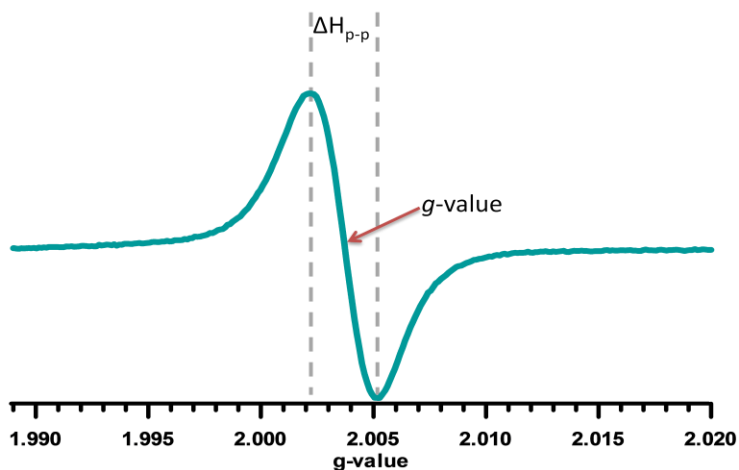


Figure 2.5. First-derivative EPR spectrum

other components and are interfaced to a data acquisition and processing system. The schematic set-up of the EPR instrumentation is illustrated in **Figure 2.6**.

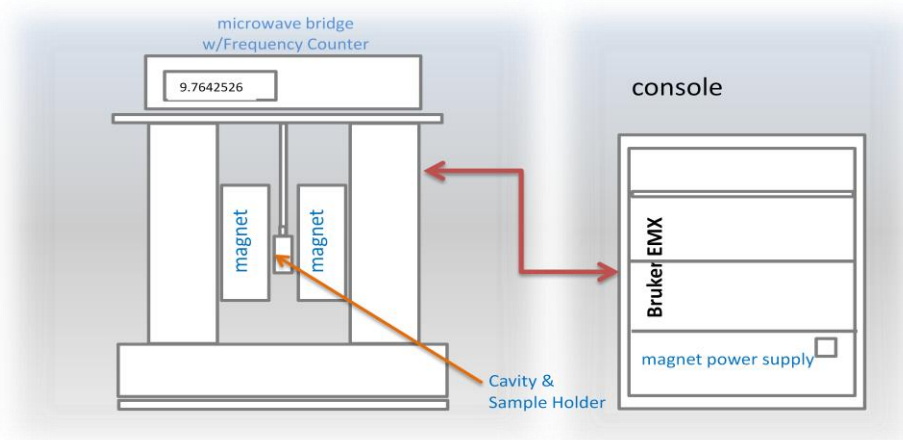


Figure 2.6. Instrument set-up of the Bruker EMX2.0/2.7 EPR spectrometer

2.12 References

1. Hoffman, R.V.; Eiceman, G.A.; Long, Y.T.; Collins, M.C.; Lu, M.Q. Mechanism of chlorination of aromatic compounds adsorbed on the surface of fly ash from municipal incinerators. *Environ. Sci. Technol.* **1990**, *24*, 11, 1635-1641.
2. Hsiao, M.C.; Wang, H.P.; Huang, Y.J.; Yang, Y.W. EXAFS study of copper in waste incineration fly ashes. *J. Synchrotron Radiat.* **2001**, *8*, 931-933.
3. Stieglitz, L.; Zwick, G.; Beck, J.; Roth, W.; Vogg, H. On the de-novo synthesis of PCDD/PCDF on fly ash of municipal waste incinerators. *Chemosphere* **1989**, *18*, 1-6, 1219-1226.
4. Lomnicki, S.; Truong, H.; Vejerano, E.; Dellinger, B. Copper oxide-based model of persistent free radical formation on combustion-derived particulate matter. *Environ. Sci. Technol.* **2008**, *42*, 13, 4982-4988.
5. Sakai, T.; Hattori, M. Thermal decarbonylation of catechol, hydroquinone and resorcinol. *Chem. Lett.* **1976**, 11, 1153-6.
6. Herring, A.M.; McKinnon, J.T.; Petrick, D.E.; Gneshin, K.W.; Filley, J.; McCloskey, B.D. Detection of reactive intermediates during laser pyrolysis of cellulose char by molecular beam mass spectroscopy, implications for the formation of polycyclic aromatic hydrocarbons. *J. Anal. Appl. Pyrolysis* **2003**, *66*, 1-2, 165-182.
7. Lomnicki, S.; Dellinger, B. Formation of PCDD/F from the pyrolysis of 2-chlorophenol on the surface of dispersed copper oxide particles. *Proc. Combust. Inst.* **2003**, *29*, 2463-2468.
8. Yordanov, N.; Christova, A. DPPH as a primary standard for quantitative EPR spectrometry. *Appl. Magn. Reson.* **1994**, *6*, 1, 341-345.
9. Yordanov, N.D.; Lubenova, S. Effect of dielectric constants, sample container dimensions and frequency of magnetic field modulation on the quantitative EPR response. *Anal. Chim. Acta* **2000**, *403*, 1-2, 305-313.
10. Nakagawa, K. Is quartz flat cell useful for the detection of superoxide radicals? *J. Act. Oxyg. Free Rad.* **1994**, *5*, 81-85.

11. Fubini, B.; Mollo, L. Role of iron in the reactivity of mineral fibers. *Toxicol. Lett.* **1995**, 82/83, 951-960.
12. Tomita, M.; Okuyama, T.; Watanabe, S.; Watanabe, H. Quantitation of the hydroxyl radical adducts of salicylic-acid by micellar electrokinetic capillary chromatography - oxidizing species formed by a Fenton reaction. *Arch. Toxicol.* **1994**, 68, 7, 428-433.
13. Yamazaki, I.; Piette, L.H. EPR spin-trapping study on the oxidizing species formed in the reaction of the ferrous ion with hydrogen-peroxide. *J. Am. Chem. Soc.* **1991**, 113, 20, 7588-7593.
14. Finkelstein, E.; Rosen, G.M.; Rauckman, E.J. Spin trapping of superoxide and hydroxyl radical - practical aspects. *Arch. Biochem. Biophys.* **1980**, 200, 1, 1-16.

CHAPTER III. RESULTS*

The data in this section has been obtained using EPR spectroscopic analyses. The g-value and ΔH_{p-p} were computed using Bruker WinEPR data processing software. To assist in the identification of the structure of the surface-bound EPFRs observed from the EPR analyses, the molecular products were analyzed by extracting the particles with methanol and dichloromethane and analyzed by GC-MS method. A vacuum-exposure system was used to generate the EPFRs on particle-metal oxide system.

3.1 Formation of Paramagnetic Species on the Surface of Transition Metal Oxide on Silica Particles

The adsorption of various hydroxylated compounds (catechol, hydroquinone, and phenol) and chlorinated aromatic adsorbates (1,2-dichlorobenzene, monochlorobenzene, and 2-monochlorophenol) on different transition metal oxides on silica particles from 150 to 400 °C resulted in formation of EPR signals that may be attributed to paramagnetic and radical species. The EPR spectra in **Figure 3.1** show complex features and probably unresolved hyperfine splitting. Almost all the adsorbates showed complex spectra except phenol which has symmetric spectra. The spectra presented in **Figure 3.1** are not to scale relative to other adsorbates.

Peak fitting analysis done on the integrated EPR spectra resulted in the identification of 3 different spectral components, denoted as g1, g2, and g3 on the basis of their increasing g-values values of approximately 1.9970, 2.0040, and 2.0050. An example of the peak fitting analysis for catechol in Fe(III)₂O₃/silica at 250 °C depicted in **Figure 3.2**. The peak fitting analysis reveals three distinct peaks. In general, the shape of the EPR spectra and the relative intensities of the g1,

* Part of this manuscript is reproduced with permission from Vejerano, E.; Lomnicki, S.; Dellinger, B. Formation and stabilization of combustion-generated environmentally persistent free radicals on an Fe(III)₂O₃/silica surface. *Environ. Sci. Technol.* 2011, 45, 2, 589-594. Copyright 2011. American Chemical Society.

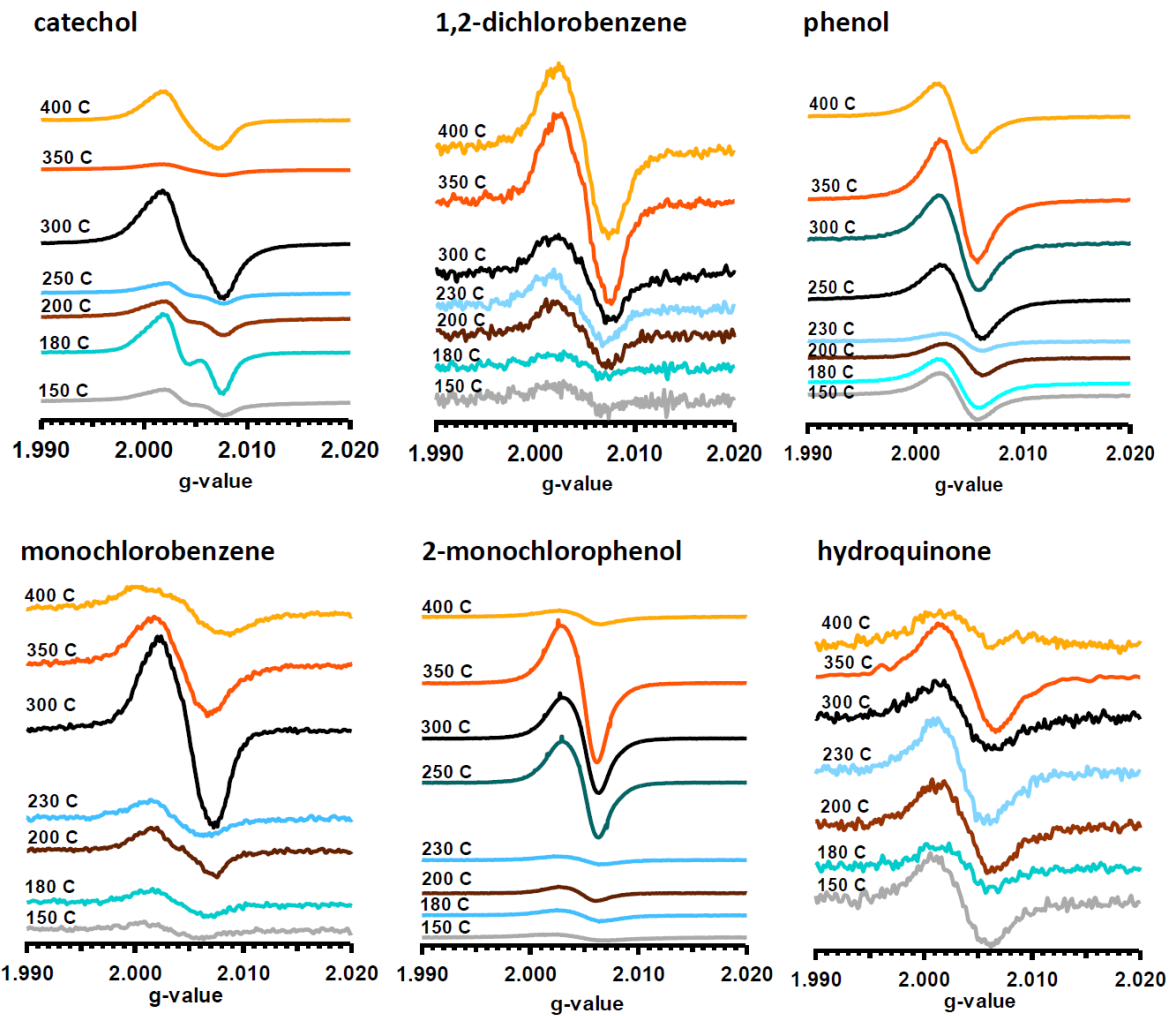


Figure 3.1. Temperature dependence of the EPR spectra of different adsorbates dosed at different temperatures on $\text{Fe(III)}_2\text{O}_3$ on silica surface

g2, and g3 signals varied with adsorption temperature. A summary of the peak fitting results for Fe(III)₂O₃ is presented in **Table 3.1** with their g-values and fitted area for different adsorbates at different temperatures.

3.1.1 Formation of g1 on Fe(III)₂O₃ and Ni(II)O on Silica Surface

The adsorption of the aromatic adsorbates on the surface of different transition metal oxides resulted in an EPR signal with a g-value of 1.9990-2.0020 designated as g1. The same signal with similar range of g-value was also observed with our previous study on Cu(II)O/silica.

However, on Fe(III)₂O₃/silica particles, the g1 band were only observable for catechol and hydroquinone following EPR spectral peak fitting (cf. **Table 3.1**). Catechol and hydroquinone exhibited high g1 intensity which facilitated peak fitting and detection, while the lower g1 intensities of EPFRs for other adsorbates are unidentifiable in these systems. Similar

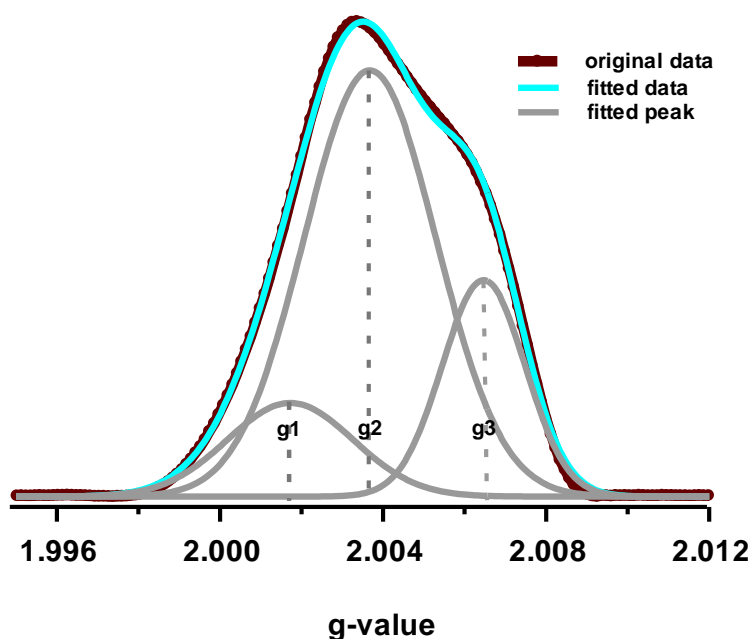


Figure 3.2. Peak fitting procedure done on catechol at 250 °C dosed on Fe(III)₂O₃ /silica surface

behavior were also observed on Ni(II)O/silica particles. In the case of Ni(II)O/silica particles, the adsorbates—catechol, monochlorobenzene, and 2-monochlorophenol showed the formation of the g1 signal at all temperatures. 1,2-Dichlorobenzene and phenol on the other hand, showed no detectable amount of g1 signal at all temperatures. The typical values of the g1 signal for Ni(II)O for the different adsorbates range from 1.9970 to 2.0021 (cf. **Table 3.3**).

3.1.2 Formation of g2 and g3 Radicals on Fe(III)₂O₃/Silica Surface

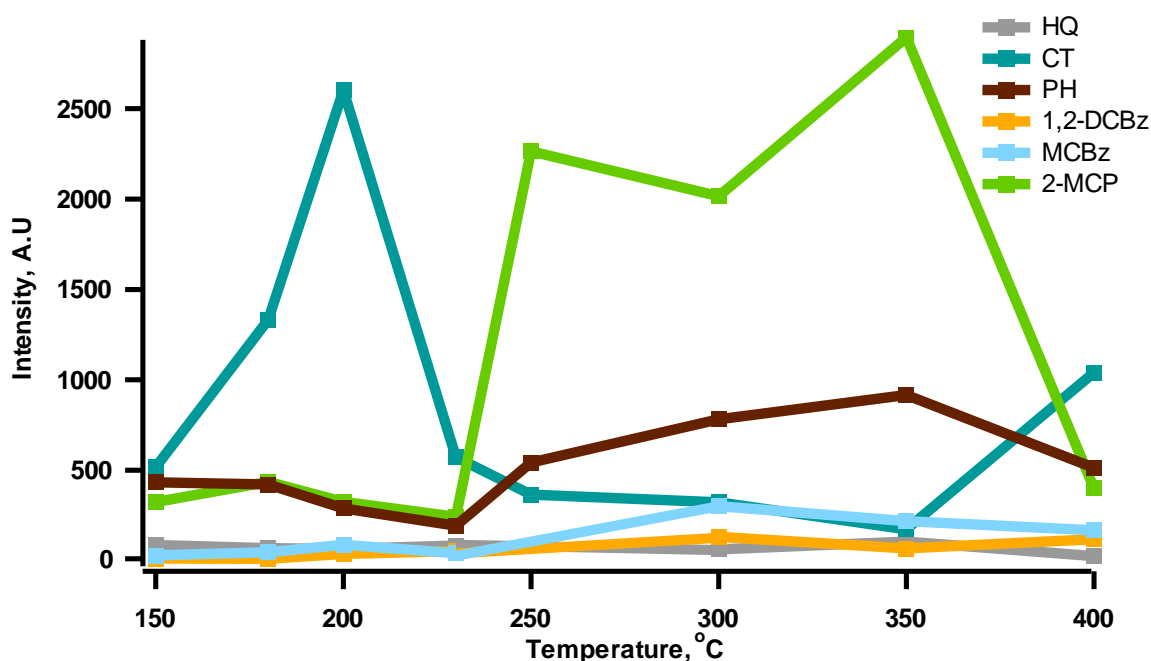


Figure 3.3. Yield of organic EPFRs (g2 + g3) adsorbed on 5% Fe(III)₂O₃/silica for different adsorbates and dosing temperatures

The adsorption of various aromatic adsorbates on Fe(III)₂O₃ on silica surface yielded one or two types of EPR signals depending on the number and type of substituent groups present. It is only in the case of phenol where a single EPFR is observed.

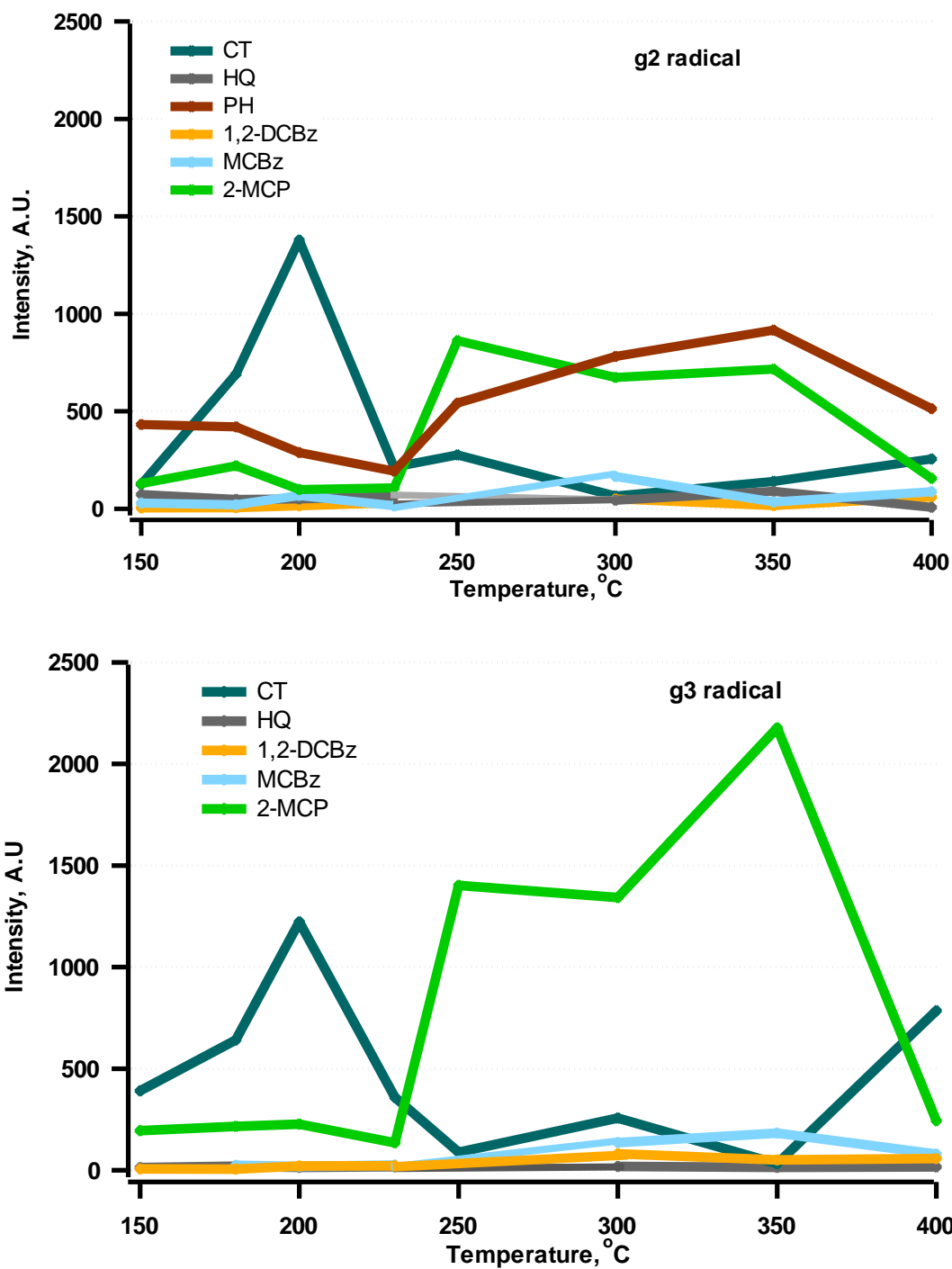


Figure 3.4. Intensity of g2 and g3 radicals on 5% Fe(III)₂O₃/silica from deconvolution of EPR spectra for different adsorbates and dosing temperatures

3.1.2.1 Phenol

Phenol formed only one type of EPR signal in moderate yield, with the EPR spectrum consisting of a symmetrical, narrow ($\Delta H_{pp} = 5.7\text{-}6.1$ Gauss), and single line with a g-value of 2.0040-2.0044 for adsorption temperatures from 150 to 400 °C (cf. **Table 3.1**). This is a g2-type radical, which exhibited a maximum yield at 300-350 °C (cf. **Figure 3.4**). At 400 °C, a sudden shift of g-value to 2.0036 is observed, together with an overall drop of EPFR yield.

3.1.2.2 Hydroquinone and Catechol

The chemisorption of catechol and hydroquinone on the $\text{Fe(III)}_2\text{O}_3$ surface resulted in spectral components with g-values of 2.0053-2.0056 for hydroquinone and 2.0057-2.0067 for catechol, respectively, for adsorption temperature of 150 to 350 °C (cf. **Table 3.1**). These values (denoted as g3) are similar to those formed over Cu(II)O surfaces (*I*). In addition, a g2-type radical was detected in high yields at all temperatures (**Figure 3.4**), with a lower g-value of 2.0033-2.0040 for hydroquinone and 2.0031-2.0040 for catechol. Whereas, the result for Cu(II)O , only the g3 signal were detected over this temperature range. The EPFR yield for the g2 and g3 components for hydroquinone was approximately constant at all temperature range and relative low from 150 to 350 °C compared to other adsorbates. Catechol displayed a maximum EPFR yield at 200 °C (cf. **Figure 3.3**). At 400 °C, EPFRs from hydroquinone became nearly undetectable, while EPFRs from catechol increased with the g-value decreasing to 2.0029.

3.1.2.3 1,2-Dichlorobenzene and 2-Monochlorophenol

The peak fitting of the EPR spectra revealed both g2- and g3-type, EPFR signals (cf. **Figure 3.4**). In contrast to catechol, neither 1,2-dichlorobenzene nor 2-monochlorophenol exhibited maxima at lower temperatures. 2-Monochlorophenol exhibited maxima in the g2 radical concentration at 250 °C and g3 radical concentration at 350 °C (cf. **Figure 3.4**). In

contrast to unchlorinated adsorbates (phenol, hydroquinone, and catechol), the chlorinated adsorbates 1,2-dichlorobenzene and 2-monochlorophenol, exhibited lower EPFR yields. In contrast to $\text{Fe(III)}_2\text{O}_3$, the chlorinated adsorbates resulted in high yields of EPFRs on Cu(II)O (1).

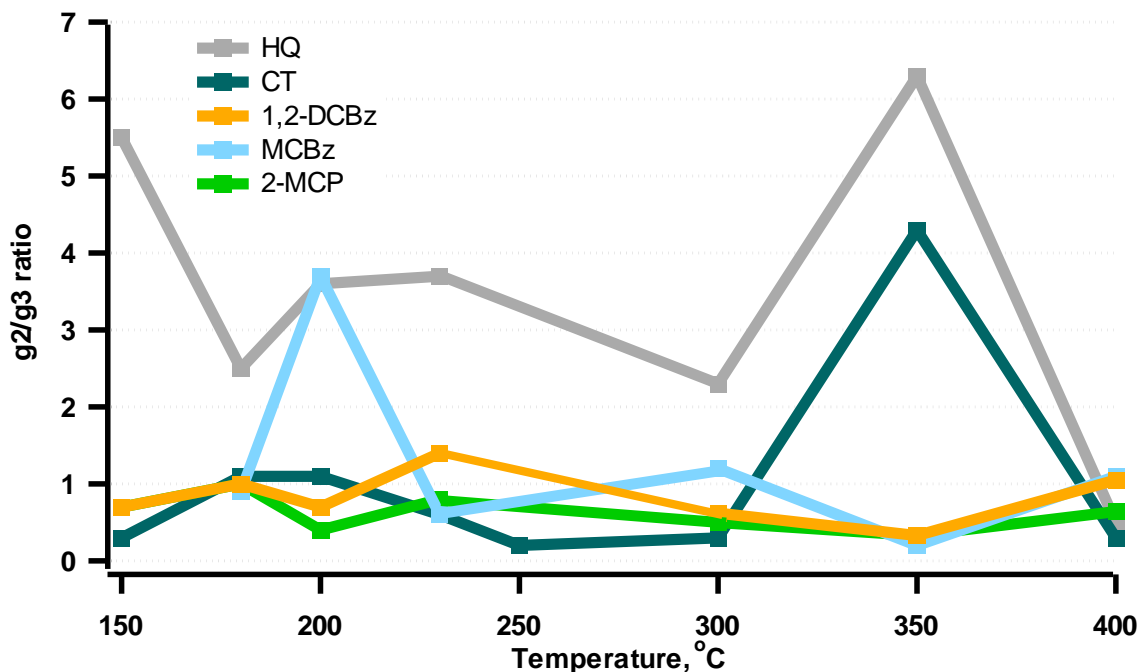


Figure 3.5. Ratio of g2 and g3 components of the different adsorbates as a function of dosing temperature on $\text{Fe(III)}_2\text{O}_3/\text{silica}$ surface

3.1.2.4 Monochlorobenzene

The chemisorption of monochlorobenzene on the surface of $\text{Fe(III)}_2\text{O}_3/\text{silica}$ forms a single signal at lower temperature which is consistent with its nearly symmetric EPR spectra. At 150 °C, a single-line EPR spectrum with a g-value of 2.0033, characteristic of g2 radical was recorded. However at higher temperatures, another EPR signal, a g3-type radical with a g-value of 2.0053-2.0060 was observed (cf. **Figure 3.4**). Moreover, the ratio of the g2 to g3 type radical

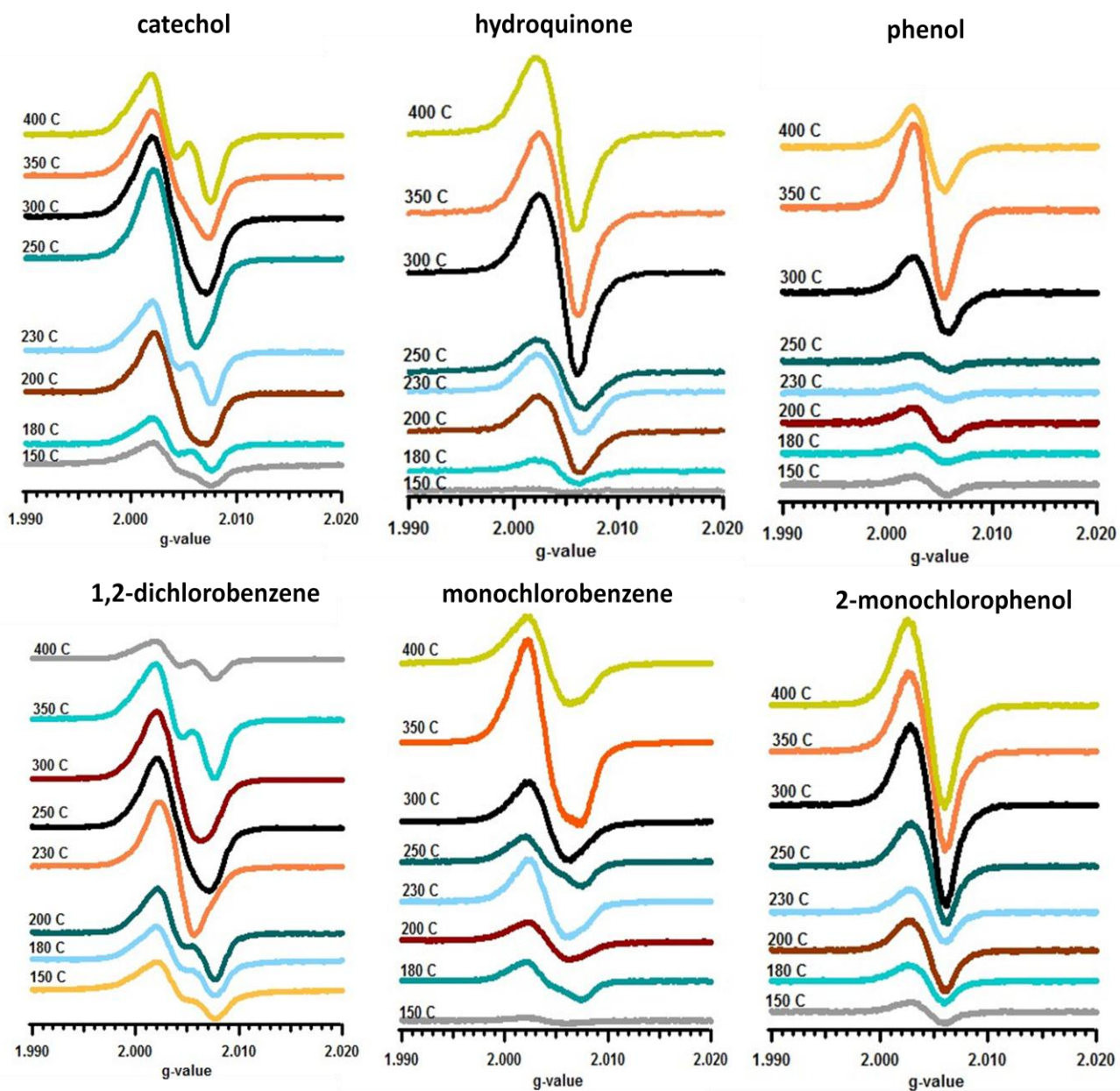


Figure 3.6. Temperature dependence of the EPR spectra of different adsorbates dosed on 5% Ni(II)O/silica

concentration was close to 1 and resembled the profile for 1,2-dichlorobenzene. The GC-MS analysis of the extract revealed the formation of 2-monochlorophenol.

3.1.3 Formation of g2 and g3 Radical on Ni(II)O on Silica Surface

The adsorption of various aromatic molecular adsorbates on the surface of 5% Ni(II)O/silica particles from 150 to 400 °C produces an EPR spectra that are asymmetrical indicating that one or more types of EPFRs are present (cf. **Figure 3.6**) similar with the studies done on Cu(II)O and Fe(III)₂O₃. In general, the yield of EPFRs from various adsorbates increases from 150 °C, until exhibiting a maximum at higher temperature between 250-300 °C except for phenol and monochlorobenzene, which have maxima at 350 °C. The peak fitting of the EPR spectra resulted in the identification of three different spectral components similar to iron and copper, denoted as g1, g2, and g3, with g-values of approximately 2.0010, 2.0040, and above 2.0050, respectively. The shape of the EPR spectra and the relative intensities of the g1, g2, and g3 signals generally varied with adsorption temperature. **Table 3.3** presents the peak fitting results for the spectra obtained from 150 to 400 °C. The total paramagnetic signal intensity of the adsorption for different adsorbates on Ni(II)O/silica is presented in **Table 3.4**

3.1.3.1 Phenol

Studies with phenol on Cu(II)O and Fe(III)₂O₃ on silica revealed only one EPFR is formed. Analysis of the EPR spectra for phenol adsorbed on Ni(II)O on silica showed similar behavior with a nearly symmetrical spectra that indicated only one type of EPFR was present. The g-value observed was between 2.0039 to 2.0043 from adsorption temperatures of 150 to 400 °C (cf. **Table 3.3**). The EPFR yield increases from 150 to 350 °C with a maximum at the latter and subsequent decline at 400 °C. A decrease in EPFR yield at 400 °C and a slight shift in the g-value were observed. In comparison with other adsorbates, phenol has the lowest EPFR yields.

Table 3.1. Summary of the peak fitting results for the different adsorbates dosed on Fe(III)₂O₃/silica at different temperatures

Temperature (°C)		HQ		PH		CT		2-MCP		MCBz		1,2-DCBz	
		g-value	Area	g-value	Area	g-value	Area	g-value	Area	g-value	Area	g-value	Area
150	g1	1.9990	2.27			2.0011	120.51						
	g2	2.0034	73.25	2.0040	432.62	2.0031	125.36	2.0028	129.22	2.0033	29.18	2.0030	4.59
	g3	2.0055	13.32			2.0057	391.33	2.0051	194.76			2.0056	6.56
180	g1	2.0015	20.48			2.0008	151.12						
	g2	2.0034	48.54	2.00403	420.76	2.0032	691.21	2.0034	220.62	2.0024	21.3	2.0032	5.06
	g3	2.0053	19.81			2.0061	641.45	2.0055	215.722	2.0053	24.54	2.0056	5.01
200	g1	2.0011	19.62			2.0000	231.71						
	g2	2.0036	50.5	2.0045	289.14	2.0031	1378.67	2.0030	98.27	2.0035	68.59	2.0031	14.88
	g3	2.0061	13.98			2.0062	1223.15	2.0050	226.81	2.0063	18.71	2.0057	21.51
230	g1	2.0006	17.38			2.0019	237.39						
	g2	2.0039	65.16	2.0044	193.02	2.0036	213.55	2.0040	107.34	2.0026	15.47	2.0030	31.18
	g3	2.0061	17.71			2.0062	358.78	2.0050	134.86	2.0049	25.71	2.0057	22.25

Table Cont'd

Temperature (°C)		HQ		PH		CAT		2-MCP		MCBz		1,2-DCBz	
		g-value	Area	g-value	Area	g-value	Area	g-value	Area	g-value	Area	g-value	Area
250	g1					2.0017	57.98						
	g2			2.0042	542.19	2.00367	276.71	2.0036	862.16				
	g3					2.0065	88.13	2.0053	1402.33				
300	g1	2.0002	9.08			2.0019	105.99						
	g2	2.0034	43.99	2.0043	781.66	2.0034	66.34	2.0033	673.33	2.0035	165.71	2.0032	50.27
	g3	2.0063	18.78			2.0057	256.67	2.0052	1342.17	2.0060	135.77	2.0058	81.13
350	g1	1.9999	7.67			2.0014	28.56						
	g2	2.0040	90.21	2.0040	916.74	2.0041	140.15	2.0030	716.14	2.0025	35.05	2.0024	16.53
	g3	2.0068	14.28			2.0067	32.67	2.0050	2177.87	2.0047	183.25	2.0055	50.51
400	g1	2.0017	3.83			2.0016	282.16						
	g2	2.0038	8.23	2.0036	513.59	2.0029	255.84	2.0033	156.25	2.0028	87.41	2.0034	60.33
	g3	2.0056	16.67			2.0053	784.81	2.0053	243.24	2.0065	80.19	2.0059	57.36

Table 3.2. Radical concentration (g2 +g3) of surface-bound EPFRS (spin/g of Fe(III)₂O₃/silica) at different temperatures dosed on Fe(III)₂O₃/silica

Temperature (°C)	Adsorbates					
	CAT	HQ	PH	1,2-DCBz	MCBz	2-MCP
150	2.45 x 10 ¹⁷	3.42 x 10 ¹⁶	1.66 x 10 ¹⁷	4.29 x 10 ¹⁵	1.12 x 10 ¹⁶	1.25 x 10 ¹⁷
180	5.71 x 10 ¹⁷	3.42 x 10 ¹⁶	1.62 x 10 ¹⁷	3.87 x 10 ¹⁶	1.76 x 10 ¹⁶	1.68 x 10 ¹⁷
200	1.00 x 10 ¹⁸	3.23 x 10 ¹⁶	1.11 x 10 ¹⁷	1.40 x 10 ¹⁶	3.36 x 10 ¹⁶	1.25 x 10 ¹⁷
230	3.11 x 10 ¹⁷	3.86 x 10 ¹⁶	7.42 x 10 ¹⁶	2.05 x 10 ¹⁶	1.58 x 10 ¹⁶	9.31 x 10 ¹⁶
250	1.40 x 10 ¹⁷		2.09 x 10 ¹⁷			8.71 x 10 ¹⁷
300	1.65 x 10 ¹⁷	2.76 x 10 ¹⁶	3.01 x 10 ¹⁷	5.05 x 10 ¹⁶	1.16 x 10 ¹⁷	7.75 x 10 ¹⁷
350	7.74 x 10 ¹⁶	4.31 x 10 ¹⁶	3.53 x 10 ¹⁷	2.58 x 10 ¹⁶	8.40 x 10 ¹⁶	1.11 x 10 ¹⁸
400	5.09 x 10 ¹⁷	1.10 x 10 ¹⁶	1.98 x 10 ¹⁷	4.53 x 10 ¹⁶	6.45 x 10 ¹⁶	1.54 x 10 ¹⁷

Table 3.3. Summary of the peak fitting results for the different adsorbates dosed on Ni(II)O/silica at different temperatures

Temperature oC	g	CAT		DCBz		PH		MCP		MCBz		HQ	
		g-value	Area	g-value	Area	g-value	Area	g-value	Area	g-value	Area	g-value	Area
150	g1	1.9980	5.08					2.0017	11.32	2.0020	2.67		
	g2	2.0039	360.74	2.0037	799.41		28.44	2.0043	55.96	2.0041	62.59		
	g3	2.0070	89.50	2.0066	241.82	2.0044	37.43	2.0054	18.36			2.0044	7.84
180	g1	1.9970	51.67					2.0021	18.59				
	g2	2.0043	446.09	2.0039	824.12		24.08	2.0044	96.75	2.0039	356.21		
	g3	2.0065	194.35	2.0063	666.88	2.0044	38.66	2.0062	17.93	2.0067	61.05	2.0044	93.21
200	g1	2.0005	52.93					2.0021	43.19				
	g2	2.0030	221.43	2.0035	870.23		20.63	2.0044	157.75	2.0036	344.02	2.0014	36.91
	g3	2.0051	643.74	2.0050	1081.66	2.0044	29.61	2.0055	55.14	2.0054	210.32	2.0046	295.48
230	g1	2.0021	29.32					2.0016	17.37			1.9986	12.80
	g2	2.0035	453.16	2.0041	1152.86		29.04	2.0044	138.52	2.0032	411.31		
	g3	2.0063	352.88	2.0071	148.33	2.0045	20.53	2.0055	36.11	2.0059	251.14	2.0045	348.14

Table Cont'd

Temperature (°C)	g	CAT		DCBz		PH		MCP		MCBz		HQ	
		g-value	Area	g-value	Area	g-value	Area	g-value	Area	g-value	Area	g-value	Area
250	g1	1.9996	27.20	1.9995	65.04		22.91	2.0013	20.57	2.0007	50.65	1.99947	24.92
	g2	2.0042	1209.90	2.0034	654.68	2.0042	89.14	2.0045	324.56	2.0035	391.35		
	g3	2.0054	117.71	2.0065	418.72			2.0052	22.55	2.0063	219.83	2.0046	335.44
300	g1	2.0016	181.19	2.0008	130.76			2.0020	64.91	2.0009	115.88	2.0001	44.60
	g2	2.0034	615.02	2.0036	1198.83		109.85	2.0046	530.19	2.0042	839.52		
	g3	2.0058	616.55	2.0058	544.29	2.0042	160.84	2.0059	56.39	2.0081	102.78	2.0044	605.2
350	g1	2.0007	86.63	2.0018	432.70			2.0020	64.72	2.0009	352.23	2.0002	40.13
	g2	2.0034	592.67	2.0034	525.89	2.0040	470.06	2.0045	526.05	2.0035	1279.93		
	g3	2.0061	416.23	2.0062	794.79			2.0049	57.43	2.0060	844.24	2.0057	560.72
400	g1	2.0021	315.10	2.0016	85.26			2.0020	77.43	1.9991	91.21	1.9993	32.40
	g2	2.0034	286.74	2.0034	322.72	2.0039	268.08	2.0044	562.82	2.0041	1139.82		
	g3	2.0062	453.77	2.0066	157.15			2.0053	64.91	2.0073	221.12	2.0042	683.10

Table 3.4. Radical concentration (g2 +g3) (spins/g of Ni(II)O/Silica) at different temperatures dosed on Ni(II)O/Silica

Temperature (°C)	Adsorbates					
	CAT	HQ	PH	1,2-DCBz	MCBz	2-MCP
150	1.75×10^{17}	3.02×10^{15}	2.53×10^{16}	4.38×10^{17}	1.85×10^{17}	3.29×10^{16}
180	2.66×10^{17}	3.58×10^{16}	2.41×10^{16}	4.00×10^{17}	1.93×10^{17}	5.13×10^{16}
200	3.53×10^{17}	1.28×10^{17}	1.93×10^{16}	5.00×10^{17}	2.29×10^{17}	9.85×10^{16}
230	3.21×10^{17}	1.39×10^{17}	1.91×10^{16}	5.74×10^{17}	2.64×10^{17}	7.38×10^{16}
250	5.21×10^{17}	1.39×10^{17}	4.31×10^{16}	7.51×10^{17}	2.54×10^{17}	1.41×10^{17}
300	5.43×10^{17}	2.50×10^{17}	1.04×10^{17}	7.21×10^{17}	4.07×10^{17}	2.51×10^{17}
350	4.21×10^{17}	2.31×10^{17}	1.81×10^{17}	5.75×10^{17}	9.52×10^{17}	2.49×10^{17}
400	4.06×10^{17}	2.75×10^{17}	1.03×10^{17}	2.17×10^{17}	5.58×10^{17}	2.71×10^{17}

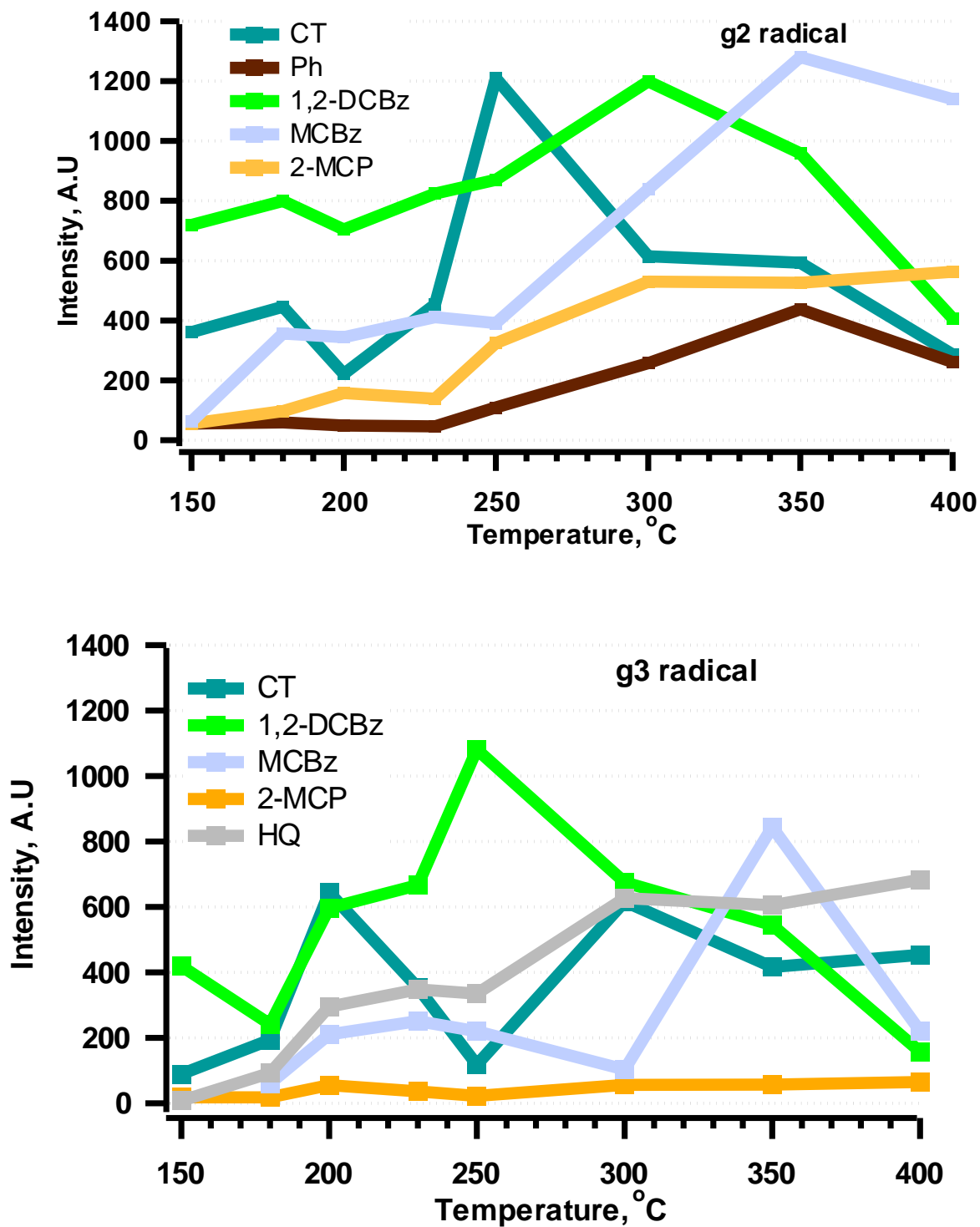


Figure 3.7. Yield of the g2 and g3 radicals on 5% Ni(II)O/silica for different adsorbates and dosing temperatures

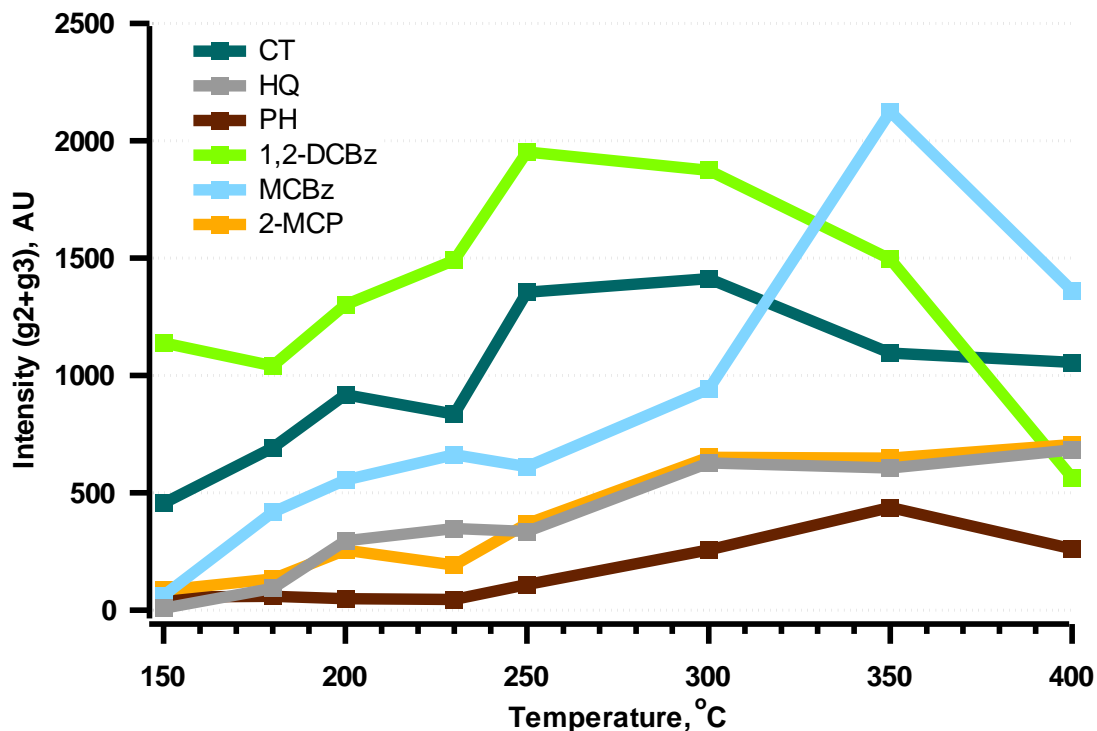


Figure 3.8. Yield of organic radical (g_2+g_3) for different precursors and dosing temperatures dosed on 5% Ni(II)O/silica

3.1.3.2 Monochlorobenzene

As shown in **Figure 3.8**, the EPFR yields of monochlorobenzene increase from 150 to 350 °C, with the maximum at 350 °C and a decrease at 400 °C. Peak fitting analysis of the EPR spectra (cf. **Figure 3.7**) showed the presence of a g_2 signal with g -value from 2.0035 to 2.0043. Analyses of the GC-MS extracts showed that the major molecular product formed at all temperatures was phenol. Another signal, g_3 , was observed at the higher temperature range of 300 to 400 °C with higher g -values from 2.0060 to 2.0081. The g -values were similar to the ones observed on Cu(II)O but were higher than those reported for Fe(III)₂O₃ whose g -value ranges from 2.0053 to 2.0060. This behavior was also observed in our previous studies with monochlorobenzene both on Cu(II)O and Fe(III)₂O₃/ silica. Analyses of the GC-MS extracts of

the 300 to 400 °C samples reveal the presence of 1,2-dichlorobenzene as one of the molecular products.

3.1.3.3 1,2-Dichlorobenzene and 2-Monochlorophenol

1,2-Dichlorobenzene has higher EPFR yields compared to the other adsorbates. The EPFR yields increase from 150 to 300 °C, with a maximum at the latter and a decrease at 350 and 400 °C. EPR spectral peak fitting procedure revealed two peaks: a g2 signal with g-values from 2.0034 to 2.0048, and a g3 signal, with g-values from 2.0050 to 2.0071. In contrast to 1,2-

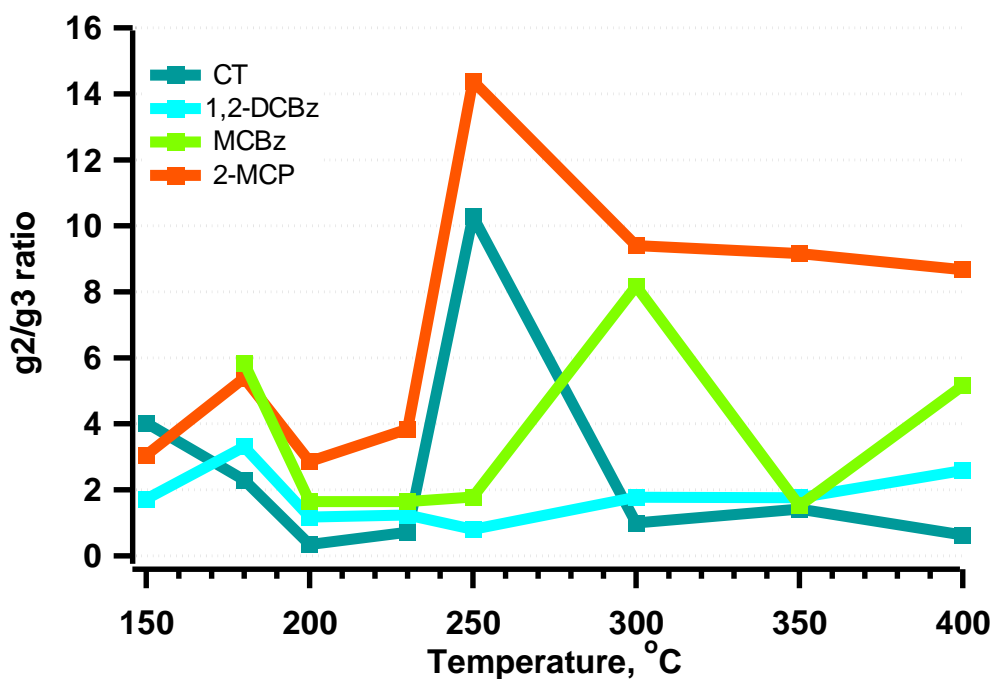


Figure 3.9. Ratio of the yield of the g2 and g3 organic radical for different adsorbates and dosing temperatures on Ni(II)O/silica

dichlorobenzene, 2-monochlorophenol exhibited no clear maximum, but the EPFR yields increase slightly from 150 to 400°C. 2-Monochlorophenol produces two EPR signals similar to 1, 2-dichlorobenzene, a g2-type signal with g-values from 2.0043 to 2.0046 and a g3-type signal with g-values from 2.0049 to 2.0059. For 1,2-dichlorobenzene, the ratio of the yields of g2-type radical with g3-type radical are approximately the same at all temperature range as depicted in **Figure 3.9**. Generally, for 2-monochlorophenol the yield of g2-type radical dominates as the temperature increases with a maximum yield at 250 °C and decreases slightly at higher temperature. The yield of g3-type radical increases with temperature but the yield of the g2-type radical still dominates at all temperatures. This behavior of 1,2-dichlorobenzene and 2-monochlorophenol were similar with the EPFRs on Cu(II)O and Fe(III)₂O₃ on silica (*1*).

3.1.3.4 Catechol and Hydroquinone

The adsorption of catechol on Ni(II)O on silica surface showed that the EPFR yields increase from 150 to 250 °C with a maximum at 250 °C and 300 °C and a slow decline thereafter up to 400 °C. EPR spectral peak fitting showed that two signals, g2 and g3, were observed. The g3 signal for catechol with g-values from 150 to 400 °C range from 2.0051 to 2.0065, which are higher than the ones reported in the literature and with the EPFRs on Cu(II)O and Fe(III)₂O₃/silica (*1*). Another EPR signal was also observed, g2 signal, with g-values ranging from 2.0031 to 2.0043 at all temperatures. From the plot of the ratio of the g2 and g3 radical yield (cf. **Figure 3.9**), the g2 signal dominates at 250 °C—the maximum, and the g2 and g3 EPFR yields are approximately equal at higher temperature range between 300 to 400 °C. However, at lower temperature, the major EPFR observed is g2-type. In contrast, the g2 signal in Cu(II)O only appears at higher temperature range. GC-MS extract analyses reveal that one of the molecular products formed at all temperatures is phenol.

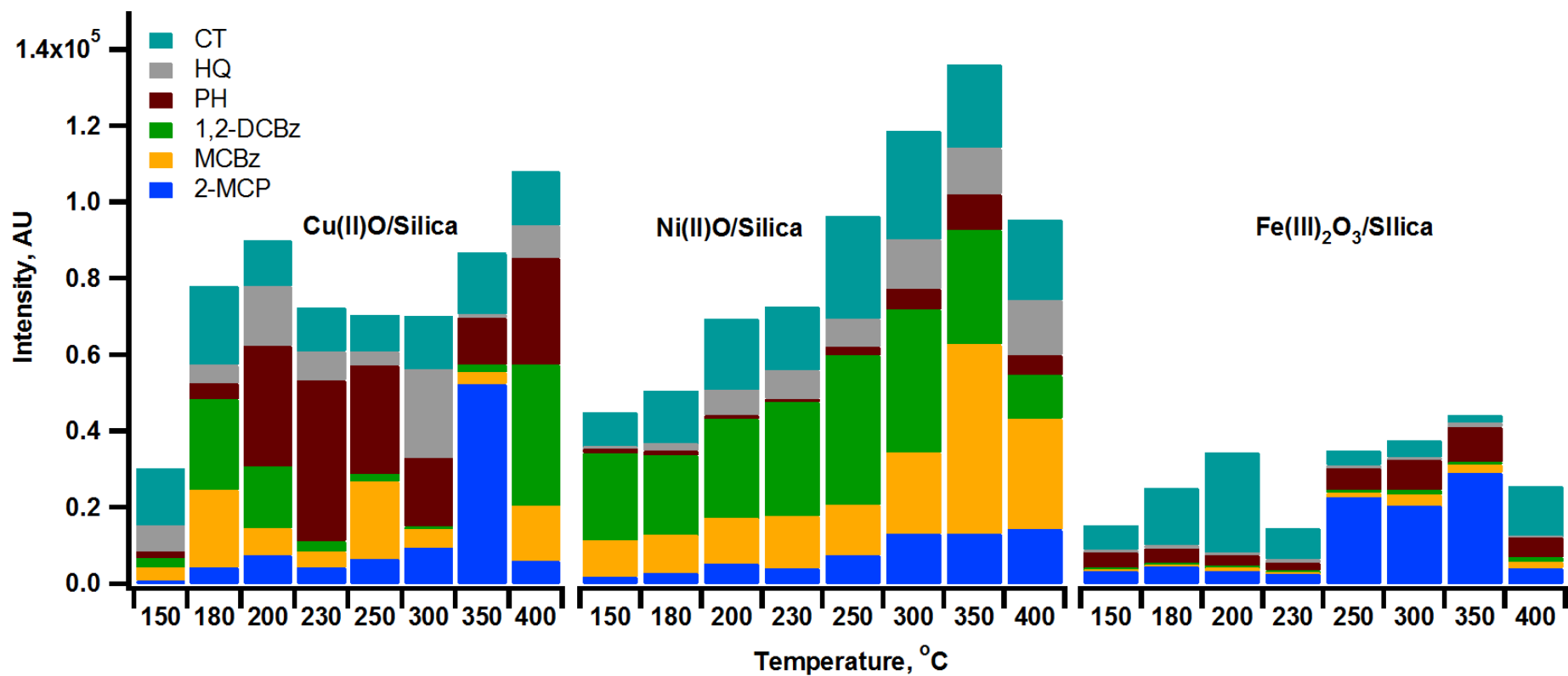


Figure 3.10. Comparative yield of the EPFR intensity (g₂ +g₃) for Cu(II)O, Fe(III)₂O₃, and Ni(II)O for different adsorbates and temperatures

The EPFR yield for hydroquinone on the other hand, generally increases from 150 to 400°C. EPR spectral peak fitting showed that only one signal was observed for hydroquinone with g-values from 2.0040 to 2.0057 which has a lower g-values compared to the EPFRs on copper. Analyses of the GC-MS extracts of hydroquinone showed no formation of phenoxy-based molecular product aside from the hydroquinone adsorbate itself.

3.2 Comparative Yields of the EPFRs on Ni(II)O, Cu(II)O, and Fe(III)₂O₃/Silica Surface

The yields of EPFRS for different transition metal oxides Cu(II)O, Ni(II)O, and Fe(III)₂O₃ on silica surface for catechol, hydroquinone, phenol, 1,2-dichlorobenzene, monochlorobenzene, and 2-monochlorophenol as adsorbates from 150 to 400 °C are presented in **Figure 3.10**. Generally, the EPFR yields for 2-monochlorophenol on Cu(II)O/silica has the highest yield compared to the other metal oxides with its maximum yield at 350 °C. The EPFR yields for 2-monochlorophenol on Ni(II)O and Fe(III)₂O₃ on silica are approximately equal. Generally, on Cu(II)O the yield for phenol was highest between 200 and 250 °C. With phenol as adsorbate, the EPFR yields shows the highest intensity on Cu(II)O, and the EPFR yields were low on both Ni(II)O and Fe(III)₂O₃ on silica surface which are approximately equal relative to each other. The EPFR yields on Cu(II)O/silica are ~10× higher than the Fe(III)₂O₃/silica. The EPFR yields for dichlorobenzene were highest on Ni(II)O which differs approximately 8× compared to the EPFRs yields on Cu(II)O, and as much by a factor of ~50 compared on Fe(III)₂O₃/silica which shows the lowest EPFR yields among all the metals. The EPFR yields for monochlorobenzene were similar to 1,2-dichlorobenzene which had the highest EPFR yield on Ni(II)O/silica compared to the yields of EPFRs on both Fe(III)₂O₃/silica and Cu(II)O/silica with the EPFRs yields on Fe(III)₂O₃/silica being the lowest and the EPFR yields for Fe(III)₂O₃/silica and Cu(II)O/silica differs by a factor of ~9 with Cu(II)O/silica having the higher yields. In

general, the EPFR yields for the chlorinated adsorbates, 1,2-dichlorobenzene and monochlorobenzene follows this trend: NiO > Cu(II)O > Fe(III)₂O₃.

For the doubly-hydroxyl substituted benzene adsorbate such as catechol, the EPFR yields are highest on Ni(II)O/silica at almost all temperatures compared to the EPFR yields on both Cu(II)O and Fe(III)₂O₃ on silica surface. However, at the lower temperature range of 150 °C to 230 °C, the EPFR yields for the three metals were approximately equal. Compared to Fe(III)₂O₃/silica, the EPFR yields on Cu(II)O/silica are higher by approximately ~8×. With hydroquinone as adsorbate, the EPFR yields measured on Ni(II)O surface compared on Cu(II)O is approximately 2×, whereas, the EPFR yields over Fe(III)₂O₃/silica surface were lower, and differ by a factor of approximately 8× compared with the two metals.

In general, the EPFR yields for the chlorinated (1,2-dichlorobenzene and monochlorobenzene) and the doubly-hydroxyl substituted adsorbates (catechol and hydroquinone) were highest on Ni(II)O/silica surface. It is only in the case of phenol were the yields were highest on Cu(II)O rather than on Ni(II)O surface. The EPFR yields over Fe(III)₂O₃/silica on the other hand, had the lowest yield for almost all the adsorbates.

3.3 Persistence and Lifetime of EPFRs on Transition Metal Oxide/Silica Surface

The persistency and stability of the combustion- and lab-generated radicals was studied by exposing them in air at ambient conditions. The variation in g-value and the ΔH_{p-p} of the EPFRs for different adsorbates on Ni(II)O, Fe(III)₂O₃ and Zn(II)O as a function of time are presented in **Appendix 1**.

3.3.1 Persistence and Lifetime of EPFRs on Fe(III)₂O₃/Silica Surface

The decays in air of the surface-bound radicals associated with Fe(III)₂O₃ are depicted in **Figure 3.11**. The half-lives of unchlorinated EPFRs of hydroquinone, phenol, and catechol were

2.9 (69.6 h), 3.8 (90.2 h), and 4.6 (111 h) days, respectively. 2-Monochlorophenol exhibited a half-life of 1.0 day (24 h). The half-lives of 1,2-dichlorobenzene and monochlorobenzene were unmeasurable. In contrast, the decay of EPFRS from 2-monochlorophenol is slow enough to be easily observed.

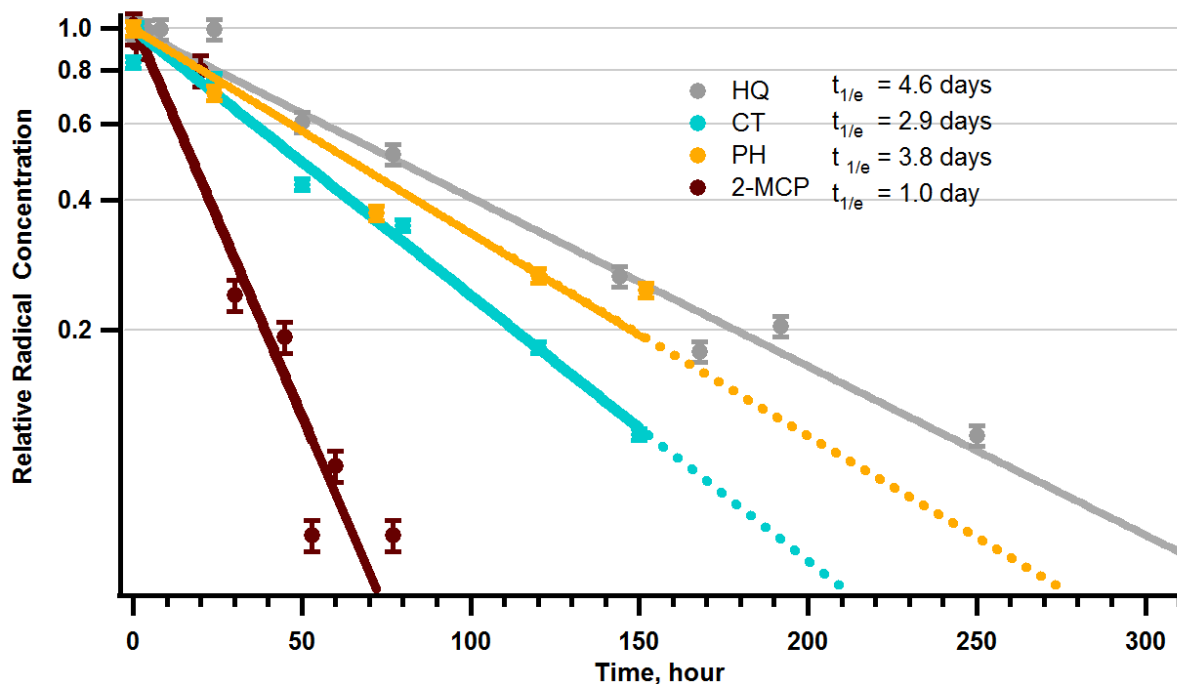


Figure 3.11. First-order decay profile of CT, HQ, PH and 2-MCP in 5% Fe(III)₂O₃/silica dosed at 230 °C and exposed to air at ambient condition

3.3.2 Persistence and Lifetime of EPFRs on Ni(II)O/Silica Surface

Exposure of the surface-bound EPFRs associated with Ni(II)O in air at ambient condition showed decay in intensities at different time intervals presented in **Figure 3.12**. The half-lives of the unchlorinated EPFRs of catechol is 2.8 days while hydroquinone has a half-life of 1.5 days. Phenol on the other hand shows two decay—a fast decay with half-life of 0.56 day and a second, slow decay with a half-life of 5.2 days, which is the longest half-life observed for all the adsorbate which is similar for the decays of EPFRs observed on Cu(II)O and Fe(III)₂O₃. The

half-lives of the EPFRs for the unchlorinated adsorbates on $\text{Fe(III)}_2\text{O}_3$ are non-measurable, however, they are measurable and have higher half-lives on Ni(II)O similar to the EPFRs on Cu(II)O/silica study. 1,2-Dichlorobenzene, monochlorobenzene, and 2-monochlorophenol have half-lives of 1.7-3.8 days. The lifetimes and persistence of the EPFRs observed on Ni(II)O/silica is similar to $\text{Fe(III)}_2\text{O}_3/\text{silica}$, which differ by 2 orders of magnitude for the ones reported on Cu(II)O/silica .

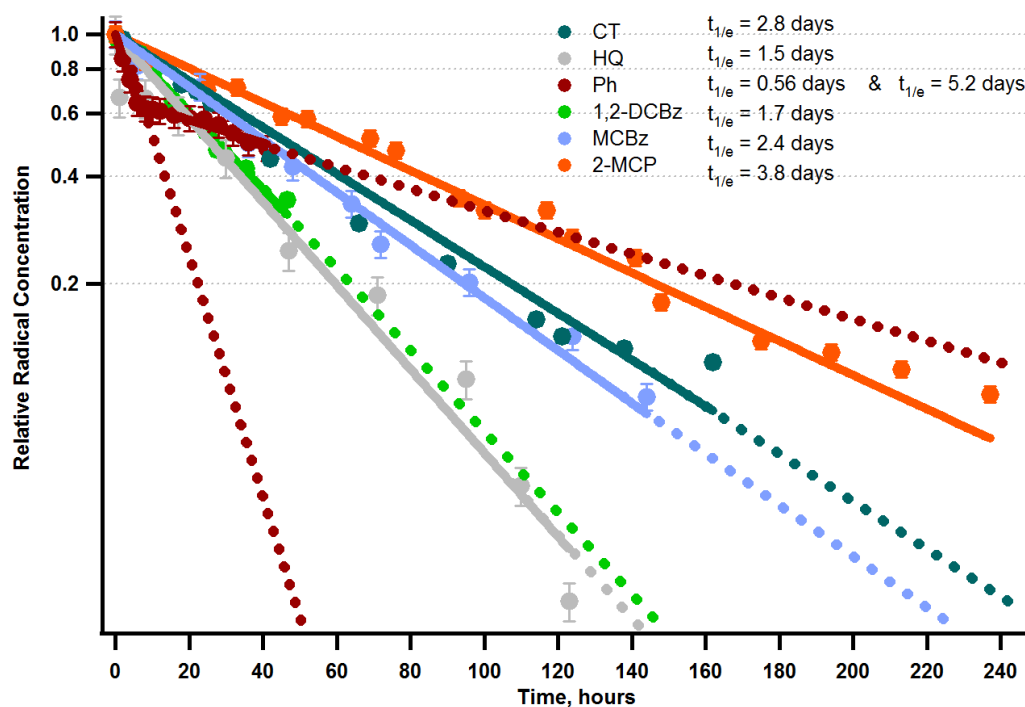


Figure 3.12. First-order decay profile of CT, HQ, PH and 2-MCP in 5% Ni(II)O/silica dosed at 230°C and exposed to air at ambient condition

3.3.3 Persistence and Lifetime of EPFRs on Zn(II)O/Silica Surface

Another metal that has been studied to determine the lifetime of EPFRs was Zn(II)O . **Figure 3.13** depicts the half-lives of the EPFRs bound on Zn(II)O . Phenol shows two half-lives, one fast decay with a half-life of 9.5 days, and another slow decay with a half-life of 73 days

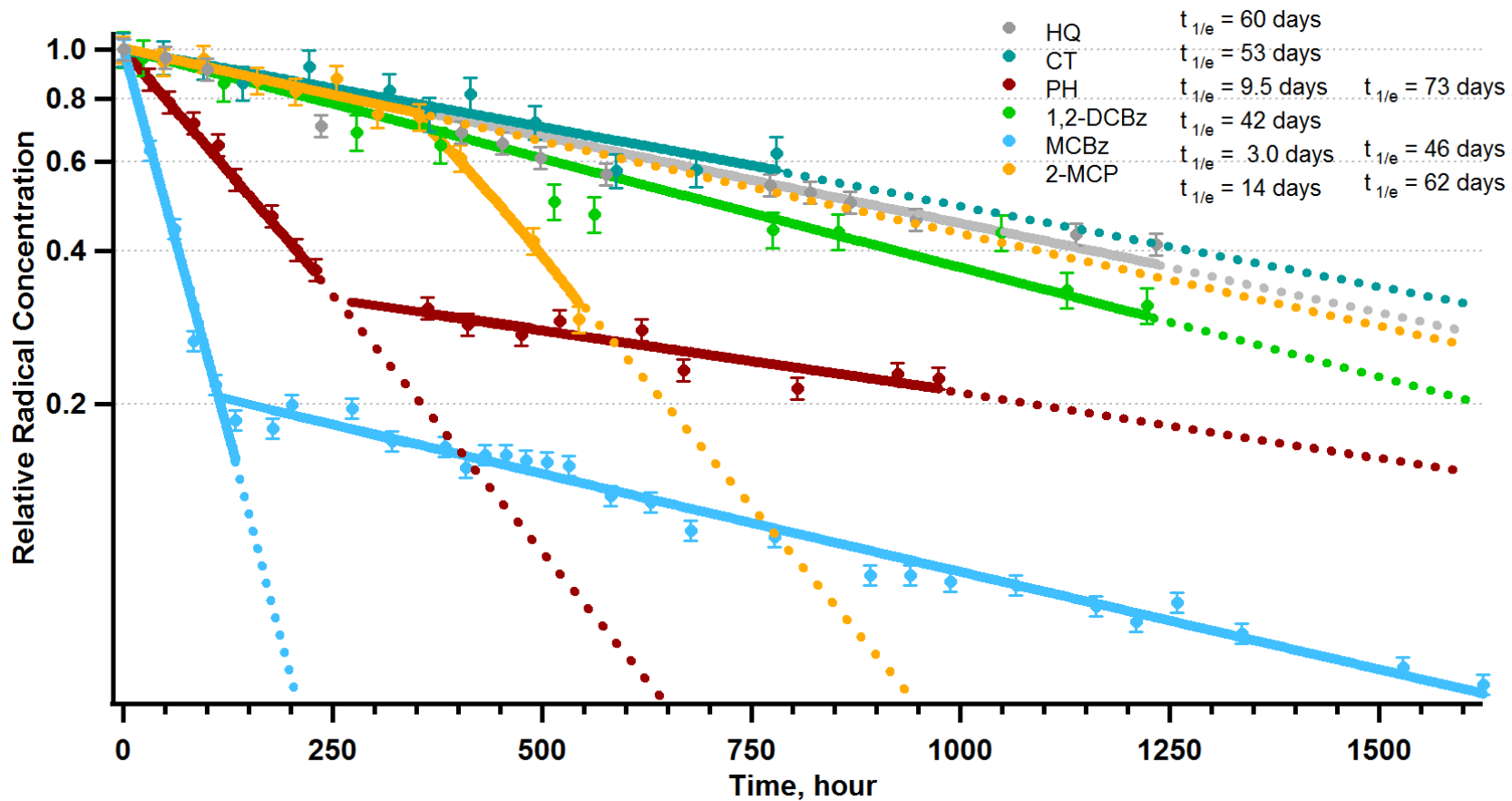


Figure 3.13. First-order decay profile of CT, HQ, PH and 2-MCP in 5% Zn(II)O/silica dosed at 230 °C and exposed to air at ambient condition

which is the longest decay observed so far for all the metals. This behavior is similar on Ni(II)O/silica both showing two decays and both are very stable. 2-Monochlorophenol and monochlorobenzene have similar behavior showing both fast and slow decays. For monochlorobenzene, the fast decay has a half-life of 3.0 days and the slow decay with a half-life of 46 days. On the other hand, 2-monochlorophenol has a fast decay with a half-life of 14 days and a slow decay of 62 days. The other remaining adsorbates (catechol, hydroquinone, and 1,2-dichlorobenzene) showed only one decay. The half-life observed for 1,2-dichlorobenzene is 42 days, while the observed half-lives for hydroquinone and catechol are 53 and 60 days, respectively.

3.4 Comparative Lifetimes of EPFRS on Different Transition Metal Oxide on Silica Surface

There were large differences in the persistence of the EPFRs observed on Fe(III)₂O₃, Ni(II)O, and Zn(II)O on silica surface, and those previously reported for Cu(II)O/silica (1). The half-lives of EPFRs of hydroquinone, phenol, and catechol were nearly 2 orders of magnitude longer for Fe(III)₂O₃, while the chlorinated compounds, 1,2-dichlorobenzene and monochlorobenzene, were so short to be virtually non-measurable on Fe(III)₂O₃. Hydroquinone did not decay at all in the first 24 h of air exposure and exhibited long overall half-life of 4.6 days. But in comparison with the two metals, the half-lives measured on Zn(II)O surface were extremely long. While the half-lives measured for Cu(II)O were on the order of hours and on the order of days for both Fe(III)₂O₃ and Ni(II)O. The half-lives on Zn(II)O/silica were remarkably very high compared to the three metals which were on the order of months. In general, the EPFR are very persistent even if it was exposed to sunlight at ambient condition as in the case of Fe(III)₂O₃ and Cu(II)O. Moreover, Zn(II)O and Ni(II)O are expected to have the same stability.

Table 3.5. Molecular extraction products from radical recombination of EPFRs on Cu(II)O/silica for different temperatures and adsorbates extracted by methanol

Temperature (°C)	150	180	200	230	250	300	350	400
Component								
Benzoquinone (1,2 or 1,4)	2	2	2	2	2	2	2 & 3	2 & 5
Biphenyl					5			
Chlorodibenzo- <i>p</i> -dioxin					6			
Chloronaphthalene						5		5
Dibenzofuran			1 & 3	3	1 & 2	3		5
1,2-Dichlorobenzene	5 & 6	5 & 6	5 & 6	5 & 6	5 & 6	5 & 6	1 & 6	1,5, & 6
Dichlorodibenzofuran							2	2
1,2-dimethoxybenzene	4 & 6	5 & 6	2 & 4	1,4,5, & 6	1,4,& 6	4,5,& 6	2,4,& 6	6
1,3-diphenoxybenzene	2 & 4	2 & 3	1 & 3	3 & 5	2	2 & 3	3	
Monochlorobenzene					6	4		
2-Monochlorophenol	4	5	4 & 5	4 & 5	4	4 & 5	5	4,5
Phenol	6	5 & 6	4	2,4,5,& 6	2,4,& 6	4,5,& 6	5 & 6	4,5, & 6
Naphthalene				2	2			
Trichlorobenzene				4	4	4	4	4
Tetrachlorobenzene				4		4	4	
Pentachlorobenzene				4			4	

Legend: 1= CT , 2=HQ, 3=PH, 4=1,2-DCBz , 5=MCBz , 6= 2-MCP

Table 3.6. Molecular extraction products from radical recombination of EPFRs on Cu(II)O/silica for different temperatures and adsorbates extracted by dichloromethane

Temperature (°C)	150	180	200	230	250	300	350	400
Component								
Benzoquinone (1,4 or 1,2)	5	2, 3, & 5	2 & 5	2 & 5	5	2	2 & 5	2 & 5
Catechol	1	1						
Chloronaphthalene	5 & 6					5	4 & 5	5
Dibenzo- <i>p</i> -dioxin	5							5
Dibenzofuran	5	3, 4, & 6		2		2, 5, & 6		5
1,2-Dichlorobenzene	5 & 6	5 & 6	5 & 6	5 & 6	5 & 6	5 & 6	5 & 6	5 & 6
1,3-Diphenoxybenzene		3		2		2		
Monochlorobenzene				6		6		
2-Monochlorophenol	4 & 5	4, & 5	4 & 5	5	5	4, 5, & 6	45	4 & 5
Phenol	1,5, & 6	4 & 5	5 & 6	5	2 & 5	2 & 5	4, 5, & 6	5
Naphthalene				3		3		
Trichlorobenzene						4 & 5	5	

Legend: 1= CT, 2=HQ, 3=PH, 4=1,2-DCBz, 5=MCBz, 6= 2-MCP

Appendix 3 depicts the EPR spectra on Cu(II)O and Fe(III)₂O₃ which shows that the intensity of the EPR spectra after exposure to sunlight.

3.5 Molecular Products from Extraction of EPFRs

3.5.1 Molecular Products from Extraction of EPFRs on Cu(II)O/Silica

The extraction of the surface-bound EPFRs formed from the adsorption of various molecular adsorbates onto Cu(II)O on silica surface at different temperatures resulted in the formation of molecular products summarized in **Table 3.5**. When catechol was the adsorbate, 1,2-dimethoxybenzene and dibenzofuran were observed in the methanol extract. The EPFRs on hydroquinone as adsorbate yielded 1,4-benzoquinone and 1,3-diphenoxybenzene which were observed at all temperature range from 150 to 400 °C. Phenol and naphthalene were observed at 230 and 250 °C, and dibenzofuran was only observed at 250 °C. Dibenzofuran and diphenoxybenzene were observed as molecular extraction with phenol as the adsorbate. For the chlorinated adsorbate, 1,2-dichlorobenzene, the molecular products observed were 1,2-dimethoxybenzene, phenol, monochlorobenzene, and 2-monochlorophenol. In addition, multiple chlorination products such as isomers of trichlorobenzene, tetrachlorobenzene, and pentachlorobenzene were observed from 230 to 400 °C. On the otherhand, monochlorobenzene yielded biphenyl, 1,2-dimethoxybenzene, phenol, and chlorinated molecules such as 1,2-dichlorobenzene and 2-monochlorophenol. Similarly, the extraction with dichloromethane of the surface-bound EPFRs yielded the same molecular products summarized in **Table 3.6**. Chloronaphthalene was not observed in the methanol extract with monochlorobenzene and 2-monochlorophenol as adsorbates, however, the dichloromethane extract showed detectable amount of the compound. Dibenzofuran was detected for all the adsorbates except catechol, and phenol was present as molecular extraction product for all the adsorbates. In contrast, dibenzo-*p*-

dioxin was only observed for monochlorobenzene at the low and high temperature ends of 150 and 400 °C, respectively. Naphthalene was observed for phenol at the middle temperature range of 230 °C and 300°C, while isomers of trichlorobenzene were observed for both the chlorinated adsorbates, monochlorobenzene, and 1,2-dichlorobenzene.

3.5.2 Molecular Products from the Extraction of EPFRs on Fe(III)₂O₃/Silica Surface

Table 3.7 summarizes the molecular extraction products of the surface-bound EPFRs on Fe(III)₂O₃ on silica for various molecular adsorbates at different temperatures. In contrast with the molecular extraction products observed on Cu(II)O, there were more products detected over Fe(III)₂O₃/silica surface. With catechol as the adsorbate, phenol was detected at all temperatures, and 2-phenoxyphenol was only observed at 230 °C together with 1,3-diphenoxybenzene. 1,4-Benzoquinone is the most commonly observed molecular extraction product of EPFRs for hydroquinone. Moreover, the presence of phenol and naphthalene were also observed, while they were no detectable amounts of these molecular products from the extraction of the surface-bound EPFRs on Cu(II)O/silica. The molecular extraction products observed for phenol includes dibenzo-*p*-dioxin at 150 °C. Dibenzofuran on the other hand, was observed at almost all temperatures. In addition, dimethylferrocene was observed at the low temperature end of 150 °C and ferrocene was detected at 200 and 230 °C. 1,3-Diphenoxybenzene and 2-methylnaphthalene were observed at 150, 250, and 400 °C. Monochlorobenzene is the only adsorbate that formed detectable amount of chlorodibenzo-*p*-dioxin at the lower temperatures of 150 and 200 °C and at the higher temperature range of 300 to 400 °C. Dichlorodibenzofuran and dibenzofuran were observed at 350 and 400 °C and 2,3'-dichloro-2'-hydroxydiphenyl ether was detected at almost all the temperature range except at 400 °C where dibenzofuran is the only product detected. For monochlorobenzene, the chlorinated molecular product 1,2-dichlorobenzene and dibenzofuran

Table 3.7. Molecular extraction products from radical recombination of EPFRs on Fe(III)₂O₃/silica for different temperatures and adsorbates extracted by methanol

Temperature (°C)	150	180	200	230	250	300	350	400
Component								
Benzoquinone (1,2 or 1,4)	2 & 3	2	2	2	2	2	2 & 3	2 & 5
Chlorodibenzodioxin	4		4			4	4	4
Chloroferrocene						5		
Chloronaphthalene							4	5
Dibenzodioxin	3							
Dibenzofuran	3		3	3	2 & 3	3		3,4, & 5
1,2-Dichlorobenzene	5 & 6	5 & 6	5 & 6	5 & 6	5 & 6	5 & 6	6	6
Dichlorodibenzofuran							4	4 & 5
2,3'-Dichloro-2'-hydroxydiphenyl ether	4	4	4	4	4 & 6	4	4	
Dimethylferrocene	3							
2,6-Dichlorophenol							4	
1,2-Dimethoxybenzene			2					
Dioxydiphenyl ether								4
1,3-Diphenoxybenzene	2	2 & 3	3	3 & 5		2 & 3		3
Ferrocene			3	3				3
Methyl benzoquinone		4						
2-Methylnaphthalene	3				3			3
Monochlorobenzene	5				6			
2-Monochlorophenol		5	5	5		5	5	5
Phenol	1 & 6	1,4,5, & 6	1 & 6	1,2,5, & 6	1,2,4, & 6	1,5, & 6	1456	4, 5, & 6
2-Phenoxyphenol				1				
Naphthalene	3	3		2	2 & 3			2 & 3

Legend: 1= CT , 2=HQ, 3=PH, 4=1,2-DCBz , 5=MCBz , 6= 2-MCP

Table 3.8. Molecular extraction products from radical recombination of EPFRs on Fe(III)₂O₃/silica for different temperatures and adsorbates extracted by dichloromethane

Temperature	150	180	200	230	250	300	350	400
Component								
(1,2 or 1,4)-Benzoquinone	2 & 5	5	2	2	2 & 3	5	2 & 5	2 & 5
Biphenyl		4						
Chlorodibenzo- <i>p</i> -dioxin			4		4	4		
Chloroferrocene			5	4				
Chloronaphthalene				5	4	4 & 5	5	
Dibenzo- <i>p</i> -dioxin				4		4		
Dibenzofuran	2 & 3		3	2 & 5			5	2 & 3
1,2-Dichlorobenzene	5 & 6	5 & 6	5 & 6	5 & 6	6	5 & 6	5 & 6	5 & 6
Dichlorodibenzofuran				4	4	4	4	
2,3'-Dichloro-2'-hydroxydiphenyl ether		4	4	4	4			
2,6-Dichlorophenol					4			
1,3-Diphenoxybenzene	2		2 & 3	2				2
Monochlorobenzene	6			6				6
2-Monochlorophenol	5	5	5	5	5	5	5	5
Phenol	5	2 & 5	1,5, & 6	2,5, & 6	1,4,5, & 6	6	5	5
2-Phenoxyphenol	3							3
Naphthalene	3			3			2	3
Trichlorobenzene				5		5		

Legend: 1= CT , 2=HQ, 3=PH, 4=1,2-DCBz , 5=MCBz , 6= 2-MCP

were observed only at the high temperature end of 400 °C. In addition, 2-monochlorophenol and phenol were observed at all temperatures.

For the adsorbate 2-monochlorophenol, phenol was observed at all temperature range of 150-400 °C. Similarly, 1,2-dichlorobenzene was observed at all temperatures which were not observed in the dichloromethane extract (cf. **Table 3.8**). In the dichloromethane extract 2,3'-dichloro-2'-hydroxydiphenyl ether was observed from monochlorobenzene adsorbate from 180 to 250 °C. In the dichloromethane extract, the only product that was detected for catechol as adsorbate was phenol, similar with the methanol extract and naphthalene was detected for phenol as adsorbate in the dichloromethane extract. The molecular products observed for the dichloromethane extract from monochlorobenzene adsorbate include dichlorodibenzofuran and dibenzo-*p*-dioxin, 2-monochlorophenol, and also the polychlorinated compound, trichlorobenzene. Chloroferrocene was observed from both chlorinated adsorbates, monochlorobenzene and 1,2-dichlorobenzene and the molecular product detected for phenol was 2-phenoxyphenol at 150 and 400 °C.

3.5.3 Molecular Products from Extraction of EPFRs on Ni(II)O/Silica

The extraction of the surface-bound EPFRs adsorbed on Ni(II)O on silica with methanol yielded molecular products that are summarized in **Table 3.9**. The most common molecular product arising from the recombination of the EPFRs is phenol. Compared to the number of molecular products identified from EPFRs bound on Cu(II)O and Fe(III)₂O₃ on silica surface only very few products were observed. Moreover, both furans and dioxins were not detected unlike in the two previous metals that were studied. Almost all the adsorbates yielded no molecular products that were observed except the adsorbates themselves. But the doubly-hydroxyl substituted benzene catechol and hydroquinone yielded phenol at all temperature range

Table 3.9. Molecular extraction products from radical recombination of EPFRs on Ni(II)O/silica for different temperatures and adsorbates extracted by methanol

Temperature	150	180	200	230	250	300	350	400
Component								
1,2-Dichlorobenzene						5	5	5
Dioxydiphenyl ether		1						
Hydroquinone			4			4		
2-Methylnaphthalene			4			5	5	
Phenol	1 & 4	1 & 4	1 & 4	1 & 4	1 & 4	1,4, & 5	1,4, & 5	1,4, & 5
Naphthalene				6			4	4
Trichlorobenzene	4	4	4	4	4	4	5	5
2,3,6-Trichlorophenol			4			4	4	4

Legend: 1= CT , 2=HQ, 3=PH, 4=1,2-DCBz , 5=MCBz , 6= 2-MCP

Table 3.10. Molecular extraction products from radical recombination of EPFRs on Ni(II)O/silica at different temperatures and adsorbates extracted by dichloromethane

Temperature	150	180	200	230	250	300	350	400
Component								
Catechol				4				
1,2-Dichlorobenzene					6	6	6	
Monochlorobenzene				4				
Phenol	1 & 4	1 & 4	1 & 4	1 & 4	1 & 4	1 & 4	1 & 4	1 & 4
Trichlorobenzene	4			4	4	4	4	4

Legend: 1= CT , 2=HQ, 3=PH, 4=1,2-DCBz , 5=MCBz , 6= 2-MCP

while 2-monochlorophenol formed phenol only at the higher temperature range of 300 to 400 °C together with some chlorinated products like 1,2-dichlorobenzene and isomers of trichlorobenzene starting from 300 to 400 °C. 2-Methylnaphthalene and naphthalene were observed for the chlorinated adsorbates, 1,2-dichlorobenzene and monochlorobenzene.

In the dichloromethane extracts, 1,2-dichlorobenzene as adsorbate formed phenol and catechol at all temperature range from 150 to 400 °C. The only observable and detectable molecular product from 2-monochlorophenol adsorbate was 1,2-dichlorobenzene. Catechol was detected at 230 °C for monochlorobenzene adsorbate and trichlorobenzene isomers were detected for the doubly-chlorinated adsorbate, 1,2-dichlorobenzene.

3.6 Biological Studies with EPFRs

Biological studies were performed to determine the interaction of the EPFRs on some biological fluids and compounds commonly found in biological environment. **Figure 3.14**

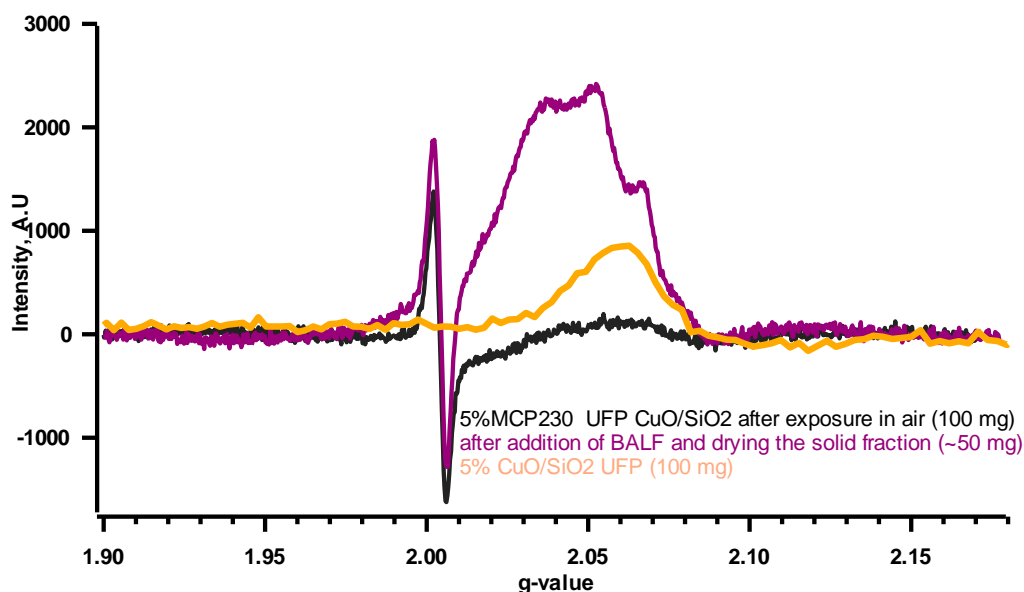


Figure 3.14. EPR spectrum of EPFRs from 2-MCP adsorbed on 5% Cu(II)O/ silica UFP with mice serum and BALF

depicts the EPR spectra for the interaction of bronchoalveolar lavage fluid (BALF) with the EPFRs of 2-monochlorophenol dosed at 230 °C on 5% Cu(II)O on silica ultrafine particles at a scan width of 1000 G.

The control, 5% Cu(II)O on silica UFP showed no peak at the region where organic radical are observed which is between 2.0023 and 2.0080, but a peak between 2.04 and 2.09 was observed which is typical for Cu²⁺ paramagnetic signal. The adsorption of 2-monochlorophenol showed the signals typical for EPFRs for this adsorbate at this region. When the particles were added to the BALF solution for 1 h and then dried in vacuum, the particles showed significant increase in EPR intensity (note that the measured fraction was only half of the original amount of EPFR particle system) and a strong signal in the region where the Cu²⁺ is found intensify.

The persistency of these EPFRs are already determined and found to be stable in air, but its stability on biological solution can be different. Thus, further studies were conducted to

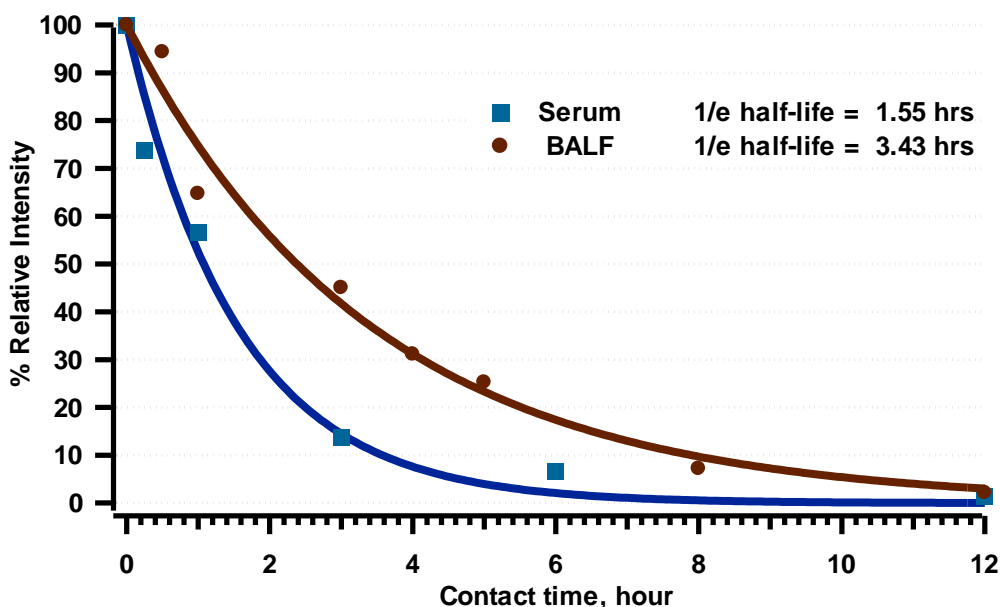


Figure 3.15. Decay of EPFR concentration with the interaction of 2-MCP adsorbed on 5% Cu(II)O/silica UFP with serum and BALF from mice

determine their persistency with biological fluids by determining the half-lives in two biological fluids, namely BALF and serum.

3.6.1 Decay of EPFR Signal on Biological Fluids

Figure 3.15 presents the decay curve of the EPFRs from 2-monochlorophenol with their interaction with BALF and serum. The decays show very good fit. The half-life of the EPFRs on BALF was 3.43 h which is two-fold higher compared with the one measured on serum. The EPR spectra of 2-monochlorophenol with BALF at different contact times are presented in **Figure 3.16**. The EPR spectra have similar features to the ones described in the previous section.

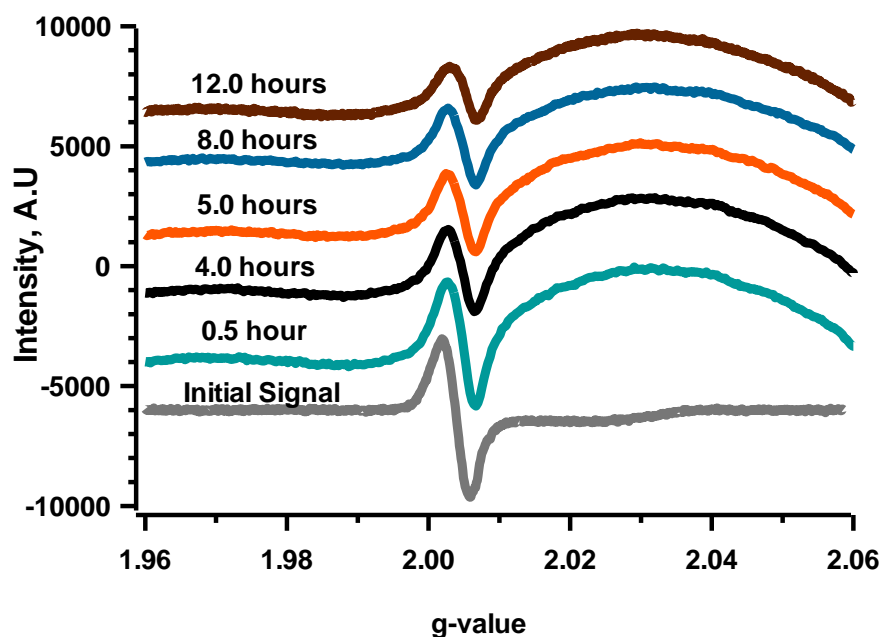


Figure 3.16. Time dependence of the EPR spectra of 2-MCP adsorbed on 5% Cu(II)O/silica UFP with mice serum and BALF

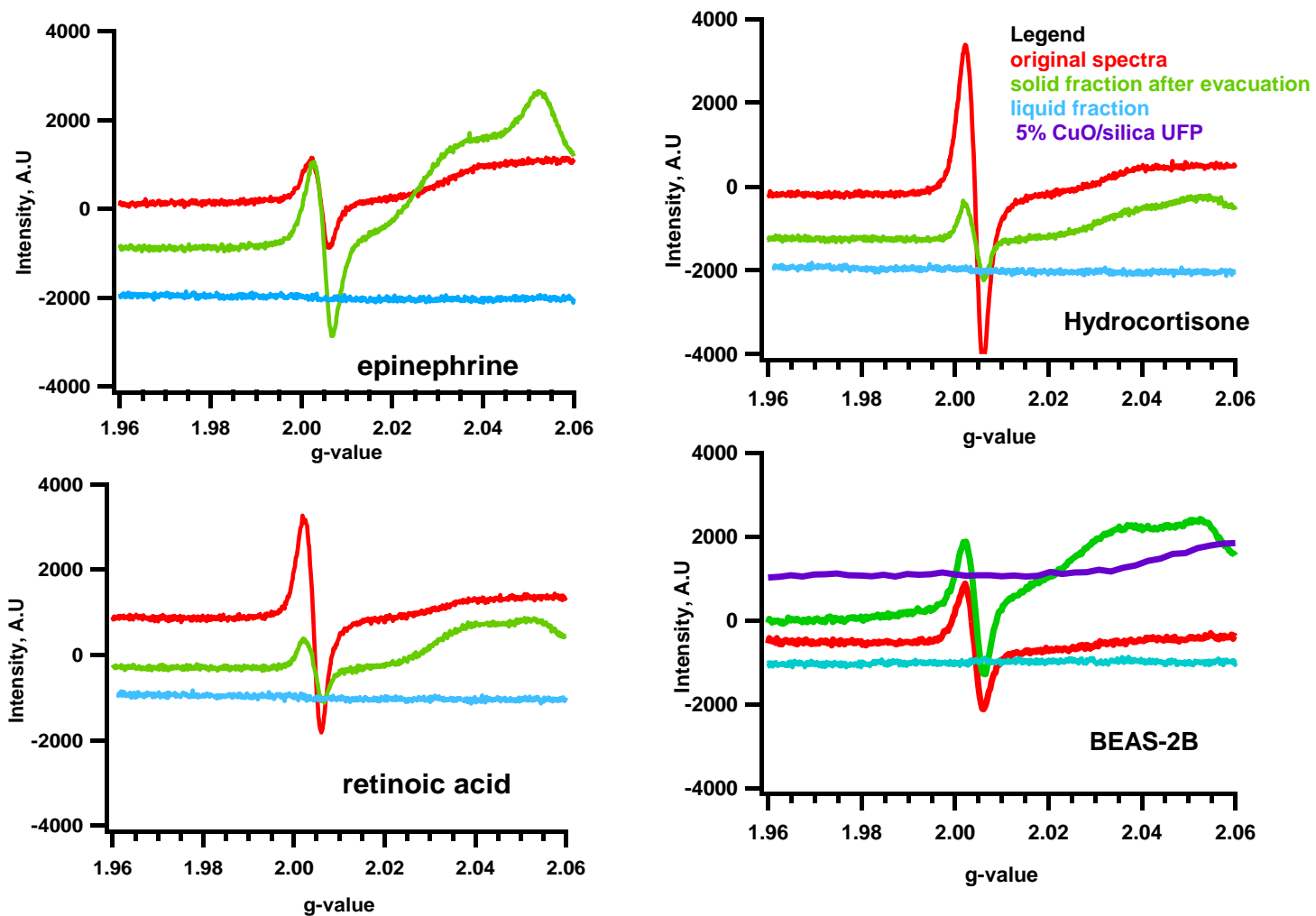


Figure 3.17. EPR spectra of 2-MCP dosed on 5% Cu(II)O/silica UFP at 230 °C on the interaction of the EPFRs with hydrocortisone, epinephrine, retinoic acid and BEAS-2B cells

3.6.2 Interaction of Some Biological Compounds with EPFRs

Studies on some molecule found in biological environment such as hydrocortisone, epinephrine (adrenaline), the antioxidant—retinoic acid, and the cell culture —BEAS-2B were conducted. **Figure 3.17** depicts the spectra of the interaction of these compounds with the EPFRs of 2-monochlorophenol. Results reveal that hydrocortisone and retinoic acid decrease the EPFR signal intensity significantly, while epinephrine significantly enhances the EPFR signal. A follow up study using undosed 5% Cu(II)O on silica particles with the solutions of the compound under study showed that no signals in the organic radical region were detected from hydrocortisone and retinoic acid, however, epinephrine showed signals that slightly higher than the noise level of the instrument.

3.7 Spin Trapping Studies

3.7.1 Spin Trapping of Hydroxyl Radical

Spin trapping studies were done for solution of EPFR- and non-EPFR-containing

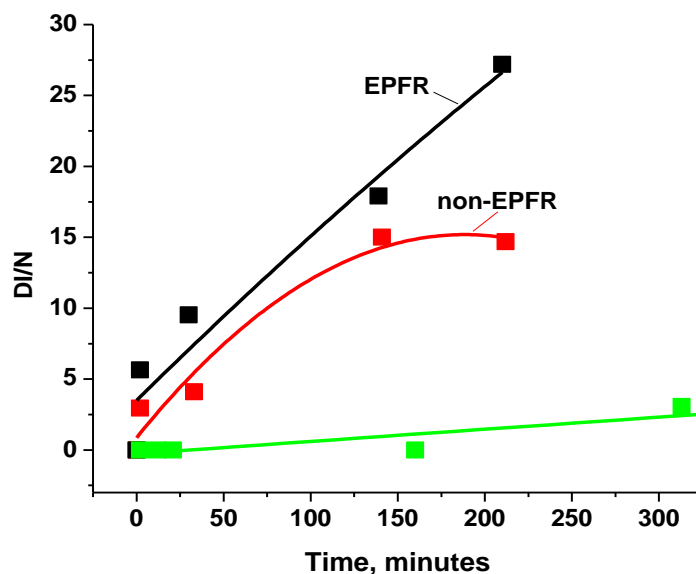


Figure 3.18. Time evolution of the DMPO-OH adduct signal in the presence of non-EPFR- and EPFR-containing particles

particles with 2-monochlorophenol as adsorbate. The sample (described in **Section 2.6**) solution generates more DMPO-OH adduct (black line in **Figure 3.18**) than reference (described in **Section 2.6**) solution (red line) which shows a very slow conversion of pure DMPO in phosphate buffer, green line (cf. **Figure 3.18**). The sample solution generates more DMPO-OH adducts than the corresponding reference solution.

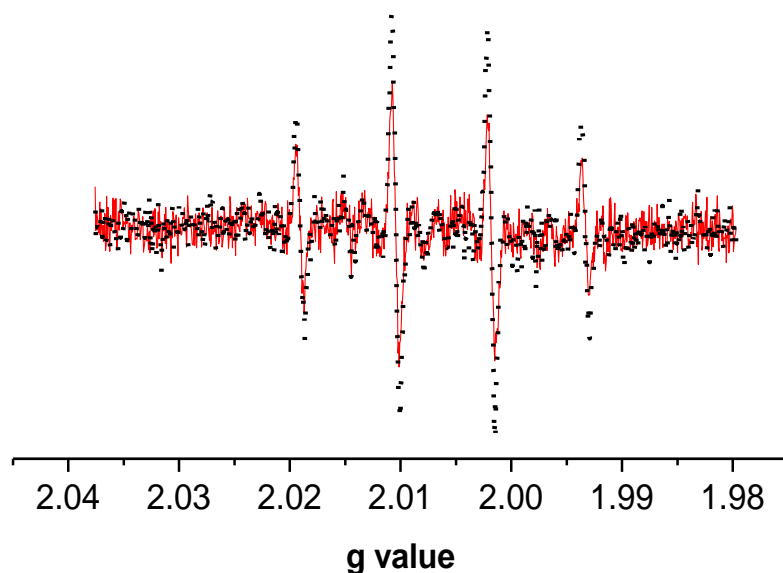


Figure 3.19. EPR spectra of DMPO-OH

The comparison of the EPR signal intensity of DMPO-OH from the reference (red line) and sample (black dashed line) from aerated solutions is depicted in **Figure 3.19**. The time evolution of the EPR signal intensity of DMPO-OH from the reference (red squares) and sample (black squares, 150 $\mu\text{g/mL}$ EPFRs+DMPO(150 mM)+Buffer) **aerated** solutions is presented in **Figure 3.18**. The green line represents the time evolution of the EPR signal intensity of DMPO-OH in pure DMPO (150 mM) balanced by phosphate buffer saline (200 μL).

3.7.2 Trapping of O_2^- by DMPO in Different Solvents

The DMPO-superoxide adduct with its characteristic 12-line spectra (2) were not detected from the sample in aqueous solution (EPFRs on catalyst (50 $\mu\text{g}/\text{mL}$) and DMPO (150 mM) in PBS) using standard EPR detection procedure. However, the DMPO-superoxide adduct was detected in different non-aqueous solvent system. In **Figure 3.21**, Spectrum 1 is the DMPO-

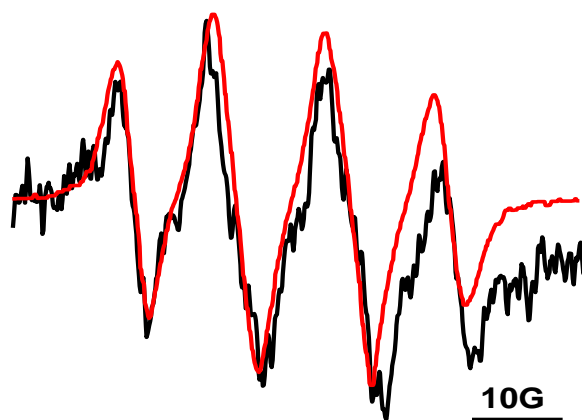


Figure 3.20. EPR spectra of DMPO-O_2^- in AcN

O_2^- EPR spectra from Fenton reaction, generated by the protocol described elsewhere containing 200 mM DMPO, 0.5mM H_2O_2 70 μM ferrous ammonium sulfate, and 5% DMSO (v/v) in nonaerated condition. Spectrum 2 is the DMPO-O_2^- adduct EPR spectra generated in pure DMSO media of EPFRs incubated for 1 h containing 50 $\mu\text{g}/\text{mL}$ EPFRs in DMSO, 150 mM DMPO in DMSO, and in aerated condition, where a weak signal was detected from the EPFRs solution in 100% DMSO (red line, spectrum 2). Spectrum 3 is the DMPO-O_2^- adduct EPR spectra generated in pure AcN media of EPFRs incubated for 1 h containing, 50 $\mu\text{g}/\text{mL}$ EPFRs, 150 mM DMPO, and in aerated condition while a broad, four-line signal appeared in pure AcN

solution (blue line spectrum 3), typical to DMPO-O₂⁻ adduct EPR spectra reported in literature for the suspension of powdery semiconductors (TiO₂, Fe₂O₃, WO₃, CdS) in AcN (3) generated by the protocol described elsewhere containing 200 mM DMPO, 0.5 mM H₂O. The resolution of the spectrum 3 was improved when the same experiment was repeated with less amount of sample. Spectrum 4 is the DMPO-O₂⁻ adduct generated in pure AcN media of EPFRs incubated for 1 h containing 25 μg/mL EPFRs, 150 mM DMPO, in aerated condition, pink line 4 (25 μg/mL EPFRs' in AcN) + 150 mM DMPO, aerated solution). The black Spectrum in **Figure 3.20** is the EPR spectrum of DMPO-O₂⁻ adduct formed in pure AcN media (the same as spectrum 3 on **Figure 3.21**).

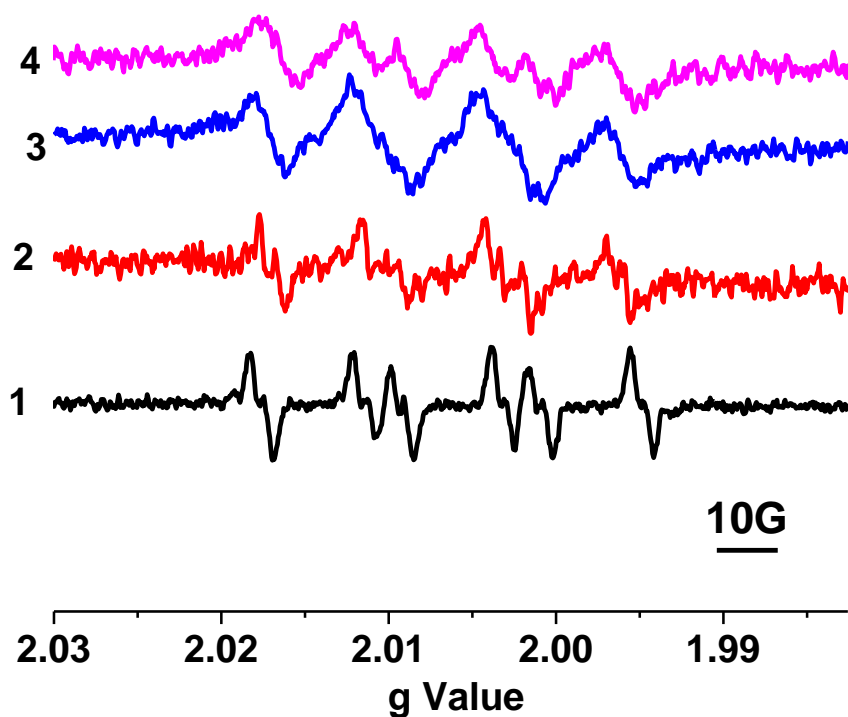


Figure 3.21. EPR Spectra of DMPO-OH in different solvent systems

The superimposed red spectrum is the DMPO-O₂⁻ spectrum formed in TiO₂ suspension in pure AcN media digitized by using UN-SCAN-IT Automated Digitizing System **Figure 3.20**. Interestingly, the DMPO-OH adduct appears in solution immediately in aqueous media and also in different concentrations of aqueous solution. To conclusively identify that the system generates superoxide the following experiment was done. Superoxide dismutase from bovine erythrocytes) (3619 U/mg) and CAT (from bovine liver, 3809 U/mg) were used in solution at concentration ranging from 20 µg/mL (70 U/mL) to 80 µg/mL (280 U/mL) (4-6). The results are presented in

Figure 3.22 and the SOD solely decreases the DMPO-OH adduct concentration in solution. The interaction between peroxide and SOD has been studied as a function of overall activity loss (7) and hence, less DMPO-OH adducts appear in solution, black line. Catalase also decreases the DMPO-OH adduct concentration, while when combined with SOD there is a significant decrease in the DMPO-OH adducts concentration (pink line, **Figure 3.22**).

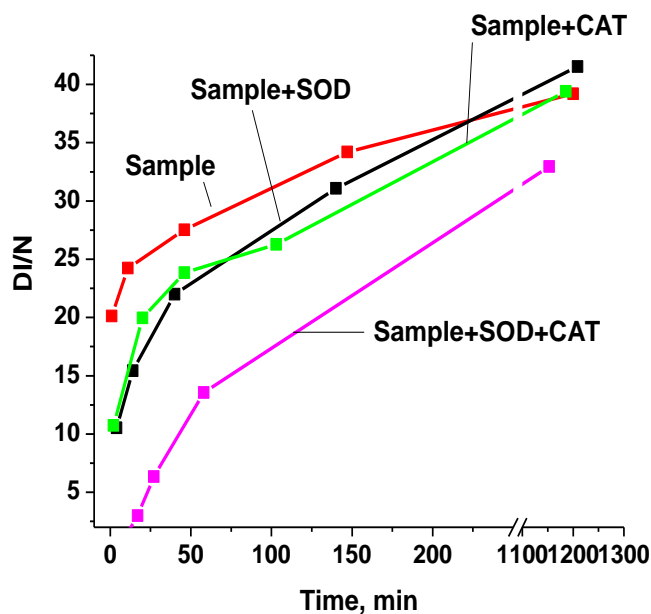


Figure 3.22. The inhibition effect of SOD and CAT on EPFRs

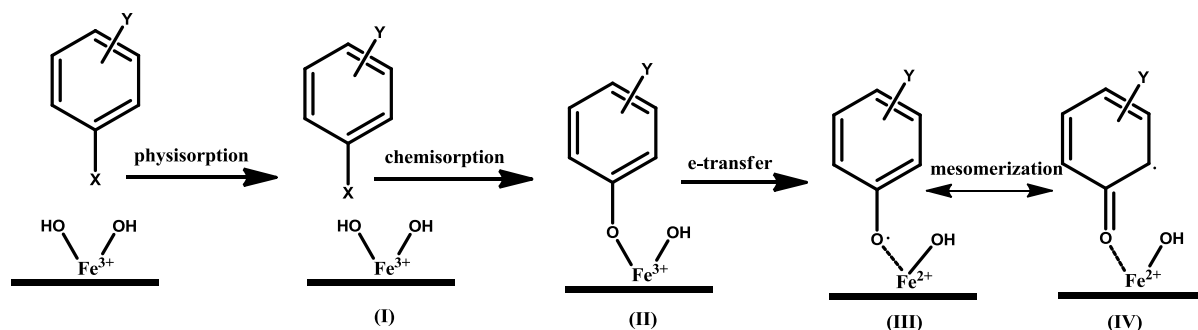
3.8 References

1. Lomnicki, S.; Truong, H.; Vejerano, E.; Dellinger, B. Copper oxide-based model of persistent free radical formation on combustion-derived particulate matter. *Environ. Sci. Technol.* **2008**, *42*, 13, 4982-4988.
2. Makino, K.; Hagiwara, T.; Murakami, A. Fundamental aspects of spin trapping with DMPO. *Radiat. Phys. Chem.* **1991**, *37*, 5-6, 657-665.
3. Noda, H.; Oikawa, K.; Ohya-Nishiguchi, H.; and Kamada, H. Detection of superoxide ions from photoexcited semiconductors in non-aqueous solvents using ESR spin-trapping technique. *Bull. Chem. Soc. Jpn.* **1993**, *66*, 12, 3542-3547.
4. Zang, L.Y.; Stone, K.; Pryor, W.A. Detection of free radicals in aqueous extracts of cigarette tar by ESR. *Free Radic. Biol. Med.* **1995**, *19*, 161-167.
5. Arroyo, C.M.; Kramer, J.H.; Dickens, B.F.; Weglicki, W.B. Identification of free-radicals in myocardial-ischemia reperfusion by spin trapping with nitron DMPO. *FEBS Lett.* **1987**, *221*, 1, 101-104.
6. Pryor, W.A.; Stone, K.; Zang, L.Y.; Bermudez, E. Fractionation of aqueous cigarette tar extracts: Fractions that contain the tar radical cause DNA damage. *Chem. Res. Toxicol.* **1998**, *11*, 441-448.
7. Cabelli, D.E.; Allen, D.; Bielski, B.H.J.; Holcman, J. The interaction between Cu(I) superoxide dismutase and hydrogen peroxide. *J. Biol. Chem.* **1989**, *264*, 17, 9967-9971.

CHAPTER IV. DISCUSSION*

4.1 General Mechanism of EPFR Formation on Transition Metal Oxide Surface

The adsorption of various aromatic molecular adsorbates on the surface of transition metal oxide resulted in the formation and detection of organic radical and paramagnetic species. The organic radical has a g-value similar to that of phenoxyl and semiquinone-type organic radicals commonly reported in the literature. Previous study using FTIR spectroscopy has demonstrated that chlorinated phenols and chlorinated benzenes resulted in the chemisorptions of these adsorbates on the surface of Cu(II)O (2). Moreover, it was observed that EPFR are formed on the surfaces of 5% Cu(II)O/silica particles from the same adsorbates, and proposed a mechanism of their formation by the interaction between the terminal hydroxyl groups on the surface of the transition metal oxide from 150 to 400 °C under typical post-combustion condition. The terminal hydroxyl group on the surface is due to the completion of the unsatisfied charges and valences of the metal ions in the terminal plane on the transition metal oxide surface



Scheme 4.1. General mechanism of the formation of EPFRs on a metal oxide/silica surface from adsorption of chlorinated and hydroxylated benzenes

* Part of this manuscript is reproduced with permission from Vejerano, E.; Lomnicki, S.; Dellinger, B. Formation and stabilization of combustion-generated environmentally persistent free radicals on an Fe(III)₂O₃/silica surface. *Environ. Sci. Technol.* 2011, 45, 2, 589-594. Copyright 2011. American Chemical Society.

(3-5). **Scheme 4.1** shows the formation of EPFRs on a generalized transition metal oxide surface, where X and Y can be a hydroxyl and/or chlorine substituents. Initially, the molecular adsorbates physisorb on the surface by forming hydrogen bonding with the hydroxyl or chlorine substituents of the molecular adsorbates and the terminal hydroxyl group on the metal oxide surface. Then, the adsorbates chemisorbed on the surface by elimination of hydrogen chloride and/or water resulting in the formation of an organic-metal oxide complex. Subsequent electron transfer from the oxygen to the metal cation center occurs and a surface-associated organic EPFRs formed and concomitant reduction of the metal cation. The surface-associated EPFRs can mesomerize between its keto and enol forms. Previous studies with X-ray Absorption Near Edge Structures (XANES) has confirmed the one-electron reduction process (6).

4.2 Metal *F*-center Formation (g1) in Fe(III)₂O₃ and Ni(II)O

Spectral peak fitting of the absorption spectra for Fe(III)₂O₃ and Ni(II)O showed a paramagnetic signal with g-value less than that of the electronic g-value between 1.9970 to 2.0021 which are due to formation of *F*-centers. When an electron transfers from the adsorbed molecule to the metal ion center resulting in the reduction of the associated metal ion, *F*-centers can form. They are electrons trapped in the anionic vacancies on the metal oxide surface leading to a paramagnetic signal with characteristically low g-value. Strained sites which result from the dehydration of hydroxylated oxide surface creates anionic vacancies (7-9) where the electrons are trapped. Previous studies with EPFRs on Cu²⁺-containing surfaces for all the adsorbates also formed *F*-centers. In contrast to Fe(III)₂O₃/silica particles, *F*-centers (g1) were only observable for catechol and hydroquinone following EPR spectral peak fitting. Similar behavior were also observed on Ni(II)O on silica particles. The results indicate that some adsorbates readily generate *F*-center. In the case of Ni(II)O on silica particles, the adsorbates—catechol,

monochlorobenzene, and 2-monochlorophenol showed the formation of *F*-center at all temperatures. In general, adsorbates that produce *F*-centers are those that 1) are monosubstituted and chemisorbed via HCl elimination, 2) those which chemisorbed via water and/or HCl and still contains a residual hydroxyl-substituent after the EPFRs are formed.

4.3 Adsorbate EPFR Formation (g2 and g3 radicals) on Fe(III)₂O₃ and Ni(II)O

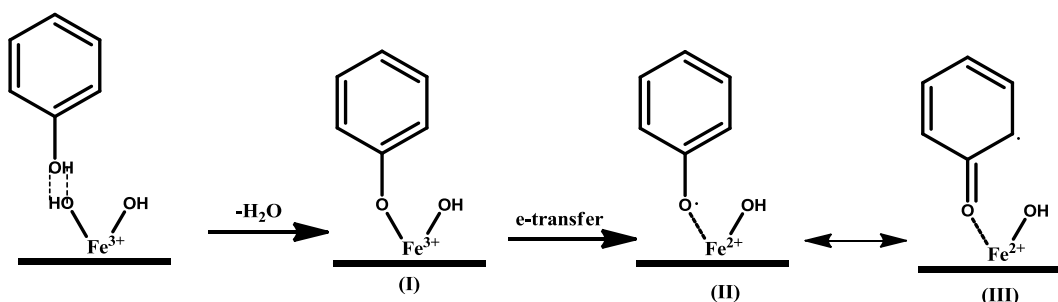
Aside from *F*-centers, the anticipated signal from organic radical species were observed after adsorption of various molecular adsorbates on Fe(III)₂O₃ and Ni(II)O silica surfaces. Depending on the number and type of substituent groups on the adsorbates, one or two types of EPFRs were observed. It is only in the case of phenol where a single EPFR was observed. The general scheme is depicted in **Figure 4.1** for a generalized transition metal and adsorbate.

4.3.1 Phenol

The adsorption of phenol on both Ni(II)O and Fe(III)₂O₃ surface resulted to the formation of only one type of radical. **Scheme 4.3** shows the mechanism of the adsorption of phenol on an iron surface. The same mechanism is true on nickel surface except that the Ni²⁺ is reduced to Ni⁺. This is expected since phenol has only one hydroxyl substituent that can chemisorb on the surface which is similar behavior observed on Cu(II)O. The g₂ signal for phenol is ascribed to that of the anticipated phenoxyl radical and is consistent with the literature spectra of phenoxyl radical with g-values of 2.0030-2.0040 (10). Our slightly higher observed g-values can be a result of the matrix effect on the spin-orbit coupling. For both Ni(II)O and Fe(III)₂O₃, a sudden shift of g-value to 2.0036 is observed, together with an overall drop of EPFR yield at 400 °C, which is indicative of formation of a new radical from the decomposition of phenoxyl radical. Indeed, phenoxyl radicals have been reported to decompose to form cyclopentadienyl ketene compounds (11) and, through CO elimination, to form cyclopentadienyl radicals (12).

Extraction and GC-MS analyses of the 400 °C from Fe(III)₂O₃ sample revealed the presence of ferrocene in the extract, suggesting the higher temperature radical is cyclopentadienyl formed from the partial decomposition of phenoxy radical (cf. **Scheme 4.3**).

Moreover, naphthalene and methyl naphthalene is observed with the GC-MS extract with phenol as the adsorbates indicating

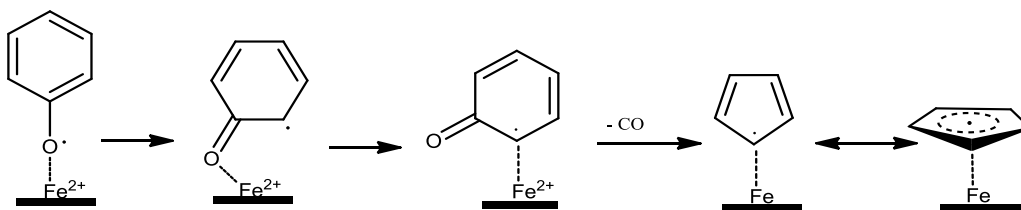


Scheme 4.2. Formation of phenoxy radical on Fe(III)₂O₃ surface from H₂O elimination

the formation of cyclopentadienyl radical. It is an established mechanism that naphthalene is formed from recombination of this radical (13).

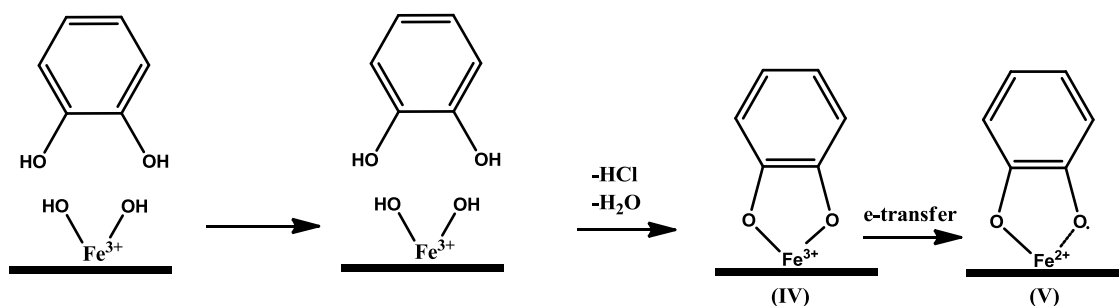
4.3.2 Hydroquinone and Catechol

Dihydroxybenzenes such as catechol (*ortho*-dihydroxy-) and hydroquinone (*para*-



Scheme 4.3. Formation of cyclopentadienyl radical from decomposition of surface-bound phenoxy radical through CO elimination on Fe(III)₂O₃ surface

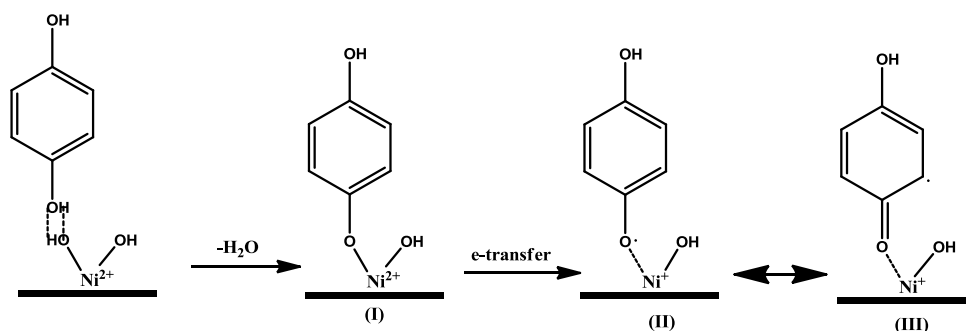
dihydroxy-) are known to form resonance-stabilized semiquinone radicals. Semiquinone radicals exist primarily as oxygen-centered radicals, with g-values greater than 2.0045 (14). The chemisorption of catechol and hydroquinone on the Fe(III)₂O₃ surface resulted in spectral components with g-values of 2.0053-2.0056 for hydroquinone and 2.0057-2.0067 for catechol, respectively, for adsorption at 150-350 °C.



Scheme 4.4. Formation of *o*-semiquinone radical from adsorption of catechol on an Fe(III)₂O₃ surface via double-H₂O elimination

The mechanism of formation for *o*-semiquinone radical from catechol is depicted in **Scheme 4.5**. These values (denoted as g₃) are typical for semiquinone-type radicals and are similar to those formed over Cu(II)O surfaces (15). In addition, a g₂-type radical was detected in high yields at all temperatures, with a lower g-value of 2.0033-2.0040 for hydroquinone and 2.0031-2.0040 for catechol. This is in contrast to the result for Cu(II)O (15), where only semiquinone radicals were detected over this temperature range. The formation of g₂-type radical is consistent with the decomposition of surface semiquinone-type radicals to phenoxyl-type radicals. In fact, extraction of the Fe(III)₂O₃/silica particles dosed with hydroquinone and catechol revealed the formation of phenol from both, as well as small amounts of the 2-phenoxyphenol dimer from catechol and 1,3-diphenoxybenzene trimer from hydroquinone. In the case of EPFRS on Ni(II)O. Another EPR signal was also observed, g₂ signal, with g-values

ranging from 2.0031 to 2.0043 at all temperatures. From the plot of the ratio of the g2 and g3 radical yield, the g2 signal dominates at 250 °C—the maximum, and the g2 and g3 EPFR yields are almost equal at higher temperatures. This shows that at lower temperature, chemisorption on a single hydroxyl substituent is the dominant reaction mechanism

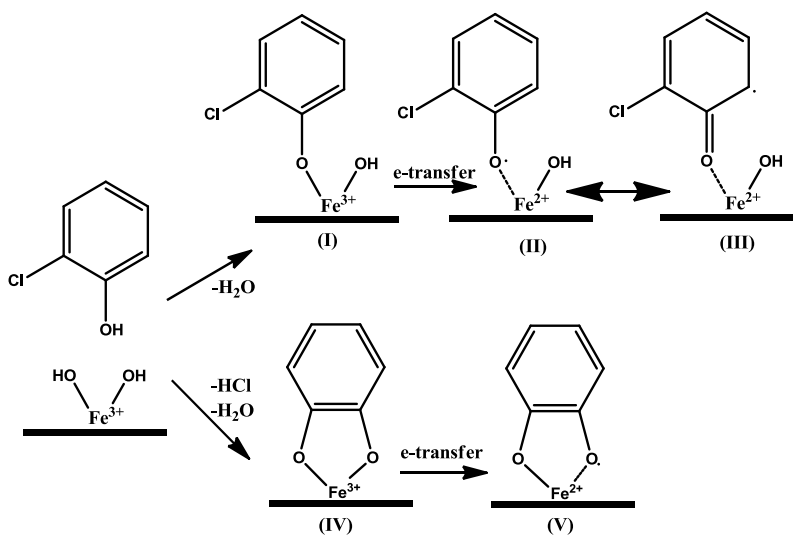


Scheme 4.5. Formation of *p*-semiquinone radical from hydroquinone on an Ni(II)O/silica surface

to form phenoxyl-type radical. However, at lower temperature, the major EPFR formed is g2-type radical. At 300 to 400 °C, g2 and g3 have approximately equal yields. In contrast, the g2 signal in Cu(II)O only appears at higher temperature range. This indicates that both single and double elimination of water on nickel surfaces are both energetically feasible and probably occurs simultaneously, to form a phenoxyl-type radical and an *o*-semiquinone-type radical, respectively. GC-MS extract analyses reveal that one of the molecular products formed at all temperatures is phenol.

In the case of hydroquinone on Ni(II)O, the EPFR yield for hydroquinone, generally increases from 150 to 400 °C. EPR spectral deconvolution showed that only one signal was observed for hydroquinone with g-values from 2.0040 to 2.0057, a g3 signal which is assigned to a *p*-semiquinone radical. The formation of *p*-semiquinone radical from hydroquinone of Ni(II)O/silica surface is depicted in **Scheme 4.5** The formation of only one signal for

hydroquinone like on Cu(II)O is expected since the hydroquinone molecules is symmetric and would therefore react with the surface in the same manner as phenol. The EPFRs on copper however, has higher g-value compared to nickel because of its lower atomic mass. The g3 signal for hydroquinone is similar to those reported on the literature for *p*-semiquinone radical anion in solution which is between 2.0045-2.0060 (16, 17). Analyses of the GC-MS extracts of



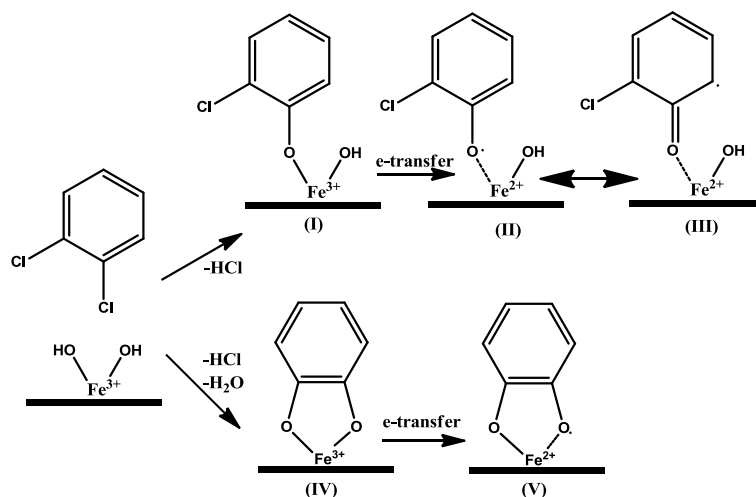
Scheme 4.6. Formation of 2-chlorophenoxy radical and *o*-semiquinone radical from 2-monochlorophenol on an Fe(III)₂O₃/silica surface

hydroquinone showed no formation of phenoxy-based molecular products which further corroborates the EPR spectral peak fitting that indeed only *p*-semiquinone radical was formed in Ni(II)O.

4.3.3 1,2-Dichlorobenzene and 2-Monochlorophenol

1,2-Dichlorobenzene and 2-monochlorophenol are substituted in the same positions as catechol and were anticipated to form similar EPFRs. The chemisorption for *o*-chlorine- and *o*-hydroxy-substituted molecules can occur by reaction with both substituents, either by H₂O or

HCl elimination (cf. **Scheme 4.6**). If both substituents react with the surface, a chemisorbed *o*-semiquinone radical is formed. The spectral peak fitting procedure of the EPR spectra revealed



Scheme 4.7. Formation of 2-chlorophenoxy radical and *o*-semiquinone radical from 1,2-dichlorobenzene on an $\text{Fe(III)}_2\text{O}_3/\text{silica}$ surface

both g2, phenoxy-type, and g3, semiquinone-type, EPFR signals. In contrast to catechol, neither 1,2-dichlorobenzene nor 2-monochlorophenol exhibited maxima at lower temperatures.

2-Monochlorophenol exhibited maxima in the g2 radical concentration at 250 °C and g3 radical concentration at 350 °C and 1,2-dichlorobenzene exhibited consistently low yields of EPFRs. 2,2'-Dichloro-3-hydroxydiphenyl ether (a dimer of 2-chlorophenoxy) and *o*-benzoquinone (formed from loss of H^\bullet from *o*-semiquinone) were observed as molecular products in the solution extracts for 1,2-dichlorobenzene and 2-monochlorophenol, respectively. For both adsorbates, the structures of the radicals are assigned as 2-chlorophenoxy radical for g2 and *o*-semiquinone radical for g3, which are consistent with the EPR spectra and molecular product distributions. In contrast to unchlorinated adsorbates (phenol, hydroquinone, and

catechol), the chlorinated adsorbates 1,2-dichlorobenzene and 2-monochlorophenol, exhibited lower EPFR yields. There are two possible explanations for this: 1) the chlorine substituent does not chemisorb with the surface by HCl elimination as readily as hydroxyl substituent reacts by H₂O elimination and 2) the surface abstracts chlorine from the adsorbate or reacts with HCl formed during chemisorption to form surface hypochlorites, which then reacts with the initially formed EPFRs (18). The first explanation is supported by the relatively low yields of EPFRs for 1,2-dichlorobenzene and 2-monochlorophenol as well as monochlorobenzene (*vide infra*). In contrast to Fe(III)₂O₃, the chlorinated adsorbates resulted in high yields of EPFRs on Cu(II)O (15). There may simply be a difference in the relative reactivity of chlorine substituents with the Fe(III)₂O₃ surface. In general, the chemisorption bonds are weaker as one move to the left in a period of transition metals, and iron should form weaker bonds than copper. Hence, the thermodynamically less favorable elimination of HCl may not occur readily on Fe(III)₂O₃ surface. However, the chlorinated adsorbates may also react efficiently, and rapidly form surface hypochlorites, which attack and destroy the chemisorbed species. Hypochlorite species are known to be strong oxidizing and chlorinating agents and contribute to decomposition of the adsorbed species (3, 18, 19), and iron is known to be especially prone to forming hypochlorites (20). In fact, the analysis of the extract from the 1,2-dichlorobenzene and 2-monochlorophenol adsorbates revealed the presence of chlorination products, including 2,3-dichlorophenol and 1,2-dichlorobenzene, respectively, which were not observed in the copper oxide studies. Increase in the EPFR yields at higher temperatures simply indicates that the rate of semiquinone radical formation exceeded the rate of the chlorination/destruction of the surface species for 2-monochlorophenol adsorption.

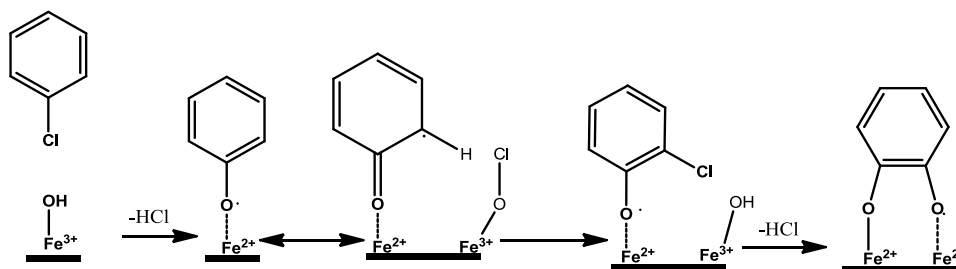
On the other hand, while the EPFR yields on Fe(III)₂O₃ for 1,2-dichlorobenzene are

relatively lower, the converse is true on Ni(II)O surface which has the highest EPFR yields. The EPFRs yields for 2-monochlorophenol was lower in Ni(II)O compared to the ones on Fe(III)₂O₃. Chlorination products such as 1,2,3-trichlorobenzene and 2,6-dichlorophenol were observed on iron, the high EPFR yield on Ni(II)O suggests that the hypochlorite species mainly chlorinates the aromatic ring and does not interfere with the stability and persistency of the EPFRs on the surface of nickel (*vide infra*). We can hypothesize therefore, that probably, there is a higher electron density on the oxygen, and thus the majority of the EPFRs on Ni(II)O are oxygen-centered radical, and the addition of the chlorine on the benzene ring is through electrophilic aromatic substitution and therefore, the EPFRs are unaffected by the chlorination process. As in the case on Fe(III)₂O₃, the EPR spectral peak fitting revealed two peaks. For both adsorbates, the g2-type radical is assigned to a 2-chlorophenoxy radical and the g3 signal to an *o*-semiquinone radical.

4.3.4 Monochlorobenzene

The chemisorption of monochlorobenzene on the surface of Fe(III)₂O₃ was expected to form phenoxy radical via HCl elimination (cf. **Scheme 4.6**). Moreover, the ratio of g2 to g3 concentration was close to 1 and resembled the profile observed for 1,2-dichlorobenzene. The GC-MS analysis of the solvent extracts revealed the formation of 2-monochlorophenol which suggests surface chlorination occurs, leading to the formation of chlorophenoxy radicals, which then react further with the surface to form *o*-semiquinone radicals (cf. **Scheme 4.5**) on Ni(II)O. As shown in **Figure 3**, the EPFR yields of monochlorobenzene increase from 150 to 350 °C, with the maximum at 350 °C and a decrease at 400 °C. Peak fitting of the EPR spectra showed the presence of a g2 signal attributed to the formation of a phenoxy radical, and since monochlorobenzene is monosubstituted, it is expected to react with the surface similar to phenol

except that it chemisorbs by HCl elimination. Analyses of the GC-MS extracts showed that the major molecular product formed at all temperatures was phenol. However, another signal, g3, was observed at the higher temperature range of 300 to 400 °C which is attributed to the



Scheme 4.8. Chlorination mechanism of benzene catalyzed by surface formation of hypochlorite species and subsequent formation of *o*-semiquinone radicals

formation of a semiquinone-type EPFRs with higher *g*-values from 2.0060 to 2.0081. The *g*-values were similar to the ones observed on Cu(II)O but were higher than those reported for Fe(III)₂O₃ whose *g*-value ranges from 2.0053 to 2.0060. The difference is due to the heavier atomic masses of both nickel and copper compared to that of iron, thus, nickel and copper have strong spin-orbit interactions. Monochlorobenzene is a monosubstituted adsorbate, but the formation of the g3, semiquinone-type EPFRs is observed due to chlorination of the adsorbed aromatic species catalyzed by surface hypochlorite. Indeed, analyses of the GC-MS extracts of the 300 to 400 °C samples reveal the presence of 1,2-dichlorobenzene and 1,2,3-trichlorobenzene were observed from the molecular products distribution. Similar behavior was also observed for monochlorobenzene on both Cu(II)O and Fe(III)₂O₃/silica studies. The HCl produced in the chemisorption step reacts with the surface to form surface-hypochlorite species on Ni(II)O surface similar to the mechanism elucidated on Fe(III)₂O₃ surface (cf. **Scheme 4.8**).

4.4 Comparative Yields of EPFRs on Different Transition Metal Oxide/Silica Surface

At higher temperature the doubly-substituted adsorbates have higher yield on Ni(II)O due to the higher probability of bonding with the surface because of the higher number of substituent which increases the number of successful collision with the surface hydroxyl. EPFRs formed on the surface of Ni(II)O are stable since it has lower propensity to form hypochlorite species which prevents destruction of the EPFRs after they were formed compared to iron. The chlorinated benzenes have lower yields compared to hydroxylated benzenes except at 400 °C where the majority of the radical observed are *o*-semiquinone. The EPFR yield of the chlorinated adsorbates are higher on Ni(II)O than in Cu(II)O, since Ni(II)O is more stable and again because of their lower propensity to form hypochlorite species and the EPFR yield of hydroxylated benzenes are highest on Ni(II)O because of the favorable adsorption on the surface via H₂O elimination.

4.5 Persistence and Lifetimes of EPFRs on Fe(III)₂O₃, Ni(II)O, and Zn(II)O Surface

The principal reaction of most radicals is with molecular oxygen which is the major pathway for its conversion to non-radical species (21). The half-lives of unchlorinated EPFRs of hydroquinone, phenol, and catechol were 2.9-4.6 days (69.6-111 h). 2-Monochlorophenol exhibited a half-life of 1.0 day (24 h) while the half-lives of 1,2-dichlorobenzene and monochlorobenzene were unmeasurable due to their low initial concentration and, perhaps, greater reactivity. The presence of chlorine appears to reduce the persistence and initial yield of formation of EPFRs on iron surfaces due to their lower reactivity with the surface and subsequent reactions with surface hypochlorites. 1,2-Dichlorobenzene and monochlorobenzene chemisorb by HCl elimination, and results in hypochlorite formation, which oxidizes the radicals so fast they are virtually not observable except at very short times. In contrast, 2-

monochlorophenol, which chemisorbs primarily by elimination of H₂O and secondarily by HCl elimination, only forms limited hypochlorites, and the decay is slow enough for their corresponding EPFRs to be easily observed. The remaining adsorbates are non-chlorinated and have remarkably long lifetimes.

In contrast, the half-lives of the EPFRs for the unchlorinated adsorbates are measurable and have higher half-lives on Ni(II)O similar to the Cu(II)O study. 1,2-Dichlorobenzene, monochlorobenzene, and 2-monochlorophenol have half-lives of 1.67-3.79 days. The lifetimes and persistence of the EPFRs observed on Ni(II)O is similar to Fe(III)₂O₃ which differs by 2 orders of magnitude for the ones reported for copper. The result suggest that as the number of chlorine substituent increases, the half-lives decreases, as such 2-monochlorophenol has a higher half-life compared to 1,2-dichlorobenzene. Probably, the chlorine group destabilizes the molecule by withdrawing the electron density from the ring. On the other hand, the hydroxyl group on 2-monochlorophenol are electron-donating and enhances the stability of the molecule and counteracts the electron-withdrawing ability of chlorine. In the case of iron, the higher propensity to form surface hypochlorite which are known to be strong oxidizing agent decreases the stability of the surface-bound EPFRs of the chlorine-substituted adsorbates—1,2-dichlorobenzene and monochlorobenzene. The half-life of the EPFRs of catechol in Ni(II)O is 2.78 days. Phenol on the other hand exhibits two decays—a fast decay with a half-life of 0.56 day, and a second slow decay, with a half-life of 5.21 days, which is the longest half-life observed for all the adsorbates. The short half-life is probably due to the formation of secondary radical from the decomposition of phenoxyl radical(12). Likewise, this behavior was also observed for phenol in Zn(II)O surface which have the highest half-lives measured so far of 73 days and another fast decay of 9.5 days. The half-lives of EPFRs on Zn(II)O are on the order of

months compared to $\text{Fe(III)}_2\text{O}_3$ and Ni(II)O , which are only on the order of days, and only on the order of hours on Cu(II)O . The other two hydroxyl substituted adsorbates, catechol and hydroquinone also have very long half-lives. In contrast with iron, all the chlorinated compounds show a remarkably long lifetime. This is because Ni(II)O and Zn(II)O has less propensity to form hypochlorite species that would otherwise destroy and perturb the stability of the EPFR-metal systems (22). The single decay observed for hydroquinone is attributed to the formation of *p*-semiquinone radical. The slow decay for phenol is from the decay of phenoxyl radical, while the faster decay is attributed to the decay of secondary radical, cyclopentadienyl. Likewise, monochlorobenzene also formed the same radicals, although the half-life of the slow decay is 3x less than the half-life observed for phenol. The presence of the electron-withdrawing chlorine substituent decreases the stability of the corresponding chlorocyclopentadienyl radical. At 230 °C, only one radical was observed for catechol which is attributed to the formation of *o*-semiquinone radical. The very long half-lives on zinc and their higher stability and persistency are probably the consequence of all the electrons in the *d*-orbitals being paired. When the one-electron reduction occurs, (cf. **Scheme 4.1**) the electron from the *2p* orbital of oxygen transfer to the *4s* sublevel of zinc and not to the *3d* sublevel, since it can no longer accommodate electron, resulting in a more stable EPFR-Zn complex.

There were large differences in the persistence of the EPFRs observed on Zn(II)O , Ni(II)O , $\text{Fe(III)}_2\text{O}_3$, and those previously reported for Cu(II)O (15) (cf. **Figure 4.1**). The half-lives of EPFRs of hydroquinone, phenol and catechol were nearly 2 orders of magnitude longer for $\text{Fe(III)}_2\text{O}_3$, while the chlorinated compounds, 1,2-dichlorobenzene and monochlorobenzene, were so short to be virtually non-measurable on $\text{Fe(III)}_2\text{O}_3$ but were not structurally different from the other EPFRs for Cu(II)O . This is attributed to the greater propensity for $\text{Fe(III)}_2\text{O}_3$ to

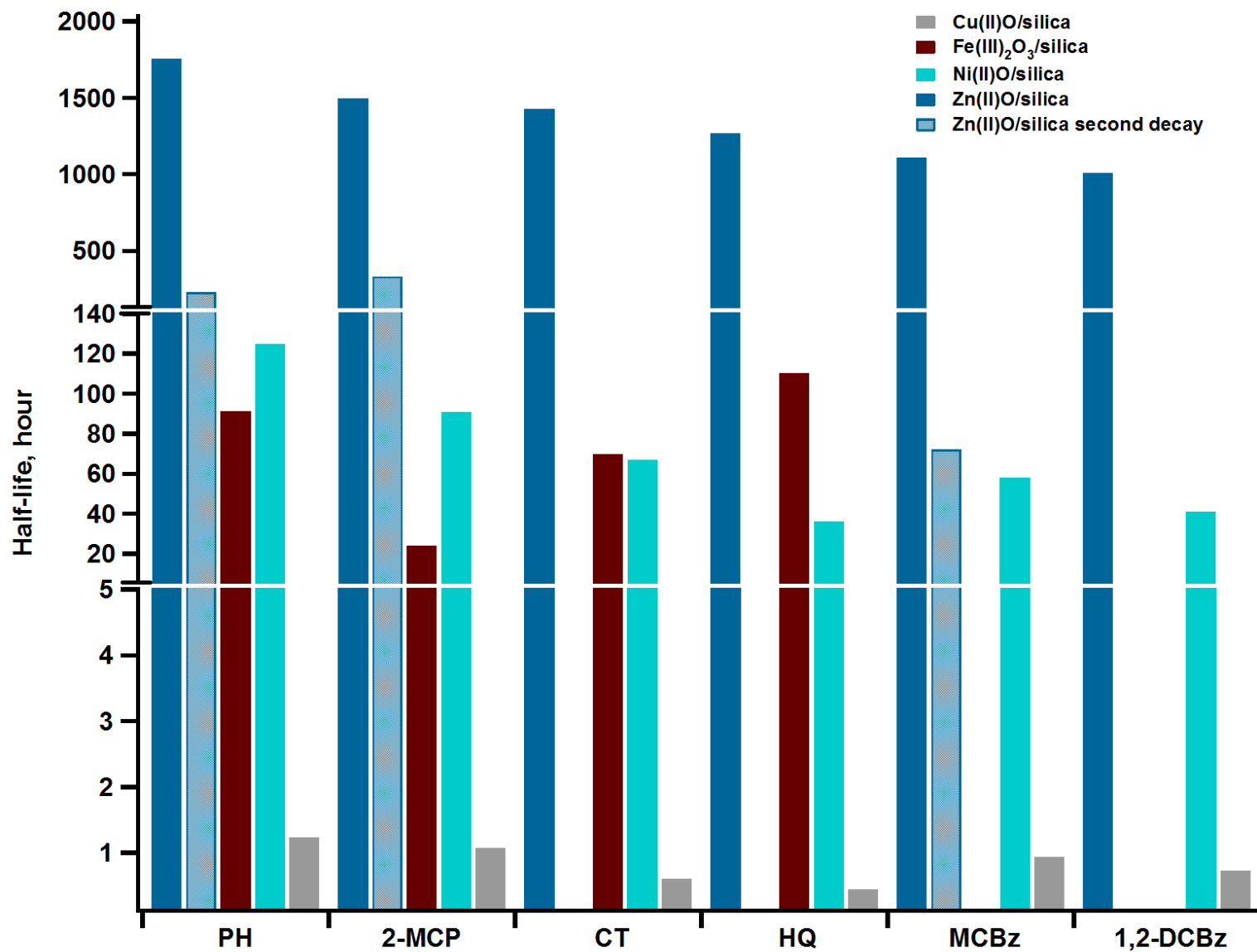


Figure 4.1. Comparison of the half-lives of EPFRs over 5% Fe(III)₂O₃, Cu(II)O, Ni(II)O, and Zn(II)O on silica surface dosed at 230 °C and exposed in air at room temperature.

form hypochlorites than Cu(II)O, Ni(II)O and Zn(II)O. But the half-lives observed on Zn(II)O were the longest compared to the three metals. *p*-Semiquinone from hydroquinone exhibited long overall half-life of 4.6 days. The decays exhibit very good exponential fits, which indicate the decay of a single species. However, for some adsorbates, such as phenol and catechol, the formation of cyclopentadienyl radicals and other secondary radicals, which may be factors in the measured half-lives at longer times, cannot be ruled out. As in the case on Ni(II)O two decays were observed for phenol which may be due to formation of cyclopentadienyl radical.

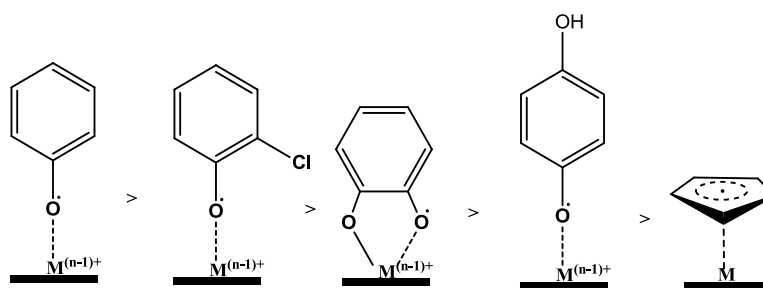


Figure 4.2. Relative persistency and stability of EPFRs on metal oxide surface

This behavior was also observed for monochlorobenzene and 2-monochlorophenol. If only the nature of the adsorbates determines the stability and persistency of the EPFRs, then we would expect them to have similar half-lives regardless of the metal they are bound to. But this is not the case, it is evident from the results, that their stability and persistency are most importantly determined by the metals they are bound to, as in the case of Zn(II)O which have extremely long half-lives on the order of months. Gas phase calculation of phenoxyl and semiquinone type radical shows that it is highly resistant to oxidation with molecular oxygen (23). This observation was also true for the EPFRs stabilized on the surface of transition metals. The remarkably consistent stability and persistency for all metals attests, that phenoxyl radical is most stable when bound on surface. Moreover, *ab initio* calculations suggests that the phenoxyl radical are

more stable than semiquinone radicals (23) which is contrary to its behavior in solution as reported in the literature. The relative stability of the different radicals is depicted in **Figure 4.2**. Chlorophenoxy radical is less persistent compared to phenoxy radical, with the chlorine substituent reducing the resonance stability by withdrawing the electron density from the ring. Semiquinone radicals in general, are less stable than phenoxy-type radical, but *o*-semiquinone radical on the other hand, are more stable and persistent than the corresponding *p*-semiquinone radical. This has been observed for copper, nickel, and zinc with the exception *p*-semiquinone radical bound on iron surface. Calculation of the reaction of gas phase semiquinone radicals with molecular oxygen suggest that the reaction of *o*-semiquinone radical are highly endothermic compared with *p*-semiquinone radical with calculated activation energies of 79.8 and 72.9 kcal mol⁻¹ (23), respectively, suggesting that *o*-semiquinone radical are more resistant to oxidation compared to the corresponding *p*-semiquinone radical. Experimental data suggest the same observation is true with surface-bound EPFRs.

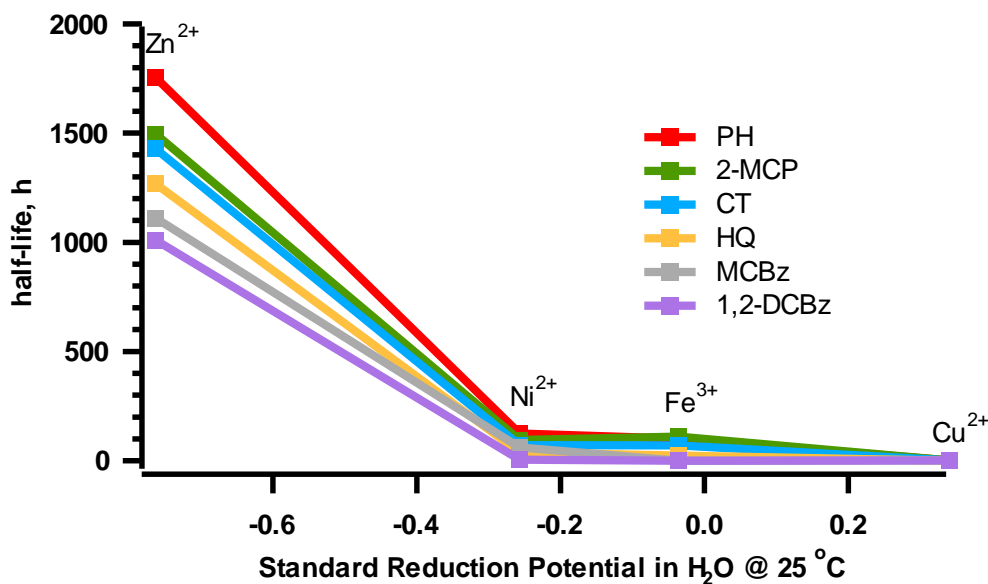
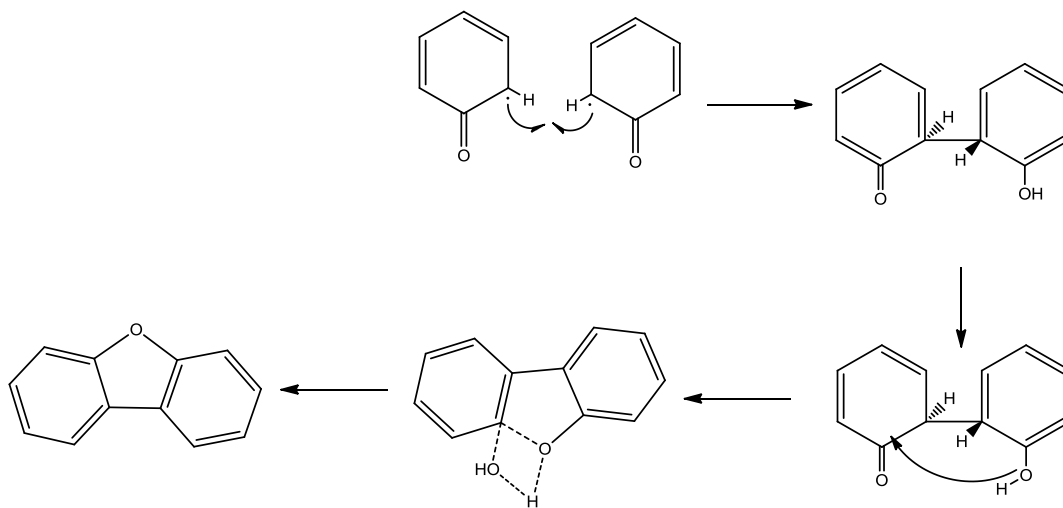


Figure 4.3. Dependence of the EPFR half-lives with the standard reduction potential

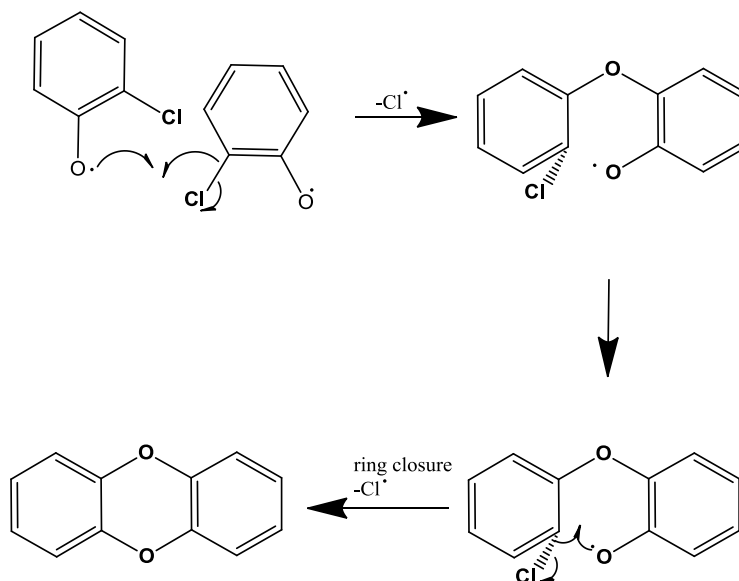
Figure 4.3 shows the plot of the half-lives for the different adsorbates versus the standard electrode potential at 25 °C in water. The standard potential used was from the reduction of the cation to its metallic form since there are no standard potential for the other metal to their one electron reduction form. The plot shows that the lower the standard electrode potential the more stable the EPFRs, since the ΔG of the reaction is more positive, and thus the reactivity towards a molecule is non-spontaneous.

4.6 Formation of Molecular Products from Radical Recombination

The extraction of the particles containing transition metal oxides dosed with different adsorbates yielded molecular products. The majority of the products observed in the extraction of the particles after dosing primarily come from phenoxy radicals. Dioxin and furans were observed in the extraction products from Cu(II)O and Fe(III)₂O₃, but not on Ni(II)O on silica particles. Moreover, few products were observed for Ni(II)O compared to the two metals. It is



Scheme 4.9. Formation of dibenzofuran from recombination of two keto forms of phenoxy radical (I)



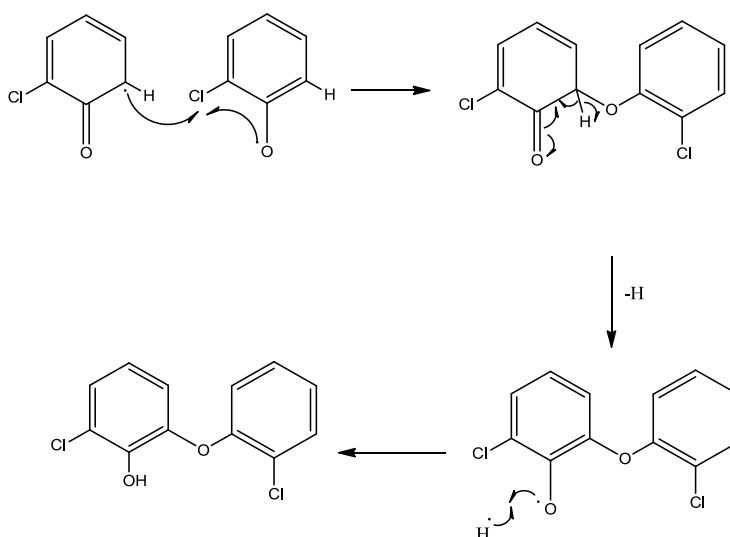
Scheme 4.10. Formation of dibenzo-*p*-dioxin from reaction of 2-monochlorophenol and chlorophenoxy radical (*I*)

already established that iron and copper catalyze the formation of dioxins and furans (24-26).

The formation of furans is thought to proceed via the mechanism. The mechanism of formation is shown in **Scheme 4.9** from two keto form of a phenoxy radical. The electrons on the radical recombine and tautomerize to form a biphenyl-like structure (**II**). The oxygen attacks the carbon (**III**) which leads to ring closure. The formation of dioxins in solution between a molecular precursor and a radical react to form dioxin depicted in **Scheme 4.10**. The electron on the oxygen atom on the phenoxy radical combines with the electron on the C-Cl bond forming an ether linkage between the two aromatic rings and produces an intermediate species (**II**), and concomitantly, eliminates a chlorine radical in the process. A hydrogen atom then abstract an electron from the O-H bond forming another radical intermediate (**III**), induces ring cyclization, consequently eliminates chlorine radical, and forms dibenzo-*p*-dioxin. Moreover, the dioxin can also undergo chlorination reaction in chlorine-rich environment to give its polychlorinated analogue. Another product that was observed from 1,2-dichlorobenzene is 2,3'-dichloro-2'-

hydroxydiphenyl ether, the carbon (III) and induces cyclization mechanism and leads to a cyclic transition species, which competes with dioxin depicted in **Scheme 4.11**.

While furans and dioxins are of highly significant environmental and health interest, other non-dioxin and non-furan products were observed. One of the most commonly seen molecular products is phenol, since most of the adsorbates have parent phenolic structure. Moreover, semiquinone radical can decompose at higher temperature to form phenoxy radical as secondary radical as demonstrated by the adsorption of catechol where phenols were detected in the extract along with 2-phenoxyphenol dimers and 1,3-diphenoxybenzene trimers. The mechanism of formation of 2-phenoxyphenol is similar to the formation of 2,3'-dichloro-2'-hydroxydiphenyl ether as shown in **Scheme 4.11**. On the other hand, the trimer, 1,3-

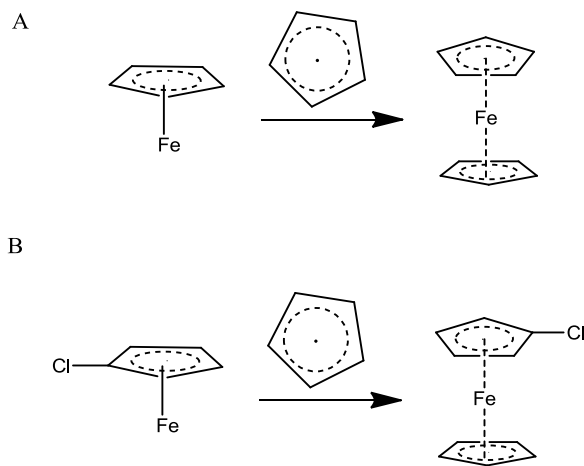


Scheme 4.11. Formation of 2,3'-dichloro-2'-hydroxydiphenyl ether

diphenoxybenzene is formed when the electron on surface-associated phenoxy radical combines with one of the mesomeric forms of the radical on the carbon at the *ortho* position on the aromatic ring. The proposed mechanism for the formation of 1,3-diphenoxybenzene and 2-

phenoxyphenol are depicted in **Appendix 2**.

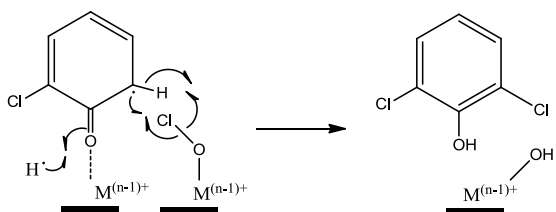
Semiquinone and phenoxy radicals are principally the major radicals in combustion system. However, other secondary radicals from decomposition of semiquinone and phenoxy radicals can undoubtedly form, such as the resonance-stabilized cyclopentadienyl radical. But its detection as molecular species is difficult, since the cyclopentadienyl ring are converted to a more stable resonance structure such as phenoxy ring. However, a direct evidence of the formation of cyclopentadienyl radical was observed on iron. The organometallic compound ferrocene and chloroferrocene were found in the extract when 1,2-dichlorobenzene and monochlorobenzene were dosed on iron as shown in **Scheme 4.3** and iron are known to stabilize cyclopentadienyl radical (27). In addition, the observation of naphthalene and its substituted



Scheme 4.12. Formation of (chloro)ferrocene from cyclopentadienyl radical

derivative, methylnaphthalene and chloronaphthalene, is an indirect evidence of the existence of cyclopentadienyl radical in combustion system. Naphthalene are known to form from cyclopentadienyl radical through a mechanism elucidated in **Scheme 4.14** (13).

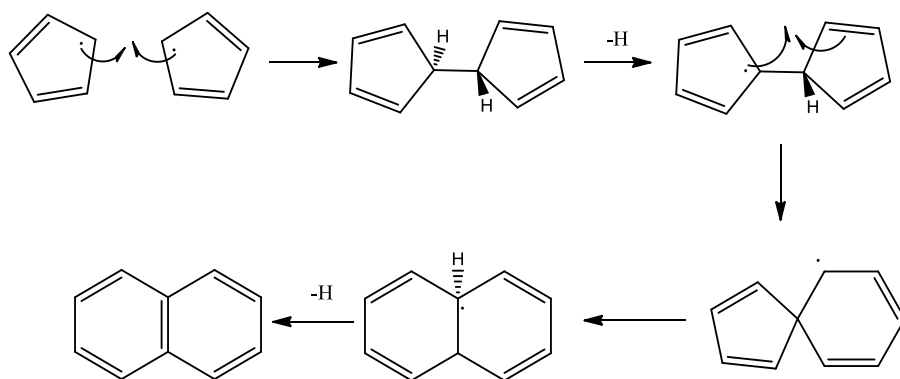
Additionally, formation of chlorinated species were detected in the extracts of the particles after dosing. The formation of chlorinated compounds such as 2,6-dichlorophenol, dichlorobenzene, trichlorobenzene, and tetrachlorobenzene suggest that chlorination reaction



Scheme 4.13. Formation of 2,6-dichlorophenol by surface hypochlorite chlorination

occurs. The mechanism is thought to proceed via the following steps depicted in **Scheme 4.13** for 2,6-dichlorophenol whereby, the chlorination process is catalyzed by surface hypochlorite species on the metal oxide, which chlorinates the aromatic ring. The higher chlorinated compound iterates this process several times to yield multiply-chlorinated species.

4.7 Interaction of EPFRs with Biological Compounds



Scheme 4.14. Formation of naphthalene and chloronaphthalene from recombination of cyclopentadienyl radical

The interactions of the EPFRs with some biologically important molecules were studied. As depicted in **Figure 3.5** an increase in radical intensity for the particles containing EPFRs from 2-monochlorophenol in BALF was observed suggesting that there are probably components in BALF which amplify the generation of EPFRs. Since BALF contains numerous component such as organic molecules having phenolic structures like tyrosine and adrenaline, and numerous metallo-proteins and proteins systems (28) it is difficult to identify which components are

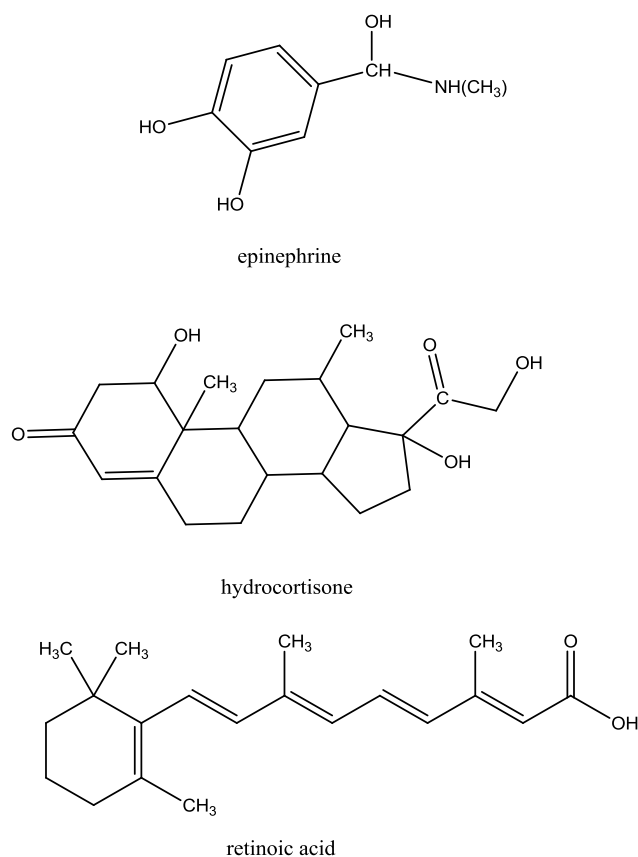


Figure 4.4: Structure of epinephrine, hydrocortisone, and retinoic acid

responsible for the amplification of the signal intensity, thus, additional experiments were performed and showed hydrocortisone and retinoic acid decrease the signal intensity, the structures are depicted in **Figure 4.4**. This is expected since retinoic acid or vitamin A is an

antioxidant and acts as a radical scavenger. However, similar study conducted for epinephrine showed a significant increase in intensity by as much as twice the original signal suggesting that molecules having similar structure with the adsorbates (i.e., containing phenolic structures) might chemisorb in the surface of the particle and amplify the generation of the EPFRs signal on the particle surface. A sample containing just epinephrine (also known as adrenaline) and pure Cu(II)O/silica, however, produces a small signal slightly higher than the noise level, but still cannot account for the doubling of the EPFR signal with the Cu(II)O/silica containing adsorbed EPFRs. Therefore, we can hypothesize that the EPFR already present on the particles surface have a synergistic effect on catalyzing additional EPFR through a yet to be identified mechanism. The structure on **Figure 4.4** for epinephrine is similar to catechol and might produce *o*-semiquinone radical or phenoxyl radical in solution.

Kinetic study on the half-lives of the EPFRs on BALF and serum showed that the half-life was ~2x higher in BALF than on serum and the EPFR signals do not decay immediately. Probably due to diffusion-limitation, since BALF contains bigger molecules such as protein systems that prevents and hinders the reaction of the EPFRs with smaller components of BALF.

On the other hand, the serum component, which predominantly contains smaller molecules, can effectively approach the particle surface and interacts faster and, thus, a faster decay was observed. The overarching observation is that the half-lives on both systems (serum and BALF) are long enough that the EPFRs on the particles can possibly be translocated to different organ systems such as the lower respiratory system where most of the EPFR-induced damages are observed or worst the smaller fractions of the particles containing EPFRs can circumvent the blood-brain barrier system and induce their adverse health effects on the central nervous system (29-32). The intensification of the signal for the Cu²⁺ region is probably due to

the numerous metals in protein systems and is not due to an organic radical or EPFRs.

From this study we have shown that there is an increase on EPFRs concentration when EPFRs are already on the surface, but most of the toxicological damages attributed to PM are thought to be the generation of ROS. The next section discusses a spin-trapping experiment to detect whether EPFRs indeed generates ROS such as superoxide and hydroxyl radical and the mechanism being operative in their formations.

4.8 Spin Trapping Studies

These EPFR radicals were found to generate reactive oxygen species in biological media (33), though the mechanism behind ROS formation is not clear. The works by Pryor *et al.* have indicated that organic radicals such as for example semiquinone radicals can undergo a cyclic process in biological media producing a large output of ROS (34). Since the EPFRs attached to

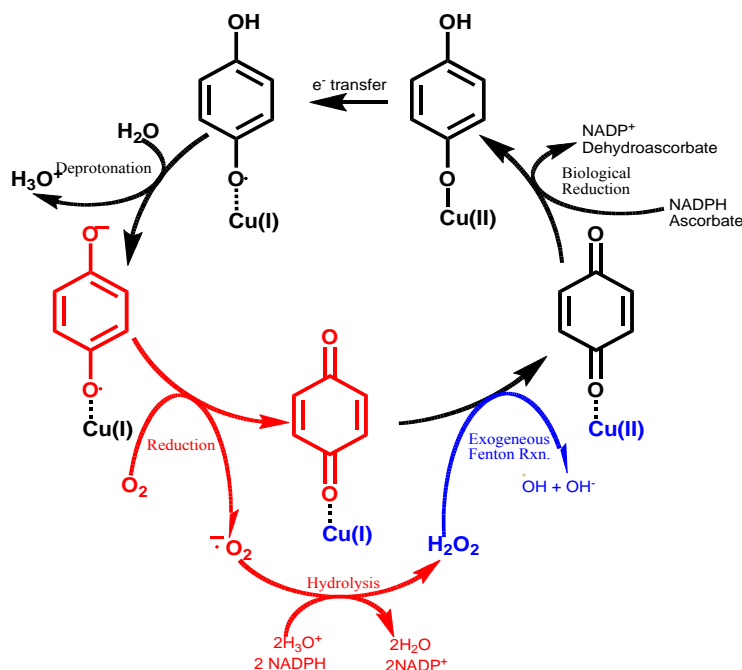


Figure 4.5. A hypothesis of a redox cycle of EPFRs originating from hydroquinone molecule adsorbed on Cu(II)O domain in biological system

the surface of particulate are similar to those described by Pryor (35, 36), and have been shown to produce ROS (37) (2, 37), we hypothesize, that they can undergo a similar cyclic process (cf. **Figure 4.4**). This hypothesis combines both the radical transformation and the associated metal center as a medium of Fenton reaction and source of ROS. Fenton process is a very important contributor to the overall ROS production (38-40).

It is very often assumed in the literature that the OH radical formation by the particulate matter in the exposed cell cultures is a result of Fenton reaction of transition metals present therein. However, since most of the fine and ultrafine particulate matter is combustion-borne, the metals present therein are in their higher oxidation state and, thus, inactive in Fenton process. Our hypothesis, by conjunction of surface radicals with metal center (and thus formation of

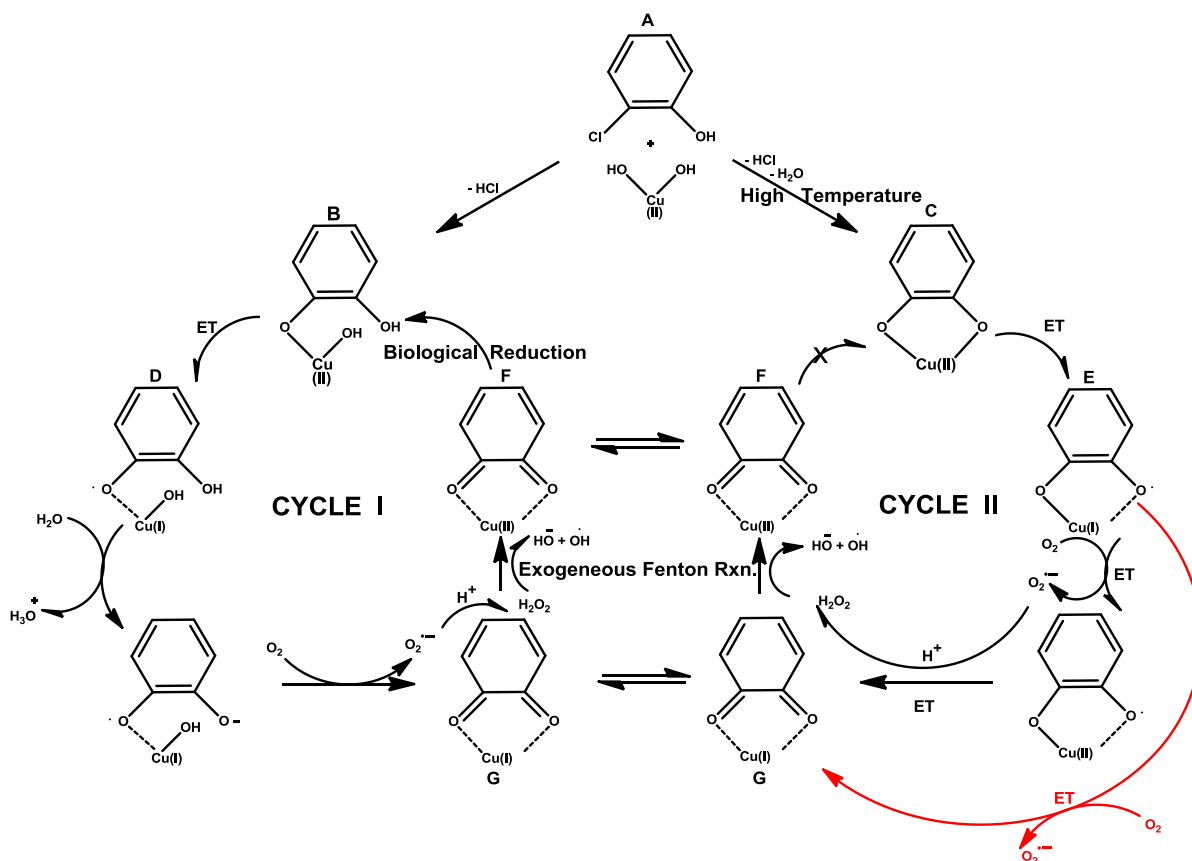
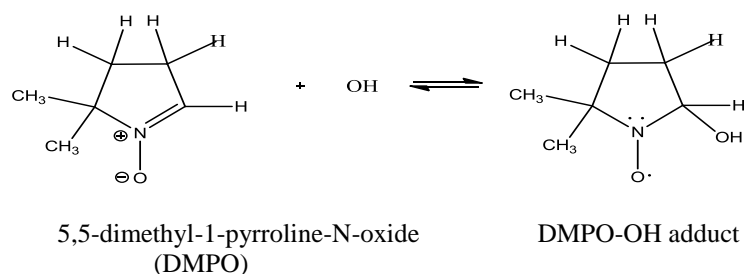


Figure 4.6: A hypothesis of a red-ox cycle of EPFRs originating from 2-MCP molecule adsorbed on Cu(II)O domain in biological system. (ET – Electron Transfer)

reduced metal site) provides an explanation of observed biological reactivity. Another example of redox cycling of EPFRs originating from 2-monochlorophenol molecule adsorbed on Cu(II)O domain in biological system is presented in **Figure 4.6**. The EPFRs formed from 2-monochlorophenol adsorbed on Cu(II)O/Silica are 2-chlorophenoxy (D), *o*-semiquinone (E) radicals. 2-Hydroxyphenoxy (E) radicals may generate a complete redox cycle (**Figure 4.6** left-hand side cycle) similar to that presented in **Figure 4.5** for 4-hydroxyphenoxy radicals.

Whereas the left hand cycle by participation of primary *o*-semiquinone radical (G) bound to the Cu(I) center (which may form only at high temperature (37) in sequence of transformation E→G→F) is not complete; i.e. *o*-semiquinone radical (G) is not generated during the cycle. The cycle ended on particle F which may participate only in right hand cycle. It is remarkable that both complete and auxiliary cycles may operate in aqueous media and generate ROS.

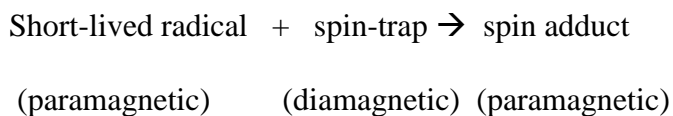


Scheme 4.15. Formation of DMPO-OH adduct

Current manuscript presents experimental evidences of the formation of some ROS in the presence of EPFRs in PBS solution using 5,5-dimethyl-1-pyrroline-N-oxide (DMPO) as a spin-trapping agent. The technique of trapping short-lived radicals with nitrones and nitroso compounds was developed by several groups in later part of 1960's (41, 42). The spin-trapping process is based on a reaction between the spin trap molecule and a radical to produce a stable paramagnetic aminoxyl (or nitroxide) species, which are referred to as a spin adduct (**Scheme**

4.1).

The spin trapping method for identifying radicals is based on a simple principle:



and takes advantage of the stability of the nitroxyl radicals. The aminoxyl product has a unique EPR spectrum which is dependent on the nature of the short-lived radical. In principle, therefore, any short-lived radical which is trapped can be unambiguously identified. In practice, however, there are some adducts which are difficult to assign.

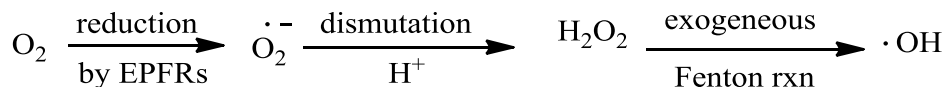
4.8.1 Hydroxyl Radical Generation

According to hypothesis presented in **Figure 4.6**, superoxide, hydrogen peroxide, and OH radicals are created due to redox cycling of EPFRs in aqueous media. The simplified sequence of ROS generation is summarized in **Scheme 4.16**, where OH radicals are the final product of the series. The identification of the OH radicals in aqueous solutions containing EPFRs and their relative concentration compared to other media with non-EPFR particles is of utmost importance for the EPFRs redox cycle validation. The experiments in the presence of DMPO spin trap were performed for both EPFR and non-EPFR samples to achieve that.

The 4-line EPR spectrum of DMPO-OH adducts was detected in solutions containing either EPFR- or non-EPFR-containing particles with DMPO in PBS media (cf. **Figure 3.18**). In the presence of EPFR particles, more DMPO-OH adduct was formed compared to non-EPFR containing particles, while a particle free solution (DMPO only) produce trace amounts of the DMPO-OH adduct (cf. **Figure 3.19**, green line). The amount of the DMPO-OH spin adduct formed in the presence of non-EPFR and EPFR particles changes with the incubation time, the longer the incubation time the bigger the difference in the amount of DMPO-OH formed in case

of non-EPFR and EPFR particles (cf. **Figure 3.19**). On average, twice as much DMPO-OH spin adducts was formed in the presence of EPFR particle compared to non-EPFR particles at long time of incubation, for instance at 220 min. (cf. **Figure 3.19**). It is also worthwhile to mention, that while in the case of non-EPFR particles the amount of DMPO-OH formed plateaued at earlier incubation time, the number of detected DMPO-OH spin adducts from EPFR particles monotonically increased and plateaued at long time of incubation (more than 12 hours, not shown). The concentration of OH radicals generated according to the cycle presented in **Figure 4.6** might be measured as a difference between the amounts of DMPO-OH adducts accumulated in EPFR and non-EPFRs solutions at the same incubation time, **Figure 3.19**.

With this comparative approach it is not critical how are DMPO-OH adducts generated in non-EPFR solution. We are not aware of any literature data confirming generation of OH radicals in fresh solution of Cu(II)O/silica (non-EPFR particles). Even in presence of H₂O₂ no evidence could be obtained for OH formation from the Cu(II)_(aq)/H₂O₂ reaction system despite the detection of a prominent signal from the DMPO-OH adduct due solely to nucleophilic addition of water to DMPO (43). The nonradical nucleophilic reaction of water with DMPO, is a significant pathway for the formation of DMPO-OH radical adduct (43). The direct



Scheme 4.16. Conversion of molecular oxygen to hydroxyl radical catalyzed by EPFRs

hydroxylation of DMPO in aqueous media (nucleophilic attack of water without participation of OH radicals) by oxidants, for instance by catalyst, H₂O₂, Fe and Cu ions, etc. may easily happen (43, 44). Therefore the difference in the DMPO-OH adducts concentration between solutions

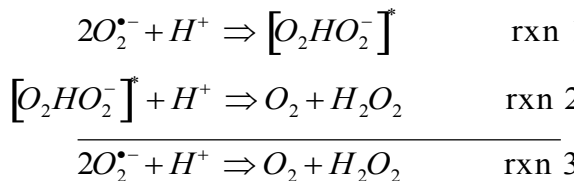
containing EPFR and non-EPFR particles may indicate the existence of OH radicals in EPFR solution. The number of OH radicals was quantified with the assumption of 1:1 stoichiometry OH to DMPO for DMPO-OH spin adduct formation, and calibrated using a TEMPOL solution as a standard and was found to be $\sim 1.39 \times 10^{14}$ spins /mL, which corresponds to $\sim 0.23 \mu\text{M}$ concentration of OH radicals at incubation time of 140 min. This value may be the lower concentration limit of OH radicals because the decay of DMPO-OH during accumulation as well as the effectiveness of trapping OH radicals by DMPO was not considered. Note that the micromolar concentration of OH radicals were also detected in solution from airborne particulate matter (urban dust SRM 1649, Washington DC area), diesel particulate matter (SRM 2975) etc using high-sensitivity fluorescence method (45) and the integrated concentration of OH radical reached $\leq 1 \mu\text{M}$ at time of incubation 140 minutes. Less than $2 \mu\text{M}$ DMPO-OH (or OH radicals) adduct was detected in Fenton mixture at concentration of $\text{Fe}^{2+} 10 \mu\text{M}$ ($100 \mu\text{M}$ DMPO + H_2O_2 + $10 \mu\text{M}$ FeSO_4)(46) or less than $1 \mu\text{M}$ DMPO-OH adduct at concentration of $\text{Fe}^{2+} 1 \mu\text{M}$ (in Fenton reaction (40)). The extrapolation of the OH radical concentration to the number of EPFR radicals ($[\text{OH}] / [\text{EPFRs}] = 1.39 \times 10^{14} \text{ (spins/mL)} / 1.50 \times 10^{-4} \text{ (g/mL)} \times 10^{17} \text{ (spins/g)}$) indicates, that 1 EPFR radical generates ~ 10 OH radicals at incubation time of 140 min. The monotonical increase of the amount of DMPO-OH adduct with the incubation time as well as large number of OH radicals formed per unit EPFR indeed indicates a cyclic nature of the process.

4.8.2 The Effect of Superoxide Dismutase (SOD) and Catalase (CAT)

The principal source of OH radicals in the presence of EPFR outside of the biological systems is superoxide dismutation, reactions 1-3, resulting in the formation of hydrogen peroxide (38, 47). The reaction is usually a second-order process, where one superoxide molecule transfers an electron to another superoxide molecule with the generation of excessive charge

density being avoided by the involvement of a proton (47). This reaction has been proven to occur over a very broad pH range of 5 to 10. The reaction involves the incorporation of a single proton into the transition state $[O_2HO_2^-]^*$, rxn 1. The overall rate of superoxide dismutation, a second-order reaction 3, is usually slow in aqueous media ($k_3 \sim 10^5 M^{-1}.s^{-1}$ at pH = 7.4 (38, 47)) and is catalyzed by the presence of transition metals. For example, k_3 can change from 10^6 to $10^9 M^{-1}.s^{-1}$ in presence of copper-containing compounds (38, 48). We have unsuccessfully attempted to spin-trap superoxide radicals for the solutions containing either EPFR or non-EPFR particles using a DMPO spin trapping agent. One of the probable reasons for inability to detect superoxide radicals is a fast dismutation of superoxide catalyzed by Cu(II)O/silica. Except that the DMPO-superoxide adduct (abbreviated as DMPO-OOH at neutral and higher pH media in aqueous and as DMPO- O_2^- in aprotic solutions (49)) has a very short lifetime (less than 1 min at pH = 7.4 (50)).

One of the biological agents for the decomposition of superoxide is the superoxide dismutase (SOD) enzyme, which is a soluble copper-complex protein, with a high superoxide decomposition rate constant of $1.3 \times 10^9 M^{-1}.s^{-1}$ (48). Therefore, SOD may accelerate rxn 3 by about 4 orders of magnitude in aqueous media and can be used as an effective indicator of



superoxide involvement in the current experiment by inhibiting the sequence: $O_2^{\bullet-} \rightarrow H_2O_2 \rightarrow OH \rightarrow DMPO-OH$ at the very beginning. In other words, SOD alone, should transform superoxide into H_2O_2 . The interaction between peroxide and SOD has been studied as a function

of overall activity loss (51). As a result less DMPO-OH adduct forms during the process. Otherwise, a different mechanism is responsible for DMPO-OH formation (52).

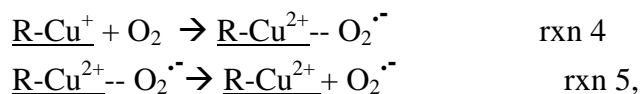
A standard procedure to verify the existence of superoxide radicals and hydrogen peroxide molecules is to introduce SOD and CAT, respectively, to the working solutions. Catalase (CAT), converts hydrogen peroxide into water and oxygen, and thus its addition to the reaction system will also inhibit OH formation, though at a different stage of the process. In the current experiment, both SOD and CAT should decrease the DMPO-OH adduct concentration if DMPO-OH forms in sequence: $O_2^{\cdot -} \rightarrow H_2O_2 \rightarrow OH \rightarrow DMPO-OH$ (51, 52). Both SOD and CAT decreased separately the DMPO-OH adducts concentration in solution. Introduction of combined SOD and CAT to the solution resulted in a significantly higher reduction of DMPO-OH adduct concentration. These results unambiguously demonstrate the interconnection of superoxide and hydrogen peroxide formed from EPFRs.

4.8.3 Trapping of Superoxide Radical by DMPO in Aprotic Solvents

The effect of SOD on the formation of DMPO-OH adduct in the presence of EPFR particles have confirmed the involvement of superoxide radicals in the process, though the radicals could not be spin-trapped in aqueous media. Unfortunately, the commonly used nitron spin traps (including DMPO) have very low efficiency for trapping superoxide radicals in aqueous media and the DMPO-superoxide radical adduct (DMPO-OOH) is not stable (50, 53). Although the spin trapping EPR method is one of the sensitive and definitive methods to trap the superoxide radicals (49, 53, 54), the experiments were unsuccessful, as mentioned above, to trap superoxide using DMPO in aqueous media of EPFRs. To address the deficiency in aqueous media, the experiments were performed in different aprotic solvents taking into consideration the fact that DMPO is an excellent probe in non-aqueous media for detecting superoxide (55). On

the other hand, superoxide has considerable nucleophilic character in aprotic solvents (47, 56), the application of such solvents can facilitate trapping of the superoxide radicals. Note that generation of superoxide in aprotic solvents can proceed easily by participation of *o*-semiquinone radicals, **Figure 4.6** (particle G, auxiliary cycle). In the *o*-semiquinone radical bound to the Cu(I) center, the non-radical bearing oxygen-copper bond is highly polarized and the species can be considered a radical anion regardless of aproticity of the solvent. Accordingly, the reaction of oxygen molecule with the *o*-semiquinone type EPFR will yield superoxide, even in aprotic media. While the same type of reaction may not occur in aprotic media in case of consideration of full cycle, **Figure 4.6**. Except that there might be an alternative pathway (transformation of E→G, colored by red) for formation of superoxide by reacting of dissolved oxygen with a lower valence transition metal complex (*o*-semiquinone radical (E) bound on the Cu⁺ assigned R-Cu⁺),

Figure 4.6, rxn 4



where R represents *o*-semiquinone radical. This type of reaction, one-electron reduction of neutral oxygen by metal complexes is discussed in the literature and in fact, the superoxide might be coordinated with the metal (47, 56), rxn 4. Subsequently, in aprotic solvents, O₂^{•-} is both a good nucleophile and a good one-electron reductant. To directly prove the formation of superoxide from the reaction of EPFRs with oxygen, experiments were performed in DMSO and AcN solvents. The selection of the solvents was based on a unique affinities of superoxide radical toward DMSO (56, 57) or AcN, particularly in suspension of metal oxides (58). Solubility of oxygen in these solvents, as a precursor for superoxide anion formation, is different and follows the order: H₂O < DMSO < AcN (58-60). On the other hand the calculated rate

constant of interaction of superoxide with DMPO in different media is also in the order H_2O ($5.85 \times 10^{-5} \text{ M}^{-1} \text{ s}^{-1}$) < DMSO ($8.71 \times 10^{-4} \text{ M}^{-1} \text{ s}^{-1}$) < AcN ($1.81 \times 10^{-3} \text{ M}^{-1} \text{ s}^{-1}$) (49) showing that the trapping results for superoxide radical by DMPO are expected to be dominant in ACN or DMSO. The results of the DMPO-O₂⁻ spin adduct formation in those solvents and in the presence of EPFR particles are summarized in **Table 4.1**. A weak signal was detected from the EPFRs solution in DMSO (**Figure 3.20**, spectrum 2), while a broad, four-line signal was detected in AcN solution (**Figure 3.20**, spectrum 3) typical for DMPO-O₂⁻ adduct for the suspension of powdery semiconductors (TiO₂, Fe₂O₃, WO₃, CdS) in AcN (58). Such broadening of the DMPO-O₂⁻ spectra might be explained by the high content of oxygen in AcN and the interaction of oxygen with paramagnetic probe (DMPO-O₂⁻) signal (61). The resolution of this spectrum was improved when the same experiment was repeated with smaller amount of the EPFR suspended in solution (**Figure 3.20**, spectrum 4).

The polarity effect of solvents on hyperfine splitting constants (hfsc) of DMPO-O₂⁻ adducts (spectra 2,4) is visible when compared to the EPR spectra of DMPO-O₂⁻ spin adduct from Fenton reaction in homogeneous water environment in presence of 5% DMSO (**Figure 3.20**, spectrum 1). The hfsc values for spectrum 1 are $\alpha_{\text{N}} = 14.50 \text{ G}$, $\alpha_{\text{H}}^{\beta} = 10.67 \text{ G}$, $\alpha_{\text{H}}^{\alpha} = 1.40 \text{ G}$ (see (43)), for spectrum 2 $\alpha_{\text{N}} = 14.00 \text{ G}$, $\alpha_{\text{H}}^{\beta} = 9.8 \text{ G}$, $\alpha_{\text{H}}^{\alpha} = 1.40 \text{ G}$ for DMPO-superoxide radical in DMSO (cf. **Figure 3.20**, 2)) and spectrum 4 $\alpha_{\text{N}} = 13.00 \text{ G}$, $\alpha_{\text{H}}^{\beta} = 9.0 \text{ G}$ for DMPO-superoxide radical in AcN. The value of $\alpha_{\text{H}}^{\alpha}$ in can were undetermined, probably due to high content of dissolved oxygen causes spectral broadening (58). The decrease in the hfsc parameters for DMPO-O₂⁻ in different solvents, H₂O, DMSO, and AcN, correlates with the decreasing polarity of the solvents (55, 62-66). According to the Burdick and Jackson's polarity index, the solvent's polar property is as follows: H₂O (10.2) > DMSO (7.2) > AcN (5.8), with the polarity indices

(66) given in parenthesis. In agreement with the polarity, the highest hfsc were detected in H₂O and the lowest in AcN.

Finally, the literature digitized EPR spectrum of DMPO-O₂⁻ spin adduct formed in photoexcitation processes of powdery semiconductor TiO₂ in AcN solution (58) (red line) fits well with our experimental DMPO-O₂⁻ spectrum (**Figure 3.21**) from EPFR solution. This result provides a direct proof of the superoxide radicals being formed from molecular oxygen in the presence of EPFR particles.

The inability to identify superoxide radicals in the aqueous media, while a DMPO-O₂⁻ spin adduct is detected in the aprotic solvents, suggests a very quick transformation of the O₂⁻ in water environment. Indeed, the experiments with the mixed AcN-Water solution has shown, that even small amount of water results in an immediate formation of OH radicals and detection of DMPO-OH spin adduct product (cf. **Table 4.1**). At the same time, the characteristic ΔH_{p-p} value for DMPO-OH adduct (for the second intense line at low magnetic field) change slowly with the addition of AcN from ~ 1.2 G in water solution to 1.3 G at 20 % of AcN and 1.8 G at 50 % of AcN. At the same time the hfsc values also decrease slowly from 14.95 G (in water) to 14.28 (50% water, 50% AcN). The changes within the EPR spectra upon introduction of aprotic solvent into water solution are related to the high content of oxygen in AcN as well as the high

Table 4.1. EPR measured parameters of DMPO-OH adduct in water solution as a function of AcN concentration

EPR measured Parameters	% of AcN in Sample solution; 50 ug EPFRs'+150mM DMPO + AcN + buffer		
	0	20	50
ΔH_{p-p} , G	1.2	1.3	1.8
hfsc values, G	$\alpha_N = \alpha_H = 14.95$	$\alpha_N = \alpha_H = 14.60$	$\alpha_N = \alpha_H = 14.28$

polarity character of AcN. There might be also some superposition of DMPO-OH and DMPO-

OOH spectra (43). These results indirectly show that the superoxide anions are self-dismutated in protic environment (47) and form OH radicals elucidated in **Scheme 4.16**.

4.9 References

1. Lomnicki, S., Dellinger, B. A detailed mechanism of the surface-mediated formation of PCDD/F from the oxidation of 2-chlorophenol on a CuO/silica surface. *J. Phys. Chem. A* **2003**, *107*, 4387-4395.
2. Balakrishna, S.; Lomnicki, S.; McAvey, K.M.; Cole, R.B.; Dellinger, B.; and Cormier, S.A. Environmentally persistent free radicals amplify ultrafine particle mediated cellular oxidative stress and cytotoxicity. *Part. Fibre Toxicol.* **2009**, *6*, 11.
3. Bandara, J.; Mielczarski, J.A.; Kiwi, J. I. Adsorption mechanism of chlorophenols on iron oxides, titanium oxide and aluminum oxide as detected by infrared spectroscopy. *Appl. Catal., B* **2001**, *34*, 4, 307-320.
4. Farquar, G.R.; Alderman, S.L.; Poliakoff, E.D.; Dellinger, B. X-ray spectroscopic studies of the high temperature reduction of Cu(II)O by 2-chlorophenol on a simulated fly ash surface. *Environ. Sci. Technol.* **2003**, *37*, 5, 931-935.
5. Lomnicki, S.; Dellinger, B. Formation of PCDD/F from the pyrolysis of 2-chlorophenol on the surface of dispersed copper oxide particles. *Proc. Combust. Inst.* **2003**, *29*, 2463-2468.
6. Alderman, S.L., Dellinger, B. FTIR investigation of 2-chlorophenol chemisorption on a silica surface from 200 to 500 °C. *J. Phys. Chem.* **2005**, *109*, 7725-7731.
7. Hindin, S.G.; Weller, S.W.; Adalbert, F., *10 catalysis of ethylene hydrogenation and hydrogen-deuterium exchange by dehydrated alumina*, in *Adv. Catal.* 1957, Academic Press. p. 70-75.
8. Voltz, S.E.; Weller, S.W. The oxidation of carbon monoxide over chromic oxide. *J. Phys. Chem.* **1955**, *59*, 6, 566-569.
9. Voltz, S.E.; Weller, S.W. Decomposition of aqueous hydrogen peroxide over chromic oxide catalysts. *J. Am. Chem. Soc.* **1954**, *76*, 6, 1586-1587.
10. Boyd, S.A.; Mortland, M.M. Dioxin radical formation and polymerization on Cu(II)-

smectite. *Nature* **1985**, *316*, 6028, 532-535.

11. Voncina, E.; Somaljer, T. Thermolysis of 2,4,6-trichlorophenol chemisorbed on aluminum oxides as example of fly ash mediated surface catalysis reaction of PCDD/PCDF formation. *Chemosphere* **2002**, *46*, 1279-1286.

12. Khachatryan, L.; Adoukpe, J.; Maskos, Z.; Dellinger, B. Formation of cyclopentadienyl radical from the gas-phase pyrolysis of hydroquinone, catechol, and phenol. *Environ. Sci. Technol.* **2006**, *40*, 16, 5071-5076.

13. Melius, C.F.; Colvin, M.E.; Marinov, N.M.; Pit, W.J.; Senkan, S.M. Reaction mechanisms in aromatic hydrocarbon formation involving the C₅H₅ cyclopentadienyl moiety. *Symp. (Int.) Combust.* **1996**, *26*, 1, 685-692.

14. Neta, P.; Fessenden, R.W. Hydroxyl radical reactions with phenols and anilines as studied by electron spin resonance. *J. Phys. Chem.* **1974**, *78*, 5, 523-9.

15. Lomnicki, S.; Truong, H.; Vejerano, E.; Dellinger, B. Copper oxide-based model of persistent free radical formation on combustion-derived particulate matter. *Environ. Sci. Technol.* **2008**, *42*, 13, 4982-4988.

16. Hales, B.J.; Case, E.E. Immobilized radicals. IV. Biological semiquinone anions and neutral semiquinones. *Biochim. Biophys. Acta, Bioenerg.* **1981**, *637*, 2, 291-302.

17. Yonezawa, T.; Kawamura, T.; Ushio, M.; Nakao, Y. Solvent effects on the g factors of semiquinones. *Bull. Chem. Soc. Jap.* **1970**, *43*, 4, 1022-7.

18. Lomnicki, S.; Dellinger, B. A detailed mechanism of the surface-mediated formation of PCDD/F from the oxidation of 2-chlorophenol on a CuO/silica surface. *J. Phys. Chem. A* **2003**, *107*, 22, 4387-4395.

19. Alderman, S.L., Farquar, G.R., Poliakoff, E.D., Dellinger, B. FTIR investigation of 2-chlorophenol chemisorption on Cu(II)O/SiO₂. *Environ. Sci. Technol.* **2003**, *37*, 935.

20. Hoffman, R.V.; Eiceman, G.A.; Long, Y.T.; Collins, M.C.; Lu, M.Q. Mechanism of chlorination of aromatic compounds adsorbed on the surface of fly ash from municipal incinerators. *Environ. Sci. Technol.* **1990**, *24*, 11, 1635-1641.

21. Dellinger, B., Lomnicki, S., Khachatryan, L., Maskos, Z., Hall R., Adoukpe, J., McFerrin, C., Truong, H. Formation and stabilization of persistent free radicals. *31st Intern. Symp. on Combustion, University of Heidelberg, Germany* **2006**, Abstracts, 88.
22. Eiceman, G.A.; Clement, R.E.; Karasek, F.W. Variations in concentrations of organic compounds including polychlorinated dibenzo-p-dioxins and polynuclear aromatic hydrocarbons in fly ash from a municipal incinerator. *Anal. Chem.* **1981**, *53*, 7, 955-959.
23. McFerrin, C.A.; Hall, R.W.; Dellinger, B. Ab initio study of the formation and degradation reactions of semiquinone and phenoxy radicals. *J. Mol. Struct. THEOCHEM* **2008**, *848*, 1-3, 16-23.
24. Addink, R.; Cnubben, P.A.J.P.; Olie, K. Formation of polychlorinated dibenzo-p-dioxins/dibenzofurans on fly ash from precursors and carbon model compounds. *Carbon* **1995**, *33*, 10, 1463-1471.
25. Stieglitz, L.; Vogg, H. Formation and degradation of polychlorodibenzodioxins and -furans in fly ashes from waste incineration. *Gewaesserschutz, Wasser, Abwasser* **1990**, *112*, Abwasser- Abfalltech.: Konzepte Prax., 849-878.
26. Ismo, H.; Kari, T.; Juhani, R. Formation of aromatic chlorinated compounds catalyzed by copper and iron. *Chemosphere* **1997**, *34*, 12, 2649-2662.
27. Federman Neto, A.; Pelegriño, A.C.; Darin, V.A. Ferrocene: 50 years of transition metal organometallic chemistry — from organic and inorganic to supramolecular chemistry. *ChemInform* **2004**, *35*, 43, no-no.
28. Agerberth, B.; Grunewald, J.; Castanos-Velez, E.; Olsson, B.; Jornvall, H.; Wigzell, H.; Eklund, A.; Gudmundsson, G.H. Antibacterial components in bronchoalveolar lavage fluid from healthy individuals and sarcoidosis patients. *Am. J. Respir. Crit. Care Med.* **1999**, *160*, 1, 283-290.
29. Nemmar, A.; Vanquickenborne, B.; Dinsdale, D.; Thomeer, M.; Hoylaerts, M.F.; Vanbilloen, H.; Mortelmans, L.; Nemery, B. Passage of inhaled particles into the blood circulation in humans. *Circulation* **2002**, *105*, 4, 411-414.
30. Frampton, M.W. Systemic and cardiovascular effects of airway injury and inflammation: Ultrafine particle exposure in humans. *Environ. Health Perspect. Suppl.* **2001**, *109*, 4, 529-532.

31. Oberdorster, G. Significance of particle parameters in the evaluation of exposure-dose-response relationships of inhaled particles. *Part. Sci. Technol.* **1996**, *14*, 2, 135-151.
32. Utell, M.J.; Frampton, M.W. Acute health effects of ambient air pollution: The ultrafine particle hypothesis. *J. Aerosol Med.* **2000**, *13*, 4, 355-59.
33. Cormier, S.A.; Lomnicki, S.; Backes, W.; and Dellinger, B. Origin and health impacts of emissions of toxic by-products and fine particles from combustion and thermal treatment of hazardous wastes and materials. *Environ. Health Perspect.* **2006**, *114*, 810-817.
34. Stone, K., Bermudez, E., Zang, L.Y., Carter, K. M. The ESR properties, DNA nicking, and DNA association of aged solutions of catechol versus aqueous extracts of tar from cigarette smoke. *Arch. Biochem. Biophys.* **1995**, *319*, 1, 196-203.
35. Dellinger, B., Pryor, W. A., Ceuto, R., Squadrito, G. L., Hedge, V., Deutsch, W. A. Role of free radicals in the toxicity of airborne fine particulate matter. *Chem. Res. Toxicol.* **2001**, *14*, 1371-1377.
36. Truong, H.; Lomnicki, S.; Dellinger, B. Potential for misidentification of environmentally persistent free radicals as molecular pollutants in particulate matter. *Environ. Sci. Technol.* **2010**, *44*, 6, 1933-1939.
37. Balakrishna, S.; Fahmy, B.; Lomnicki, S.; Dellinger, B.; Ahlert, T.; You, D.; Cormier, S.A. *Combustion generated nanoparticles: Pro-inflammatory effects and role of oxidative stress in neonatal rat exposure models*. 2008: American Chemical Society.
38. Halliwell, B., and Gutteridge, J.M.C. Free radicals and metal ions in human disease in methods in enzymology. *Methods Enzymol.* **1990**, *186*, 1-85.
39. Yamazaki, I.; Piette, L.H. EPR spin-trapping study on the oxidizing species formed in the reaction of the ferrous ion with hydrogen-peroxide. *J. Am. Chem. Soc.* **1991**, *113*, 20, 7588-7593.
40. Yamazaki, I.; Piette, L.H. ESR spin-trapping studies on the reaction of Fe²⁺ ions with H₂O₂-reactive species in oxygen-toxicity in biology. *J. Biol. Chem.* **1990**, *265*, 23, 13589-13594.
41. Forshult, S.; Lagercrantz, C. Use of nitroso compounds as scavengers for study of short-lived free radicals in organic reactions. *Acta Chem. Scand.* **1969**, *23*, 2, 522-&.

42. Janzen, E.G.; Blackburn, B.J. Detection and identification of short-lived free radicals by an electron spin resonance trapping technique. *J. Am. Chem. Soc.* **1968**, *90*, 21, 5909-5916.
43. Burkitt, M.J.; Tsang, S.Y.; Tam, S.C.; Bremner, I. Generation of 5,5-dimethyl-1-pyrroline N-oxide hydroxyl and scavenger radical adducts from copper/H₂O₂ mixtures - effects of metal-ion chelation and the search for high-valent metal-oxygen intermediates. *Arch. Biochem. Biophys.* **1995**, *323*, 1, 63-70.
44. Finkelstein, E.; Rosen, G.M.; Rauckman, E.J. Spin trapping of superoxide and hydroxyl radical - practical aspects. *Arch. Biochem. Biophys.* **1980**, *200*, 1, 1-16.
45. Alaghmand, M.; Blough, N.V. Source-dependent variation in hydroxyl radical production by airborne particulate matter. *Environ. Sci. Technol.* **2007**, *41*, 7, 2364-2370.
46. Tomita, M.; Okuyama, T.; Watanabe, S.; Watanabe, H. Quantitation of the hydroxyl radical adducts of salicylic-acid by micellar electrokinetic capillary chromatography - oxidizing species formed by a Fenton reaction. *Arch. Toxicol.* **1994**, *68*, 7, 428-433.
47. Fee, J.A.; Valentine, J.S., *Chemical and physical properties of superoxide in superoxide and superoxide dismutases.*, ed. A.M. Michelson, McCord, J. M., and Fridovich, I., . Vol. Academic Press, New York. **1977** 19-60.
48. Bielski, B.H.J.; Allen, A.O. Mechanism of disproportionation of superoxide radicals. *J. Phys. Chem.* **1977**, *81*, 11, 1048-1050.
49. Villamena, F.A.; Locigno, E.J.; Rockenbauer, A.; Hadad, C.M.; Zweier, J.L. Theoretical and experimental studies of the spin trapping of inorganic radicals by 5,5-dimethyl-1-pyrroline N-oxide (DMPO). 2. Carbonate radical anion. *J. Phys. Chem. A* **2007**, *111*, 2, 384-391.
50. Buettner, G.R.; Oberley, L.W. Considerations in spin trapping of superoxide and hydroxyl radical in aqueous systems using 5,5-dimethyl-1-pyrroline-N-oxide. *Biochem. Biophys. Res. Commun.* **1978**, *83*, 1, 69-74.
51. Cabelli, D.E.; Allen, D.; Bielski, B.H.J.; Holcman, J. The interaction between Cu(I) superoxide dismutase and hydrogen peroxide. *J. Biol. Chem.* **1989**, *264*, 17, 9967-9971.
52. Buettner, G.R.; Mason, R.P. Critical reviews of oxidative stress and aging: Advances in

basic science, diagnostics and intervention. Chapter 2. *Ed. Cutler, R.G., and Rodrigues, H.* **2003**, 27-38.

53. Dikalov, S.I.; Dikalova, A.E.; Mason, R.P. Noninvasive diagnostic tool for inflammation-induced oxidative stress using electron spin resonance spectroscopy and an extracellular cyclic hydroxylamine. *Arch. Biochem. Biophys.* **2002**, *402*, 2, 218-226.

54. Bacic, G.; Spasojevic, I.; Secerov, B.; Mojovic, M. Spin-trapping of oxygen free radicals in chemical and biological systems: New traps, radicals and possibilities. *Spectrochim. Acta Part A Mol. Biomol. Spectrosc.* **2008**, *69*, 5, 1354-1366.

55. Harbour, J.R.; Bolton, J.R. Involvement of hydroxyl radical in destructive photo-oxidation of chlorophylls in vivo and in vitro. *Photochem. Photobiol.* **1978**, *28*, 2, 231-234.

56. Valentine, J.S.; Foote, C.S.; Grenbery, A.; Liebman, J.F.E. Active oxygen in biochemistry. **1995**, 3, Blackie Academic & Professional.

57. Dvoranova, D.; Brezova, V.; Mazur, M.; Malati, M.A. Investigations of metal-doped titanium dioxide photocatalysts. *Appl. Catal., B* **2002**, *37*, 2, 91-105.

58. Hasegawa, K.; Murase, M.; Saida, H.; Shinoda, M.; Miyamoto, M.; Shimasaki, C.; Yoshimura, T.; Tsukurimichi, E. Photooxidation of naphthalenamines adsorbed on particles under simulated atmospheric conditions. *Environ. Sci. Technol.* **1993**, *27*, 1819-1825.

59. Baird, W.R.; Foley, R.T. Solubility of oxygen in selected organic-solvents. *J. Chem. Eng. Data* **1972**, *17*, 3, 355-&.

60. Greenwald, R., A. Handbook of method for oxygen radical research. *CRC Press, Florida* **1985**, 65.

61. Roubaud, V.; Sankarapandi, S.; Kuppasamy, P.; Tordo, P.; Zweier, J.L. Quantitative measurement of superoxide generation using the spin trap 5-(diethoxyphosphoryl)-5-methyl-1-pyrroline-N-oxide. *Anal. Biochem.* **1997**, *247*, 2, 404-411.

62. Janzen, E.G.; Haire, D.L.; Coulter, G.A.; Stronks, H.J.; Krygsman, P.H.; Towner, R.A.; Hilborn, J.W. Locating spin traps in heterogeneous media by C-13 NMR-spectroscopy - investigations in SDS micelles, DMPC vesicles, and rat-liver microsomes. *J. Org. Chem.* **1989**, *54*, 12, 2915-2920.

63. Buettner, G.R. Spin trapping - electron-spin-resonance parameters of spin adducts. *Free Radic. Biol. Med.* **1987**, 3, 4, 259-303.
64. Harbour, J.R.; Hair, M.L. Transient radicals in heterogeneous systems - detection by spin trapping. *Adv. Colloid Interface Sci.* **1986**, 24, 2-3, 103-141.
65. Reszka, K.; Bilski, P.; Sik, R.H.; Chignell, C.F. Photosensitized generation of superoxide radical in aprotic solvents - an EPR and spin-trapping study. *Free Radic. Res. Commun.* **1993**, 19, S33-S44.
66. Lee, M.L.; and Markides., K.E. Analytical supercritical fluid chromatography and extraction, chromatography conferences supercritical fluid chromatography and extraction, chromatography conferences. *Supercritical Fluid Chromatography and Extraction, Chromatography Conferences* **1990**, Inc., Provo, Utah.

CHAPTER V. SUMMARY

5.1 EPFR Formation on Transition Metal Oxide/Silica Surface

The formation of environmentally persistent free radicals in combustion-generated particulate matter has been investigated. Our hypothesis suggests that EPFRs on ambient particulate matter are formed from the interaction of organic pollutants and transition metals. EPFRs such as semiquinone-type and phenoxy-type radicals are known to exist in combustion system and are highly resonance stabilized (1-3). Semiquinone radicals are known to be very potent species which can undergo redox cycling and are implicated in oxidative stress which results to cardiopulmonary dysfunction and even cancer (4-7). Phenoxy-type radicals on the other hand, can recombine and are known to form PCDD/Fs which are the most toxic compound known. The association of the EPFRs with transition metals makes EPFRs to become highly stable compared to previously identified atmospheric free radicals, and are very persistent, thus, they can travel over long distances and exert their adverse health and environmental effects.

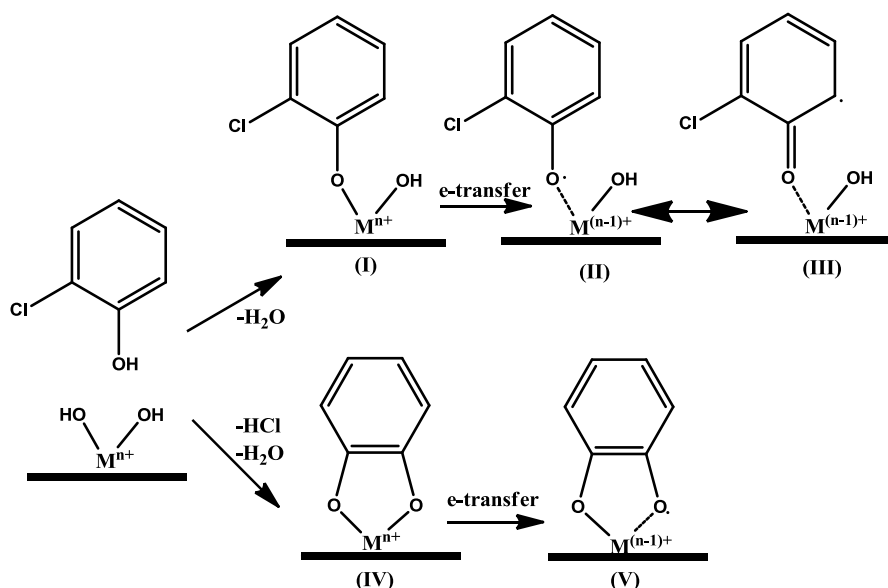
Our study suggests that the adsorption of various aromatic adsorbates forms and stabilizes free radicals on the surface of different transition metals from 150-400 °C and semiquinone and phenoxy-type radicals were observed together with cyclopentadienyl-type radicals which results from decomposition of phenoxy radicals. Semiquinone and phenoxy radical are environmentally persistent and are biologically active. EPFRs were studied by EPR measurement and their g-values were determined from peak fitting analyses of the first-derivative EPR spectra, and the lifetime and the condition for their formation. Nickel, iron, copper, and zinc were the transition metals studied as they are dominant components in combustion system and are known to catalyze pollutant formation in particulate matter. Chlorinated adsorbates such as 1,2-dichlorobenzene, 2-monochlorophenol, and

monochlorobenzene were studied as they are the dominant chlorinated compound in combustion system containing chlorine, such as hazardous waste and municipal incinerators (8-10).

The phenolic compounds such as catechol, hydroquinone, and phenol were chosen as they are major component of biomass system (11-16) and catechol and hydroquinone are known to form semiquinone radicals (1-3).

5.2 Formation and Stabilization of EPFRs on Fe(III)₂O₃ and Ni(II)O on Silica Surface

In our previous study we investigated the formation of EPFRs on Cu(II)O as they are



Scheme 5.1. Formation of cyclopentadienyl radical from decomposition of surface-bound phenoxyl radical through CO elimination

known to catalyze the formation of PCDD/Fs. However, since iron is typically the more dominant transition metal in airborne PM_{2.5} as well as emissions from some types of combustion sources, the formation and stabilization of EPFRs involving reaction with iron might contribute more than copper to the total number of the metal-radical complexes in PM. Like EPFRs on copper, EPFRS on iron and nickel surface undergo essentially the same mechanism.

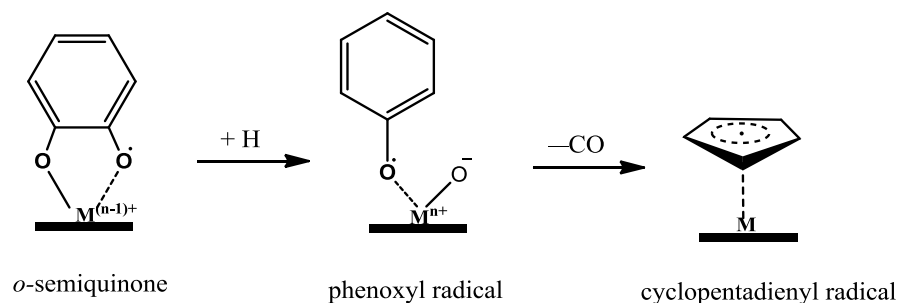
We have identified 3 key steps in the formation of EPFRs. First, the molecular adsorbate physisorbs on the surface of the terminal hydroxyl group of the metal oxide surface. The adsorbate chemisorbs on the surface via two possible pathways. First, is by single elimination of the chlorine substituent, and second by elimination of both substituents to form a bidentate species. Once chemisorb, the electron from the oxygen atom is transferred from the metal cation forming the surface stabilized EPFRs and concomitant reduction of the metal cation center. **Scheme 5.1** illustrates the mechanism of formation for 2-monochlorophenol on a generalized metal oxide surface. For monosubstituted benzene containing chlorine and hydroxy substituents, the resulting EPFRs lead to the formation of a phenoxyl-type EPFR. On the other hand, the doubly-substituted benzene can form phenoxyl-type EPFRs if adsorption occurs on a single site and/or a semiquinone-type radicals if chemisorptions occurs on both substituents.

5.3 Temperature Dependence of EPFR Yields

This study investigates the formation of EPFRs from different aromatic adsorbates from 150-400 °C and what radicals are formed under these conditions. Depending on the metals and substituents, variation in the yield of metal and type of EPFRs formed are observed. In general, the maximum yield for iron were observed at higher temperature from 300-350 °C, similar observation was noted for EPFR yield on Ni(II)O. Compared to copper, EPFR yields on iron are ~10x lower which has the lowest yield among the metals. Theoretical calculations suggest that only Ni(II)O and Cu(II)O lead to exothermic reaction thus generation of EPFRs are very favorable compared to the formation of EPFRs over Fe(III)₂O₃ (17). The yields of EPFRs on iron for chlorinated adsorbates are among the lowest. For the chlorinated adsorbates, the higher the number of chlorine substituents the lower the EPFR yield because of the electron-withdrawing character of the substituent which destabilizes the ring. However, the hydroxyl substituent for 2-

monochlorophenol counteracts the electron withdrawing ability of the chlorine-substituent, thus, the resulting EPFRs are stable, which resulted in higher yield. Another possible explanations for the lower EPFR yield for chlorinated adsorbates are: 1) the chlorine substituent does not chemisorb with the surface by HCl elimination as readily as hydroxyl substituent reacts by H₂O elimination and 2) the surface abstracts chlorine from the adsorbate or reacts with HCl formed during chemisorption to form surface hypochlorites, which then reacts with the initially formed EPFR (18). The unchlorinated adsorbates generally, have higher yield than the chlorinated adsorbate possibly since the elimination of H₂O is more favorable than HCl elimination.

A different behavior was observed for the EPFRs on Ni(II)O. In general, the chlorinated adsorbates have higher EPFR yield than the chlorinated adsorbates, specifically phenol and hydroquinone, except for catechol which essentially forms *o*-semiquinone radicals. This shows that for Ni(II)O, the molecules that can form bidentate species on the surface are favored, thus, 1,2-dichlorobenzene and 2-monochlorophenol have higher yield. Monochlorobenzene has higher yield, especially at higher temperature since it can undergo chlorination reaction by the



Scheme 5.2. Surface decomposition of *o*-semiquinone radical to phenoxyl radical and subsequent conversion to cyclopentadienyl radical through CO elimination

hypochlorite mechanism to form 1,2-dichlorobenzene which can chemisorb on two sites and ultimately form *o*-semiquinone radical. In general, the yield of EPFRs on Ni(II)O is similar to Cu(II)O and differs by as much as ~10x compared to Fe(III)₂O₃. Therefore, Ni(II)O favors the formation of EPFRs from adsorbates that can chemisorb on two sites to form bidentate species. Semiquinone radicals are known to decompose to phenoxyl radical, and phenoxyl radical can be decomposed further to form secondary cyclopentadienyl radicals **Scheme 5.2**.

5.4 Persistence of EPFRs on Transition Metal Oxide/Silica Surface

While atmospheric free radicals have very short lifetime, EPFRs associated with transition metals are very stable and persistent. They are resistant to further oxidation with molecular oxygen which is the primary sink of free radicals to molecular species in the environment. However, the half-lives of EPFRs show strong dependence on the metals they are tethered to. The half-lives for the different adsorbates on Cu(II)O range from 27-74 min (19), while that of EPFRs on Ni(II)O and Fe(III)₂O₃ range from 1.5 to 5.2 and from 1.0 to 4.6 days, respectively. On the other hand for transition metals having a completely filled *d*-orbitals such as Zn(II)O the EPFRs for the different adsorbates have a remarkably long half-lives on the order of months (43-72 days). Moreover, a second decay, possibly from secondary radicals such as cyclopentadienyl radicals showed half-lives that are even longer than the primary radical (semiquinone and phenoxyl type radicals) observed on Cu(II)O, Ni(II)O, and Fe(III)₂O₃ and the half-lives of the EPFRs on the different metals follow this trend: Zn > Ni~Fe > Cu. The half-lives of the EPFRs correlate well with the standard reduction potential of the metals. The more negative the reduction potential, the higher the half-lives of the EPFRs.

5.5 Formation of Molecular Products from Radical-Radical Recombination

Although the same adsorbates were used in all studies, there were differences in

reactivity of Cu(II)O, Fe(III)₂O₃, and Ni(II)O surface, which resulted in different EPFRs being formed and different molecular products being observed from the extraction of these particles in methanol and dichloromethane. More products were formed on both Cu(II)O and Fe(III)₂O₃, which includes PCDD/Fs as one of the molecular products observed. However, PCDD/Fs were not detected as molecular products on Ni(II)O surface. This is expected since the lower reactivity of the nickel surface does not catalyze the formation of PCDD/Fs, however, this low reactivity of the EPFRs on the surface suggests that once bound, the EPFRs are very stable and would no longer undergo further reactions compared to iron and copper. Phenol was one of the most abundant and easily identifiable molecular products, which attests to the relative ease of forming this radical. In addition semiquinone radical can decompose to phenoxy radical at higher temperature. To understand the formations of molecular products, mechanism were proposed from the free radical pathway.

5.6 *In Vitro* Studies and Interaction of EPFRs with Biological Compounds

The interaction of EPFRs with biological compounds was of high importance in the study of particulate matter. Kinetic study on the half-lives of the EPFRs on BALF and serum showed that the EPFR half-life was ~2x higher in BALF than in serum. The EPFRs signals do not decay immediately owing to diffusion-limitation of the components of BALF which hinders the reaction of the EPFRs with smaller molecular components of BALF. However, the half-lives on both systems (serum and BALF) are long enough that the EPFRs on the particles can possibly be translocated to different organ systems such as the lower respiratory system where most of the EPFR-induced damages occur (20).

The spin trapping studies were conducted to verify if the cyclical process we hypothesized occurs and that, the EPFRs are the ones responsible for the generation of ROS in

biological system. This hypothesis combines both the radical transformation and the associated metal center as a medium of Fenton reaction and source of ROS. The identification of the OH radical in aqueous solutions containing EPFRs and their relative concentration compared to other media with non-EPFR-containing particles is of utmost importance for the EPFRs redox cycle validation. The experiments in the presence of DMPO spin trap were performed for both EPFR and non-EPFR-containing samples. In the presence of EPFR particles, more DMPO-OH adduct was formed compared to non-EPFR containing particles, while a particle free solution (DMPO only) produce trace amounts of the DMPO-OH adduct. The amount of the DMPO-OH spin adduct formed in the presence of non-EPFR and EPFR particles changes with incubation time, the longer the incubation time the larger the difference in the amount of DMPO-OH formed in the case of non-EPFR- and EPFR-containing particles. On average, twice as much DMPO-OH spin adducts was formed in the presence of EPFR-containing particle compared to non-EPFR-containing particles at long incubation time. Even in presence of H_2O_2 no evidence could be obtained for OH formation from the $Cu(II)_{(aq)}/H_2O_2$ reaction system despite the detection of a prominent signal from the DMPO-OH adduct due solely to the nucleophilic addition of water to DMPO (21). The number of OH radicals was quantified with the assumption of 1:1 stoichiometry of OH to DMPO for DMPO-OH spin adduct formation. This value may be the lower concentration limit of OH radicals because the decay of DMPO-OH during accumulation as well as the effectiveness of trapping OH radicals by DMPO was not considered. The extrapolation of the OH radical concentration to the number of EPFR radicals indicates that 1 EPFR radical generates ~10 OH radicals at incubation time of 140 min which indicates a cyclic nature of the process. The effect of SOD on the formation of DMPO-OH adduct in the presence of EPFR particles have confirmed the involvement of superoxide radicals in the process although

it could not be spin-trapped in the aqueous media. The inability to identify superoxide radicals in the aquatic media, while a DMPO-O₂⁻ spin adduct is detected in the aprotic solvents, suggests a very quick transformation of the O₂⁻ in water environment. These results indirectly show that the superoxide anions are self-dismutated in protic environment (22) and form OH radicals. The polarity effect of solvents on hyperfine splitting constants (hfsc) of DMPO-O₂⁻ adducts is visible when compared to the EPR spectra of DMPO-O₂⁻ spin adduct from Fenton reaction in homogeneous water environment in presence of 5% DMSO. A decrease in the hfsc parameters for DMPO-O₂⁻ in different solvents, H₂O, DMSO and AcN, correlates with the decreasing polarity of the solvent (23-28). The result provides a direct proof of the superoxide radicals being formed from molecular oxygen in the presence of EPFR particles.

5.7 Concluding Remarks

In summary, our results indicate the reactions of different aromatic molecules on Cu(II)O, Fe(III)₂O₃, Ni(II)O, and Zn(II)O silica surface produce EPFRs. These EPFRs are stable and do not react rapidly with air, which results in atmospheric lifetimes of days. The study has proven that semiquinone-type and phenoxyl type radicals are formed in combustion system from 150-400 °C, which is the same condition most particulate matter would undergo in the post-combustion zone. These EPFRs are stabilized by their association with different metals existing on the surface of particulate matter. This suggests the EPFRs can be transported in the atmosphere, eventually participate in atmospheric reactions, or directly exert health and environmental impacts. Chlorinated EPFRs were formed and persisted on copper-, nickel- and zinc-, and iron-containing particles, which suggest their importance in the environmental and health impacts of combustion-generated particles in municipal and hazardous wastes. The EPFRs forms ROS and undergoes redox cycling as proven by the spin trapping experiment. The longer

lifetimes observed for these EPFR-metal system suggest their greater importance in atmospheric processes. The differences between the EPFRs and their lifetimes on different transition metals suggest an urgent need to study other metal oxides as potential sources of EPFR-containing particles.

The author suggests that further studies be done on the formation of EPFRs with the following considerations. Other metals and transition metals which are of significant concentration in particulate matter like vanadium, manganese, magnesium, chromium, and titanium be investigated. In addition, mixture of these metals should be studied to closely simulate real fly ash system and conduct parallel experiments using real fly ash system and to compare the formation and stabilization of combustion-generated EPFRs. This is to determine whether these metal systems enhance EPFR formation or whether they actively decompose EPFRs after they are formed. Furthermore, photochemical studies should be conducted to understand their fate in the environment. In addition, simulate the conditions where EPFR-containing particulate matter are exposed to, and determine the effect of these conditions on their stability and persistency, and determine if they can catalyze the formation of new atmospheric pollutants such as NO_x.

5.8 References

1. Lomnicki, S.; Dellinger, B. A detailed mechanism of the surface-mediated formation of PCDD/F from the oxidation of 2-chlorophenol on CuO/ silica surface. *J. Phys. Chem. A* **2003**, *107*, 22, 4387-4395.
2. Lomnicki, S.; Dellinger, B. Formation of PCDD/F from the pyrolysis of 2-chlorophenol on the surface of dispersed copper oxide particles. *Proceedings of the International Symposium on Combustion* **2003**, *29*, 2463-2468.
3. Pryor, W.A., Prier, D. G., Church, D. F. Electron spin resonance study of mainstream and sidestream smoke: Nature of the free radicals in gas-phase smoke and in cigarette tar.

Environ. Health Perspect. **1983**, *47*, 345-355.

4. Han, J.Y.; Takeshita, K.; Utsumi, H. Noninvasive detection of hydroxyl radical generation in lung by diesel exhaust particles. *Free Radic. Biol. Med.* **2001**, *30*, 5, 516-525.
5. Knaapen, A.M.; Shi, T.M.; Borm, P.J.A.; Schins, R.P.F. Soluble metals as well as the insoluble particle fraction are involved in cellular DNA damage induced by particulate matter. *Mol. Cell. Biochem.* **2002**, *234*, 1, 317-326.
6. Prahalad, A.K.; Soukup, J.M.; Inmon, J.; Willis, R.; Ghio, A.J.; Becker, S.; Gallagher, J.E. Ambient air particles: Effects on cellular oxidant radical generation in relation to particulate elemental chemistry. *Toxicol. Appl. Pharmacol.* **1999**, *158*, 2, 81-91.
7. Prahalad, A.K.; Inmon, J.; Dailey, L.A.; Madden, M.C.; Ghio, A.J.; Gallagher, J.E. Air pollution particles mediated oxidative DNA base damage in a cell free system and in human airway epithelial cells in relation to particulate metal content and bioreactivity. *Chem. Res. Toxicol.* **2001**, *14*, 7, 879-887.
8. Fine, P.M.; Cass, G.R.; Simoneit, B.R.T. Chemical characterization of fine particle emissions from the fireplace combustion of woods grown in the southern United States. *Environ. Sci. Technol.* **2002**, *36*, 1442-1451.
9. Bonte, J.L.; Fritsky, K.J.; Plinke, M.A.; Wilken, M. Catalytic destruction of PCDD/F in a fabric filter: Experience at a municipal waste incinerator in Belgium. *Waste Manag.* **2002**, *22*, 4, 421-426.
10. Blumenstock, M.; Zimmermann, R.; Schramm, K.-W.; Kaune, A.; Nikolai, U.; Lenoir, D.; Kettrup, A. Estimation of the dioxin emission (PCDD/FI-TEQ) from the concentration of low chlorinated aromatic compounds in the flue and stack gas of a hazardous waste incinerator. *J. Anal. Appl. Pyrolysis* **1999**, *49*, 1-2, 179-190.
11. Fine, P.M.; Cass, G.R.; Simoneit, B.R.T. Chemical characterization of fine particle emissions from the wood stove combustion of prevalent United States tree species. *Environ. Eng. Sci.* **2004**, *21*, 6, 705-721.
12. Hays, M.D.; Fine, P.M.; Geron, C.D.; Kleeman, M.J.; Gullett, B.K. Open burning of agricultural biomass: Physical and chemical properties of particle-phase emissions. *Atmos. Environ.* **2005**, *39*, 36, 6747-6764.

13. Høgl, O. Some non-volatile extracts of coffee. *Mitteilungen aus dem Gebiete der Lebensmitteluntersuchung und Hygiene* **1958**, 49, pp. 433-441.
14. Sheesley, R.J.; Schauer, J.J.; Chowdhury, Z.; Cass, G.R.; Simoneit, B.R.T. Characterization of organic aerosols emitted from the combustion of biomass indigenous to south Asia. *J Geophys Res-Atmos* **2003**, 108, D9, -.
15. Varagnal, J., *Hydroquinone, resorcinol, and catechol* 3rd ed. Kirk-othmer. Encyclopedia of chemical technology., ed. D.E. M. Grayson, G.J. Bushey, C.I. Eastman, A. Klingsberg, L. Spiro and M. Wainwright. Vol. 13. **1981**, New York John Wiley & Sons pp. 39-69.
16. Visser, R.; Harbers, A.A.M.; Hovestad, A.; Stevens, T.W. *Identification of organic compounds in waste water of wood gasifiers with capillary gas chromatography*. 1985: Huethig.
17. Sun, Q.; Altarawneh, M.; Dlugogorski, B.Z.; Kennedy, E.M.; Mackie, J.C. Catalytic effect of CuO and other transition metal oxides in formation of dioxins: A theoretical investigation of reaction between 2,4,5-trichlorophenol and CuO. *Environ. Sci. Technol.* **2007**, 41, 16, 5708-5715.
18. Lomnicki, S.; Dellinger, B. A detailed mechanism of the surface-mediated formation of PCDD/F from the oxidation of 2-chlorophenol on a CuO/silica surface. *J. Phys. Chem. A* **2003**, 107, 22, 4387-4395.
19. Lomnicki, S.; Truong, H.; Vejerano, E.; Dellinger, B. Copper oxide-based model of persistent free radical formation on combustion-derived particulate matter. *Environ. Sci. Technol.* **2008**, 42, 13, 4982-4988.
20. Oberdorster, G.; Sharp, Z.; Atudorei, V.; Elder, A.; Gelein, R.; Kreyling, W.; Cox, C. Translocation of inhaled ultrafine particles to the brain. *Inhal. Toxicol.* **2004**, 16, 6-7, 437-445.
21. Burkitt, M.J.; Tsang, S.Y.; Tam, S.C.; Bremner, I. Generation of 5,5-dimethyl-1-pyrroline N-oxide hydroxyl and scavenger radical adducts from copper/H₂O₂ mixtures - effects of metal-ion chelation and the search for high-valent metal-oxygen intermediates. *Arch. Biochem. Biophys.* **1995**, 323, 1, 63-70.
22. Fee, J.A.; Valentine, J.S., *Chemical and physical properties of superoxide in superoxide and superoxide dismutases.*, ed. A.M. Michelson, McCord, J. M., and Fridovich, I., . Vol. Academic Press, New York. **1977** 19-60.

23. Harbour, J.R.; Bolton, J.R. Involvement of hydroxyl radical in destructive photo-oxidation of chlorophylls *in vivo* and *in vitro*. *Photochem. Photobiol.* **1978**, *28*, 2, 231-234.
24. Janzen, E.G.; Haire, D.L.; Coulter, G.A.; Stronks, H.J.; Krygsman, P.H.; Towner, R.A.; Hilborn, J.W. Locating spin traps in heterogeneous media by C-13 NMR-spectroscopy - investigations in SDS micelles, DMPC vesicles, and rat-liver microsomes. *J. Org. Chem.* **1989**, *54*, 12, 2915-2920.
25. Buettner, G.R. Spin trapping - electron-spin-resonance parameters of spin adducts. *Free Radic. Biol. Med.* **1987**, *3*, 4, 259-303.
26. Harbour, J.R.; Hair, M.L. Transient radicals in heterogeneous systems - detection by spin trapping. *Adv. Colloid Interface Sci.* **1986**, *24*, 2-3, 103-141.
27. Reszka, K.; Bilski, P.; Sik, R.H.; Chignell, C.F. Photosensitized generation of superoxide radical in aprotic solvents - an EPR and spin-trapping study. *Free Radic. Res. Commun.* **1993**, *19*, S33-S44.
28. Lee, M.L.; and Markides., K.E. Analytical supercritical fluid chromatography and extraction, chromatography conferences supercritical fluid chromatography and extraction, chromatography conferences. *Supercritical Fluid Chromatography and Extraction, Chromatography Conferences* **1990**, Inc., Provo, Utah.

APPENDIX 1. VARIATION OF G-VALUE AND ΔH_{p-p} WITH TIME ON $\text{Fe(III)}_2\text{O}_3$, Ni(II)O , AND Zn(II)O ON SILICA SURFACE WITH AIR

Table A1.1. Variation of ΔH_{p-p} and g-value with time for catechol dosed on $\text{Fe(III)}_2\text{O}_3/\text{silica}$ at 230 °C upon exposure to air at ambient condition

Time (h)	ΔH_{p-p}	g-value
0	9.7	2.0041
0.50	9.4	2.0042
0.75	9.7	2.0040
1.0	9.7	2.0040
18	8.9	2.0041
24	8.7	2.0040
144	5.3	2.0043
168	5.8	2.0044
192	5.6	2.0044
216	5.6	2.0044
292	5.6	2.0045
360	9.8	2.0040

Table A1.2. Variation of ΔH_{p-p} and g-value with time for 2-monochlorophenol dosed on $\text{Fe(III)}_2\text{O}_3/\text{silica}$ at 230 °C upon exposure to air at ambient condition

Time (h)	ΔH_{p-p}	g-value
0	6.0	2.0043
15	7.3	2.0045
20	7.2	2.0042
34	7.2	2.0044
45	7.1	2.0044
53	6.8	2.0041
77	6.8	2.0041
0	6.0	2.0043
15	7.3	2.0045
20	7.2	2.0042
34	7.2	2.0044
45	7.1	2.0044
53	6.8	2.0041
77	6.8	2.0041

Table A1.3. Variation of ΔH_{p-p} and g-value with time for phenol dosed on Fe(III)₂O₃/silica at 230 °C upon exposure to air at ambient condition.

Time (h)	ΔH_{p-p}	g-value
0	6.2	2.0044
0.5	6.5	2.0044
1	6.9	2.0044
1.5	6.6	2.0044
24	5.3	2.0041
48	5.6	2.0039
72	5.4	2.0038
168	5.6	2.0044

Table A1.4. Variation of ΔH_{p-p} and g-value with time for hydroquinone dosed on Fe(III)₂O₃/silica at 230 °C upon exposure to air at ambient condition

Time (h)	ΔH_{p-p}	g-value
0	8.9	2.0044
0.5	8.0	2.0043
1	8.2	2.0045
24	9.2	2.0046
120	9.0	2.0044

Table A1.5. Variation of ΔH_{p-p} and g-value with time for catechol dosed on Ni(II)O/silica at 230 °C upon exposure to air at ambient condition

Time (h)	ΔH_{p-p}	g-value	Time (h)	ΔH_{p-p}	g-value
0	9.8	2.0040	32	6.6	2.0041
1	9.7	2.0040	48	6.4	2.0044
2	9.6	2.0040	52	6.6	2.0044
4	9.8	2.0040	55	5.5	2.0043
6	9.8	2.0040	120	5.3	2.0043
8	9.2	2.0039	144	5.6	2.0045
24	8.8	2.0042	168	5.6	2.0045
28	8.6	2.0043			

Table A1.6. Variation of ΔH_{p-p} and g-value with time for monochlorobenzene dosed on Ni(II)O/silica at 230 °C upon exposure to air at ambient condition

Time (h)	ΔH_{p-p}	g-value
0	5.9	2.0042
0.5	6.3	2.0043
1	6.2	2.0043
2	6.3	2.0044
4	5.8	2.0043
6	5.8	2.0043
23	5.8	2.0042
25	5.8	2.0042
120	5.8	2.0041
124	5.6	2.0041
144	5.8	2.0040

Table A1.7. Variation of ΔH_{p-p} and g-value with time for 2-monochlorophenol dosed on Ni(II)O/silica at 230 °C upon exposure to air at ambient condition

Time (h)	ΔH_{p-p}	g-value	Time (h)	ΔH_{p-p}	g-value
0	5.7	2.0042	93	5.2	2.0040
1	6.0	2.0042	100	5.7	2.0042
5	5.8	2.0043	117	5.4	2.0040
7	5.6	2.0043	124	5.3	2.0042
8	5.7	2.0042	141	5.6	2.0040
24	5.6	2.0042	148	5.3	2.0043
25	5.6	2.0040	151	5.3	2.0043
33	5.8	2.0041	175	5.3	2.0041
45	5.5	2.0040	213	5.4	2.0041
52	5.3	2.0042	237	5.3	2.0039
69	5.6	2.0040	261	5.2	2.0040
76	5.5	2.0042	1000	5.6	2.0041

Table A1.8. Variation of ΔH_{p-p} and g-value with time for phenol dosed on Ni(II)O/silica at 230 °C upon exposure to air at ambient condition

Time (h)	ΔH_{p-p}	g-value	Time (h)	ΔH_{p-p}	g-value
0	5.8	2.0043	27	5.3	2.0041
1	5.4	2.0042	32	5.2	2.0042
5	6.0	2.0042	43	5.3	2.0038
19	5.7	2.0039	47	5.2	2.0040

21	5.6	2.0040	51	5.2	2.0005
23	5.6	2.0041	66	5.4	2.0039
25	5.9	2.0041	67	5.5	2.0042

Table A1.9. Variation of ΔH_{p-p} and g-value with time for hydroquinone dosed on Ni(II)O/silica at 230 °C upon exposure to air at ambient condition

Time (h)	ΔH_{p-p}	g-value
0	6.7	2.0045
0	7.2	2.0045
1	7.1	2.0045
2	7.5	2.0046
18	7.6	2.0042
23	6.5	2.0044
120	6.4	2.0039
124	6.4	2.0043
144	6.2	2.0059

Table A1.10. Variation of ΔH_{p-p} and g-value with time for 1,2-dichlorobenzene dosed on Ni(II)O/silica at 230 °C upon exposure to air at ambient condition

Time (h)	ΔH_{p-p}	g-value
0	6.2	2.0042
1	6.3	2.0042
2	6.3	2.0042
3	6.3	2.0042
4	6.1	2.0042
6	6.1	2.0042
7	6.0	2.0042
24	6.1	2.0041
25	6.0	2.0041
27	5.8	2.0041
29	5.8	2.0041
30	6.0	2.0041
46	6.0	2.0039

Table A1.11. Variation of ΔH_{p-p} and g-value with time for catechol dosed on Zn(II)O/silica at 230 °C upon exposure to air at ambient condition

Time (h)	ΔH_{p-p}	g-value	Time (h)	ΔH_{p-p}	g-value
-----------------	------------------------------------	----------------	-----------------	------------------------------------	----------------

0	10.7	2.0036	673	4.8	2.0044
1	10.2	2.0033	722	4.7	2.0044
17	10.7	2.0033	772	4.7	2.0043
24	10.2	2.0035	822	4.7	2.0045
40	8.9	2.0036	958	4.5	2.0044
47	7.1	2.0043	1012	4.7	2.0039
65	6.4	2.0041	1030	4.5	2.0044
165	5.3	2.0043	1078	4.8	2.0046
185	5.3	2.0041	1126	4.8	2.0047
209	4.9	2.0041	1174	4.8	2.0045
233	4.9	2.0041	1220	4.5	2.0045
254	4.9	2.0041	1268	4.8	2.0046
283	4.9	2.0042	1300	4.8	2.0045
304	4.7	2.0043	1348	4.8	2.0047
330	4.9	2.0042	1396	4.8	2.0048
353	4.7	2.0043	1444	4.8	2.0044
397	4.7	2.0043	1492	4.8	2.0046
420	4.7	2.0043	1570	4.8	2.0047
444	4.7	2.0042	1666	4.8	2.0046
468	4.7	2.0043	1762	4.8	2.0044
516	4.6	2.0045	1858	4.8	2.0046
563	4.7	2.0044	2319	4.8	2.0045
627	4.6	2.0042			

Table A1.12. Variation of ΔH_{p-p} and g-value with time for monochlorobenzene dosed on Zn(II)O/silica at 230 °C upon exposure to air at ambient condition

Time (h)	ΔH_{p-p}	g-value	Time (h)	ΔH_{p-p}	g-value
0	10.0	2.0037	678	5.2	2.0045
1	10.0	2.0040	532	5.1	2.0044
32	8.9	2.0041	582	5.2	2.0044
61	7.0	2.0042	718	5.0	2.0044
84	7.0	2.0042	772	5.1	2.0045
110	6.4	2.0042	778	5.0	2.0045
134	5.7	2.0044	844	5.2	2.0044
178	5.2	2.0041	892	5.1	2.0046
201	5.1	2.0042	940	5.1	2.0045
225	4.9	2.0044	988	5.1	2.0044
273	4.9	2.0438	1036	4.9	2.0046
321	5.0	2.0439	1066	5.0	2.0045
384	4.9	2.0042	1114	5.0	2.0045
409	5.0	2.0044	1162	5.0	2.0045

432	5.0	2.0044	1210	5.2	2.0045
457	5.0	2.0044	1258	5.1	2.0046
481	5.2	2.0045	1336	5.1	2.0046
506	4.9	2.0045	1410	5.2	2.0045
532	5.1	2.0044	1528	4.9	2.0044
582	5.2	2.0044	1624	4.9	2.0046
630	5.1	2.0043			

Table A1.13. Variation of ΔH_{p-p} and g-value with time for 2-monochlorophenol dosed on Zn(II)O/silica at 230 °C upon exposure to air at ambient condition

Time (h)	ΔH_{p-p}	g-value	Time (h)	ΔH_{p-p}	g-value
0	7.3	2.0038	732	4.8	2.0045
19	7.0	2.0037	782	5.0	2.0046
91	5.6	2.0042	732	4.8	2.0045
119	5.4	2.0042	966	5.2	2.0047
137	5.3	2.0039	972	5.3	2.0045
185	5.2	2.0041	1044	5.4	2.0046
215	6.2	2.0037	1042	5.3	2.0047
244	4.9	2.0043	1140	5.2	2.0046
265	4.7	2.0043	1186	5.3	2.0047
291	4.6	2.0044	1234	5.1	2.0045
314	4.3	2.0044	1312	5.2	2.0046
358	4.3	2.0044	1360	5.3	2.0046
381	4.0	2.0044	1408	5.3	2.0046
404	4.1	2.0044	1456	5.3	2.0044
428	4.3	2.0043	1504	5.1	2.0046
476	4.3	2.0045	1582	5.4	2.0046
524	4.3	2.0048	1672	5.3	2.0046
588	4.3	2.0045	1774	5.5	2.0045
634	4.6	2.0047	1870	5.3	2.0046
682	4.9	2.0045	2337	5.2	2.0044

Table A1.14. Variation of ΔH_{p-p} and g-value with time for phenol dosed on Zn(II)O/silica at 230 °C upon exposure to air at ambient condition

Time (h)	ΔH_{p-p}	g-value	Time (h)	ΔH_{p-p}	g-value
0	6.8	2.0042	564	3.7	2.0044

0	6.8	2.0042	628	4.4	2.0042
1	6.8	2.0043	674	3.9	2.0044
17	5.9	2.0043	722	4.0	2.0044
24	5.9	2.0043	772	4.0	2.0043
41	5.9	2.0042	822	3.9	2.0044
48	5.9	2.0044	958	4.0	2.0043
73	5.9	2.0041	1012	4.0	2.0045
91	5.9	2.0043	1030	4.0	2.0043
113	5.9	2.0041	1078	3.9	2.0044
141	4.4	2.0043	1126	4.4	2.0042
159	4.0	2.0041	1126	4.0	2.0044
183	4.0	2.0041	1172	4.0	2.0044
207	3.9	2.0042	1220	4.2	2.0045
237	3.9	2.0043	1298	4.0	2.0044
266	3.9	2.0043	1346	3.9	2.0044
287	3.9	2.0044	1394	4.0	2.0045
313	3.7	2.0043	1444	4.4	2.0043
331	3.9	2.0043	1492	4.0	2.0048
336	4.0	2.0044	1570	4.0	2.0045
360	3.9	2.0043	1666	4.0	2.0045
382	3.8	2.0042	1762	4.0	2.0043
468	3.9	2.0043	1858	3.8	2.0043
516	3.9	2.0043	2319	3.9	2.0044

Table A1.15. Variation of ΔH_{p-p} and g-value with time for hydroquinone dosed on Zn(II)O/silica at 230 °C upon exposure to air at ambient condition

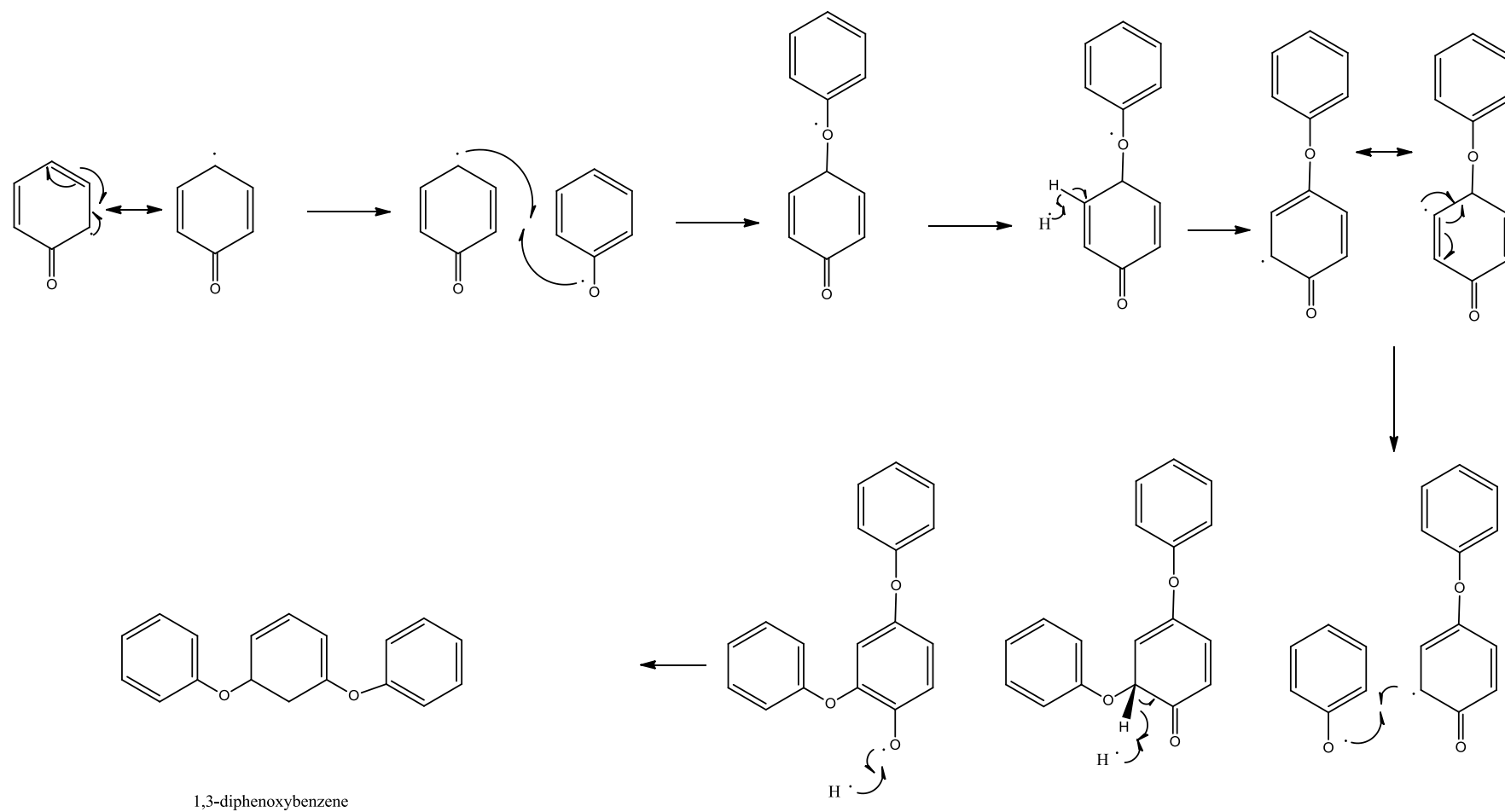
Time (h)	ΔH_{p-p}	g-value	Time (h)	ΔH_{p-p}	g-value
1	10.2	2.0030	806	5.0	2.0043
61	6.2	2.0048	854	4.9	2.0044
82	6.1	2.0043	902	4.9	2.0044
108	6.2	2.0041	950	4.9	2.0047
131	5.8	2.0043	996	5.0	2.0045
175	5.6	2.0042	1044	4.8	2.0046
198	5.3	2.0042	1074	5.0	2.0046
221	5.1	2.0041	1222	5.0	2.0046
245	5.1	2.0043	1270	4.8	2.0043
293	5.3	2.0043	1318	4.8	2.0043
340	5.3	2.0043	1366	5.0	2.0044
404	4.9	2.0041	1444	5.0	2.0045
450	4.9	2.0044	1540	4.8	2.0046
498	5.0	2.0044	1636	4.8	2.0045

548	5.0	2.0043	1732	4.8	2.0044
598	5.0	2.0044	2193	5.0	2.0044
734	4.9	2.0043			

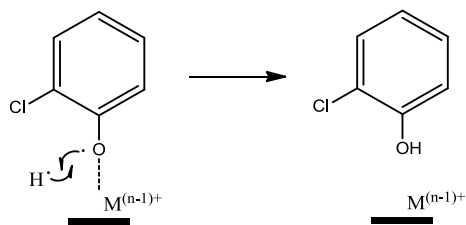
Table A1.16. Variation of ΔH_{p-p} and g-value with time for 1,2-dichlorobenzene dosed on Zn(II)O/silica at 230 °C upon exposure to air at ambient condition

Time (h)	ΔH_{p-p}	g-value	Time (h)	ΔH_{p-p}	g-value
0	9.1	2.0038	420	5.0	2.0045
1	8.1	2.0040	443	5.0	2.0043
18	7.5	2.0037	467	5.0	2.0045
24	7.5	2.0040	563	5.0	2.0045
49	6.8	2.0040	627	5.0	2.0044
56	6.6	2.0043	721	5.0	2.0045
63	7.0	2.0037	821	5.0	2.0045
81	6.1	2.0040	957	5.0	2.0043
153	5.0	2.0040	1005	5.0	2.0045
181	5.0	2.0044	1219	4.9	2.0046
200	5.0	2.0041	1297	4.9	2.0045
224	5.0	2.0042	1444	5.0	2.0046
254	5.0	2.0043	1492	5.1	2.0046
283	5.0	2.0045	1570	5.1	2.0046
304	5.0	2.0045	1666	5.1	2.0047
330	5.0	2.0043	2223	5.1	2.0044
353	5.0	2.0045			

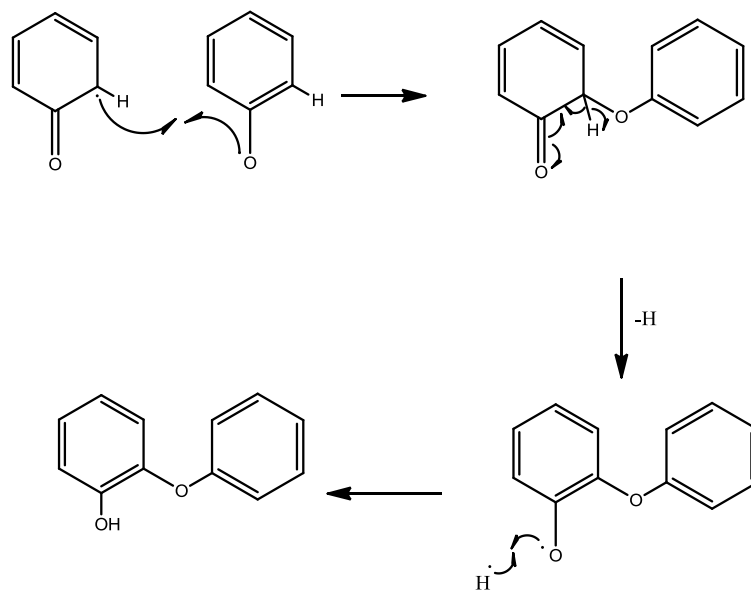
APPENDIX 2. PROPOSED REACTION MECHANISMS FOR THE FORMATION OF MOLECULAR PRODUCT FROM RADICALS



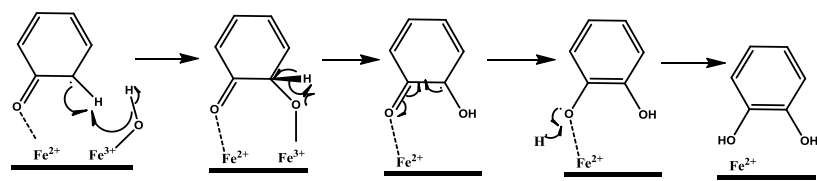
Scheme A2.1. Formation of 1,3-diphenoxybenzene from phenoxy radical



Scheme A2.2. Formation of monochlorophenol from 2-chlorophenoxy radical



Scheme A2.3. Formation of 2-phenoxyphenol from recombination of mesomeric forms of phenoxy radical in the surface



Scheme A2.5. Formation of catechol from phenol

APPENDIX 3. PEAK FITTING ANALYSIS EXAMPLE OF EPR SPECTRA FOR CT, HQ, PH, 1,2-DCBz, MCBz, AND 2-MCP

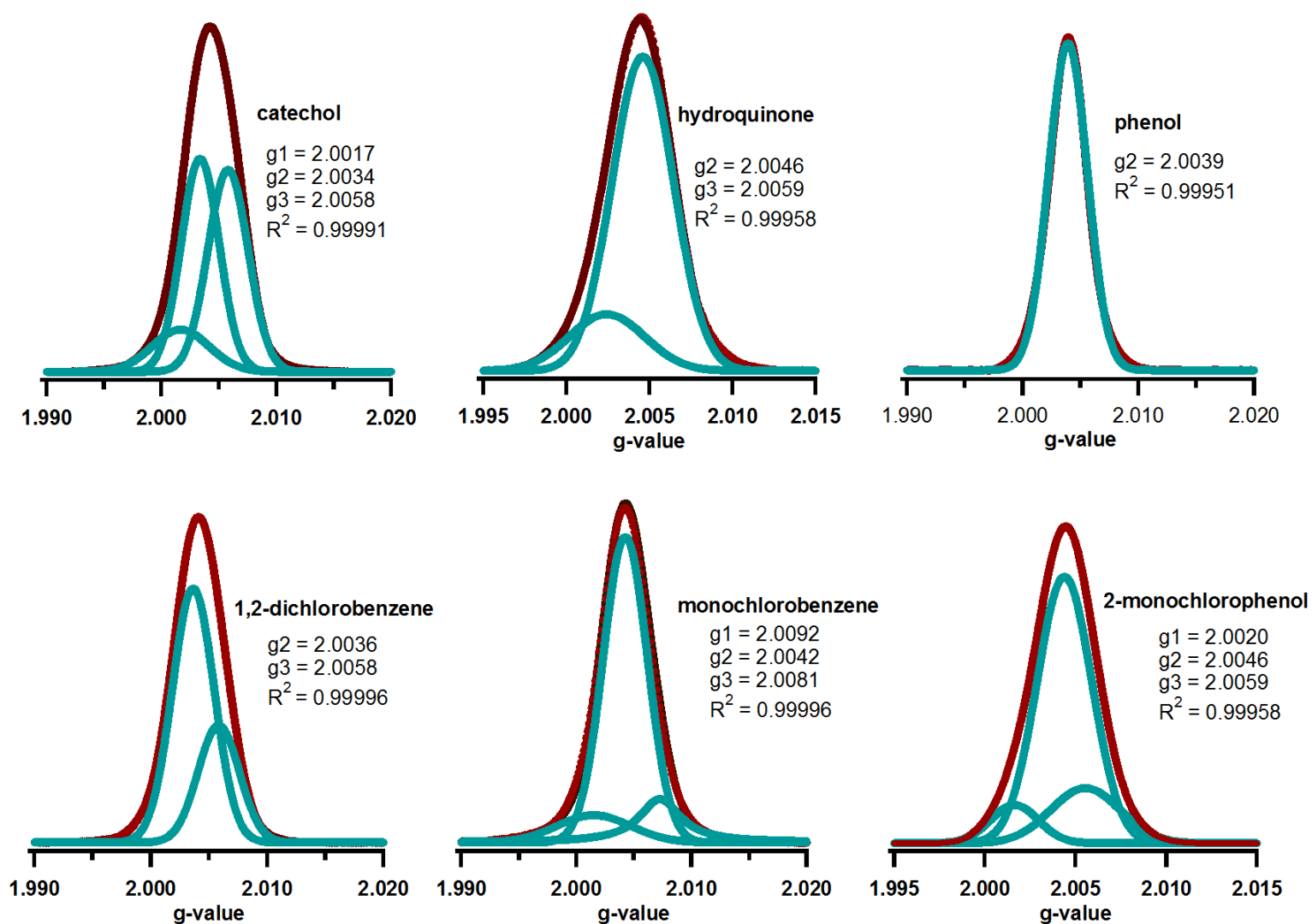


Figure A3.1. Examples of spectral peak fitting of EPR signals from Ni(II)O/silica dosed with CT, HQ, PH, 1,2-DCBz, MCBz, and 2-MCP

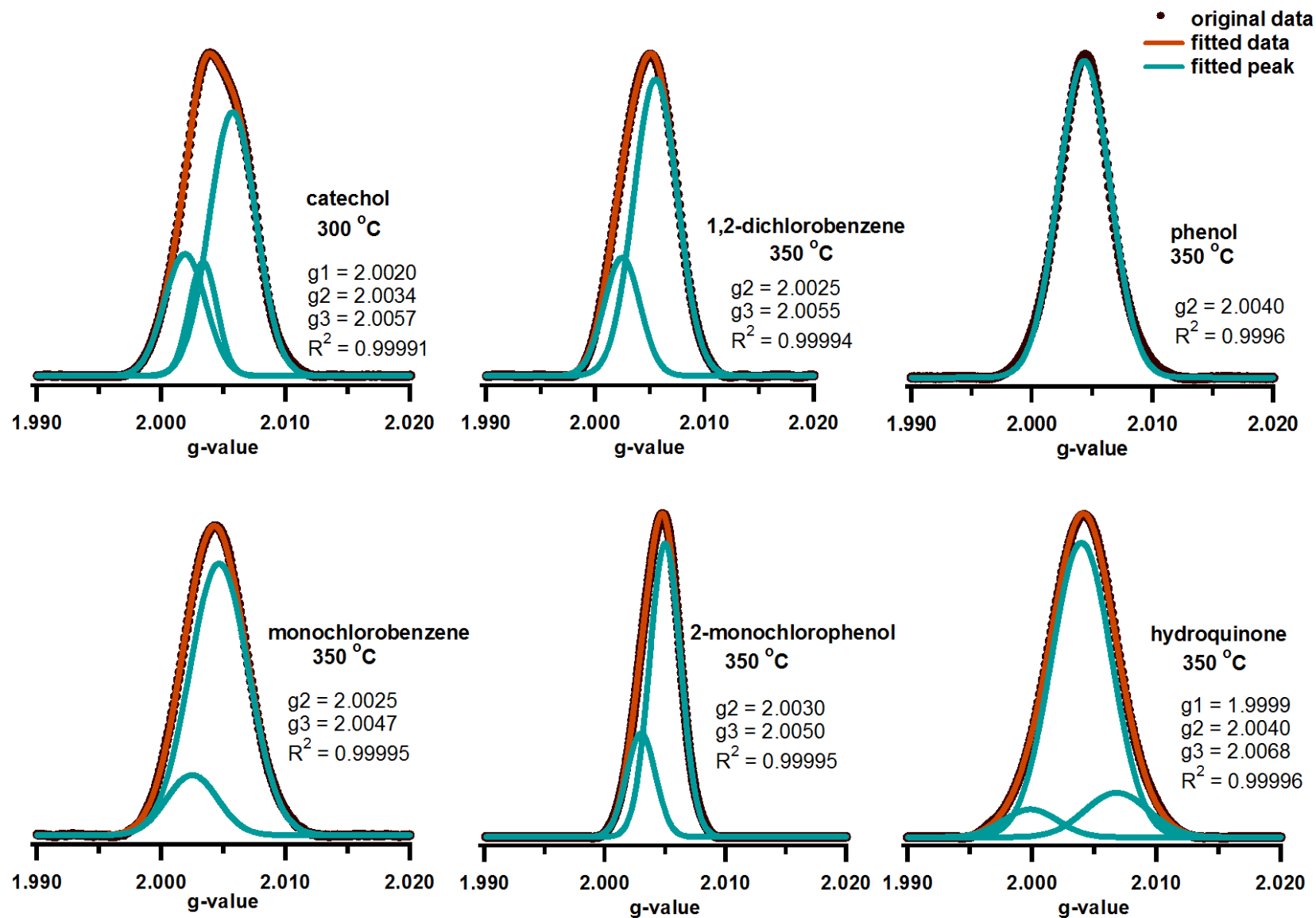


Figure A3.2. Examples of spectral peak fitting of EPR signals from $\text{Fe(III)}_2\text{O}_3/\text{silica}$ dosed with CT, HQ, PH, 1,2-DCBz, MCBz, and 2-MCP

APPENDIX 4. EPFRs ON Cu(II)O AND Fe₂(III)O₃/SILICA EXPOSED TO SUNLIGHT AT AMBIENT CONDITION

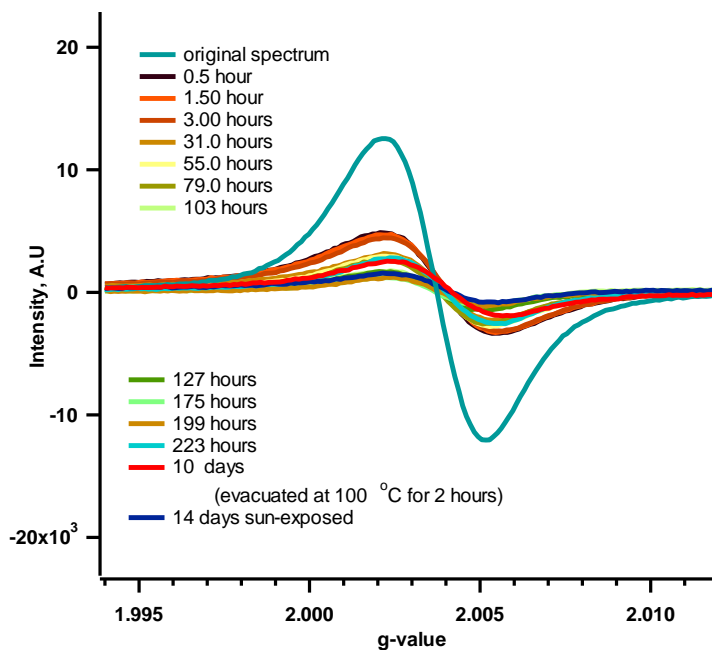


Figure A3.1. EPFRs on Cu(II)O/silica surface from adsorption of CT, HQ, and PH exposed to air and then sunlight

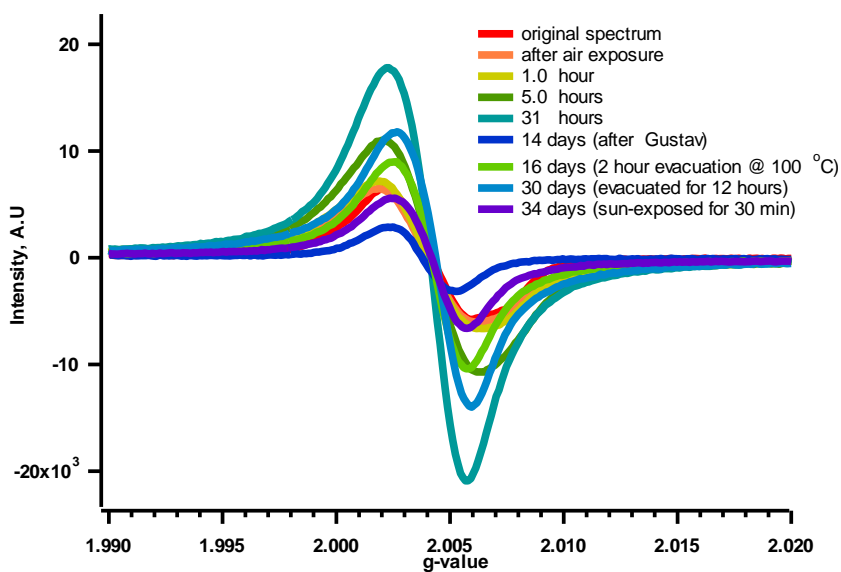


Figure A3.2. EPFRs on Fe(III)₂O₃/silica surface from adsorption of CT, HQ, and PH exposed to air and then sunlight

APPENDIX 5. AMERICAN CHEMICAL SOCIETY'S POLICY ON THESES AND DISSERTATIONS

If your university requires a signed copy of this letter see contact information below.

Thank you for your request for permission to include **your** paper(s) or portions of text from **your** paper(s) in your thesis. Permission is now automatically granted; please pay special attention to the implications paragraph below. The Copyright Subcommittee of the Joint Board/Council Committees on Publications approved the following:

Copyright permission for published and submitted material from theses and dissertations

ACS extends blanket permission to students to include in their theses and dissertations their own articles, or portions thereof, that have been published in ACS journals or submitted to ACS journals for publication, provided that the ACS copyright credit line is noted on the appropriate page(s).

Publishing implications of electronic publication of theses and dissertation material

Students and their mentors should be aware that posting of theses and dissertation material on the Web prior to submission of material from that thesis or dissertation to an ACS journal may affect publication in that journal. Whether Web posting is considered prior publication may be evaluated on a case-by-case basis by the journal's editor. If an ACS journal editor considers Web posting to be "prior publication", the paper will not be accepted for publication in that journal. If you intend to submit your unpublished paper to ACS for publication, check with the appropriate editor prior to posting your manuscript electronically.

If your paper has not yet been published by ACS, we have no objection to your including the text or portions of the text in your thesis/dissertation in **print and microfilm formats**; please note, however, that electronic distribution or Web posting of the unpublished paper as part of your thesis in electronic formats might jeopardize publication of your paper by ACS. Please print the following credit line on the first page of your article: "Reproduced (or 'Reproduced in part') with permission from [JOURNAL NAME], in press (or 'submitted for publication'). Unpublished work copyright [CURRENT YEAR] American Chemical Society." Include appropriate information.

If your paper has already been published by ACS and you want to include the text or portions of the text in your thesis/dissertation in **print or microfilm formats**, please print the ACS copyright credit line on the first page of your article: "Reproduced (or 'Reproduced in part') with permission from [FULL REFERENCE CITATION.] Copyright [YEAR] American Chemical Society." Include appropriate information.

Submission to a Dissertation Distributor: If you plan to submit your thesis to UMI or to another dissertation distributor, you should not include the unpublished ACS paper in your thesis if the thesis will be disseminated electronically, until ACS has published your paper. After publication of the paper by ACS, you may release the entire thesis (**not the individual ACS article by itself**) for electronic dissemination through the distributor; ACS's copyright credit line should be printed on the first page of the ACS paper.

Use on an Intranet: The inclusion of your ACS unpublished or published manuscript is permitted in your thesis in print and microfilm formats. If ACS has published your paper you may include the manuscript in your thesis on an intranet that is not publicly available. Your ACS article cannot be posted electronically on a publicly available medium (i.e. one that is not password protected), such as but not limited to, electronic archives, Internet, library server, etc. The only material from your paper that can be posted on a public electronic medium is the article abstract, figures, and tables, and you may link to the article's DOI or post the article's author-directed URL link provided by ACS. This paragraph does not pertain to the dissertation distributor paragraph above.

Questions? Call +1 202/872-4368/4367. Send e-mail to copyright@acs.org or fax to +1 202-776-8112. 10/10/03, 01/15/04, 06/07/06

VITA

Eric Warren Pimentel Vejerano was born on January 1978, in the Republic of the Philippines. He completed his Bachelor of Science in agricultural chemistry from the University of the Philippines Los Baños in April 1999. He pursued his doctoral degree in physical environmental chemistry at Louisiana State University in Baton Rouge on August 2005. His research was under the mentorship of Dr. Barry Dellinger, Professor and Patrick F. Taylor Chair, Director of LSU Inter-college Environmental Co-operative, and Director of LSU Superfund Research Center. He will receive his Doctor of Philosophy degree in May 2011.